



Global Carbon Budget 2025

- 2 Pierre Friedlingstein[1,2], Michael O'Sullivan[1], Matthew W. Jones[3], Robbie M. Andrew[4],
- 3 Dorothee C. E. Bakker[5], Judith Hauck[6,7], Peter Landschützer[8], Corinne Le Quéré[3], Hongmei
- 4 Li[9,10], Ingrid T. Luijkx[11], Glen P. Peters[4], Wouter Peters[11,12], Julia Pongratz[13,10], Clemens
- 5 Schwingshackl[13], Stephen Sitch[1], Josep G. Canadell[14], Philippe Ciais[15], Kjetil Aas[4], Simone
- 6 R. Alin[16], Peter Anthoni[17], Leticia Barbero[18], Nicholas R. Bates[19,20], Nicolas Bellouin[21],
- 7 Alice Benoit-Cattin[22], Carla F. Berghoff[23], Raffaele Bernardello[24], Laurent Bopp[2], Ida Bagus
- 8 Mandhara Brasika[1,25], Matthew A. Chamberlain[26], Naveen Chandra[27], Frédéric Chevallier[15],
- 9 Louise P. Chini[28], Nathan O. Collier[29], Thomas H. Colligan[30], Margot Cronin[31], Laique M.
- 10 Djeutchouang[32,33,34], Xinyu Dou[35], Matt P. Enright[19,20], Kazutaka Enyo[36], Michael
- 11 Erb[37,38], Wiley Evans[39], Richard A. Feely[16], Liang Feng[40,41], Daniel J. Ford[1], Adrianna
- Foster[42], Filippa Fransner[43,44], Thomas Gasser[45], Marion Gehlen[15], Thanos Gkritzalis[8],
- 13 Jefferson Goncalves De Souza[1], Giacomo Grassi[46], Luke Gregor[47,48], Nicolas Gruber[47],
- 14 Bertrand Guenet [49], Özgür Gürses [6], Kirsty Harrington [50], Ian Harris [51], Jens Heinke [52], George
- 15 C. Hurtt[28], Yosuke Iida[36], Tatiana Ilyina[53,9,10], Akihiko Ito[54], Andrew R. Jacobson[55,56],
- 16 Atul K. Jain[57], Tereza Jarníková[3], Annika Jersild[30], Fei Jiang[58], Steve D. Jones[8], Etsushi
- 17 Kato[59], Ralph F. Keeling[60], Kees Klein Goldewijk[61], Jürgen Knauer[62], Yawen Kong[63,64],
- Jan Ivar Korsbakken[4], Charles Koven[65], Taro Kunimitsu[4], Xin Lan[55,56], Junjie Liu[66,67],
- 19 Zhiqiang Liu[68], Zhu Liu[69], Claire Lo Monaco[70], Lei Ma[28], Gregg Marland[37,38], Patrick C.
- 20 McGuire[71], Galen A. McKinley[72], Joe R. Melton[73], Natalie Monacci[74], Erwan Monier[75,76],
- 21 Eric J. Morgan[60], David R. Munro[55,56], Jens D. Müller[77], Shin-Ichiro Nakaoka[78], Lorna R.
- 22 Nayagam[78], Yosuke Niwa[78], Tobias Nutzel[13], Are Olsen[43,44], Abdirahman M. Omar[79,44],
- 23 Naiqing Pan[80], Sudhanshu Pandey[66], Denis Pierrot[81], Zhangcai Qin[82], Pierre Regnier[83],
- 24 Gregor Rehder[84], Laure Resplandy[85], Alizée Roobaert[8], Thais M. Rosan[1], Christian
- 25 Rödenbeck[86], Jörg Schwinger[44,79], Ingunn Skjelvan[79,44], T. Luke Smallman[40,41], Victoria
- 26 Spada[87], Mohanan G. Sreeush[6], Qing Sun[88], Adrienne J. Sutton[16], Colm Sweeney[56], Didier
- 27 Swingedouw[89], Roland Séférian[90], Shintaro Takao[78], Hiroaki Tatebe[91,92], Hanqin Tian[80],
- 28 Xiangjun Tian[93,94], Bronte Tilbrook[26,95], Hiroyuki Tsujino[96], Francesco Tubiello[97], Erik van
- 29 Ooijen[26], Guido R. van der Werf[11], Sebastiaan J. van de Velde[98,99], Anthony P. Walker[100],
- 30 Rik Wanninkhof[81], Xiaojuan Yang[100], Wenping Yuan[101], Xu Yue[102], Jiye Zeng[78]

31

- 32 1: Faculty of Environment, Science and Economy, University of Exeter, Exeter, EX4 4QF, UK
- 2: Laboratoire de Météorologie Dynamique, Institut Pierre-Simon Laplace, CNRS, École Normale
- 34 Supérieure, Université PSL, Sorbonne Université, École Polytechnique, Paris, France
- 35 3: Tyndall Centre for Climate Change Research, School of Environmental Sciences, University of East
- 36 Anglia, Norwich Research Park, Norwich NR4 7TJ, UK





- 4: CICERO Center for International Climate Research, Oslo 0349, Norway
- 38 5: School of Environmental Sciences, University of East Anglia, Norwich NR4 7TJ, UK
- 39 6: Alfred-Wegener-Institut, Helmholtz-Zentrum für Polar- und Meeresforschung, Am Handelshafen 12,
- 40 27570 Bremerhaven
- 41 7: Universität Bremen, FB02 Biology/Chemistry Bremen, Germany
- 42 8: Flanders Marine Institute (VLIZ), Jacobsenstraat 1, 8400, Ostend, Belgium
- 43 9: Helmholtz-Zentrum Hereon, Max-Planck-Straße 1, 21502 Geesthacht, Germany
- 44 10: Max Planck Institute for Meteorology, Bundesstraße 53, 20146 Hamburg, Germany
- 45 11: Wageningen University, Environmental Sciences Group, P.O. Box 47, 6700AA, Wageningen, The
- 46 Netherlands
- 47 12: University of Groningen, Centre for Isotope Research, Groningen, The Netherlands
- 48 13: Ludwig-Maximilians-Universität München, Luisenstr. 37, 80333 München, Germany
- 49 14: CSIRO Oceans and Atmosphere, Canberra, ACT 2101, Australia
- 50 15: Laboratoire des Sciences du Climat et de l'Environnement, LSCE/IPSL, CEA-CNRS-UVSQ,
- 51 Université Paris-Saclay, F-91198 Gif-sur-Yvette, France
- 52 16: National Oceanic and Atmospheric Administration, Pacific Marine Environmental Laboratory
- 53 (NOAA/PMEL), 7600 Sand Point Way NE, Seattle, WA 98115, USA
- 54 17: Karlsruhe Institute of Technology, Institute of Meteorology and Climate Research/Atmospheric
- 55 Environmental Research, 82467 Garmisch-Partenkirchen, Germany
- 56 18: Rosenstiel School of Marine Atmospheric and Earth Science, Cooperative Institute for Marine and
- 57 Atmospheric Studies (CIMAS), University of Miami, 4600 Rickenbacker Causeway, Miami, FL, USA
- 58 19: Arizona State University, Tempe, Arizona, AZ 85287-5502, USA
- 59 20: Bermuda Institute of Ocean Sciences (BIOS), 17 Biological Lane, St. Georges, GE01, Bermuda
- 60 21: Department of Meteorology, University of Reading, Reading, RG6 6BB, UK
- 61 22: Marine and Freshwater Research Institute, Reykjavik, Iceland
- 62 23: Instituto Nacional de Investigación y Desarrollo Pesquero (INIDEP), Paseo Victoria Ocampo Nº1,
- 63 B7602HSA, Mar del Plata, Argentina
- 64 24: Barcelona Supercomputing Center, Barcelona, Spain
- 65 25: Faculty of Marine Science & Fisheries, Udayana University, Denpasar, Bali, 80361, Indonesia
- 66 26: CSIRO Environment, Castray Esplanade, Hobart, Tasmania 7004, Australia
- 67 27: Research Institute for Global Change, JAMSTEC, 3173-25 Showa-machi, Kanazawa, Yokohama,
- 68 236-0001, Japan
- 69 28: Department of Geographical Sciences, University of Maryland, College Park, MD 20742, USA
- 70 29: Computer Science and Engineering Division, Oak Ridge National Laboratory, Oak Ridge, TN
- 71 37831, USA
- 72 30: Earth System Science Interdisciplinary Center, University of Maryland, College Park, MD 20740,
- 73 USA

© Author(s) 2025. CC BY 4.0 License.





- 74 31: Marine Institute, Rinville, Oranmore, Co Galway H91 R673, Ireland
- 75 32: School for Climate Studies, Stellenbosch University, Private Bag X1, Matieland, Stellenbosch,
- 76 7602, South Africa
- 77 33: Southern Ocean Carbon Climate Observatory, CSIR, Rosebank, Cape Town, 7700, South Africa
- 78 34: Engr. Computer Science, University of California, Davis, CA 95616, USA
- 79 35: Department of Earth System Science, Stanford University, Stanford, CA 94305, USA
- 80 36: Japan Meteorological Agency, 3-6-9 Toranomon, Minato City, Tokyo, 105-8431, Japan
- 81 37: Research Institute for Environment, Energy, and Economics, Appalachian State University, Boone,
- 82 North Carolina, USA
- 83 38: Department of Geological and Environmental Sciences, Appalachian State University, Boone,
- 84 North Carolina, USA
- 85 39: Hakai Institute, 1713 Hyacinthe Bay Rd, Heriot Bay, BC, V0P 1H0, Canada
- 86 40: National Centre for Earth Observation, University of Edinburgh, Edinburgh, EH9 3FE, UK
- 41: School of Geosciences, University of Edinburgh, Edinburgh, EH9 3FE, UK
- 88 42: Climate and Global Dynamics Laboratory, National Center for Atmospheric Research
- 89 43: Geophysical Institute, University of Bergen, Allégaten 70, 5007 Bergen, Norway
- 90 44: Bjerknes Centre for Climate Research, Bergen, Norway
- 91 45: International Institute for Applied Systems Analysis (IIASA), Schlossplatz 1 A-2361 Laxenburg,
- 92 Austria
- 93 46: European Commission, Joint Research Centre (JRC), Ispra, Italy
- 94 47: Environmental Physics Group, Institute of Biogeochemistry and Pollutant Dynamics and Center for
- 95 Climate Systems Modeling (C2SM), ETH Zürich, Zurich, Switzerland
- 96 48: Swiss Data Science Center, 8050 Zurich, Switzerland
- 97 49: Laboratoire de Géologie, Ecole Normale Supérieure, CNRS UMR 8538, Institut Pierre-Simon
- 98 Laplace, PSL Research University, Paris, France
- 99 50: Smith School for Enterprise and the Environment, University of Oxford, Oxford, UK
- 100 51: NCAS-Climate, Climatic Research Unit, School of Environmental Sciences, University of East
- 101 Anglia, Norwich Research Park, Norwich, NR4 7TJ, UK
- 102 52: Potsdam Institute for Climate Impact Research (PIK), member of the Leibniz Association, P.O. Box
- 103 60 12 03, 14412 Potsdam, Germany
- 104 53: Universität Hamburg, Bundesstraße 55, 20146 Hamburg, Germany
- 105 54: Graduate School of Agricultural and Life Sciences, University of Tokyo, Tokyo, Japan
- 106 55: Cooperative Institute for Research in Environmental Sciences (CIRES), University of Colorado
- 107 Boulder, Boulder, CO 80305, USA
- 108 56: National Oceanic and Atmospheric Administration Global Monitoring Laboratory (NOAA/GML),
- 109 325 Broadway R/GML, Boulder, CO 80305, USA





- 110 57: Department of Climate, Meteorology and Atmospheric Sciences, University of Illinois, Urbana, IL
- 111 61801, USA
- 112 58: Jiangsu Provincial Key Laboratory for Advanced Remote Sensing and Geographic Information
- 113 Technology, International Institute for Earth System Science, Nanjing University, Nanjing, 210023,
- 114 China
- 115 59: Institute of Applied Energy (IAE), Minato-ku, Tokyo 105-0003, Japan
- 116 60: University of California, San Diego, Scripps Institution of Oceanography, La Jolla, CA 92093-
- 117 0244, USA
- 118 61: Utrecht University, Faculty of Geosciences, Department IMEW, Copernicus Institute of Sustainable
- Development, Heidelberglaan 2, P.O. Box 80115, 3508 TC, Utrecht, the Netherlands
- 120 62: School of Life Sciences, Faculty of Science, University of Technology Sydney, Ultimo, NSW 2007,
- 121 Australia
- 122 63: State Key Laboratory of Remote Sensing and Digital Earth, Aerospace Information Research
- 123 Institute, Chinese Academy of Sciences, Beijing 100101, China
- 124 64: Ministry of Education Key Laboratory for Earth System Modeling, Department of Earth System
- 125 Science, Tsinghua University, Beijing 100084, China
- 126 65: Lawrence Berkeley National Laboratory, USA
- 127 66: Jet Propulsion Laboratory, California Institute of Technology, Pasadena, CA, USA
- 128 67: Division of Geological and Planetary Sciences, California Institute of Technology, Pasadena, CA,
- 129 USA
- 130 68: CMA Key Open Laboratory of Transforming Climate Resources to Economy, Chongqing Institute
- of Meteorological Sciences, Chongqing 401147, China
- 132 69: Department of Earth System Science, Tsinghua University, Beijing, China
- 133 70: LOCEAN Laboratory (Sorbonne Université, CNRS, IRD, MNHN), 4 Place Jussieu, F-75005 Paris,
- 134 France
- 135 71: Department of Meteorology and National Centre for Atmospheric Science, University of Reading,
- 136 Reading, UK
- 137 72: Lamont-Doherty Earth Observatory, Columbia University, New York, NY, USA
- 138 73: Climate Research Division, Environment and Climate Change Canada, Victoria, BC, Canada
- 139 74: College of Fisheries and Ocean Sciences, University of Alaska Fairbanks, Fairbanks, Alaska 99775-
- 140 7220, USA
- 141 75: Department of Land, Air and Water Resources, University of California, Davis, CA 95616, USA
- 76: Climate Adaptation Research Center, University of California, Davis, CA 95616, USA
- 143 77: Carbon to Sea Initiative, Washington D.C., USA
- 144 78: Earth System Division, National Institute for Environmental Studies (NIES), 16-2 Onogawa,
- 145 Tsukuba Ibaraki, 305-8506, Japan
- 146 79: NORCE Research, Jahnebakken 5, 5007 Bergen, Norway





- 147 80: Schiller Institute of Integrated Science and Society, Department of Earth and Environmental
- 148 Sciences, Boston College, Chestnut Hill, MA 02467, USA
- 149 81: National Oceanic and Atmospheric Administration, Atlantic Oceanographic & Meteorological
- Laboratory (NOAA/AOML), 4301 Rickenbacker Causeway, Miami, FL 33149, USA
- 151 82: School of Atmospheric Sciences, Sun Yat-sen University, Zhuhai 519000, China
- 152 83: Department of Geoscience, Environment & Society-BGEOSYS, Université Libre de Bruxelles,
- 153 1050 Brussels, Belgium
- 154 84: Leibniz Institute for Baltic Sea Research Warnemünde (IOW), Seestrasse 15, 18119 Rostock,
- 155 Germany
- 156 85: Princeton University, Department of Geosciences and Princeton Environmental Institute, Princeton,
- 157 NJ, USA
- 158 86: Max Planck Institute for Biogeochemistry, P.O. Box 600164, Hans-Knöll-Str. 10, 07745 Jena,
- 159 Germany
- 160 87: Canadian Centre for Climate Modelling and Analysis, Environment and Climate Change Canada,
- 161 Victoria, BC, Canada
- 162 88: Institute for Climate and Environmental Physics, University of Bern, Bern, Switzerland
- 163 89: Environnements et Paléoenvironnements Océaniques et Continentaux (EPOC) UMR CNRS 5805
- 164 EPOC OASU, Université de Bordeaux, Allée Geoffroy Saint Hilaire, 33615 Pessac, France
- 165 90: Centre National de Recherches Météorologiques, Université de Toulouse, Météo-France, CNRS,
- 166 UMR 3589, Toulouse, France
- 167 91: Research Center for Environmental Modeling and Application, Japan Agency for Marine-Earth
- 168 Science and Technology, Yokohama, Japan
- 169 92: Advanced Institute for Marine Ecosystem Change, Japan Agency for Marine-Earth Science and
- 170 Technology, Yokohama, Japan
- 171 93: State Key Laboratory of Tibetan Plateau Earth System and Resource Environment, Institute of
- 172 Tibetan Plateau Research, Chinese Academy of Sciences, Beijing 100101, China
- 173 94: University of Chinese Academy of Sciences, Beijing 101408, China
- 174 95: Australian Antarctic Partnership Program, University of Tasmania, Hobart, Australia
- 175 96: JMA Meteorological Research Institute, Tsukuba, Ibaraki, Japan
- 176 97: Statistics Division, Food and Agriculture Organization of the United Nations, Via Terme di
- 177 Caracalla, Rome 00153, Italy
- 178 98: Earth Sciences New Zealand, Wellington, New Zealand
- 179 99: Department of Marine Science, University of Otago, Dunedin, New Zealand
- 180 100: Climate Change Science Institute and Environmental Sciences Division, Oak Ridge National
- 181 Laboratory, Oak Ridge, TN 37831, USA
- 182 101: Institute of Carbon Neutrality, College of Urban and Environmental Sciences, Peking University,
- 183 Beijing 100091, China





184 102: School of Environmental Science and Engineering, Nanjing University of Information Science and

Accurate assessment of anthropogenic carbon dioxide (CO2) emissions and their redistribution among

185 Technology (NUIST), Nanjing, 210044, China

186 187

188

189

Correspondence to: Pierre Friedlingstein (p.friedlingstein@exeter.ac.uk)

Abstract

190 the atmosphere, ocean, and terrestrial biosphere in a changing climate is critical to better understand 191 the global carbon cycle, support the development of climate policies, and project future climate 192 change. Here we describe and synthesise datasets and methodologies to quantify the five major 193 components of the global carbon budget and their uncertainties. Fossil CO2 emissions (EFOS) are based 194 on energy statistics and cement production data. Emissions from land-use change (ELUC) are estimated 195 by bookkeeping models based on land-use and land-use change data. Atmospheric CO2 concentration is measured at surface stations, and the global atmospheric CO_2 growth rate (G_{ATM}) is computed from 196 197 the annual changes in concentration. The global net uptake of CO2 by the ocean (SOCEAN, called the 198 ocean sink) is estimated with global ocean biogeochemistry models and observation-based fCO2-199 products. The global net uptake of CO₂ by the land (S_{LAND}, called the land sink) is estimated with 200 dynamic global vegetation models. Additional lines of evidence on land and ocean sinks are provided 201 by atmospheric inversions, atmospheric oxygen measurements, ocean interior observation-based 202 estimates, and Earth System Models. The sum of all sources and sinks results in the carbon budget 203 imbalance (B_{IM}), a measure of imperfect data and incomplete understanding of the contemporary 204 carbon cycle. All uncertainties are reported as $\pm 1\sigma$. 205 For the year 2024, E_{FOS} increased by 1.1% relative to 2023, with fossil emissions at 10.3 ± 0.5 GtC yr⁻¹ 206 (including the cement carbonation sink, 0.2GtC/yr), E_{LUC} was 1.3 ± 0.7 GtC yr⁻¹, for total anthropogenic CO₂ emissions of 11.6 ± 0.9 GtC yr⁻¹ (42.4 ± 3.2 GtCO₂ yr⁻¹). Also, for 2024, G_{ATM} was 207 208 7.9 ± 0.2 GtC yr⁻¹ (3.73 ± 0.1 ppm yr⁻¹), 2.2 GtC above the 2023 growth rate. S_{OCEAN} was 3.4 ± 0.4 209 GtC yr⁻¹ and S_{LAND} was 1.9 ± 1.1 GtC yr⁻¹, leaving a large negative B_{IM} (-1.7 GtC yr⁻¹), suggesting that the total sink or GATM is strongly overestimated in 2024. The global atmospheric CO2 concentration 210 averaged over 2024 reached 422.8 ± 0.1 ppm. Preliminary data for 2025 suggest an increase in E_{FOS} 211 212 relative to 2024 of +1.1% (0.2% to 2.2%) globally, and atmospheric CO2 concentration increasing by 2.3 ppm reaching 425.7 ppm, 52% above the pre-industrial level (around 278 ppm in 1750). Overall, 213 the mean and trend in the components of the global carbon budget are consistently estimated over the 214 period 1959-2024, with a near-zero overall budget imbalance, although discrepancies of up to around 215 1 GtC yr⁻¹ persist for the representation of annual to decadal variability in CO₂ fluxes. Comparison of 216 estimates from multiple approaches and observations shows: (1) a persistent large uncertainty in the 217 218 estimate of land-use change emissions, (2) a low agreement between the different methods on the





219 magnitude of the land CO2 flux in the northern extra-tropics, and (3) a discrepancy between the 220 different methods on the mean ocean sink. 221 This living data update documents changes in methods and datasets applied to this most-recent global carbon budget as well as evolving community understanding of the global carbon cycle. The data 222 223 presented in this work are available at https://doi.org/10.18160/GCP-2025 (Friedlingstein et al., 224 2025c). 225 226 **Executive Summary** 227 Global fossil CO2 emissions (including cement carbonation) are expected to further increase in 228 2025 by 1.1% relative to 2024 (range 0.2% to 2.2%), bringing fossil emissions to an expected 10.4 229 GtC yr⁻¹ (38.1 GtCO₂ yr⁻¹) ¹. Emissions from coal, oil and gas in 2025 are all expected to be above their 230 2024 levels (by 0.8%, 1.0% and 1.3% respectively). These preliminary estimates are based on available 231 data for 2025. Consolidated data confirm a growth of 1.1% in 2024 relative to 2023, with fossil CO2 emissions of 10.3 ± 0.5 GtC yr⁻¹ (37.8 ± 1.8 GtCO₂ yr⁻¹) in 2024. 232 233 Regionally, fossil emissions are projected to grow in 2025 in the USA and the European Union, 234 reversing long-term decreases, and also in China and India, albeit more slowly compared to 235 recent trends. The increase in fossil emissions in 2025 relative to 2024 is projected to be 0.4% (-0.9% 236 to 2.0%) for China, 1.9% (-0.2% to 4.1%) for the United States, 1.4% (-0.3% to 3.1%) for India, and 237 0.4% (-2.1% to 2.8%) for the European Union. Projected emissions in Japan, provided this year for the first time, are for a decrease of -2.2% (-8.1% to 3.7%). Emissions are also projected to increase by 6.8% 238 239 for international aviation but to remain flat for international shipping, and to increase by 1.1% (-1.1% to 240 3.3%) for the rest of the world in aggregate. The global carbon intensity of energy has consistently decreased over the past decade (-0.7% yr⁻¹), indicating decarbonisation of the energy system in China (-241 1.4% yr⁻¹), the European Union (-1.5% yr⁻¹), and the USA (-1.3% yr⁻¹), but no decline in India and an 242 243 increase in the rest of the world in aggregate. These trends are not sufficient to offset the growth in 244 global energy demand, which is driven by growing GDP globally and a weakening decline in energy 245 per GDP, particularly in China and the US. Fossil CO₂ emissions decreased (p<0.05) in 35 countries with growing economies (p<0.05) during 246 247 the decade 2015-2024. The list of decarbonising countries nearly doubled since the previous decade 248 (2005-2014; 18 countries). The 35 decarbonising countries contribute 2.7 GtC yr⁻¹ (9.7 GtCO₂) fossil 249 fuel CO2 emissions over the last decade in aggregate, representing 27% of the world CO2 fossil

¹ All growth rates use a leap year adjustment that corrects for the extra day in 2024.





250	emissions.
251	Global net CO ₂ emissions from land use averaged 1.4 \pm 0.7 GtC yr ⁻¹ (5.0 \pm 2.6 GtCO ₂ yr ⁻¹) for the
252	2015-2024 period. Emissions from deforestation, the main driver of global gross emissions, remain
253	high at around 1.9 GtC yr ⁻¹ over the 2015-2024 period, highlighting the strong potential of halting
254	deforestation for emissions reductions. Sequestration of 1.3 GtC yr ⁻¹ through re-/afforestation and forest
255	regrowth in shifting cultivation cycles offsets two third of the deforestation emissions. In addition,
256	smaller net emissions are due to wood harvest & forest management, peat drainage and peat fire.
257	Regionally, the highest net emitters during 2015-2024 were Brazil, Indonesia, and the Democratic
258	Republic of the Congo, with these 3 countries contributing more than half of global land-use CO ₂
259	emissions. Net carbon dioxide removals (CDR) from re-/afforestation were highest in China, the USA,
260	and the EU27, with combined removals of 0.3 GtC/yr during 2015-2024.
261	Since the late-1990s, emissions from land use show a statistically significant decrease at a rate of
262	around 0.2 GtC per decade, with a larger drop within the most recent decade. Preliminary data
263	for 2025 suggest emissions decreased to around 1.1 GtC (4.1 GtCO ₂ yr ⁻¹), mainly attributable to
264	the end of the El Niño conditions.
265	Total anthropogenic emissions (fossil and land use, including the carbonation sink) were 11.6 GtC
266	yr ⁻¹ (42.4 GtCO ₂ yr ⁻¹) in 2024, with a slightly lower preliminary estimate of 11.5 GtC yr ⁻¹ (42.2
267	GtCO ₂ yr ⁻¹) for 2025. Total anthropogenic emissions have grown more slowly over the last decade
268	$(0.3\%~yr^{-1}~over~the~2015-2024~period)$ compared to the previous decade $(1.9\%~yr^{-1}~over~2005-2014)$.
269	The remaining carbon budget from the beginning of 2026 for a 50% likelihood to limit warming
270	to 1.5°C is nearly exhausted (50 GtC, 170 GtCO ₂ left, equivalent to around 4 years at the 2025
271	emissions levels), consistent with the warming of the planet attributed to human activities, which
272	reached 1.36°C in 2024. Each additional cumulative emission of about 180 GtCO ₂ will lead to
273	approximately 0.1°C of warming. The remaining carbon budgets to limit warming to 1.7°C and 2°C
274	above the 1850-1900 level have been reduced to 145 GtC (525 GtCO ₂ , 12 years) and 290 GtC (1055 GtCO ₂ , 25 years) respectively.
275	
276	The concentration of CO ₂ in the atmosphere is set to reach 425.7 ppm in 2025, 52% above pre-
277	industrial levels. The atmospheric CO_2 growth rate was 5.6 ± 0.02 GtC yr ⁻¹ (2.6 ppm) during the
278	decade 2015-2024 (50% of total CO ₂ emissions). 2024 had a record-high growth rate of 7.9 ± 0.02 GtC
279	yr ⁻¹ (3.7 ppm) mainly due to the 2023/2024 El Niño conditions. The preliminary 2025 growth rate
280	estimate is 4.9 GtC (2.3 ppm).
281	The ocean sink, the global net uptake of CO_2 by the ocean, has taken up 29% of the total
282	emissions in the past decade, after being re-evaluated upwards based on new evidence and
283	process understanding. The ocean sink has been stagnant since 2016, largely in response to
284	climate variability modulating the growing sink trend, but further affected by the ocean heatways





285 of 2023-2024 in the Northern Hemisphere. The ocean CO₂ sink was 3.2 ± 0.4 GtC yr⁻¹ during the decade 2015-2024, with a preliminary estimate of 3.2 GtC yr-1 for 2025, slightly below 2024 levels, due 286 to the end of the El Niño conditions in 2024 and associated reduced atmospheric CO2 growth rate. 287 288 The land sink, which is the global net uptake of CO₂ by the land excluding land use, has taken up 289 21% of the total emissions in the past decade, after being re-evaluated downwards based on improved process representation. The land sink has been relatively stagnant since 2000, largely in 290 291 response to climate variability and climate change offsetting the CO2 induced growth. The land 292 CO_2 sink was 2.4 ± 0.8 GtC yr⁻¹ during the 2015-2024 decade, but was reduced to 1.9 GtC ± 0.8 GtC yr⁻¹ ¹ in 2024. The preliminary estimate for the land sink in 2025 is an increase to 3.1 GtC, recovering 293 294 entirely from its strong drop during the 2023-2024 El Niño conditions. 295 The effects of climate change and climate variability act to reduce the land and ocean CO2 sinks 296 by 25% and 7.9% respectively, on average for the 2015-2024 period. The land sink is negatively 297 affected by warming with decreased tropical plant productivity and enhanced ecosystem respiration globally. The ocean sink is negatively affected by altered oceanic circulation and surface warming 298 299 which decreases CO2 solubility. 300 So far in 2025, global fire CO₂ emissions have been approximately 20% lower than the 2015-2024 301 average due to low fire activity in Africa and the tropics, reaching 1.2-1.4 GtC globally during 302 January-September. This contrasts with the above average fire emissions in 2023 (1.7-2.1 GtC yr⁻¹) 303 and 2024 (1.6-2.2 GtC yr⁻¹) due to extensive fires in Canada (2023) and Brazil and Bolivia (2024). 304 These fire emissions estimates should not be directly compared with the land-use emissions or the land 305 sink, because they represent a gross carbon flux to the atmosphere and do not account for post-fire 306 recovery. They also do not distinguish between natural, climate-driven, and land-use-related fires.





309

1 Introduction

310 The concentration of carbon dioxide (CO₂) in the atmosphere has increased from approximately 278 311 parts per million (ppm) in 1750 (Gulev et al., 2021), the beginning of the Industrial Era, to 422.8 ± 0.1 312 ppm in 2024 (Lan et al., 2025a; Figure 1). The atmospheric CO₂ increase above pre-industrial levels 313 was, initially, primarily caused by the release of carbon to the atmosphere from deforestation and other land-use change activities (Canadell et al., 2021). While emissions from fossil fuels started before the 314 315 Industrial Era, they became the dominant source of anthropogenic emissions to the atmosphere from 316 around 1950 and their relative share has continued to increase until present. Anthropogenic emissions 317 occur on top of an active natural carbon cycle that circulates carbon between the reservoirs of the 318 atmosphere, ocean, and terrestrial biosphere on time scales from sub-daily to millennial, while 319 exchanges with geologic reservoirs occur on longer timescales (Archer et al., 2009). 320 The global carbon budget (GCB) presented here refers to the mean, variations, and trends in the 321 perturbation of CO₂ in the environment, referenced to the beginning of the Industrial Era (defined here 322 as 1750). This paper describes the components of the global carbon cycle over the historical period with 323 a stronger focus on the recent period (since 1959, onset of robust atmospheric CO₂ measurements), the 324 last decade (2015-2024), the last year (2024) and the current year (2025). Finally, it provides 325 cumulative emissions from fossil fuels and land-use change since the year 1750, and since the year 1850 (the reference year for historical simulations in IPCC). 326 327 We quantify the input of CO₂ to the atmosphere by emissions from human activities, the growth rate of 328 atmospheric CO2 concentration, and the resulting changes in the storage of carbon in the land and ocean 329 reservoirs in response to increasing atmospheric CO2 levels, climate change and variability, and other 330 anthropogenic and natural changes (Figure 2). An understanding of this perturbation budget over time 331 and the underlying variability and trends of the natural carbon cycle is necessary to understand the 332 response of natural sinks to changes in climate, CO2 and land-use change drivers, and to quantify 333 emissions compatible with a given climate stabilisation target. 334 The components of the CO2 budget that are reported annually in this paper include separate and 335 independent estimates for the CO₂ emissions from (1) fossil fuel combustion and oxidation from all 336 energy and industrial processes; also including cement production and carbonation (E_{FOS}; GtC yr⁻¹) and 337 (2) the emissions resulting from deliberate human activities on land, including those leading to land-use 338 change (E_{LUC}; GtC yr⁻¹); and their partitioning among (3) the growth rate of atmospheric CO₂ 339 concentration (G_{ATM}; GtC yr⁻¹), and the uptake of CO₂ (the 'CO₂ sinks') in (4) the ocean (S_{OCEAN}; GtC 340 yr¹) and (5) on land (S_{LAND}; GtC yr¹). The CO₂ sinks as defined here conceptually include the response of the land (including inland waters and estuaries) and ocean (including coastal and marginal seas) to 341





- 342 elevated CO₂ and changes in climate and other environmental conditions, although in practice not all
- processes are fully accounted for (see Section 2.10). Note that the term sink means that the net transfer
- 344 of carbon is from the atmosphere to land or the ocean, but it does not imply any permanence of that sink
- 345 in the future.
- 346 Global emissions and their partitioning among the atmosphere, ocean and land are in balance in the real
- 347 world. Due to the combination of imperfect spatial and/or temporal data coverage, errors in each
- 348 estimate, and smaller terms not included in our budget estimate (discussed in Section 2.10), the
- 349 independent estimates (1) to (5) above do not necessarily add up to zero. We hence estimate a budget
- 350 imbalance (B_{IM}), which is a measure of the mismatch between the estimated emissions and the
- 351 estimated changes in the atmosphere, land and ocean, as follows:

352
$$B_{IM} = E_{FOS} + E_{LUC} - (G_{ATM} + S_{OCEAN} + S_{LAND})$$
 (1)

- 353 G_{ATM} is usually reported in ppm yr⁻¹, which we convert to units of carbon mass per year, GtC yr⁻¹, using
- 1 ppm = 2.124 GtC (Ballantyne et al., 2012; Table 1). Units of gigatonnes of CO₂ (or billion tonnes of
- 355 CO₂) used in policy are equal to 3.664 multiplied by the value in units of GtC.
- 356 We also assess a set of additional lines of evidence derived from global atmospheric inversion system
- results (Section 2.7), observed changes in oxygen concentration (Section 2.8) and Earth System Models
- 358 (ESMs) simulations (Section 2.9), all of these methods closing the global carbon balance (zero B_{IM}).
- We further quantify E_{FOS} and E_{LUC} by country, including both territorial and consumption-based
- 360 accounting for E_{FOS} (see Section 2), and discuss missing terms from sources other than the combustion
- 361 of fossil fuels (see Section 2.10). We also assess carbon dioxide removal (CDR) (see Sect. 2.2 and 2.3).
- Land-based CDR is significant, but already accounted for in ELUC in equation (1) (Sect 3.2.2). Other
- 363 CDR methods, not based on vegetation, are currently several orders of magnitude smaller than the other
- components of the budget (Sect. 3.3), hence these are not included in equation (1), or in the global
- 365 carbon budget tables or figures (with the exception of Figure 2 where CDR is shown primarily for
- 366 illustrative purpose).
- 367 The global CO₂ budget has been assessed by the Intergovernmental Panel on Climate Change (IPCC) in
- all assessment reports (Watson et al., 1990; Schimel et al., 1995; Prentice et al., 2001; Denman et al.,
- 369 2007; Ciais et al., 2013; Canadell et al., 2021), and by others (e.g. Ballantyne et al., 2012). The Global
- 370 Carbon Project (GCP, www.globalcarbonproject.org, last access: 23 October 2025) has coordinated this
- 371 cooperative community effort for the annual publication of global carbon budgets for the year 2005
- 372 (Raupach et al., 2007; including fossil emissions only), year 2006 (Canadell et al., 2007), year 2007
- 373 (GCP, 2008), year 2008 (Le Quéré et al., 2009), year 2009 (Friedlingstein et al., 2010), year 2010
- 374 (Peters et al., 2012a), year 2012 (Le Quéré et al., 2013; Peters et al., 2013), year 2013 (Le Quéré et al.,
- 375 2014), year 2014 (Le Quéré et al., 2015a; Friedlingstein et al., 2014), year 2015 (Jackson et al., 2016;





376 Le Quéré et al., 2015b), year 2016 (Le Quéré et al., 2016), year 2017 (Le Quéré et al., 2018a; Peters et al., 2017a), year 2018 (Le Quéré et al., 2018b; Jackson et al., 2018), year 2019 (Friedlingstein et al., 377 2019; Jackson et al., 2019; Peters et al., 2020), year 2020 (Friedlingstein et al., 2020; Le Quéré et al., 378 379 2021), year 2021 (Friedlingstein et al., 2022a; Jackson et al., 2022), year 2022 (Friedlingstein et al., 380 2022b), the year 2023 (Friedlingstein et al., 2023), and most recently the year 2024 (Friedlingstein et 381 al., 2025a). Each of these papers updated previous estimates with the latest available information for the 382 entire time series. 383 We adopt a range of ± 1 standard deviation (σ) to report the uncertainties in our global estimates, 384 representing a likelihood of 68% that the true value will be within the provided range if the errors have 385 a gaussian distribution, and no bias is assumed. This choice reflects the difficulty of characterising the 386 uncertainty in the CO2 fluxes between the atmosphere and the ocean and land reservoirs individually, 387 particularly on an annual basis, as well as the difficulty of updating the CO2 emissions from land-use 388 change. A likelihood of 68% provides an indication of our current capability to quantify each term and 389 its uncertainty given the available information. The uncertainties reported here combine statistical 390 analysis of the underlying data, assessments of uncertainties in the generation of the datasets, and expert judgement of the likelihood of results lying outside this range. The limitations of current information 391 392 are discussed in the paper and have been examined in detail elsewhere (Ballantyne et al., 2015; 393 Zscheischler et al., 2017). We also use a qualitative assessment of confidence level to characterise the 394 annual estimates from each term based on the type, amount, quality, and consistency of the different 395 lines of evidence as defined by the IPCC (Stocker et al., 2013). 396 This paper provides a detailed description of the datasets and methodology used to compute the global 397 carbon budget estimates for the industrial period, from 1750 to 2025, and in more detail for the recent 398 period since 1959. This paper is updated every year using the format of 'living data' to keep a record of 399 budget versions and the changes in new data, revision of data, and changes in methodology that lead to 400 changes in estimates of the carbon budget. All underlying data used to produce the budget and 401 additional materials associated with the release of each new version are available via the Global Carbon 402 Budget website (https://globalcarbonbudget.org/, last access: 23 October 2025), with emissions also 403 available through the Global Carbon Atlas (http://www.globalcarbonatlas.org, last access: 23 October 404 2025). With this approach, we aim to provide the highest transparency and traceability in the reporting of CO₂, the key driver of climate change. 405

2 Methods

- 407 Multiple organisations and research groups around the world generated the original measurements and
- data used to complete the global carbon budget. The effort presented here is thus mainly one of
- 409 synthesis, where results from individual groups are collated, analysed, and evaluated for consistency.
- 410 We facilitate access to original data with the understanding that primary datasets will be referenced in





- 411 future work (see Table 2 for how to cite the datasets, and Section on data availability). Descriptions of
- 412 the measurements, models, and methodologies follow below, with more detailed descriptions of each
- 413 component provided as Supplementary Information (Supplement Tables S1 to S5).
- 414 This is the 20th version of the global carbon budget and the 14th revised version in the format of a living
- 415 data update in Earth System Science Data. It builds on the latest published global carbon budget of
- 416 Friedlingstein et al. (2025a). The main changes this year are: the inclusion of (1) data to year 2024 and
- 417 a projection for the global carbon budget for year 2025; (2) transient carbon densities in the estimate of
- 418 E_{LUC}, (3) a correction on S_{LAND} to account for the historical changes in forest cover, (4) a correction on
- 419 Socean to account for the underestimation of the sink by GOBMs and for the ocean temperature
- 420 gradients in the fCO₂-products estimate, (5) an estimate of the atmospheric CO₂ growth rate derived
- 421 from satellite observations, and (6) decadal estimates of change in the dissolved inorganic carbon
- 422 inventory in the interior ocean. Other methodological differences are summarised in Table 3 and
- 423 previous changes since 2006 are provided in Table S9.

424 2.1 Fossil CO₂ emissions (E_{FOS})

425 **2.1.1** Historical period 1850-2024

- 426 The estimates of global and national fossil CO₂ emissions (E_{FOS}) include the oxidation of fossil fuels
- 427 through both combustion (e.g., transport, heating) and chemical oxidation (e.g. carbon anode
- 428 decomposition in aluminium refining) activities, and the decomposition of carbonates in industrial
- processes (e.g. the production of cement). We also include CO₂ uptake from the cement carbonation
- 430 process. Several emissions sources are not estimated or not fully covered: coverage of emissions from
- 431 lime production are not global, and decomposition of carbonates in glass and ceramic production are
- 432 included only for the "Annex 1" countries of the United Nations Framework Convention on Climate
- 433 Change (UNFCCC) for lack of activity data. These omissions are considered to be minor. Short-cycle
- 434 carbon emissions for example from combustion of biomass are not included here but are accounted
- for in the CO_2 emissions from land use (see Section 2.2).
- 436 Our estimates of fossil CO₂ emissions rely on data collection by many other parties. Our goal is to
- 437 produce the best estimate of this flux, and we therefore use a prioritisation framework to combine data
- 438 from different sources that have used different methods, while being careful to avoid double counting
- 439 and undercounting of emissions sources. The CDIAC-FF emissions dataset, derived largely from UN
- 440 energy data, forms the foundation, and we extend emissions to 2024 using energy growth rates reported
- by the Energy Institute (a dataset formerly produced by BP). We then proceed to replace estimates
- using data from what we consider to be superior sources, for example Annex 1 countries' official
- submissions to the UNFCCC. All data points are potentially subject to revision, not just the latest year.
- 444 For full details see Andrew and Peters (2025).





445	Other estimates of global fossil CO ₂ emissions exist, and these are compared by Andrew (2020a). The
446	most common reason for differences in estimates of global fossil CO2 emissions is a difference in which
447	emissions sources are included in the datasets. Datasets such as those published by the Energy Institute
448	the US Energy Information Administration, and the International Energy Agency's 'CO2 emissions
449	from fuel combustion' are all generally limited to emissions from combustion of fossil fuels. In
450	contrast, datasets such as PRIMAP-hist, CEDS, EDGAR, and GCP's dataset aim to include all sources
451	of fossil CO ₂ emissions. See Andrew (2020a) for detailed comparisons and discussion.
452	Cement products absorb CO ₂ from the atmosphere over their lifetimes, a process known as 'cement
453	carbonation'. We estimate this CO2 sink, from 1931 onwards, as the average of two studies in the
454	literature (Cao et al., 2020; Guo et al., 2021). Both studies use the same model, developed by Xi et al.
455	(2016), with different parameterisations and input data, with the estimate of Guo and colleagues being
456	revision of Xi et al. (2016). The trends of the two studies are very similar. Since carbonation is a
457	function of both current and previous cement production, we extend these estimates to 2024 by using
458	the growth rate derived from the smoothed cement emissions (10-year smoothing) fitted to the
459	carbonation data. In the present budget, we always include the cement carbonation carbon sink in the
460	fossil CO ₂ emission component (E _{FOS}) unless explicitly stated otherwise.
461	We use the Kaya Identity for a simple decomposition of CO ₂ emissions into the key drivers (Raupach of CO ₂)
462	al., 2007). While there are variants (Peters et al., 2017b), we focus here on a decomposition of CO2
463	emissions into population, GDP per person, energy use per GDP, and CO2 emissions per energy.
464	Multiplying these individual components together returns the CO ₂ emissions. Using the decomposition
465	it is possible to attribute the change in CO2 emissions to the change in each of the drivers. This method
466	gives a first-order understanding of what causes CO2 emissions to change each year.
467	2.1.2 2025 projection
468	We provide a projection of global fossil CO ₂ emissions in 2025 by combining separate projections for
469	China, USA, EU, India, Japan, and for all other countries combined. The methods are different for each
470	of these. For China we combine monthly fossil fuel production data from the National Bureau of
471	Statistics and trade data from the Customs Administration, giving us partial data for the growth rates to
472	date of natural gas, petroleum, and cement, and of the apparent consumption itself for raw coal. We
473	then use a regression model to project full-year emissions based on historical observations. For the
474	USA our projection is taken directly from the Energy Information Administration's (EIA) Short-Term
475	Energy Outlook (EIA, 2025), combined with the year-to-date growth rate of cement clinker production
476	For the EU we use monthly energy data from Eurostat to derive estimates of monthly CO ₂ emissions
477	(Andrew, 2021), with (i) coal emissions extended using a statistical relationship with reported
478	electricity generation from coal and other factors, (ii) natural gas emissions extended using Holt-





480	and the EIA's estimates of oil consumption for Europe, which include a forecast. EU cement emissions
481	are based on available year-to-date data from three of the largest producers, Germany, Poland, and
482	Spain. India's projected emissions are derived from monthly estimates through August/September using
483	the methods of Andrew (2020b) and extrapolated through December assuming seasonal patterns from
484	before 2019. Japan's emissions are also projected based on monthly estimates through July and normal
485	seasonal patterns. Emissions from international transportation (bunkers) are estimated separately for
486	aviation and shipping. Changes in aviation emissions are derived primarily from OECD monthly
487	estimates, extrapolated using the growth rates of global flight miles from Airportia, and then the final
488	months are projected assuming normal patterns from previous years. Shipping emissions are assumed to
489	be unchanged in 2025, based on available sub-annual evidence from multiple sources. Emissions for the
490	rest of the world are derived for coal and cement using projected growth in economic production from
491	the IMF (2025) combined with extrapolated changes in emissions intensity of economic production; for
492	oil using a global constraint from EIA; and for natural gas using a global constraint from IEA. More
493	details on the E_{FOS} methodology and its 2025 projection can be found in Supplement S.1.
494	We compare our 2025 projection with the Carbon Monitor (2025). Carbon Monitor is a dataset of daily
495	emissions constructed using hourly to daily proxy data (e.g., electricity consumption, travel patterns,
496	etc) instead of energy use data (Liu et al., 2020a; Liu et al., 2020b). Emissions estimates from January
497	to August are combined to a new projection for September-December to give a full-year 2025 estimate.
498	The projections are estimated by leveraging seasonal patterns from 2019-2024 daily CO ₂ emission data
499	from Carbon Monitor. A regression model is applied separately for individual countries to obtain their
500	respective forecast. First, the seasonality component for each month is assessed based on daily average
501	emissions from 2019 to 2023, excluding 2020 due to the COVID-19 pandemic. Then, a linear
502	regression model is constructed using the calculated seasonal components and the daily average
503	emissions for the months from January to August 2025. The resulting model is used to project carbon
504	emissions for September-December 2025. The uncertainty range is calculated by using historical
505	monthly variance of seasonal components (See Supplement S.1.5).

2.2 CO₂ emissions from land-use, land-use change and forestry (E_{LUC})

2.2.1 Historical period 1850-2024

506

507

The net CO₂ flux from land-use, land-use change and forestry (E_{LUC}, called land-use change emissions in the rest of the text) includes CO₂ fluxes from deforestation, afforestation, logging and forest degradation (including harvest activity), shifting cultivation (cycle of cutting forest for agriculture, then abandoning), regrowth of forests (following wood harvest or agriculture abandonment), peat burning, and peat drainage.





313	Opdated estimates from three bookkeeping models are used to quantify gross emissions, gross removals
514	and the resulting net E _{LUC} : BLUE (Hansis et al., 2015), LUCE (Qin et al. 2024), and OSCAR (Gasser et
515	al., 2020). Different to previous GCBs, all three bookkeeping models use transient carbon densities, i.e.
516	they consider the effects of environmental changes, such as atmospheric CO2 increase, on vegetation
517	and soil carbon densities, to estimate E_{LUC} (Gasser et al., 2020; Dorgeist et al., 2024). The GCB
518	assessments have for a long time also (and initially exclusively) used estimates from the bookkeeping
519	model H&C2023 (Houghton and Castanho, 2023), its predecessor H&N2017 (Houghton and Nassikas,
520	2017), and earlier versions. However, H&C2023 does not consider transient carbon densities and only
521	provides data up to 2020, which implies the need to extrapolate its data to the time after 2020. As the
522	model does thus not incorporate the most recent developments in bookkeeping modeling, it is not used
523	anymore in GCB2025.
524	Emissions from peat burning and peat drainage are added from external datasets (see Supplement
525	S.2.2): peat fire emissions from the Global Fire Emission Database (GFED4s; van der Werf et al.,
526	2017) and peat drainage emissions averaged from estimates of the Food Agriculture Organization
527	(Conchedda and Tubiello, 2020; FAO, 2025a) and from simulations with the DGVM ORCHIDEE-
528	PEAT (Qiu et al., 2021) and the DGVM LPX-Bern (Lienert and Joos, 2018; Müller and Joos, 2021).
529	Uncertainty estimates were derived from the Dynamic Global Vegetation Models (DGVMs) ensemble
530	for the time period prior to 1960, and using for the recent decades an uncertainty range of ± 0.7 GtC yr-1
531	which is a semi-quantitative measure for annual and decadal emissions and reflects our best value
532	judgement that there is at least 68% chance ($\pm 1\sigma$) that the true land-use change emission lies within the
533	given range, for the range of processes considered here.
534	The GCB E_{LUC} estimates follow the CO_2 flux definition of global carbon cycle models and differ from
535	IPCC definitions adopted in National GHG Inventories (NGHGI) for reporting under the UNFCCC.
536	The latter typically include terrestrial fluxes occurring on all land that countries define as managed,
537	following the IPCC managed land proxy approach (Grassi et al., 2018). This partly includes fluxes due
538	to environmental change (e.g. atmospheric CO_2 increase), which are part of S_{LAND} in our definition. As
539	a result, global emission estimates are smaller for NGHGI than for the global carbon budget definition
540	(Grassi et al., 2023). The same is the case for the FAO estimates of carbon fluxes on forest land, which
541	include both anthropogenic and natural fluxes on managed land (Tubiello et al., 2025; FAO, 2025b).
542	Using the NGHGI data collected and processed in the LULUCF data hub V3.1 (Melo et al. 2025), we
543	translate the GCB and NGHGI definitions to each other, to provide a comparison of the anthropogenic
544	carbon budget as reported in GCB to the official country reporting to the UNFCCC convention. We
545	further compare these estimates with the net atmosphere-to-land flux from atmospheric inversion
546	systems (see Section 2.7), averaged over managed land only.





547	ELUC contains a range of fluxes that are related to Carbon Dioxide Removal (CDR). CDR is defined as
548	the set of anthropogenic activities that remove CO2 from the atmosphere, in addition to the Earth's
549	natural processes (such as carbon uptake in response to atmospheric CO2 increase), and store it in
550	durable form, such as in forest biomass, soils, long-lived products, oceans or geological reservoirs.
551	Here, we quantify vegetation-based CDR that is implicitly or explicitly captured by land-use fluxes
552	(CDR not based on vegetation is discussed in Section 2.3). We quantify CDR through re/afforestation
553	from the three bookkeeping estimates by separating permanent increases in forest cover, which counts
554	as CDR, from forest regrowth in shifting cultivation cycles (not part of CDR; see Supplement S.2.2). It
555	should be noted that the permanence of the storage under climate risks such as fire is increasingly
556	questioned. Other CDR activities related to land use but not fully accounted for in our E_{LUC} estimate
557	include the transfer of carbon to harvested wood products (HWP), bioenergy with carbon capture and
558	storage (BECCS), and biochar production (Babiker et al., 2022; Smith et al., 2024). The different
559	bookkeeping models all represent HWP but with varying details concerning product usage and their
560	lifetimes. BECCS and biochar are currently only represented in bookkeeping and DGVM models with
561	regard to the CO_2 removal through photosynthesis, without accounting for the durable storage. HWP,
562	BECCS, and biochar are typically counted as CDR once the transfer to the durable storage site occurs
563	and not when the CO_2 is removed from the atmosphere, which complicates a direct comparison to the
564	GCB approach to quantify annual fluxes to and from the atmosphere. We provide estimates for CDR
565	through HWP, BECCS, and biochar based on independent studies in Section 3.2.2. HWP and BECCS
566	estimates reflect updated 2024 data of the State of CDR report (Smith et al., 2024), while biochar
567	estimates correspond to 2023 due to unavailability of newer data. We do not add them to our E_{LUC}
568	estimate to avoid potential double-counting that arises from the partial consideration of HWP, BECCS,
569	and biochar in the bookkeeping and DGVM models and to avoid inconsistencies from the temporal
570	discrepancy between transfer to storage and removal from the atmosphere. More details on the $E_{\text{\tiny LUC}}$
571	methodology can be found in Supplement S.2.

2.2.2 2025 Projection

- 573 We project the 2025 land-use emissions for BLUE, OSCAR, and LUCE based on their E_{LUC} estimates
- 574 for 2023 and adding the anomalies in carbon emissions from peat fires in equatorial Asia and tropical
- 575 deforestation and degradation fires (2025 emissions relative to 2023 emissions) from GFED4s (van der
- Werf et al., 2017) estimated using active fire data (MCD14ML; Giglio et al., 2016). 2023 is used as
- base year since the E_{LUC} estimate for the year 2024 is informed by extrapolated land-use data
- 578 (Supplement S.2.1). Peat drainage is assumed to be unaltered as it has low interannual variability.

579 2.3 Carbon Dioxide Removal (CDR) not based on vegetation

- 580 Some CDR involves CO₂ fluxes via land use, which is included in our estimate of E_{LUC}
- (re/afforestation) or provided separately in Section 3.2.2 (biochar, HWP, and BECCS). Other CDR

595

616





582	occurs through CO2 fluxes directly from the air to the geosphere, which is reported in Section 3.3. The
583	majority of this derives from bio-oil storage in geological reservoirs, enhanced weathering through the
584	application of crushed rock to soils, and the production of solid mineral products with CO2 captured
585	from the atmosphere, with smaller contributions from Direct Air Carbon Capture and Storage
586	(DACCS), sinking of terrestrial (e.g., straw) or marine (e.g., macroalgae) biomass into the deep ocean
587	through human intervention, and others like intentional ocean or river alkalinity enhancement. For these
588	methods, we use updated 2024 data (Smith et al., 2024), which compiles and harmonises reported CDR
589	from a combination of existing databases, surveys, and novel research. Currently, there are no
590	internationally agreed methods for reporting these types of CDR, implying that estimates are based on
591	self-disclosure by projects following their own protocols or protocols produced by third party registries.
592	As such, the fractional uncertainty on these numbers should be viewed as substantial, and numbers are
593	liable to change in future years as protocols are harmonised and improved.

2.4 Growth rate in atmospheric CO₂ concentration (G_{ATM})

2.4.1 Historical period 1850-2024

396	The rate of growth of the atmospheric CO ₂ concentration is provided for years 1959-2024 by the US
597	National Oceanic and Atmospheric Administration Global Monitoring Laboratory (NOAA/GML; Lan
598	et al., 2025a), which includes recent revisions to the calibration scale of atmospheric CO2
599	measurements (WMO-CO2-X2019; Hall et al., 2021). For the 1959-1979 period, the global growth rate
600	is based on measurements of atmospheric CO_2 concentration averaged from the Mauna Loa and South
601	Pole stations, as observed by the CO ₂ Program at Scripps Institution of Oceanography (SIO, Keeling et
602	al., 1976). For the 1980-2024 time period, the global growth rate is based on the average of multiple
603	stations selected from the marine boundary layer sites with well-mixed background air (Lan et al.,
604	2024), after fitting a smooth curve through the data for each station as a function of time, and averaging
605	by latitude band (Masarie and Tans, 1995). The annual growth rate is estimated by Lan et al. (2025a)
606	from atmospheric CO2 concentration by taking the average of the most recent December-January
607	months corrected for the average seasonal cycle and subtracting this same average one year earlier. To
608	obtain G_{ATM} , the observation-based growth rate in units of ppm $yr^{\text{-}1}$ is converted to units of GtC $yr^{\text{-}1}$ by
609	multiplying by a factor of 2.124 GtC per ppm, assuming instantaneous mixing of CO ₂ throughout the
610	atmosphere (Ballantyne et al., 2012; Table 1). There is high confidence in the observations because
611	they are based on direct measurements from stations distributed around the world (Lan et al., 2024)
612	with all CO_2 measurements consistently measured against the same CO_2 standard scale (WMO X2019)
613	defined by a suite of gas standards (Hall et al., 2021). However, the conversion to estimates of G_{ATM} in
614	GtC/yr incurs large uncertainty on annual time scale as discussed next.
615	The uncertainty around G _{ATM} is due to three main factors. First, the network composition of the marine

boundary layer sites with some sites coming or going, gaps in the time series at each site, etc. This





617 uncertainty was estimated with a bootstrap method by constructing 100 "alternative" networks (Steele et al., 1992; Masarie and Tans, 1995; Lan et al., 2025a). Second, the analytical uncertainty that 618 describes the short- and long-term uncertainties associated with the CO2 analyzers. A Monte Carlo 619 620 method was used to estimate the total analytical uncertainty by randomly selecting errors to add to each 621 observation from a normal distribution of combined short- and long-term uncertainties. Prior to the 622 1980s when analyzers were less precise and CO2 measurement scale was slightly less well defined, 623 larger analytical errors were assigned to account for these factors. However, the network uncertainty 624 remains the larger term of uncertainty. The first and second uncertainties are reported as 1-sigma 625 standard deviations (i.e., 68% confidence interval), and summed in quadrature to determine the global surface growth rate uncertainty, which averaged to 0.085 ppm (Lan et al., 2024b). Third, the uncertainty 626 627 associated with using the average CO2 concentration from a surface network to approximate the true 628 atmospheric average CO₂ concentration (mass-weighted, in 3 dimensions) as needed to assess the total 629 atmospheric CO₂ burden. In reality, CO₂ variations measured at the stations will not exactly track 630 changes in total atmospheric burden, with offsets in magnitude and phasing due to vertical and 631 horizontal mixing (Pandey et al., 2025). This effect must be very small on decadal and longer time scales, when the atmosphere can be considered well mixed. The long-term CO2 increase in the 632 633 stratosphere lags the increase (meaning lower concentrations) that we observe in the marine boundary 634 layer, while the continental boundary layer (where most of the emissions take place) leads the marine 635 boundary layer with higher concentrations. These effects nearly cancel each other on decadal time 636 scales, when the growth rate is nearly the same everywhere (Ballantyne et al., 2012). We therefore 637 maintain an uncertainty around the annual growth rate based on the multiple stations dataset ranges 638 between 0.11 and 0.72 GtC yr⁻¹, with a mean of 0.61 GtC yr⁻¹ for 1959-1979 and 0.17 GtC yr⁻¹ for 639 1980-2024, when more measurement sites were available (Lan et al., 2025a). We estimate the 640 uncertainty of the decadal averaged growth rate after 1980 at 0.02 GtC yr⁻¹ based on the annual growth 641 rate uncertainty but stretched over a 10-year interval. For years prior to 1980, we estimate the decadal 642 averaged uncertainty to be 0.07 GtC yr⁻¹ based on a factor proportional to the annual uncertainty prior and after 1980 (0.02 * [0.61/0.17] GtC yr⁻¹). 643 644 To estimate the total carbon accumulated in the atmosphere since 1750 or 1850, we use an atmospheric 645 CO_2 concentration of 278.3 \pm 3 ppm or 285.1 \pm 3 ppm, respectively (Gulev et al., 2021). For the 646 construction of the historical budget shown in Figure 3, we use the fitted estimates of CO2 concentration from Joos and Spahni (2008) to estimate the annual atmospheric growth rate (see 647 Supplement S.7). The uncertainty of ± 3 ppm (converted to $\pm 1\sigma$) is taken directly from the IPCC's AR5 648 649 assessment (Ciais et al., 2013). Typical uncertainties in the growth rate in atmospheric CO2 650 concentration from ice core data are equivalent to ± 0.1 -0.15 GtC yr⁻¹ as evaluated from the Law Dome 651 data (Etheridge et al., 1996) for individual 20-year intervals over the period from 1850 to 1960 (Bruno 652 and Joos, 1997).





2.4.2 Satellite-based (2015-present)

- 654 Further opportunities to estimate global CO₂ growth rates are offered by space-based platforms such as
- 655 GOSAT (since 2010) and OCO-2 (since 2015). Their recorded short-wave infrared spectra allow
- 656 retrieval of column CO₂ abundances (XCO₂) over cloud-free scenes over land and ocean with footprints
- 657 of 80 (GOSAT) and 3 (OCO-2) km² respectively. The columns are not full integrals; the sensitivity to
- 658 surface and lower-tropospheric CO₂ mole fractions is much higher than to upper tropospheric and
- 659 stratospheric CO₂. However, for the purpose of calculating atmospheric growth rates, the sensitivity is
- 660 not limiting, as the pressure-weighted sensitivity is still above 0.5 in the stratosphere (Pandey et al.
- 661 2024) and priors used in OCO-2 account for the slow stratospheric-tropospheric exchanges using the
- age of air (Laughner et al. 2023). Here, we use OCO-2 based whole atmosphere growth rates using the
- 663 Growth Rate from Satellite Observations (GRESO) approach (Pandey et al., 2024). We specifically
- 664 note that their retrievals are evaluated against surface-based remote sensing (Total Column Carbon
- 665 Observing Network) data, which in turn are tied to atmospheric observations (from aircraft and using
- 666 aircore) (Wunch et al., 2017). Furthermore, OCO-2 retrievals use a priori CO₂ mole fraction profiles
- 667 tied to NOAA GML in-situ flask records at Mauna Loa (MLO) and American Samoa (SMO)
- 668 measurement stations (Laughner et al., 2023). For details on evaluation, bias-correction, and
- spatiotemporal coverage of OCO-2 we refer to O'Dell et al (2018).
- Relative to surface observations, the GRESO product typically reflects tropical growth rate anomalies
- 671 earlier, and sees whole atmosphere carbon stock changes with a lower latency. The GRESO growth
- 672 rates presented here use both land and ocean observations of OCO-2 providing global sampling of the
- atmosphere. We used GRESO post 2015 to present an alternative quantification of the atmospheric
- 674 carbon stock changes in G_{ATM}, using the reported 1-sigma uncertainty of 0.08 ppm/yr. The mean
- differences between GRESO and surface-data derived G_{ATM} is 0.05 ± 0.26 ppm/yr over the 2015-2024
- 676 (n=10 years) period.

677 **2.4.3 2025 projection**

- We provide an assessment of G_{ATM} for 2025 as the average of two methods. First,the GCB regression
- 679 method models monthly global-average atmospheric CO₂ concentrations and derives the increment and
- annual average from these. The model uses lagged observations of concentration (Lan et al., 2025a):
- 681 both a 12-month lag, and the lowest lag that will allow model prediction to produce an estimate for the
- 682 following January, recalling that the G_{ATM} increment is derived from December/January pairs. The
- 683 largest driver of interannual changes is the ENSO signal (Betts et al., 2016), so the monthly ENSO 3.4
- 684 index (Huang et al., 2023) is included in the model. Given the natural lag between sea-surface
- temperatures and effects on the biosphere, and in turn effects on globally mixed atmospheric CO₂
- 686 concentration, a lagged ENSO index is used, and we use both a 5-month and a 6-month lag. The
- 687 combination of the two lagged ENSO values helps reduce possible effects of noise in a single month.





- To help characterise the seasonal variation, we add month as a categorical variable. Finally, we flag the
- period affected by the Pinatubo eruption (August 1991 November 1993) as a categorical variable.
- 690 The second method uses the multi-model mean and uncertainty of the 2025 GATM estimated by the
- 691 ESMs prediction system (see Section 2.9). We then take the average of the GCB regression and ESMs
- 692 G_{ATM} estimates, with their respective uncertainty combined quadratically.
- 693 Similarly, the projection of the 2025 global average CO₂ concentration (in ppm), is calculated as the
- 694 average of the estimates from the two methods. For the GCB regression method, it is the annual average
- 695 of global concentration over the 12 months of 2025; for the ESMs, it is the observed global average
- 696 CO₂ concentration for 2024 plus the annual increase in 2025 of the global average CO₂ concentration,
- 697 which is an average of NOAA/GML measurements from January to June (Lan et al., 2025) and
- 698 predictions of the ESMs multi-model mean from July to December (see Section 2.9).

699 2.5 Ocean CO2 sink

700 **2.5.1** Historical period 1850-2024

- 701 The reported estimate of the global ocean anthropogenic CO₂ sink S_{OCEAN} is derived as the average of
- 702 two estimates. The first estimate is derived as the mean over an ensemble of ten global ocean
- 503 biogeochemistry models (GOBMs, Table 4 and Table S2). The second estimate is obtained as the mean
- 704 over an ensemble of nine surface ocean fCO₂-observation-based data-products (Table 4 and Table S3).
- 705 The GOBMs simulate both the natural and anthropogenic CO₂ cycles in the ocean. They constrain the
- anthropogenic air-sea CO₂ flux (the dominant component of S_{OCEAN}) by the transport of carbon into the
- ocean interior, which is also the controlling factor of present-day ocean carbon uptake in the real world.
- They cover the full globe and all seasons and were evaluated against surface ocean carbon observations,
- suggesting they are suitable to estimate the annual ocean carbon sink (Hauck et al., 2020). We derive
- 710 Socean from GOBMs by using a simulation (sim A) with historical forcing of climate and atmospheric
- 711 CO₂ from GCB (Section 2.4), accounting for model biases and drift from a control simulation (sim B)
- 712 with constant atmospheric CO₂ and normal year climate forcing. A third simulation (sim C) with
- 713 historical atmospheric CO₂ increase and normal year climate forcing is used to attribute the ocean sink
- 714 to CO₂ (sim C minus sim B) and climate (sim A minus sim C) effects. A fourth simulation (sim D;
- 715 historical climate forcing and constant atmospheric CO₂) is used to compare the change in
- 716 anthropogenic carbon inventory in the interior ocean (sim A minus sim D) to the observation-based
- 717 estimates of Gruber et al. (2019) and Müller et al. (2023) with the same flux components (steady state
- and non-steady state anthropogenic carbon flux).
- As there is accumulating evidence for a 10-20% underestimation of S_{OCEAN} by the GOBMs based on
- ocean interior data (section 3.6.5), atmospheric oxygen (section 3.6.2), atmospheric inversions (section





- 3.8) and supported by eddy-covariance measurements (Dong et al., 2024), we scale up the global
- 722 GOBM multi-model mean estimates by 10% for estimating S_{OCEAN} (Friedlingstein et al., 2025b) (see
- Supplement S3.3). Analysis of Earth System Models and GOBMs indicate that an underestimation by
- about 10% may be due to biases in ocean carbon transport and mixing from the surface mixed layer to
- 725 the ocean interior (Goris et al., 2018, Terhaar et al., 2021, Bourgeois et al., 2022, Terhaar et al., 2022),
- 726 biases in the chemical buffer capacity (Revelle factor) of the ocean (Vaittinada Ayar et al., 2022;
- 727 Terhaar et al., 2022) and partly due to a late starting date of the simulations (mirrored in atmospheric
- 728 CO₂ chosen for the pre-industrial control simulation, Table S2, Bronselaer et al., 2017, Terhaar et al.,
- 729 2022; 2024). GOBMs are evaluated against key metrics and their capability to reproduce various
- 730 statistical measures of physical and biogeochemical fields using the International Ocean Model
- 731 Benchmarking (IOMB) Scheme (Fu et al., 2022, Text S3.3).
- 732 The fCO₂-products are tightly linked to observations of fCO₂ (fugacity of CO₂, which equals pCO₂
- 733 corrected for the non-ideal behaviour of the gas; Pfeil et al., 2013), which carry imprints of temporal
- 734 and spatial variability, but are also sensitive to uncertainties in gas-exchange parameterizations and
- data-sparsity (Fay et al., 2021, Gloege et al., 2021, Hauck et al., 2023a). Their asset is the assessment of
- the mean spatial pattern of variability and its seasonality (Hauck et al., 2020, Gloege et al. 2021, Hauck
- et al., 2023a). To benchmark biases and trends derived from the fCO₂-products, we update a model
- 738 subsampling exercise following Hauck et al. (2023a, see section S3) and use independent measurements
- al., 2016) and calculated fCO₂ from the Global Ocean Data Analysis Project GLODAP (Lauvset et al.,
- 741 2024). New in GCB2025, we now also include the UExP-FNN-U product in the ensemble mean, which
- vas previously shown but not included. We include it since new evidence emerged from field and
- 743 modelling studies, recommending the adjustment of the fCO_2 to the surface skin layer where the gas
- exchange takes place (Dong et al., 2024, Ford et al., 2024, Bellenger et al., 2022). Furthermore, a
- second fCO₂-product submitted temperature adjusted fCO₂ (JMA-MLR) this year, so we now include
- 746 these corrected estimates in the ensemble mean. Additionally, following Friedlingstein et al (2025b),
- 747 we now also add 0.18 PgC yr⁻¹ (multiplied by 7/9 as two products already include a temperature
- 748 correction) to the multi fCO2-product average in the calculation of Socian to account for the warm
- 749 layer and cool skin effect (See Supplement S3.1). This correction is based on a recent field study (Ford
- 750 et al., 2024) and broadly consistent in magnitude with a GOBM study (Bellenger et al 2022) .
- 751 The global fCO₂-based flux estimates were adjusted to remove the pre-industrial natural ocean source of
- 752 CO_2 to the atmosphere of 0.65 ± 0.3 GtC yr⁻¹, arising from the transfer of carbon from land to ocean via
- 753 rivers (Regnier et al., 2022), to satisfy our definition of S_{OCEAN} (Hauck et al., 2020). This CO₂
- 754 outgassing adjustment was distributed over the latitudinal bands using the regional distribution of
- 755 Lacroix et al. (2020; North: 0.14 GtC yr⁻¹, Tropics: 0.42 GtC yr⁻¹, South: 0.09 GtC yr⁻¹).
- 756 Acknowledging that this distribution is based on only one model, the advantage is that a gridded field is





757 available, and the adjustment can be calculated for the three latitudinal bands and the RECCAP regions 758 (REgional Carbon Cycle Assessment and Processes (RECCAP2; Ciais et al., 2020, Poulter et al., 2022, DeVries et al., 2023). This dataset suggests that more of the river-induced outgassing is located in the 759 760 tropics than in the Southern Ocean and is thus opposed to the previously used dataset of Aumont et al. 761 (2001). Accordingly, the regional distribution is associated with an additional uncertainty in addition to 762 the large uncertainty around the global estimate (Crisp et al., 2022; Gruber et al., 2023). Anthropogenic perturbations of river carbon and nutrient transport to the ocean are not represented in the process 763 764 models used to quantify Socean, but an a-posteriori correction is applied to the global Socean estimate (see Section 2.10 and Supplement S.8.3). We calculate SOCEAN as the average of the GOBM ensemble 765 mean and the fCO₂-product ensemble mean from 1990 onwards. For the 1959-1989 period, it is 766 767 calculated as the GOBM ensemble mean plus half of the offset between GOBMs and fCO2-products 768 ensemble means over 1990-2001. In addition, two diagnostic ocean models are used to estimate Social over the industrial era (1781-1958, Khatiwala et al. (2013) and DeVries (2014)). 769 770 Socean is evaluated against the change in the total dissolved inorganic carbon inventory in the interior 771 ocean from the observation-based estimates of Keppler et al. (2023) and Ehmen et al. (2025, in review) 772 with the same flux components. 773 We assign an uncertainty of \pm 0.4 GtC yr⁻¹ to the ocean sink based on a combination of random 774 (ensemble standard deviation) and systematic uncertainties (GOBMs bias in anthropogenic carbon 775 accumulation, previously reported uncertainties in fCO₂-products; see Supplement S.3.4). While this 776 approach is consistent within the GCB, an independent uncertainty assessment of the fCO2-products alone suggests a somewhat larger uncertainty of up to 0.7 GtC yr⁻¹ (Ford et al. 2024). We assess a 777 778 medium confidence level to the annual ocean CO2 sink and its uncertainty because it is based on 779 multiple lines of evidence, it is consistent with ocean interior carbon estimates (see Section 3.6.5) and 780 the interannual variability in the GOBMs and data-based estimates is largely consistent and can be 781 explained by climate variability. We refrain from assigning a high confidence because of the deviation 782 between the GOBM and fCO2-product trends between around 2002 and 2020 and the higher SOCEAN 783 estimate from O₂:N₂ (section 2.8). More details on the S_{OCEAN} methodology can be found in Supplement 784 S.3. 785

2.5.2 2025 Projection

The Social forecast for the year 2025 is based on (a) the historical (Lan et al., 2025a) and our 2025 786 787 estimate of atmospheric CO₂ concentration, (b) the historical and our 2025 estimate of global fossil 788 emissions, and (c) the boreal spring (March, April, May) Oceanic Niño Index (ONI) (NCEP, 2025). 789 Using a non-linear regression approach, i.e., a feed-forward neural network, atmospheric CO₂, ONI, and 790 the fossil emissions are used as training data to best match Social from 1959 through 2024 from this 791 year's carbon budget. Using this relationship, the 2025 Socean can then be estimated from the projected

805





overfitting, the neural network training was done using a Monte Carlo approach, with a variable number of artificial neurons (varying between 2-5) and 20% of the randomly selected training data were withheld for independent internal testing.

Based on the best output performance (tested using the 20% withheld input data), the best performing number of neurons was selected. In a second step, we trained the network 10 times using the best number of neurons identified in step 1 and different sets of randomly selected training data. The mean of the 10 trainings is considered our best forecast, whereas the standard deviation of the 10 ensembles

2025 input data using the non-linear relationship established during the network training. To avoid

- provides a first order estimate of the forecast uncertainty. This uncertainty is then combined with the Social uncertainty (0.4 GtC yr⁻¹) to estimate the overall uncertainty of the 2025 projection. As an
- additional line of evidence, we also assess the 2025 atmosphere-ocean carbon flux from the ESM
- prediction system (see Section 2.9).

804 2.6 Land CO₂ sink

2.6.1 Historical Period 1850-2024

- 806 The terrestrial land sink (SLAND) is thought to be due to the combined effects of rising atmospheric CO₂,
- 807 increasing N inputs, and climate change, on plant growth and terrestrial carbon storage. SLAND does not
- 808 include land sinks directly resulting from land-use and land-use change (e.g., regrowth of vegetation) as
- 809 these are part of the land-use change emissions (E_{LUC}), although system boundaries make it difficult to
- attribute exactly CO_2 fluxes on land between S_{LAND} and E_{LUC} (Erb et al., 2013).
- 811 S_{LAND} is estimated from the multi-model mean of 22 DGVMs (Table 4 and Table S1). DGVMs
- 812 simulations include all climate variability and CO₂ effects over land. In addition to the carbon cycle
- 813 represented in all DGVMs, 15 models also account for the nitrogen cycle and hence can include the
- 814 effect of N inputs on S_{LAND}. The DGVMs estimates of S_{LAND} do not explicitly include the export of
- 815 carbon to aquatic systems or its historical perturbation, which is discussed in Supplement S.8.3.
- DGVMs need to meet several criteria to be included in this assessment (see Supplement S.4.2). In
- 817 addition, we use the International Land Model Benchmarking system (ILAMB; Collier et al., 2018) for
- the DGVMs evaluation (see Supplement S.4.2), with an additional comparison of DGVMs with a data-
- 819 informed, Bayesian model-data fusion framework (CARDAMOM) (Bloom and Williams, 2015; Bloom
- et al., 2016). The uncertainty on S_{LAND} is taken from the DGVMs standard deviation.
- 821 New to GCB2025 is a correction applied to the S_{LAND} to account for its overestimation resulting from
- 822 the assumption of pre-industrial land-use in the DGVM simulations, when in reality a large portion of
- 823 the land surface has been converted to pasture and cropland, with a lower sink capacity. This bias is
- termed the Replaced Sinks and Sources (RSS) (Gitz and Ciais, 2003; Sitch et al., 2005, Pongratz et al.,





825 2009; Gasser et al., 2021; Obermeier et al. 2021; Dorgeist et al., 2024). The correction applied on SLAND 826 utilises results from a subset of DGVMs that were able to supply Net Biome Productivity estimates at a Plant Functional Type basis combined with time-varying PFT area fractions from the simulation with 827 828 land use and land use change considered (O'Sullivan et al., 2025; Friedlingstein et al. 2025b), see S.4.1 for details on methodology. SLAND is reduced by 19% globally when accounting for the RSS. More 829 details on the S_{LAND} methodology can be found in Supplement S.4. 830 831 2.6.2 2025 Projection 832 In previous versions of the GCB, the land sink projection was similar to the ocean sink forecast, based 833 on a non-linear regression approach with a feed-forward neural network. This approach, however, 834 resulted in a large uncertainty and underestimated the land sink variability in the past. This year, we 835 update the projection and simply calculate the land sink for 2025 as the residual of the projection of the 836 other components of the carbon cycle (SLAND=EFOS+ELUC-GATM-SOCEAN). 837 2.7 Atmospheric inversion estimate 838 The world-wide network of in-situ atmospheric measurements and satellite derived atmospheric CO2 839 column (XCO₂) observations put a strong constraint on changes in the atmospheric abundance of CO₂. 840 This allows atmospheric inversion methods to constrain the magnitude and location of the combined 841 total surface CO2 fluxes from all sources, including fossil and land-use change emissions and land and 842 ocean CO2 fluxes. The inversions assume EFOS to be well known, and they solve for the spatial and 843 temporal distribution of land and ocean fluxes from the residual gradients of CO2 between stations that 844 are not explained by fossil fuel emissions. By design, such systems thus close the carbon balance ($B_{\rm IM}$ = 845 0) and provide an additional perspective on the independent estimates of the ocean and land fluxes. 846 This year's release includes fourteen inversion systems that are described in Table S4. Each system is 847 rooted in Bayesian inversion principles but uses different methodologies. These differences concern the 848 selection of atmospheric CO2 data or XCO2, and the choice of a-priori fluxes to refine. They also differ 849 in spatial and temporal resolution, assumed correlation structures, and mathematical approach of the 850 models (see references in Table S4 for details). Importantly, the systems use a variety of transport models, which was demonstrated to be a driving factor behind differences in atmospheric inversion-851 852 based flux estimates, and specifically their distribution across latitudinal bands (Gaubert et al., 2019; 853 Schuh et al., 2019). Six inversion systems used surface observations from the global measurement 854 network (Schuldt et al., 2024, 2025). Eight inversion systems used satellite XCO2 retrievals from 855 GOSAT and/or OCO-2, scaled to the WMO 2019 calibration scale, of which three inversions this year

used these XCO₂ datasets in addition to the in-situ observational CO₂ mole fraction records.





857	The original products delivered by the inverse modellers were modified to facilitate the comparison to
858	the other elements of the budget, specifically on two accounts: (1) global total fossil emissions
859	including cement carbonation CO2 uptake, and (2) riverine CO2 transport. We note that with these
860	adjustments the inverse results no longer represent the net atmosphere-surface exchange over
861	land/ocean areas as sensed by atmospheric observations. Instead, for land, they become the net uptake
862	of CO ₂ by vegetation and soils that is not exported by fluvial systems, similar to the DGVMs estimates.
863	For oceans, they become the net uptake of anthropogenic CO ₂ , similar to the GOBMs estimates.
864	The inversion systems prescribe global fossil emissions based on e.g. the GCP's Gridded Fossil
865	Emissions Dataset versions 2025.1 (GCP-GridFED; Jones et al., 2025), which are updates to GCP-
866	GridFEDv2021 presented by Jones et al. (2021b). GCP-GridFEDv2025.1 scales gridded estimates of
867	CO ₂ emissions from EDGARv4.3.2 (Janssens-Maenhout et al., 2019) within national territories to
868	match national emissions estimates provided by the GCB for the years 1959-2024, which were
869	compiled following the methodology described in Section 2.1. Small differences between the systems
870	due to for instance regridding to the transport model resolution, or use of different fossil fuel emissions
871	than GCP-GridFEDv2025.1, are adjusted in the latitudinal partitioning we present, to ensure agreement
872	with the estimate of E_{FOS} in this budget. We also note that the ocean fluxes used as prior by 8 out of 14
873	inversions are part of the suite of the ocean process model or fCO ₂ -products listed in Section 2.5.
874	Although these fluxes are further adjusted by the atmospheric inversions (except for Jena CarboScope),
875	it makes the inversion estimates of the ocean fluxes not completely independent of S_{OCEAN} assessed
876	here.
877	To facilitate comparisons to the independent Socian and Sland, we used the same adjustments for
878	transport and outgassing of carbon transported from land to ocean, as done for the observation-based
879	estimates of S _{OCEAN} (see Supplement S.5.1).
880	The atmospheric inversions are evaluated using vertical profiles of atmospheric CO ₂ concentrations
881	(Figure S13). More than 50 aircraft programs over the globe, either regular programs or repeated
882	surveys over at least 9 months (except for SH programs), have been used to assess system performance
883	(with space-time observational coverage sparse in the SH and tropics, and denser in NH mid-latitudes;
884	Table S8). The fourteen systems are compared to the independent aircraft CO2 measurements between 2
885	and 7 km above sea level between 2001 and 2024. Results are shown in Figure S13 and discussed in
886	Supplement S.5.2.
887	We note that as of GCB2025, the ensemble of inverse models covering a full decade is deemed
888	sufficiently large to report the 1-sigma standard deviation as uncertainty, following the convention of
889	the other components in GCB.More details on the atmospheric inversion methodology can be found in
890	Supplement S.5.

915

916





2.8 Atmospheric oxygen based estimate

892 Long-term atmospheric O2 and CO2 observations allow estimation of the global ocean and land carbon 893 sinks, due to the coupling of O2 and CO2 with distinct exchange ratios for fossil fuel emissions and land 894 uptake, and uncoupled O2 and CO2 ocean exchange (Keeling and Manning, 2014). The global ocean 895 and net land carbon sinks were calculated following methods and constants used in Keeling and 896 Manning (2014) but modified to also include the effective O2 source from metal refining (Battle et al., 897 2023). For the exchange ratio of the net land sink at value of 1.05 is used, following Resplandy et al. 898 (2019). For fossil fuels, the following values are used: gas: 1.95 (+/-) 0.04, liquid: 1.44, (+/-) 0.03, solid: 1.17 (+/-) 0.03, cement: 0 (+/-) 0, gas flaring: 1.98 (+/-) 0.07 (Keeling, 1988). Atmospheric O₂ is 899 900 observed as δ(O₂/N₂) and combined with CO₂ mole fraction observations into Atmospheric Potential 901 Oxygen (APO, Stephens et al., 1998). The APO observations from 1990 to 2024 were taken from a 902 weighted average of flask records from three stations in the Scripps O2 program network (Alert, Canada (ALT), La Jolla, California (LJO), and Cape Grim, Australia (CGO), weighted per Keeling and 903 904 Manning (2014). Observed CO₂ was taken from the globally averaged marine surface annual mean 905 growth rate from the NOAA/GML Global Greenhouse Gas Reference Network (Lan et al., 2025a). The 906 O₂ source from ocean warming is based on ocean heat content from updated data from NOAA/NCEI 907 (Levitus et al., 2012). The effective O₂ source from metal refining is based on production data from 908 Bray (2020), Flanagan (2021), and Tuck (2022). Uncertainty was determined through a Monte Carlo approach with 20,000 iterations, using uncertainties prescribed in Keeling and Manning (2014), 909 910 including observational uncertainties from Keeling et al. (2007) and autoregressive errors in fossil fuel 911 emissions (Ballantyne et al., 2015). The reported uncertainty is 1 standard deviation of the ensemble. 912 As for the atmospheric inversions, the O_2 based estimates also closes the carbon balance ($B_{IM} = 0$) by 913 design and provides another independent estimate of the ocean and land fluxes. Note that the O2 method 914 requires a correction for global air-sea O2 flux, which has the largest uncertainty at annual time scales,

2.9 Earth System Models estimate

917 Reconstructions and predictions from decadal prediction systems based on Earth system models 918 (ESMs) provide a novel line of evidence in assessing the atmosphere-land and atmosphere-ocean 919 carbon fluxes in the past decades and predicting their changes for the current year and years to come. 920 By assimilating physical atmospheric and oceanic data products into the ESMs, the models are able to reproduce the historical variations of the atmosphere-sea CO2 fluxes, atmosphere-land CO2 fluxes, and 921 922 atmospheric CO2 growth rate (Li et al., 2016, 2019; Lovenduski et al., 2019a,b; Ilyina et al., 2021; Li et 923 al., 2023). Furthermore, the ESM-based predictions have proven their skill in predicting the air-sea CO2 924 fluxes for up to 6 years, the air-land CO2 fluxes and atmospheric CO2 growth for 2 years (Lovenduski et

but which is still non-negligible for decadal estimates (Nevison et al., 2008).





al., 2019a,b; Ilyina et al., 2021; Li et al., 2023). The reconstructions from the fully coupled model simulations ensure a closed budget within the Earth system, i.e., no budget imbalance term.

927 Six ESMs have performed the set of prediction simulations. The ensemble size of initialized prediction 928 simulations is 10, and the ensemble mean for each individual model is used here. Each ESM uses a 929 different assimilation method and combination of data products incorporated in the system, more details 930 on the models configuration can be found in Table 4 and Supplement Table S5. Reconstructions of 931 atmosphere-ocean CO2 fluxes (Socean) and atmosphere-land CO2 fluxes (SLAND-ELUC) for the time period 932 from 1960-2024 are assessed here. Predictions of the atmosphere-ocean CO2 flux, atmosphere-land CO2 933 flux, and atmospheric CO2 growth for 2025 are calculated based on the predictions at lead year 1. The 934 predictions of atmosphere-ocean CO2 flux and atmosphere-land CO2 flux are bias corrected by removing 935 the climatological mean and linear trend biases from 1981-2021 referring to GCB2022 (Friedlingstein et 936 al., 2022), the atmospheric CO₂ growth (G_{ATM}) is then calculated as the residual of the CO₂ emissions 937 subtracting the carbon sinks into the ocean and the land. With the ESMs simulations, we also compute 938 the GATM in another way based on monthly atmospheric CO2 concentrations at 1000hPa level over the 939 oceans to be comparable to the NOAA/GML global measurements of atmospheric CO2 concentrations (Lan et al., 2025a). The bias correction is done referring to NOAA/GML monthly CO2 concentrations in 940 941 recent 10 years from 2015-2024 regarding mean state and linear trend, a shorter period is used because a 942 non-linear trend for the whole period is observed from both NOAA/GML measurements and model 943 simulations. The 2025 GATM is then calculated by the increment of atmospheric CO2 concentration in 944 December 2025 minus that in December 2024 multiplied by 2.124 to convert the unit from ppm to GtC. 945 The prediction of 2025 atmospheric CO₂ concentration is an average of the available NOAA/GML 946 measurements from January to June (Lan et al., 2025) and ESMs' predictions from July to December. 947 Note that the two methods, i.e., one based on the residual of carbon sources and sinks and another based 948 on atmospheric concentration increment, of calculation of GATM result in different magnitudes, which 949 suggests the consideration of variable ratio rather than a constant value in converting CO₂ concentration 950 to mass. More details on methods of bias correction of decadal predictions can be found in Kharin et al. 951 (2012), Boer et al. (2016) and Li et al. (2023). The ESMs are used here to support the assessment of 952 Socean and net atmosphere-land CO2 flux (SLAND - ELUC) over the 1960-2024 period, and to provide an 953 estimate of the 2025 prediction of G_{ATM} and atmospheric CO₂ concentration.

2.10 Processes not fully included in the global carbon budget

The contribution of anthropogenic CO and CH₄ to the global carbon budget is not fully accounted for in Eq. (1) and is described in Supplement S.8.1. The contributions to CO₂ emissions of decomposition of carbonates not accounted for is described in Supplement S.8.2. The contribution of anthropogenic changes in river fluxes is conceptually included in Eq. (1) in Socean and in Sland, but it is not represented in the process models used to quantify these fluxes. However, a correction of -0.07 GtC/yr





- is applied a posteriori to the S_{LAND} estimate for the 2015-2024 period, as proposed in Friedlingstein et
 al. (2025b). This effect is discussed in Supplement S.8.3. Similarly, the Replaced Sinks and Sources
- 962 effect from reduced forest cover over the historical period is missing from the DGVMs used here to
- 963 estimate S_{LAND}. However, a correction (-19%) is applied a posteriori to the S_{LAND} estimate from
- DGVMs, based on O'Sullivan et al. (2025; see Section 2.6 and Supplement S.4.1).

965 3 Results

- 966 For each component of the global carbon budget, we present results for three different time periods: the
- 967 full historical period, from 1850 to 2024, the decades in which we have atmospheric concentration
- 968 records from Mauna Loa (1959-2024), a specific focus on last year (2024), and the projection for the
- 969 current year (2025). Subsequently, we assess the estimates of the budget components of the last decades
- 970 against the top-down constraints from inverse modelling of atmospheric observations and the
- 971 land/ocean partitioning derived from the atmospheric O₂ measurements. Atmospheric inversions further
- 972 allow for an assessment of the budget components with a regional breakdown of land and ocean sinks.

974 3.1 Fossil CO₂ Emissions

975 **3.1.1 Historical period 1850-2024**

- 976 Cumulative fossil CO₂ emissions for 1850-2024 were 495 ± 25 GtC, including the cement carbonation
- 977 sink (Table 8, with all cumulative numbers rounded to the nearest 5GtC). In this period, 46% of global
- 978 fossil CO₂ emissions came from coal, 35% from oil, 15% from natural gas, 3% from decomposition of
- 979 carbonates for cement production, and 1% from flaring. In 1850, the UK stood for 62% of global fossil
- 980 CO₂ emissions. In 1893 the combined cumulative emissions of the current members of the European
- 981 Union reached and subsequently surpassed the level of the UK. Since 1917 US cumulative emissions
- have been the largest. Over the entire period 1850-2024, US cumulative emissions amounted to 120
- 983 GtC (24% of world total), the EU's to 80 GtC (16%), China's to 80 GtC (15%), and India's to 18 GtC
- 984 (4%).

- 985 In addition to the estimates of fossil CO₂ emissions that we provide here (see Section 2.1), there are
- 986 three global datasets with long time series that include all sources of fossil CO₂ emissions: CDIAC-FF
- 987 (Erb and Marland, 2025), CEDS version 2024 07 08 (Hoesly et al., 2024) and PRIMAP-hist version
- 988 2.6 (Gütschow et al., 2016; Gütschow et al., 2024), although these datasets are not entirely independent
- 989 from each other (Andrew, 2020a). CEDS has cumulative emissions over 1750-2022 at 480 GtC,
- 990 CDIAC-FF has 481 GtC, GCP 484 GtC, PRIMAP-hist CR 490 GtC, and PRIMAP-hist TR 492 GtC.
- 991 CDIAC-FF excludes emissions from lime production. CEDS estimates higher emissions from
- 992 international shipping in recent years, while PRIMAP-hist has higher fugitive emissions than the other





datasets. However, in general these four datasets are in relative agreement as to total historical global emissions of fossil CO₂.

995 3.1.2 Recent period 1959-2024

- 996 Global fossil CO₂ emissions, E_{FOS} (including the cement carbonation sink), have increased every decade
- 997 from an average of 3.0 ± 0.2 GtC yr⁻¹ for the decade of the 1960s to an average of 9.8 ± 0.5 GtC yr⁻¹
- 998 during 2015-2024 (Table 7, Figure 2 and Figure 4). The growth rate in these emissions decreased
- 999 between the 1960s and the 1990s, from 4.3% yr⁻¹ in the 1960s (1960-1969), 3.1% yr⁻¹ in the 1970s
- (1970-1979), 1.5% yr⁻¹ in the 1980s (1980-1989), to 1.0% yr⁻¹ in the 1990s (1990-1999). After this
- period, the growth rate began increasing again in the 2000s at an average growth rate of 2.8% yr⁻¹,
- decreasing to 1.2% yr⁻¹ in the 2010s, and 0.8% yr⁻¹ for the last decade (2015-2024). China's emissions
- increased by +2.5% yr⁻¹ on average over the last 10 years dominating the global trend, and India's
- emissions increased by +3.6% yr⁻¹, while emissions decreased in EU27 by 2.5% yr⁻¹, and in the USA by
- 1005 1.2% yr⁻¹ (Figure 5a). Figure 6 illustrates the spatial distribution of fossil fuel emissions for the 2015-
- 1006 2024 period.
- 1007 E_{FOS} reported here includes the uptake of CO₂ by cement via carbonation which has increased with
- 1008 increasing stocks of cement products, from an average of 20 MtC yr⁻¹ (0.02 GtC yr⁻¹) in the 1960s to an
- average of 210MtC yr⁻¹ (0.21 GtC yr⁻¹) during 2015-2024 (Figure 5b).

1010 3.1.3 Final year 2024

- 1011 Global fossil CO₂ emissions were slightly higher, 1.1%, in 2024 than in 2023, with an increase of 0.11
- 1012 GtC to reach 10.3 ± 0.5 GtC (including the 0.22 GtC cement carbonation sink) in 2024 (Figure 4),
- $1013 \qquad \text{distributed among coal (41\%), oil (32\%), natural gas (21\%), cement (4\%), flaring (1\%), and others} \\$
- 1014 (1%). Compared to 2023, the 2024 emissions from coal, oil, and gas increased by 0.8%, 1.3%, and
- 1015 2.4% respectively, while emissions from cement decreased by 4.6%. All annual growth rates presented
- are adjusted for the leap year, unless stated otherwise.
- 1017 In 2024, the largest absolute contributions to global fossil CO₂ emissions were from China (32%), the
- 1018 USA (13%), India (8%), and the EU27 (6%). These four regions account for 59% of global fossil CO₂
- 1019 emissions, while the rest of the world contributed 41%, including international aviation and marine
- bunker fuels (3% of the total). Growth rates for these countries from 2023 to 2024 were +0.7% (China),
- 1021 -0.6% (USA), -2.6% (EU27), and +4.0% (India), with +1.3% for the rest of the world, including
- 1022 international aviation and marine bunker fuels (+9.8%). The per-capita fossil CO₂ emissions in 2024
- 1023 were 1.3 tC person⁻¹ yr⁻¹ for the globe, and were 3.9 (USA), 2.4 (China), 1.5 (EU27) and 0.6 (India) tC
- 1024 person⁻¹ yr⁻¹ for the four highest emitters (Figure 5c).





1025	3.1.4 Year 2025 Projection
1026 1027 1028 1029 1030	Globally, we estimate that global fossil CO ₂ emissions (including cement carbonation, -0.21 GtC) will grow by 1.1% in 2025 (0.2% to +2.2%) to 10.4 GtC (38.1 GtCO ₂), an historical record high ² . The estimates of changes in 2025 emissions per fuel types, relative to 2024, are projected to be 0.8% (range -0.1% to 1.9%) for coal, +1.0% (range 0.3% to 1.8%) for oil, +1.3% (range 0.0% to 2.5%) for natural gas, and 0.5% (range -1.5% to 2.6%) for cement (Figure 5b).
1031 1032 1033 1034	For China, projected fossil emissions in 2025 are expected to increase slightly by 0.4% (range -0.9% to 2.0%) compared with 2024 emissions, bringing 2024 emissions for China around 3.4 GtC yr ⁻¹ (12.3 GtCO ₂ yr ⁻¹). Our projected changes by fuel for China are +0.3% for coal, +2.1% for oil, +1.3% for natural gas, and -2.8% for cement.
1035 1036 1037 1038	For the USA, using the Energy Information Administration (EIA) emissions projection for 2025 combined with cement clinker data from USGS, we project an increase of 1.9% (range -0.2% to 4.1%) compared to 2024, bringing USA 2025 emissions to around 1.4 GtC yr ⁻¹ (5.0 GtCO ₂ yr ⁻¹). Our projected changes by fuel are 7.5% for coal, 1.1% for oil, +1.1% for natural gas, and -8.0% for cement.
1039 1040 1041	For India, our projection for 2025 is an increase of 1.4% (range of -0.3% to 3.1%) over 2024, with 2025 emissions around 0.9 GtC yr $^{-1}$ (3.2 GtCO $_2$ yr $^{-1}$). Our projected changes by fuel are +1.7% for coal, +0.1% for oil, -6.4% for natural gas, and +9.9% for cement.
1042 1043 1044	For the European Union, our projection for 2025 is for an increase of 0.4% (range -2.1% to 2.8%) relative to 2024, with 2025 emissions around 0.7 GtC yr^{-1} (2.4 GtCO ₂ yr^{-1}). Our projected changes by fuel are -0.3% for coal, 0.6% for oil, +0.9% for natural gas, and -4.1% for cement.
1045 1046 1047	New this year, we provide a projection for Japan, with a 2025 decrease of 2.2% (range of -8.1% to +3.7%), with 2025 emissions around 0.3 GtC yr^1 (0.9 GtCO ₂ yr^1). Our projected changes by fuel are -3.1% for coal, -0.8% for oil, -2.7% for natural gas, and -3.0% for cement.
1048 1049 1050 1051 1052 1053	International aviation and shipping are projected to increase by 3.7% in 2025, reaching 0.3 GtC yr $^{-1}$ (1.2 GtCO $_2$ yr $^{-1}$), with international aviation projected to be up 6.8% over 2024, and international shipping projected to be flat (0%). For the rest of the world, the expected change for 2025 is an increase of 1.1% (range -1.1% to 3.3%) with 2025 emissions around 3.7 GtC yr $^{-1}$ (13.7 GtCO $_2$ yr $^{-1}$). The fuel-specific projected 2025 growth rates for the rest of the world are: +1.0% for coal, +0.5% for oil, +1.8% for natural gas, +2.4% for cement.
1054 1055	Compared to the GCB estimate, Carbon Monitor projects a global fossil CO ₂ emissions increase of 0.3% (-1.8% to 2.4%) for 2025, lower than GCB but with overlapping uncertainties. In contrast to

² Growth rates in this section use a leap year adjustment that corrects for the extra day in 2024.





1056 GCB, Carbon Monitor projects the 2025 emissions from China to decline by -2.4% (range -4.7% to -1057 0.2%). Conversely, Carbon Monitor projects the 2025 emissions to increase by 3.0% (0% to 6.0%) for 1058 the USA, by +0.3% (-1.9% to +2.5%) for India, by 1.6% (-2.8% to 5.8%) for the EU27, and by 0.4% (-2.8% to -2.8%) for the EU27, and by -2.8% (-2.8%) for the EU27, and -2.8% (-2.8%) for the EU27, a 1059 3.3% to 4.0%) for Japan. The Carbon Monitor projects international aviation and shipping to increase 1060 by 0.7% (-0.9% to 2.2%) in 2025. For the rest of the world, the expected change is an increase of 1.5% 1061 (range 0.3% to 2.7%). 1062 For traceability, Table S6 provides a comparison of annual projections from GCB since 2015 with the 1063 actual emissions assessed in the subsequent GCB annual report. 1064 3.2 **Emissions from Land-Use Change** 1065 3.2.1 Historical period 1850-2024 1066 Cumulative net CO₂ emissions from land-use change (E_{LUC}) for 1850-2024 are 250 \pm 60 GtC (Table 8) 1067 with a large spread among individual bookkeeping estimates of 210 GtC (OSCAR), 240 GtC (LUCE) 1068 and 290 GtC (BLUE). DGVMs show a lower estimate of 160 ± 60 GtC. Vegetation biomass 1069 observations provide independent constraints on the E_{LUC} estimates (Li et al., 2017). Over the 1901-1070 2012 period, the GCB bookkeeping models' cumulative E_{LUC} amounts to 180 GtC [155 to 210 GtC] 1071 and the DGVM cumulative E_{LUC} to 121 ± 45 GtC, both not significantly different from the observation-1072 based estimate of 155 ± 50 GtC (Li et al., 2017). The substantially lower cumulative E_{LUC} estimates 1073 from DGVMs compared to GCB2024 are due to the correction for the RSS bias, which is implemented 1074 in this assessment (see Section 2.6.1; O'Sullivan et al., 2025). 1075 Recent period 1959-2024 3.2.2 1076 In contrast to growing fossil emissions, net CO2 emissions from land use, land-use change, and forestry 1077 remained relatively constant (around 1.8 GtC yr⁻¹) over the 1959-1999 period. Since then, they have 1078 shown a statistically significant decrease of about 0.2 GtC per decade (p<0.001), reaching 1.4 ± 0.7 GtC 1079 yr⁻¹ for the 2015-2024 period (Table 7), with a spread from 1.3 to 1.6 GtC yr⁻¹ across the three 1080 bookkeeping estimates (Table 5, Figure 4b). Different from the bookkeeping average, the DGVM 1081 average grows slightly larger over the 1980-2010 period, but as bookkeeping models, DGVMs show 1082 decreasing emissions in the most recent decade, 2015-2024 (Table 5). 1083 Compared to GCB2024, the overall trends in E_{LUC} remained similar but the E_{LUC} estimates increased. The main reason for the larger estimates in this assessment is that the H&C2023 model, included up to 1084 1085 GCB2024, is not included anymore (see Section 2.2). H&C2023 had the lowest E_{LUC} estimates among 1086 all bookkeeping models (Figure S3). Larger E_{LUC} estimates in the last few decades (compared to 1087 GCB2024) are also due to the consideration of transient instead of constant carbon densities by all three





1089 for all E_{LUC} components in the last few decades (Figure S3). Net E_{LUC} increases because emissions from 1090 deforestation are still the dominating term. 1091 We separate E_{LUC} into five component fluxes to gain further insight into the drivers of net emissions: 1092 deforestation, forest (re-)growth, wood harvest and other forest management, peat drainage and peat 1093 fires, and all other transitions (Figure 7b; Supplement S.2.2). We further decompose the deforestation 1094 and the forest (re-)growth term into contributions from shifting cultivation vs permanent forest cover 1095 changes (Figure 7c). Averaged over the 2015-2024 period and over the three bookkeeping estimates, 1096 fluxes from deforestation amount to 1.9 [1.5 to 2.3] GtC yr⁻¹ (Table 5), of which 1.1 [0.9, 1.2] GtC yr⁻¹ 1097 are from permanent deforestation. Fluxes from forest (re-)growth amount to -1.3 [-1.5, -1.0] GtC yr⁻¹ 1098 (Table 5), of which -0.6 [-0.7, -0.5] GtC yr⁻¹ are from re/afforestation and the remainder from forest 1099 regrowth in shifting cultivation cycles. Wood harvest and other forest management causes net 1100 emissions of 0.4 [0.1, 0.7] GtC yr¹ (with substantial gross fluxes largely compensating each other; see Figure S2). Emissions from peat drainage and peat fires (0.2 [0.2, 0.3] GtC yr⁻¹) and the net flux from 1101 other transitions (0.1 [0.1, 0.1] GtC yr⁻¹) are of smaller magnitude globally (Table 5). 1102 1103 The split into component fluxes clarifies the potentials for emission reduction and carbon dioxide 1104 removal: emissions from permanent deforestation - the largest of our component fluxes - could be 1105 halted (largely) without compromising carbon uptake by forests, contributing substantially to emissions 1106 reduction. By contrast, reducing wood harvesting would have limited potential to reduce net emissions 1107 as it would be associated with less forest regrowth; removals and emissions cannot be decoupled here 1108 on long timescales. A similar conclusion applies to removals and emissions from shifting cultivation, 1109 which we have therefore separated out. Carbon Dioxide Removal (CDR) in forests could instead be 1110 increased by permanently increasing the forest cover through re/afforestation, for which we estimate a 1111 removal of -0.6 GtC yr⁻¹ from the atmosphere averaged over 2015-2024. This value is similar to independent estimates derived from NGHGIs for CDR in managed forests (through re/afforestation plus 1112 1113 forest management) for 2013-2022 (-0.5 GtC yr⁻¹, Pongratz et al., 2024). Re/afforestation constitutes the 1114 vast majority of all current CDR (Pongratz et al., 2024). Though they cannot be compared directly to 1115 annual fluxes from the atmosphere and are thus not included in our estimate of ELUC, CDR through 1116 transfers between non-atmospheric reservoirs such as in durable HWPs, biochar, or BECCS comprise much smaller amounts of carbon. 218 MtC yr⁻¹ have been estimated to be transferred to HWPs, 1117 1118 averaged over 2013-2022 (Pongratz et al., 2024). The net flux of HWPs, considering the re-release of 1119 CO₂ through their decay, amounts to 91 MtC yr⁻¹ over that period (Pongratz et al., 2024). Note that 1120 some double-counting between the CDR through HWPs and the CDR through re/afforestation exists if 1121 the HWPs are derived from newly forested areas. "Blue carbon", i.e. coastal wetland management such 1122 as restoration of mangrove forests, saltmarshes and seagrass meadows, though at the interface of land 1123 and ocean carbon fluxes, are counted towards the land-use sector as well. Currently, bookkeeping





1124 models do not include blue carbon; however, current CDR deployment in coastal wetlands is small 1125 globally, less than 0.003 MtC yr⁻¹ (Powis et al., 2023). 1126 The statistically significant decrease in E_{LUC} since the late-1990s, including the larger drop within the 1127 most recent decade, is due to the combination of decreasing emissions from deforestation (in particular 1128 permanent deforestation) and increasing removals from forest regrowth (with those from 1129 re/afforestation stagnating globally in the last decade). Net emissions in 2015-2024 are 23% lower than 1130 in the late-1990s (1995-2004) and 19% lower than in 2005-2014. The steep drop in E_{LUC} after 2015 is 1131 due to the combined effect from a peak in peat fire emissions in 2015 and a long-term decline in 1132 deforestation emissions in many countries over the 2010-2020 period. The processes behind gross 1133 removals, foremost forest regrowth and soil recovery, are all slow, while gross emissions include a 1134 large instantaneous component. Short-term changes in gross emissions dynamics, such as a temporary 1135 decrease in deforestation, influences E_{LUC} faster than a change in gross removals, which rather act on 1136 longer-term timescales. Component fluxes often differ more across the bookkeeping estimates than the 1137 net flux (Figure 7b), which is expected due to different process representation; in particular, the 1138 treatment of shifting cultivation, which increases both gross emissions and gross removals, differs 1139 across models, but also net and gross wood harvest fluxes show high uncertainty (Figure S2). By 1140 contrast, models agree relatively well for emissions from permanent deforestation. 1141 Overall, highest net land-use emissions occur in the tropical regions of all three continents. The top 1142 three emitters over 2015-2024 are Brazil (in particular the Amazon Arc of Deforestation), Indonesia, 1143 and the Democratic Republic of the Congo, with these 3 countries contributing 0.8 GtC yr⁻¹ or 57% of 1144 the global net land-use emissions (average over 2015-2024; Figure 6b, Figure 7a). This is related to 1145 massive expansion of cropland (FAO, 2025c), particularly in the last few decades in Latin America, 1146 Southeast Asia, and sub-Saharan Africa (Hong et al., 2021), to a substantial part for export of 1147 agricultural products (Pendrill et al., 2019). Emission intensity is high in many tropical countries, 1148 particularly of Southeast Asia, due to high rates of land conversion in regions of carbon-dense and often 1149 still pristine, undegraded natural forests (Hong et al., 2021). Emissions are further increased by peat 1150 fires in equatorial Asia (GFED4s, van der Werf et al., 2017). Uptake due to land-use change occurs in 1151 several regions of the world (Figure 6b) particularly due to re/afforestation. Highest CDR in the last 1152 decade is seen in China, the USA, and the EU27, partly related to expanding forest area as a consequence of the forest transition in the 19th and 20th century and subsequent regrowth of forest 1153 1154 (Mather 2001; McGrath et al., 2015). Substantial uptake through re/afforestation also exists in other 1155 regions such as Brazil, Russia, or Indonesia, where, however, emissions from deforestation and other 1156 land-use changes dominate the net land-use flux. While the mentioned patterns are robust and supported 1157 by independent literature, we acknowledge that model spread is substantially larger on regional than 1158 global levels, as has been shown for bookkeeping models (Bastos et al., 2021) as well as DGVMs 1159 (Obermeier et al., 2021). Assessments for individual regions are being performed as part of the





1160	REgional Carbon Cycle Assessment and Processes 2 initiative (RECCAP2; Ciais et al., 2020, Poulter et
1161	al., 2022) or already exist for selected regions (e.g., for Europe by Petrescu et al., 2020; for Brazil by
1162	Rosan et al., 2021; for China by Zhu et al., 2025; and for 8 selected countries/regions in comparison to
1163	inventory data by Schwingshackl et al., 2022).
1164	The NGHGI data under the land-use, land-use change, and forestry (LULUCF) sector (Melo et al.
1165	2025) and the LULUCF estimates from FAOSTAT (FAO, 2025d) differ from the global models'
1166	definition of E_{LUC} (see Section 2.2.1). In the NGHGI reporting, natural land fluxes (S_{LAND}) are counted
1167	towards E_{LUC} when they occur on managed land (Grassi et al., 2018) whereas FAOSTAT LULUCF
1168	estimates generally include natural fluxes in managed and unmanaged forests (Tubiello et al., 2021). To
1169	compare our results to the NGHGI approach, we perform a translation of our E_{LUC} estimates by adding
1170	S_{LAND} in managed forest from the DGVMs simulations (1.9 GtC yr $^{\text{-}1}$ in 2015-2024) to the bookkeeping
1171	E _{LUC} estimate (following the methodology described in Grassi et al., 2023; see Supplement S.2.4).
1172	Adding this sink changes E _{LUC} from being a source of 1.4 GtC yr ⁻¹ to a sink of 0.5 GtC yr ⁻¹ , much
1173	closer to the NGHGI estimate reporting a sink of 1.0 GtC yr ⁻¹ (Figure 8a, Table S10). Remaining
1174	differences in the bookkeeping and NGHGI estimates are mainly stemming from fluxes due to other
1175	transitions and permanent deforestation, whereas peat emissions and the net flux in managed forests
1176	agree well (Figure 8b,c). We further apply a mask of managed land to the net atmosphere-to-land flux
1177	estimate from atmospheric inversions to obtain inverse estimates that are comparable to the NGHGI
1178	estimates and to the translated E_{LUC} estimates from bookkeeping models (see Supplement S.2.4). The
1179	inversion-based net flux in managed land indicates a sink of 0.7 GtC yr ⁻¹ for 2015-2024, which is in
1180	broad agreement with the NGHGI and the translated E_{LUC} estimates (Figure 8, Table S10).
1181	Additionally, the interannual variability of the inversion estimates and the translated E_{LUC} estimates
1182	show a remarkable agreement (Pearson correlation of 0.71 in 2000-2024), which supports the suggested
1183	translation approach. Though estimates of NGHGI, FAOSTAT, and atmospheric inversions and the
1184	translated bookkeeping estimates still differ in value and need further analysis, the approach suggested
1185	by Grassi et al. (2023), which we adopt here, provides a feasible way to relate the global models' and
1186	NGHGI approach to each other and thus link the anthropogenic carbon budget estimates of land-use
1187	CO2 fluxes directly to the Global Stocktake, as part of the UNFCCC Paris Agreement. The translation
1188	approach has been shown to be generally applicable also at the country-level (Grassi et al., 2023;
1189	Schwingshackl et al., 2022).
1190	3.2.3 Final year 2024
1191	The global CO_2 emissions from land-use change are estimated as 1.3 ± 0.7 GtC in 2024, similar to the
1192	2023 estimate. However, confidence in the annual change remains low, as the land-use forcing
1193	underlying the E_{LUC} estimates was informed directly by data only up to and including 2023, with a trend
1194	extrapolation to 2024 (see Supplement Section S.2.1). The anomalously large fire emissions in South





1193	America in 2024 that resulted from the impacts of the 2023/2024 droughts linked to El Niño are thus
1196	not yet fully reflected in the 2024 E_{LUC} estimate, even if they led to permanent deforestation. The extent
1197	of degradation was anomalously high in the Amazon in 2024 and partly masked relatively low
1198	deforestation rates (https://terrabrasilis.dpi.inpe.br). However, this is not captured by our approach that
1199	is based on forest cover changes. For degradation it is currently impossible to be separated into effects
1200	of land-use activity versus effects of climate variability.
1201	3.2.4 Year 2025 Projection
1202	In equatorial Asia, peat fire emissions remained low (1 TgC in 2025 through October 15 2025, after 2
1203	TgC in 2024; GFED4.1s, van der Werf et al., 2017), as did deforestation and degradation fires (4 TgC
1204	in 2025; 8 TgC in 2024). South America saw a big reduction in emissions from deforestation and
1205	degradation fires, from 334 TgC in 2024 to 35 TgC up until October 15 2025. Pantropical 2025 fire
1206	emission estimates from deforestation and degradation through October 15 are 105 TgC, which is not
1207	just a massive drop compared to the anomalously high 2024 emissions, but also only about one third of
1208	the long-term average (1997-2024). The reduction in emissions is mainly attributable to anomalously
1209	low deforestation and degradation fire emissions in South America, likely connected to the ceasing of
1210	the El Niño conditions and their impacts on ecosystems.
1211	Since the E _{LUC} estimate for the year 2024 is not informed directly by data on land-use dynamics
1212	(Section 3.2.3), we estimate the 2025 projection based on fire anomalies over the year 2023. We expect
1213	E _{LUC} emissions of around 1.1 GtC (4.1 GtCO ₂) in 2025, 0.1 GtC below the 2024 level (0.3 GtC below
1214	the 2015-2024 average). Note that the confidence in the 2025 E_{LUC} projection remains low, as it is
1215	based on deforestation, degradation and peat fire emissions, which are only a proxy for land-use
1216	change. Projections in past GCB assessments are only partially confirmed by updated E_{LUC} estimates
1217	based on bookkeeping models in the following GCB assessments (Figure S4). Although our
1218	extrapolation includes tropical deforestation and degradation fires, the degradation attributable to
1219	selective logging, edge-effects or fragmentation is not captured. Further, deforestation and fires in
1220	deforestation zones may become more disconnected, partly due to changes in legislation in some
1221	regions. For example, Van Wees et al. (2021) found that the contribution from fires to forest loss
1222	decreased in the Amazon and in Indonesia over the period of 2003-2018.
1223	3.3 CDR not based on vegetation
1224	Besides the CDR through land use (Sec. 3.2), the atmosphere-to-geosphere flux of carbon resulting
1225	from carbon dioxide removal (CDR) activities in 2024 is estimated at 0.0088 MtC/yr. This results
1226	primarily from 0.002 MtC/yr and 0.00022 MtC/yr of mineralisation and enhanced weathering projects
1227	respectively, 0.003 MtC/yr of bio-oil geological storage, and 0.0004 MtC/yr of DACCS (Pongratz et
1228	al., 2024). This represents a decrease of 20% in the anthropogenic sink compared to the 0.011 MtC/yr





1229	estimate for 2023, and it remains roughly a million times smaller than current fossil CO ₂ emissions.
1230	Note that the lower DACCS estimates reflect more accurate annual data from registries, indicating that
1231	operational projects are currently removing less CO2 than their expected capacities. Similarly, reported
1232	CDR via Enhanced Rock Weathering decreased in 2024; however, this may not indicate a real decline
1233	in activity. The decline likely reflects a transition toward third party verification, with some removals
1234	not yet appearing on registries. Other novel CDR methods, including ocean and river alkalinity
1235	enhancement (0.0002 MtC/yr and 0.00001 MtC/yr in 2024 respectively), and biomass direct storage
1236	(compressing waste biomass to store underground, 0.0008 MtC/yr), jointly contributed just under 0.004
1237	MtC/yr according to updated 2024 estimates of the State of CDR report (Smith et al., 2024). CDR
1238	through intentional biomass sinking into the deep ocean was reported at 0.001 MtC/yr for 2023, but no
1239	activities have been identified for 2024.
1240	3.4 Total anthropogenic emissions
1241	Cumulative anthropogenic CO ₂ emissions (fossil, including cement carbonation, and land-use change)
1242	for 1850-2024 totalled 745 \pm 65 GtC (2730 \pm 240 GtCO ₂), of which 71% (530 GtC) occurred since
1243	1959 and 35% (260GtC) since 2000 (Table 7 and 8). Total anthropogenic emissions more than doubled
1244	since the 1960s, from 4.9 \pm 0.7 GtC yr^1 for the decade of the 1960s to an average of 11.2 \pm 0.9 GtC yr^1
1245	during 2015-2024, and reaching 11.6 \pm 0.9 GtC (42.4 \pm 3.2 GtCO2) in 2024. However, total
1246	anthropogenic CO ₂ emissions have been almost stable over the last decade (0.3% yr ⁻¹ average growth
1247	rate over the 2015-2024 period), much lower than the 1.9% growth rate over the previous decade
1248	(2005-2014). This slower growth is due both to the reduced growth in E_{FOS} between the two decades,
1249	and to the decrease in emissions from $E_{\scriptsize LUC}$ over the past decade.
1250	During the historical period 1850-2024, 67% of historical emissions were from fossil emissions and
1251	33% from land-use change. However, fossil emissions have grown significantly since the 1960s while
1252	net land-use change emissions have not, and consequently the contributions of land-use change to total
1253	anthropogenic emissions were smaller during recent periods, 21% during the period 1959-2024 and
1254	down to 12% over the last decade (2015-2024).
1255	For 2025 we project global total anthropogenic CO ₂ emissions from fossil and land-use changes to be
1256	around 11.5 GtC (42.2 GtCO ₂), marginally below the 2024 level due to lower net land-use emissions (-
1257	0.13 GtC) compensating the growth in fossil emission (+0.09 GtC).
1258	3.5 Atmospheric CO ₂
1259	3.5.1 Historical period 1850-2024
1260	Atmospheric CO ₂ concentration was approximately 278 parts per million (ppm) in 1750, reaching 300
1261	ppm in the late 1900s, 350 ppm in the late 1980s, and reaching 422.80 ± 0.1 ppm in 2024 (Lan et al.,





1262 2025a; Figure 1). The mass of carbon in the atmosphere increased by 51% from 590 GtC in 1750 to 898 1263 GtC in 2024. Current CO₂ concentrations in the atmosphere are unprecedented in the last 2 million years and the current rate of atmospheric CO2 increase is at least 10 times faster than at any other time 1264 1265 during the last 800,000 years (Canadell et al., 2021). 1266 3.5.2 Recent period 1959-2024 1267 The growth rate in atmospheric CO₂ level increased from 1.7 ± 0.07 GtC yr⁻¹ in the 1960s to 5.6 ± 0.02 1268 GtC yr⁻¹ during 2015-2024 with important decadal variations (Table 7, Figure 3 and Figure 4c). During 1269 the last decade (2015-2024), the growth rate in atmospheric CO₂ concentration continued to increase, 1270 albeit with large interannual variability (Figure 9). This interannual variability is highly consistent 1271 between the surface-based CO2 growth rate and GRESO, the XCO2-based growth rate (r= 0.84), but 1272 substantial differences are seen in 2019 and 2022-2024. These reflect differences in the total 1273 atmospheric carbon stock seen within the set boundaries of Jan-1 and Dec-31 used to create an annual 1274 growth rate, as discussed in Section 2.4.2. Especially with large anomalies in tropical regions and close 1275 to January 1st, the calculation becomes sensitive to when the change is detected. This affected the 2023 1276 and 2024 growth rates most strongly as they originated from tropical regions, and late in the calendar 1277 year (see next section). Figure 9 also shows the total annual fluxes (in GtC yr⁻¹) from the inverse 1278 models, which are derived to match the observed atmospheric increase while numerically accounting 1279 for the atmospheric transport-related delay in detection. The inversely modeled values generally match 1280 the GRESO growth rate better than the surface observations-based growth rate, indicating that the latter is more strongly influenced by the delay between the fluxes occurring and the actual observation of 1281 1282 these signals. Note that this effect is mainly important on the annual timescale, and not over longer 1283 periods. 1284 Final year 2024 3.5.3 1285 The growth rate in the surface based atmospheric CO₂ concentration was 7.9 ± 0.2 GtC (3.73 ± 0.08 1286 ppm) in 2024 (Figure 4c; Lan et al., 2025a), well above the 2023 growth rate $(5.7 \pm 0.2 \text{ GtC}, 2.7 \pm 0.08 \text{ m})$ ppm) or the 2015-2024 average (5.6 ± 0.02 GtC, 2.6 ± 0.008 ppm), as to be expected during an El Niño 1287 1288 year. The 2024 atmospheric CO2 growth rate was the largest over the 1959-2024 atmospheric 1289 observational record, more than 1.5 GtC above the growth rates of 1998, 2015, and 2016 and 1998, all 1290 strong El Niño years. 1291 In contrast, the satellite-based GRESO growth rate was 6.8±0.2 GtC/yr (3.20±0.09 ppm/yr) for 2024 1292 which was also above its 2023 growth rate (6.5±0.2 GtC/yr, 3.06±0.07 ppm/yr) and the highest on its 1293 10-year record. But it shows a more equal split of the anomaly between both years (2023-2024). This 1294 likely reflects more accurately that a substantial fraction of the flux anomaly occurred in 2023, but this 1295 was only detected by the surface network in 2024. For the interpretation of the annual global budget





1296	this has strong implications, as 2024 surface fluxes would need to add up to a smaller anomaly (by >1
1297	GtC/yr) than when using the surface-based annual growth rate. Hence the budget imbalance in 2024
1298	(Table 7) would be reduced from -1.7 GtC to -0.6 GtC if the GRESO growth rate was used for the
1299	budget estimate.
1300	3.5.4 Year 2025 Projection
1301	Based on a projection of the 2025 surface fluxes, we estimate the annual growth in atmospheric CO ₂
1302	$\left(G_{ATM}\right)$ to be about 4.9 GtC (equivalent to a 2.3 ppm increase in the global mean concentration), in line
1303	with a neutral ENSO year. This is the average of the GCB regression method (4.4 GtC, 2.1 ppm) and
1304	ESMs the multi-model mean (5.5 GtC, 2.6 ppm). The 2025 atmospheric CO ₂ concentration, averaged
1305	over the year, is expected to reach the level of 425.7 ppm, 53% over the pre-industrial level (278 ppm).
1306	3.6 Ocean Sink
1307	3.6.1 Historical period 1850-2024
1308	Cumulated since 1850, the ocean sink S_{OCEAN} adds up to 200 ± 35 GtC, with more than 70% of this
1309	amount (145 \pm 25 GtC) being taken up by the global ocean since 1959. Over the historical period, the
1310	ocean sink increased in pace with the anthropogenic emissions exponential increase (Figure 3). Since
1311	1850, the ocean has removed 27% of total anthropogenic emissions.
1312	3.6.2 Recent period 1959-2024
1313	S_{OCEAN} increased from 1.3 ± 0.4 GtC yr ⁻¹ in the 1960s to 3.2 ± 0.4 GtC yr ⁻¹ during 2015-2024 (Table 7),
1314	with interannual variations of the order of a few tenths of GtC yr1 (Figure 4d, Figure 10b). The ocean-
1315	borne fraction (Socean/(Efos+Eluc)) has been remarkably constant around 27% on average, with
1316	variations around this mean illustrating the decadal variability of the ocean carbon sink. So far, there is
1317	no evidence of a sustained decrease in the ocean-borne fraction from 1959 to 2024 (Figure S16).
1318	The increase of the ocean sink is primarily driven by the increased atmospheric CO ₂ concentration, with
1319	the strongest CO2 induced signal in the North Atlantic and the Southern Ocean (Figure 12a, Figure
1320	S10). The effect of climate change is much weaker, reducing the ocean sink globally by 0.20 ± 0.05
1321	GtC yr ⁻¹ (-6.2% of S _{OCEAN}) during 2015-2024 (all models simulate a weakening of the ocean sink by
1322	climate change, range -4.6 to -12.2%). The climate change effect leading to a reduced ocean sink is
1323	evident in all large-scale latitudinal bands (north, tropics, south, Figure 12b, Figure S10). This is the
1324	combined effect of change and variability in all atmospheric forcing fields, previously attributed to
1325	wind and temperature changes (Le Quéré et al., 2010, Bunsen et al., 2024). The effect of warming is
1326	smaller than expected from offline calculation due to a stabilising feedback from limited exchange
1327	between surface and deep waters (Bunsen et al., 2024; Müller et al., 2025).





1328 The global net air-sea CO2 flux is a residual of large natural and anthropogenic CO2 fluxes into and out 1329 of the ocean with distinct regional and seasonal variations (Figure 6c and Figure S5). Natural fluxes dominate on regional scales, but largely cancel out when integrated globally (Gruber et al., 2009; 1330 1331 DeVries et al., 2023). Mid-latitudes in all basins and the high-latitude North Atlantic dominate the 1332 ocean CO2 uptake where low temperatures and high wind speeds facilitate CO2 uptake at the surface 1333 (Takahashi et al., 2009). In these regions, formation of mode, intermediate and deep-water masses 1334 transport anthropogenic carbon into the ocean interior, thus allowing for continued CO2 uptake at the 1335 surface. Outgassing of natural CO2 occurs mostly in the tropics, especially in the equatorial upwelling 1336 region, and to a lesser extent in the North Pacific and polar Southern Ocean, mirroring a wellestablished understanding of regional patterns of air-sea CO2 exchange (e.g., Takahashi et al., 2009, 1337 1338 Gruber et al., 2009; DeVries et al., 2023). These patterns are also noticeable in the Surface Ocean CO2 1339 Atlas dataset, where an ocean fCO₂ value above the atmospheric level indicates outgassing (Figure S5). 1340 This map further illustrates the data-sparsity in the Indian Ocean and the Southern Hemisphere in 1341 general. 1342 The largest variability in the ocean sink occurs on decadal time-scales (Figure 10b). The ensemble 1343 means of GOBMs and fCO2-products show the same patterns of decadal variability, although with a 1344 larger amplitude of variability in the fCO₂-products than in the GOBMs. The ocean sink stagnated in 1345 the 1990s and strengthened between the early 2000s and the mid-2010s (Figure 10b; Le Quéré et al., 1346 2007; Landschützer et al., 2015, 2016; DeVries et al., 2017; Hauck et al., 2020; McKinley et al., 2020, 1347 Gruber et al., 2023). Different explanations have been proposed for the decadal variability in the 1990s 1348 and 2000s, ranging from the ocean's response to changes in atmospheric wind systems (e.g., Le Quéré 1349 et al., 2007, Keppler and Landschützer, 2019), including variations in upper ocean overturning 1350 circulation (DeVries et al., 2017) to the eruption of Mount Pinatubo in the 1990s (McKinley et al., 1351 2020, Fay et al., 2023). The main origin of the decadal variability is a matter of debate with a number of 1352 studies initially pointing to the Southern Ocean (see review in Canadell et al., 2021 and Gruber et al., 1353 2023), but also contributions from the North Atlantic and North Pacific (Landschützer et al., 2016, 1354 DeVries et al., 2019), or a global signal (McKinley et al., 2020) were proposed. The GOBM 1355 decomposition into climate and CO2 effects emphasizes the role of the climate effect (that would 1356 include cooling signals from volcanic eruptions) for the stagnation in the 1990s until 2002, which are 1357 seemingly more pronounced in the tropics and north than in the south (Figure S10). The atmospheric 1358 pCO₂ growth rate is a spatially uniform driver that amplifies with large-scale averaging, while climate 1359 exerts spatially heterogeneous effects that cancel with averaging. Thus, climate dominates small-scale 1360 flux variability, but is matched on the global mean by the impact of the pCO2 growth rate (Fay et al., 1361 2024). 1362 More recently, the sink seems to have entered a phase of stagnation 2016 - 2022, largely in response to 1363 large inter-annual climate variability. The first-order effect of interannual variability stems from a





1304	stronger ocean shik during large Er wino events leading to a reduction in CO2 outgassing from the
1365	Tropical Pacific.(e.g., 1997/98, 2015/16) and a weaker sink in neutral years following El Niño (2017)
1366	and during La Niña events (2020-2022, Figure 10b; Rödenbeck et al., 2014, Hauck et al., 2020;
1367	McKinley et al. 2017). After the triple La Niña event 2020-2022, the ocean sink rebound in 2023 linked
1368	to the onset of an El Niño event. Warming in the extratropics, in particular in the Northern Hemisphere,
1369	however, weakened the overall increase in the ocean carbon sink (Müller et al., 2025). In the GOBMs,
1370	the ocean sink stagnation 2016-2022 is associated with a period of a stronger climate effect reducing
1371	the ocean sink, mostly stemming from the tropics, in line with the expected patterns from El Niño and
1372	La Niña (Figure S10). The CO ₂ effect has also shown a lower growth rate since around 2016.
1373	The unscaled ensemble means of GOBMs, and fCO ₂ -products (adjusted for the riverine flux) show a
1374	mean offset increasing from 0.28 GtC yr ⁻¹ in the 1990s (first decade available) to 0.59 GtC yr ⁻¹ in the
1375	decade 2015-2024. The offset is larger than in previous GCB versions, because two fCO ₂ -products
1376	(UExP-FNN-U, JMA-MLR), that use an adjusted version of the Surface Ocean CO2 Atlas data to
1377	represent the sea surface fCO ₂ within the surface skin layer where gas exchange takes place (Ford et al.,
1378	2025), are now included in the fCO ₂ -product mean. Additionally, an update in the SOCAT dataset with
1379	regards to Southern Ocean data led to an increase in the sink strength in three of the fCO ₂ -products
1380	(VLIZ-SOMFFN, LDEO-HPD, CMEMS-LSCE-FFNN - see section S3.1, Fay et al., 2025). In this
1381	version of the GCB, the S _{OCEAN} positive trend between GOBMs and fCO ₂ -products diverges over time
1382	by a factor of 1.6 since 2002 (GOBMs: 0.27 ± 0.05 GtC yr ⁻¹ per decade, fCO ₂ -products: 0.46 GtC yr ⁻¹
1383	per decade [0.22 to 0.81 GtC yr ⁻¹ per decade], Socean: 0.38 GtC yr ⁻¹ per decade), but the uncertainty
1384	ranges overlap. A hybrid approach recently constrained the trend for 2000 to 2022 to 0.42 ± 0.06 GtC
1385	${\rm yr}^{-1}$ decade $^{-1}$ (Mayot et al., 2024), which aligns with the updated trend of ${\rm S}_{\rm OCEAN}$ (0.46 GtC ${\rm yr}^{-1}$
1386	$decade^{-1}$), while the fCO_2 -products exhibit a larger (0.54 [0.29, 0.85] GtC yr ⁻¹ $decade^{-1}$) and the
1387	GOBMs a lower trend (0.34 \pm 0.05 GtC yr ⁻¹ per decade) over the same period.
1388	In the current budget, the discrepancy between the two types of estimates stems from a persistently
1389	larger ocean sink in the fCO ₂ -products in the northern and southern extra-tropics since around 2002
1390	(Figure 14). Note that the discrepancy in the mean flux, which was located in the Southern Ocean in
1391	GCB2022 and earlier, was reduced due to the choice of the regional river flux adjustment (Lacroix et
1392	al., 2020 instead of Aumont et al., 2001). This comes at the expense of a discrepancy in the mean
1393	S_{OCEAN} of about 0.2-0.3 GtC yr^{-1} in the tropics. Likely explanations for the discrepancy in the trends and
1394	decadal variability in the high-latitudes are data sparsity and uneven data distribution (Bushinsky et al.,
1395	2019, Gloege et al., 2021, Hauck et al., 2023a, Mayot et al., 2024). In particular, two fCO2-products
1396	were shown to overestimate the Southern Ocean CO_2 flux trend by 50 and 130% based on current
1397	sampling in a model subsampling experiment (Hauck et al., 2023a) and the largest trends in the fCO ₂ -
1398	products occurred in a data devoid region in the North Pacific (Mayot et al., 2024). In Supplement S3
1399	we show that the strength of the trends in fCO ₂ products is linked to reconstruction biases of the true
	41

stronger ocean sink during large El Niño events leading to a reduction in CO2 outgassing from the





1400	trend signal. In this respect it is highly worrisome that the coverage of fCO_2 observations has declined
1401	since 2016/17 (Dong et al., 2022, 2024; Bakker et al., 2025b) and is now down to that of the mid-2000s
1402	(Figure 10b). The temperature correction applied in two products further worsens the agreement in
1403	trends between GOBMs and fCO2-products. Similarly, model biases likely contribute to the discrepance
1404	between GOBMs and fCO ₂ -products (as indicated by the comparison with Mayot et al., 2024, and by
1405	the large model spread in the South, Figure 14).
1406	The adjusted S_{OCEAN} estimate is 2.9 ± 0.4 GtC yr ⁻¹ over the period 2004 to 2019, which agrees within
1407	the ranges of uncertainty with the ocean interior estimate of 3.2 ± 0.7 GtC yr ⁻¹ obtained with the
1408	MOBO-DIC approach (Keppler et al., 2023). The S_{OCEAN} estimate of 2.7 ± 0.4 GtC yr ⁻¹ over the period
1409	1990 to 2022 is further in excellent agreement with another recent ocean interior estimate of 2.6 ± 0.4
1410	GtC yr ⁻¹ obtained with the ResNet-DIC method (Ehmen et al., 2025, in review). The carbon flux
1411	components of both observation-based ocean interior estimates match the definition of Social used her
1412	(Hauck et al., 2020). Finally, the decadal Social estimates agree well with the corresponding ocean
1413	interior estimates for all decades from the 1960s to the 2010s, which represent a composite estimate of
1414	four observation-based products (Table 6).
1415	The S_{OCEAN} estimate agrees within uncertainties with other lines of evidence from atmospheric oxygen
1416	based estimates, atmospheric inversions, and ocean interior observation-based constraints (Table 6).
1417	The atmospheric oxygen-based estimate shows a strong growth of >1.5 GtC yr ⁻¹ from the 1990s to the
1418	recent decade 2015-2024. ESMs with data assimilation result in lower estimates of the ocean sink than
1419	all other estimates (Table 6). Also the atmospheric inversions are lower than S_{OCEAN} on average, and
1420	cover a similar range as the adjusted GOBMs and fCO2 products.
1421	3.6.3 Final year 2024
1422	The estimated ocean CO_2 sink is 3.4 ± 0.4 GtC for 2024. This is an increase of 0.1 GtC compared to
1423	2023 (Figure 4d). The sink strengthening was expected from the atmospheric CO2 growth and El Niño
1424	conditions in the beginning of the year (January to April). However, the continuation of the anomalous
1425	warm conditions in the extratropics, especially of the Atlantic Ocean, led to a weaker than expected
1426	increase in the sink (Figure 11c). The GOBMs suggest that the increase is driven by the anomalously
1427	high atmospheric CO2 growth rate and dampened by climate effects, thus suggesting that warming
1428	overcompensated the effect from El Niño (Figure S10). GOBMs and fCO2-products largely agree on
1429	patterns of ocean sink anomalies with a reduced sink in parts of the subtropical and subpolar North
1430	Atlantic and North Pacific that coincides with regions of anomalously warm sea surface temperatures
1431	(Figure S9). GOBM and fCO2-product ensemble mean estimates consistently result in an ocean sink
1432	increase in 2024 (GOBMs: 0.13 ± 0.14 GtC, f CO ₂ -products: 0.08 [-0.34,0.43] GtC). Eight GOBMs and
1433	six fCO ₂ -products show an increase in S _{OCEAN} , while only two GOBMs and three fCO ₂ -products show a
1/13/1	decrease in Secret. The fCOs products have a larger uncertainty at the end of the reconstructed time





1435	series, potentially linked to uncertainties related to fewer available observations in the final year (see
1436	e.g. Watson et al 2020, Pérez et al 2024). Specifically, the fCO ₂ -products' estimate of the last year is
1437	regularly adjusted in the following release owing to the tail effect and an incrementally increasing data
1438	availability. While the monthly grid cells covered may have a lag of only about a year (Figure 10b
1439	inset), the values within grid cells may change with 1-5 years lag (see absolute number of observations
1440	plotted in previous GCB releases), potentially resulting in annual changes in the flux magnitude from
1441	fCO ₂ -products.
1442	3.6.4 Year 2025 projection
1443	Using a feed-forward neural network method (see Section 2.5.2) we project an ocean sink of 3.3 ± 0.4
1444	GtC for 2025, which is a declining sink of 0.1 GtC compared to 2024, and can be explained by the
1445	generally lower ocean CO2 uptake following the El Niño event ending in 2024, consistent with the
1446	projected recovery of the atmospheric CO2 growth rate after a record high in 2024. The set of ESMs
1447	predictions support this estimate with a 2025 ocean sink of around 3.1 [3.0, 3.2] GtC. Taking the
1448	average of both estimates, we project an ocean sink of 3.2 \pm 0.4 GtC for 2025.
1449	3.6.5 Evaluation of ocean models and fCO ₂ -products
1450	The process-based model evaluation draws a generally positive picture with GOBMs scattered around
1451	the observational values for Southern Ocean sea-surface salinity, Southern Ocean stratification index
1452	and surface ocean Revelle factor, albeit outliers exist (Section S3.3 and Table S11). However, the
1453	Atlantic Meridional Overturning Circulation at 26°N is underestimated by 8 out of 10 GOBMs and
1454	overestimated by one GOBM. IOMB summarizes the GOBMs' performance across physical and
1455	biogeochemical data sets and various statistics relative to the GOBM ensemble (Figure S6). All
1456	GOBMs perform better in some variables compared to the other models, and worse in other variables.
1457	Despite the indication that GOBMs underestimate the ocean sink, low sink models do not perform
1458	generally worse than the other models; and similarly, high sink models do not perform better than the
1459	others.
1460	The model simulations allow to separate the anthropogenic carbon component and to compare the
1461	GOBMs DIC inventory change directly to the interior ocean estimates of Gruber et al. (2019), Müller et
1462	al. (2023) and the GOBM anthropogenic surface fluxes to DeVries (2022) without further assumptions
1463	(Table S11). The GOBMs ensemble average of anthropogenic carbon inventory changes 1994-2007
1464	amounts to 2.3 GtC yr $^{-1}$ and is thus lower than the 2.6 \pm 0.3 GtC yr $^{-1}$ estimated by Gruber et al. (2019)
1465	although within the uncertainty. Five models fall within the range reported by Gruber et al. (2019).
1466	Comparison to the decadal estimates of anthropogenic carbon accumulation (Müller et al., 2023) are
1467	close to the interior ocean data based estimate for the decade 2004-2014 (GOBMs sim D minus sim A,
1468	2.6 ± 0.4 GtC yr ⁻¹ , Müller et al. 2.7 ± 0.3 GtC yr ⁻¹), but do not reproduce the supposedly higher





1469	anthropogenic carbon accumulation in the earlier period 1994-2004 (GOBMs sim D minus sim A, 2.2 ± 10^{-2}
1470	$0.3~GtC~yr^{-1}$, Müller et al. $2.9\pm0.3~GtC~yr^{-1}$). Finally, the mean anthropogenic carbon uptake in
1471	GOBMs from 1985 to 2018 amounts to 2.3 GtC yr ⁻¹ , slightly lower than the corresponding observation-
1472	based uptake rate of 2.4 ± 0.2 Gt yr $^{-1}$ based on OCIM (DeVries, 2022; DeVries et al., 2023). Taken
1473	together, the comparison to observation-based estimates suggests that the majority of the GOBMs may
1474	underestimate anthropogenic carbon uptake by 10-20% and some models even more and are one line of
1475	evidence that supports the upscaling of GOBMs by 10% (Friedlingstein et al., 2025a, section 2.5.1).
1476	Interestingly, and in contrast to the uncertainties in the surface CO2 flux, we find the largest mismatch
1477	in interior ocean carbon accumulation in the tropics, with smaller contributions from the north and the
1478	south (Table S11). The large discrepancy in accumulation in the tropics highlights the role of interior
1479	ocean carbon redistribution for those inventories (Khatiwala et al., 2009, DeVries et al., 2023).
1480	Additional benchmarking of the fCO ₂ -products with independent data generally shows low and
1481	consistent biases and RMSEs, with the exception of the comparison with SOCAT flag E data in the
1482	tropics where the biases range from -6.6 μatm in JMA-MLR to -10.29 μatm in OceanSODA_ETHv2 ,
1483	(Figure S7) and the Northern Hemisphere, where biases range from -2.68 μatm in VLIZ-SOMFFN to -
1484	$40.47~\mu atm$ in UExP-FNN-U (Figure S7), although with few measurements covering the latter area.
1485	Furthermore, we evaluate the trends derived from a subset of fCO ₂ -products by subsampling five
1486	GOBMs used in Friedlingstein et al. (2023; covering the period up to the year 2022) following the
1487	approach of Hauck et al. (2023a) and evaluating the air-sea CO ₂ flux trend for the 2001-2021 period,
1488	i.e. the period of strong divergence in the air-sea CO ₂ exchange excluding the tail effect, against trend
1489	biases identified by the GOBM reconstruction. The results indicate a relationship between
1490	reconstruction bias and strength of the decadal trends (Figure S8), indicating a tendency of the fCO ₂ -
1491	products ensemble to overestimate the air-sea CO ₂ flux trends in agreement with Mayot et al. (2024).
1492	3.7 Land Sink
1493	3.7.1 Historical period 1850-2024
1494	Cumulated since 1850, the terrestrial carbon sink S_{LAND} amounts to 175 \pm 50 GtC, 24% of total
1495	anthropogenic emissions, with more than two thirds of this amount (120 \pm 40 GtC) being taken up by
1496	the terrestrial ecosystems since 1959. Over the historical period, the land sink increased in pace with the
1497	anthropogenic emissions exponential increase (Figure 3). As described in section 2, S_{LAND} estimate now
1498	includes the RSS correction.
1499	3.7.2 Recent period 1959-2024
1500	S_{LAND} increased from 0.9 ± 0.3 GtC yr $^{-1}$ in the 1960s to 2.4 ± 0.8 GtC yr $^{-1}$ during 2015-2024, with
1501	important interannual variations of up to 2 GtC yr ⁻¹ generally showing a decreased land sink during El





1502	Niño events (Figure 10a), responsible for the corresponding enhanced growth rate in atmospheric CO ₂
1503	concentration. The larger land CO ₂ sink during 2015-2024 compared to the 1960s is reproduced by all
1504	the DGVMs in response to the increase in both atmospheric CO ₂ , nitrogen deposition, and the changes
1505	in climate, and is broadly consistent with the residual estimated from the other budget terms
1506	(Efos+Eluc-Gatm-Socean, Table 5).
1507	Over the historical period, the increase in the global terrestrial CO ₂ sink is largely attributed to the CO ₂
1508	fertilisation effect (Prentice et al., 2001, Piao et al., 2009, Schimel et al., 2015) and increased nitrogen
1509	deposition (Huntzinger et al., 2017, O'Sullivan et al., 2019), directly stimulating plant photosynthesis
1510	and increased plant water use in water limited systems, with a smaller negative contribution of climate
1511	change (Figure 12). There is a range of evidence to support a positive terrestrial carbon sink in response
1512	to increasing atmospheric CO ₂ (Walker et al., 2021), including a new synthesis of free-air CO ₂ -
1513	enrichment experiments across forests and ages, which concluded that Net Primary Productivity
1514	increased by 22% for a common 41% CO ₂ enrichment (Norby 2025). As expected from theory, the
1515	greatest CO ₂ effect is simulated in the tropical forest regions, associated with warm temperatures and
1516	long growing seasons (Hickler et al., 2008) (Figure 12a). However, evidence from tropical intact forest
1517	plots indicate an overall decline in the land sink across Amazonia (1985-2011), attributed to enhanced
1518	mortality offsetting productivity gains (Brienen et al., 2015, Hubau et al., 2020). During 2015-2024 the
1519	land sink is positive in all regions (Figure 6d) with the exception of eastern Brazil, Bolivia, northern
1520	Venezuela, Southwest USA, central Europe and Central Asia, North and South Africa, and eastern
1521	Australia, where the negative effects of climate variability and change (i.e. reduced rainfall and/or
1522	increased temperature) counterbalance CO ₂ effects. This is clearly visible in Figure 12 where the effects
1523	of CO ₂ (Figure 12a) and climate (Figure 12b) as simulated by the DGVMs are isolated (see also Figure
1524	S12). The negative effect of climate can be seen across the globe, and is particularly strong in most of
1525	South America, Central America, Southwest US, Central Europe, western Sahel, southern Africa,
1526	Southeast Asia and southern China, and eastern Australia (Figure 12b, Figure S12). Globally, over the
1527	2015-2024 period, climate change reduces the land sink by 0.8 ± 0.7 GtC yr ⁻¹ (25% of the CO ₂ effect,
1528	which is 3.2 ± 1.1 GtC yr ⁻¹ for the corresponding period, see Supplement S4.1).
4.500	
1529	Most DGVMs have similar S _{LAND} averaged over 2015-2024, and 14/22 models fall within the 1σ range
1530	of the residual land sink [1.4 to 3.3 GtC yr ⁻¹] (see Table 5), and all models but one are within the 2σ
1531	range [0.5 to 4.3 GtC yr ⁻¹]. The ED model is an outlier, with a land sink estimate of 4.9 GtC yr ⁻¹ for the
1532	2015-2024 period (accounting for the RSS correction), driven by a strong CO ₂ fertilisation effect (6.4
1533	GtC yr ⁻¹ in the CO ₂ only (S1) simulation). There are no direct global observations of the land sink
1534	(S _{LAND}), or the CO ₂ fertilisation effect, and so we are not yet in a position to rule out models based on
1535	component fluxes if their net land sink (S_{LAND} - E_{LUC}) is within the observational uncertainty provided by
1536	O ₂ measurements. The important role of non-living carbon pools in carbon budgets has also been
1537	recently highlighted from an Earth-observation (EO) perspective, where contrary to DGVMs, EO





1538 products do not show an increase in biomass, thus inferring a larger role of dead carbon in land carbon 1539 cycle dynamics (Bar-On et al., 2025). 1540 Since 2020 the globe has experienced La Niña conditions which would be expected to lead to an 1541 increased land carbon sink. This 3-year long period of La Niña conditions came to an end by the second 1542 half of 2023 and transitioned to an El Niño which lasted until mid-2024. A clear transition from maximum to a minimum in the global land sink is evident in S_{LAND}, from 2022 to 2023 and we find that 1543 1544 an El Niño-driven decrease in tropical land sink is offset by a smaller increase in the high-latitude land 1545 sink. In the past years several regions experienced record-setting fire events (see also section 3.8.3). 1546 While global burned area has declined over the past decades mostly due to declining fire activity in 1547 savannas (Andela et al., 2017), forest fire emissions are rising and have the potential to counter the 1548 negative fire trend in savannas (Zheng et al., 2021). Noteworthy extreme fire events include the 2019-1549 2020 Black Summer event in Australia (emissions of roughly 0.2 GtC; van der Velde et al., 2021), 1550 Siberia in 2021, where emissions approached 0.4 GtC or three times the 1997-2020 average according 1551 to GFED4s, Canada in 2023 and 2024 (Byrne et al., 2024), and unprecedented wildfires in Brazil and 1552 Bolivia in 2024 (partly related to land-use activity, see Sec. 3.2.3 and 3.2.4) (Bourgoin et al., 2025), 1553 partially offset by a negative trend in wildfire over Northern Hemisphere Africa. While other regions, 1554 including Western US and Mediterranean Europe, also experienced intense fire seasons in 2021 their 1555 emissions are substantially lower. 1556 Despite these regional negative effects of climate change on SLAND, the efficiency of land to remove anthropogenic CO2 emissions has remained broadly constant over the last six decades at around 23% 1557 1558 (Figure S16). 1559 3.7.3 Final year 2024 1560 The terrestrial CO₂ sink from the DGVMs ensemble S_{LAND} was 1.9 ± 0.9 GtC in 2024, 37% below the 1561 2022 La Niña induced strong sink of 3.1 ± 1.0 GtC, and also below the 2015-2024 average of 2.4 ± 0.8 1562 GtC yr⁻¹ (Figure 4e, Table 7). We estimate that the 2024 land sink was the lowest since 2015. The 1563 severe reduction in the land sink in 2024 is likely driven by the El Niño conditions, leading to a 66% 1564 reduction in S_{LAND} in the tropics (30N-30S) from 2.8 GtC in 2022 to 1.0 GtC in 2024. This is combined with intense wildfires in Canada, Bolivia and Brazil that led to a significant CO2 source (see also 1565 1566 Section 3.8.3). We note that the S_{LAND} estimate for 2024 of 1.9 ± 0.9 GtC is much larger than the $0.3 \pm$ 1567 1.0 GtC yr⁻¹ estimate from the residual sink from the global budget (E_{FOS}+E_{LUC}-G_{ATM}-S_{OCEAN}, Table 5), 1568 although the residual sink would be substantially larger (at around 1.4 GtC yr⁻¹) if using the satellite-1569 based GRESO in this equation. A large budget imbalance is often associated with El Niño years (e.g. 1570 1986/87, 1997/98, 2005/06, 2023/24), and the possible underestimation in DGVMs of the tropical land 1571 response to drought and high temperature extremes. Few DGVMs have explicit representation of





1572	drought-mortality and only 8 from 22 include some form of forest demography, although recent efforts
1573	are underway to fill these critical research gaps (Eckes-Shephard et al., 2025 Yao et al., 2022, 2023).
1574	An overestimate in S_{LAND} in 2024 can in part be attributed to the inability in DGVMs to reproduce
1575	extreme fire emissions in 2024. Globally fire emissions as calculated by GFED were 0.43 GtC/yr higher
1576	in 2024 compared to the decadal average (2015-2024), similar to the anomaly in 2023 (0.44 GtC /yr).
1577	This was mainly due to an increase in fire over forests in Boreal North America (0.16 GtC/yr) and
1578	forests, savannahs and grasslands over Southern Hemisphere South America (0.35 GtC/yr) in 2024,
1579	partly offset by a negative trend in fires over Northern Hemisphere Africa (-0.05 GtC/yr anomaly). In
1580	fact, across the Amazon basin emissions from degradation fires (two thirds Brazil, one third Bolivia)
1581	surpassed those from deforestation fires in 2024 (Bourgoin et al., 2025). In contrast DGVMs simulate
1582	an anomaly of 0.2 GtC/yr in 2024, i.e. an underestimate of 0.23 GtC/yr in fire emissions for 2024.
1583	Finally, a large uncertainty relates to climate forcing datasets, particularly over the critical carbon-rich
1584	tropical forest regions with poor coverage of meteorological stations. For example, there are large
1585	differences in climate forcing (e.g. CRUJRA-3Q and ERA5) and downstream DGVM carbon
1586	simulations over the Congo basin and tropical central and northern Africa in 2024 (Ke et al., 2025).
1587	3.7.4 Year 2025 projection
1588	Calculating the land sink as the residual of the other projections for 2025, we project a land sink of 3.1
1589	GtC for 2025, 1.1 GtC larger than the 2024 estimate, consistent with an expected recovery of the land
1590	sink after an El Niño event. The ESMs do not provide an additional estimate of S_{LAND} as they only
1591	simulate the net atmosphere-land carbon flux (S_{LAND} - E_{LUC}).
1592	3.7.5 Evaluation of land models
1593	The evaluation of the DGVMs shows generally higher agreement across models for runoff, and to a
1594	lesser extent for GPP, and ecosystem respiration. These conclusions are supported by a more
1595	comprehensive analysis of DGVM performance in comparison with benchmark data (Sitch et al.,
1596	2024). A relative comparison of DGVM performance (Figure S11) suggests several DGVMs (CABLE-
1597	POP, CLASSIC, OCN, ORCHIDEE) may outperform others at multiple carbon and water cycle
1598	benchmarks. However, results from Seiler et al., 2022, also show how DGVM differences are often of
1599	similar magnitude compared with the range across observational datasets. All models score high
1600	enough over the metrics tests to support their use here. There are a few anomalously low scores for
1601	individual metrics from a single model, and these can direct the effort to improve models for use in
1602	future budgets (See also Supplement S.4.2).





1603 3.8 Partitioning the carbon sinks

3.8.1 Global sinks and spread of estimates

- In the period 2015-2024, the bottom-up view of global net ocean and land carbon sinks provided by the
 GCB, S_{OCEAN} for the ocean and S_{LAND}- E_{LUC} for the land, agrees closely with the top-down global
 carbon sinks delivered by the atmospheric inversions. This is shown in Figure 13, which visualises the
- 1608 individual decadal mean atmosphere-land and atmosphere-ocean fluxes from each, along with the
- 1609 constraints on their sum offered by the global fossil CO₂ emissions flux minus the atmospheric growth
- rate ($E_{FOS}-G_{ATM}$, 4.2 ± 0.5 Gt C yr⁻¹, Table 7, shown as diagonal line in Figure 13). The GCB estimate
- $1611 \qquad \text{for net atmosphere-to-surface flux } (S_{OCEAN} + S_{LAND} E_{LUC}) \ during \ 2015-2024 \ is \ 4.2 \pm 1.1 \ Gt \ C \ yr^{-1} \ during \ 2015-2024 \ is \ 4.2 \pm 1.1 \ during$
- $1612 \qquad \hbox{(Table 7), implying a zero budget imbalance (B_{IM}) (see Section 3.9). The atmospheric inversions}$
- estimate of the net atmosphere-to-surface flux during 2015-2024 is 4.3 Gt C yr^{-1} , with a \leq 0.1 GtC yr^{-1}
- 1614 imbalance, and thus scatter across the diagonal, with inverse models trading land for ocean fluxes in
- 1615 their solution. The independent constraint on the net atmosphere-to-surface flux based on atmospheric
- $1616 \qquad O_2 \ by \ design \ also \ closes \ the \ balance \ and \ is \ 4.2 \pm 0.9 \ GtC \ yr^{\text{-}1} \ over \ the \ 2015-2024 \ period \ (orange$
- symbol on Figure 13), while the ESMs estimate for the net atmosphere-to-surface flux over that period
- 1618 is 4.8 [2.4, 6.0] GtC yr⁻¹ (Tables 5 and 6).
- 1619 The distributions based on the individual models and fCO₂-products reveal substantial spread but
- 1620 converge near the decadal means quoted in Tables 5 to 7. Sink estimates for S_{OCEAN} are mostly non-
- 1621 Gaussian, while the ensemble of DGVMs and inverse models appears more normally distributed
- 1622 justifying the use of a multi-model mean and standard deviation for their errors in the budget.
- Noteworthy is that the tails of the distributions provided by the land and ocean bottom-up estimates
- would not agree with the global constraint provided by the fossil fuel emissions and the observed
- atmospheric CO2 growth rate. This illustrates the power of the atmospheric joint constraint from the
- 1626 global CO₂ observation capacity.

1627 3.8.1.1 Net atmosphere-to-land flux

- 1628 The GCB estimate of the net atmosphere-to-land flux (S_{LAND} E_{LUC}), calculated as the difference
- between S_{LAND} from the DGVMs and E_{LUC} from the bookkeeping models, amounts to a 1.0 ± 1.0 GtC
- $1630 ext{ yr}^{-1} ext{ sink during } 2015-2024 ext{ (Table 5)}. ext{ The estimate of net atmosphere-to-land flux } (S_{LAND} E_{LUC}) ext{ from}$
- 1631 the DGVMs alone $(1.4 \pm 0.7 \text{ GtC yr}^{-1}, \text{Table 5, green symbols on Figure 13})$ is slightly larger, although
- within the uncertainty of the GCB estimate and also within uncertainty of the global carbon budget
- 1633 constraint ($E_{FOS} G_{ATM} S_{OCEAN}$, 1.0 ± 0.6 GtC yr⁻¹; Table 7). Also, for 2015-2024, the inversions
- estimate the net atmosphere-to-land flux is a 1.3 ± 0.3 GtC yr⁻¹ sink, similar to the mean of the DGVMs
- estimates (purple versus grey symbols on Figure 13). The independent constraint based on atmospheric
- O_2 is slightly lower, 0.7 ± 0.8 GtC yr⁻¹ (orange symbol in Figure 13), although its uncertainty overlaps





103/	with the uncertainty range from other approaches. Last, the ESIMS estimate for the net atmosphere-to-
1638	land flux during 2014-2023 is a 2.3 $[-0.1, 3.6]$ GtC yr^{-1} sink, larger than all other estimates (Table 5).
1639	As discussed in Section 3.5.3, the atmospheric growth rate of CO ₂ derived from the NOAA surface
1640	stations was very high in 2024, 7.9 GtC (3.73 ppm) the largest on the 65 years long observational
1641	record. Both DGVMs and inversions assign this large CO2 growth rate to a continued reduction of the
1642	net atmosphere to land flux since 2023, in particular in the tropics (Figures 11 and 14), especially
1643	pronounced in the inversions. DGVMs simulate a 2024 global net atmosphere-to-land flux of 1.1 GtC
1644	yr ⁻¹ , a 50% decline relative to the 2.2 GtC yr ⁻¹ sink in 2022, primarily driven by the severe reduction in
1645	S _{LAND} (-37%, see Section 3.7.3). The tropics (30°N-30°S) are recording a dramatic decrease in the net
1646	atmosphere-to-land flux from a 1.3 GtC yr ⁻¹ sink in 2022 to a 0.2 GtC yr ⁻¹ source in 2024. The
1647	atmospheric inversions show a continued reduction with the global net atmosphere-to-land flux
1648	declining from 2.9 GtC yr ⁻¹ in 2022 to 0.8 GtC yr ⁻¹ in 2023 to 0.2 GtC yr ⁻¹ in 2024 (-94% from 2022 to
1649	2024), with the tropics turning from a 1.3 GtC yr^{-1} sink in 2022 to a 1.2 GtC yr^{-1} source in 2024.
1650	3.8.1.2 Net atmosphere-to-ocean flux
1651	For the 2015-2024 period, the unadjusted GOBMs (2.7 \pm 0.4 GtC yr ⁻¹) produce a lower estimate for
1652	S _{OCEAN} than the unadjusted fCO ₂ -products with 3.3 [2.9, 3.8] GtC yr ⁻¹ , which shows up in Figure 13 as
1653	separate peaks in the distribution from the GOBMs (dark blue symbols) and from the fCO2-products
1654	(light blue symbols). Atmospheric inversions (3.0 \pm 0.3 GtC yr $^{\!-1}$) suggest an ocean uptake more in line
1655	with the average of the GOBMs and fCO ₂ -products for the recent decade (Table 6). The inversions are
1656	not fully independent as 7 out of 14 inversions covering the last decade use fCO2-products as ocean
1657	priors and one uses a GOBM (Table S4). The independent constraint based on atmospheric O2 (3.5 \pm
1658	0.5 GtC yr 1) is at the high end of the distribution of the other methods. However, as mentioned in
1659	section 2.8, the O2 method requires a correction for global air-sea O2 flux, which induces a non-
1660	negligible uncertainty on the decadal estimates (about 0.5 GtC yr ⁻¹). The large growth in the ocean
1661	carbon sink from O2 is compatible with the GOBMs and fCO2-products estimates when accounting for
1662	their uncertainty ranges. Lastly, the ESMs estimate, 2.5 [2.2, 2.8] GtC yr ⁻¹ , suggest a lower average
1663	ocean carbon sink than the other estimates. We caution that the riverine transport of carbon taken up on
1664	land and outgassing from the ocean, accounted for here, is a substantial (0.65 \pm 0.3 GtC yr $^{\text{-}1})$ and
1665	uncertain term (Crisp et al., 2022; Gruber et al., 2023; DeVries et al., 2023) that separates the GOBMs,
1666	ESMs and oxygen-based estimates on the one hand from the fCO ₂ -products and atmospheric inversions
1667	on the other hand.
1668	3.8.2 Regional partitioning
1669	Figure 14 shows the latitudinal partitioning of the global atmosphere-to-ocean (Socean), atmosphere-to-ocean
1670	land (S _{LAND} – E _{LUC}), and their sum (S _{OCEAN} + S _{LAND} – E _{LUC}) according to the estimates from GOBMs





- and ocean fCO₂-products (S_{OCEAN}), DGVMs (S_{LAND} E_{LUC}), and from atmospheric inversions (S_{OCEAN}
- and S_{LAND} E_{LUC}). S_{OCEAN} estimates were not adjusted for the regional analysis.

1673 **3.8.2.1 North**

- Despite being one of the most densely observed and studied regions of our globe, annual mean carbon
- sink estimates in the northern extra-tropics (north of 30°N) continue to differ. The atmospheric
- inversions suggest an atmosphere-to-surface sink ($S_{OCEAN} + S_{LAND} E_{LUC}$) for 2015-2024 of 2.7 ± 0.4
- 1677 GtC yr⁻¹, which is higher than the process models' estimate of 2.0 ± 0.4 GtC yr⁻¹ (Figure 14). The
- GOBMs $(1.1 \pm 0.2 \text{ GtC yr}^{-1})$, fCO₂-products $(1.4 [1.2-1.6] \text{ GtC yr}^{-1})$, and inversion systems $(1.2 \pm 0.1) \text{ Gr}^{-1}$
- 1679 GtC yr⁻¹) produce largely consistent estimates of the ocean sink. However, the larger flux in the fCO₂-
- products may be related to data sparsity (Mayot et al., 2024). Thus, the difference mainly arises from
- the net land flux ($S_{LAND} E_{LUC}$) estimate, which is 0.9 ± 0.3 GtC yr¹ in the DGVMs compared to $1.5 \pm$
- 1682 0.4 GtC yr⁻¹ in the atmospheric inversions (Figure 14, second row).
- 1683 Discrepancies in the northern land fluxes conform with persistent issues surrounding the quantification
- of the drivers of the global net land CO₂ flux (Arneth et al., 2017; Huntzinger et al., 2017; O'Sullivan et
- al., 2022) and the distribution of atmosphere-to-land fluxes between the tropics and high northern
- latitudes (Baccini et al., 2017; Schimel et al., 2015; Stephens et al., 2007; Ciais et al., 2019; Gaubert et
- 1687 al., 2019; O'Sullivan et al. 2024).
- 1688 In the northern extra-tropics, the process models, inversions, and fCO₂-products consistently suggest
- that most of the interannual variability stems from the land (Figure 14). Inversions generally agree on
- the magnitude of interannual variations (IAV) over land, more so than DGVMs (0.27-0.38 vs 0.07-0.55
- 1691 GtC yr⁻¹, averaged over 1990-2024).

1692 **3.8.2.2 Tropics**

- 1693 In the tropics (30°S-30°N), both the atmospheric inversions and process models estimate a net carbon
- $1694 \qquad \text{balance } (S_{OCEAN} + S_{LAND} E_{LUC}) \text{ that is relatively close to neutral over the past decade (inversions: } 0.05$
- ± 0.5 GtC yr⁻¹, process models: 0.4 ± 0.6 GtC yr⁻¹). The GOBMs (-0.003 ± 0.3 GtC yr⁻¹), fCO₂-products
- 1696 (0.3 [0.1, 0.6] GtC yr¹), and inversion systems (0.3 \pm 0.1 GtC yr¹) indicate a neutral to positive tropical
- ocean flux (see Figure S5 for spatial patterns). DGVMs indicate a net land sink (S_{LAND} E_{LUC}) of 0.4
- 1698 ±0.5 GtC yr⁻¹, whereas the inversion systems indicate a small source in the net land flux although with
- larger model spread (-0.2 \pm 0.6 GtC yr⁻¹, Figure 14, third row).
- 1700 A continuing conundrum is the partitioning of the global atmosphere-land flux between the Northern
- Hemisphere land and the tropical land (Stephens et al., 2017; Pan et al., 2011; Gaubert et al., 2019). It is
- 1702 of importance because each region has its own history of land-use change, climate drivers, and impact
- 1703 of increasing atmospheric CO₂ and nitrogen deposition. Quantifying the magnitude of each sink is a





1704 prerequisite to understanding how each individual driver impacts the tropical and mid/high-latitude 1705 carbon balance. We define the North-South (N-S) difference as net atmosphere-land flux north of 30°N 1706 minus the net atmosphere-land flux south of $30^{\circ}N$. For the inversions, the N-S difference is 1.7 ± 1.0 1707 GtC yr $^{-1}$ across this year's inversion ensemble. In the ensemble of DGVMs the N-S difference is $0.6\pm$ 1708 0.5 GtC yr⁻¹, a much narrower range than the one from atmospheric inversions. The smaller spread 1709 across DGVMs than across inversions is to be expected as there is no correlation between Northern and Tropical land sinks in the DGVMs as opposed to the inversions where the sum of the two regions being 1710 1711 well-constrained by atmospheric observations leads to an anti-correlation between these two regions. 1712 The tropical lands are the origin of most of the atmospheric CO₂ interannual variability (Ahlström et al., 1713 2015), consistently among the process models and inversions (Figure 14). The interannual variability in the tropics is similar among the ocean fCO₂-products (0.06-0.18 GtC yr⁻¹) and the GOBMs (0.07-0.16 1714 GtC yr⁻¹). The DGVMs and inversions indicate that atmosphere-to-land CO₂ fluxes are more variable 1715 1716 than atmosphere-to-ocean CO₂ fluxes in the tropics, with interannual variability of 0.3 to 1.13 and 0.96 GtC yr⁻¹ for DGVMs and inversions, respectively for 1990-2024. The year 2024 saw the largest growth 1717 1718 rate in the atmosphere so far, largely caused by reductions in the tropical land sink, similar to earlier 1719 extreme years, such as during the 2015-2016 El Niño period. The inversions seem to capture the 1720 response of the tropical land sink to a larger degree than the DGVMs, with a 2024 tropical land source 1721 of 1.2 ± 0.9 GtC yr⁻¹ for the inversions versus 0.2 ± 0.7 for the DGVMs.

1722 **3.8.2.3 South**

1723 In the southern extra-tropics (south of 30°S), the atmospheric inversions suggest a net atmosphere-to-1724 surface sink ($S_{OCEAN}+S_{LAND}-E_{LUC}$) for 2015-2024 of 1.6 \pm 0.2 GtC yr¹, similar to the process models' 1725 estimate of 1.5 ± 0.4 GtC yr⁻¹ (Figure 14). An approximately neutral net land flux (S_{LAND} - E_{LUC}) for the 1726 southern extra-tropics is estimated by both the DGVMs $(0.05 \pm 0.1 \text{ GtC yr}^{-1})$ and the inversion systems 1727 $(0.01 \pm 0.1 \text{ GtC yr}^{-1})$. This means nearly all carbon uptake is due to oceanic sinks south of 30°S. The Southern Ocean flux in the fCO₂-products (1.6 [1.5, 1.9 GtC] yr⁻¹) and inversion estimates (1.6 \pm 0.2 1728 1729 GtC yr⁻¹) is marginally higher than in the GOBMs $(1.5 \pm 0.4 \text{ GtC yr}^{-1})$ (Figure 14, bottom row). This 1730 agreement is subject to the choice of the river flux adjustment (Lacroix et al., 2020, Hauck et al., 1731 2023b). Nevertheless, the time-series of atmospheric inversions and fCO₂-products diverge from the 1732 GOBMs. A substantial overestimation of the trends in the fCO₂-products could be explained by sparse 1733 and unevenly distributed observations, especially in wintertime (Figure S5; Hauck et al., 2023a; Gloege 1734 et al., 2021). Model biases likely contribute as well, with biases in mode water formation, stratification, 1735 and the chemical buffer capacity known to play a role in Earth System Models (Terhaar et al., 2021, 1736 Bourgeois et al., 2022, Terhaar et al., 2022).





1737	The interannual variability in the southern extra-tropics is low because of the dominance of ocean areas
1738	with low variability compared to land areas. The split between land (S_{LAND} - E_{LUC}) and ocean (S_{OCEAN})
1739	shows a substantial contribution to variability in the south coming from the land, with no consistency
1740	between the DGVMs and the inversions or among inversions. This is expected due to the difficulty of
1741	separating exactly the land and oceanic fluxes when viewed from atmospheric observations alone. The
1742	S_{OCEAN} interannual variability was found to be higher in the fCO_2 -products (0.04-0.18 GtC yr $^{-1}$)
1743	compared to GOBMs (0.03 to 0.06 GtC ${\rm yr}^{-1}$) in 1990-2024. Inversions give an interannual variability
1744	of 0.13 to 0.15 GtC yr ⁻¹ . Model subsampling experiments recently illustrated that fCO ₂ -products may
1745	overestimate decadal variability in the Southern Ocean carbon sink by 30% and the trend since 2000 by
1746	50-130% due to data sparsity, based on one and two fCO ₂ -products with strong variability (Gloege et
1747	al., 2021, Hauck et al., 2023a). The trend benchmark test using the method of Hauck et al., (2023a) and
1748	a subset of 6 fCO ₂ -products confirms the sensitivity of the decadal trends in fCO ₂ -products to
1749	reconstruction biases, particularly in the Southern Ocean, indicating an overestimation of the ensemble
1750	mean trend (See Supplement S.3.4). However, we also find compensating positive biases in the
1751	ensemble so that the ensemble mean bias is smaller than the bias from some individual f CO ₂ -products.
1752	3.8.2.4 RECCAP2 regions
1753	Aligning with the RECCAP-2 initiative (Ciais et al., 2022; Poulter et al., 2022; DeVries et al., 2023),
1754	we provide a breakdown of this GCB paper estimate of the E_{LUC} , S_{LAND} , Net land $(S_{LAND}$ - $E_{LUC})$, and
1755	S _{OCEAN} fluxes over the 10 land, and 5 ocean RECCAP-2 regions, averaged over the period 2015-2024
1756	(Figure 15). The DGVMs and inversions suggest a positive net land sink in all regions, except for South
1757	America, Africa, and Southeast Asia, where the inversions indicate a small net source of respectively -
1758	$0.1\pm0.5~GtC~yr^{-1}, -0.3\pm0.3~GtC~yr^{-1}, and~-0.1\pm0.3~GtC~yr^{-1}~compared~to~a~small~sink~of~0.1\pm0.3~GtC~yr^{-1}$
1759	yr^{-1} , $0.1\pm0.3~GtC~yr^{-1}$, and $0.03\pm0.1~GtC~yr^{-1}$ for the DGVMs. The uncertainty in the sign of net
1760	tropical carbon fluxes is driven by opposing gross fluxes and relatively large uncertainty in the gross
1761	fluxes themselves. For South America, DGVMs estimate S_{LAND} of 0.4 ± 0.4 GtC yr^{-1} and E_{LUC} of
1762	$0.3\pm0.2~GtC~yr^{-1}$. Bookkeeping models suggest a larger E_{LUC} source of around $0.5~GtC~yr^{-1}$. Similarly,
1763	in Southeast Asia, the DGVMs estimate an E_{LUC} of $0.2\pm0.1~GtC~yr^{-1}$, compared with the bookkeeping
1764	model estimate of 0.4 \pm 0.02 GtC yr $^{-1}$. Therefore, DGVMs may underestimate E_{LUC} in these regions,
1765	which could explain the net sink discrepancy with inversions. In Africa, E_{LUC} is similar for DGVMs and
1766	bookkeeping models (\sim 0.4 GtC yr $^{-1}$), and DGVMs estimate an S_{LAND} of 0.5 \pm 0.2 GtC yr $^{-1}$.
1767	The inversions suggest the largest net land sinks are located in North America (0.4±0.3 GtC yr ⁻¹),
1768	Russia $(0.6\pm0.2~{\rm GtC~yr}^{-1})$, Europe $(0.3\pm0.2~{\rm GtC~yr}^{-1})$, and East Asia $(0.2\pm0.3~{\rm GtC~yr}^{-1})$. This agrees
1769	well with the DGVMs in North America (0.4±0.1 GtC yr ⁻¹), which indicate a large natural land sink





- 1771 DGVMs suggest a smaller net land sink in Russia compared to inversions (0.3±0.1 GtC yr⁻¹), and a 1772 similar net sink in East Asia (0.2±0.1 GtC yr⁻¹). 1773 There is generally a higher level of agreement in the estimates of regional Socean between the different 1774 data streams (GOBMs, fCO2-products and atmospheric inversions) on decadal scale, compared to the 1775 agreement between the different land flux estimates. All data streams agree that the largest contribution 1776 to Socean stems from the Southern Ocean due to a combination of high flux density and large surface 1777 area, but with important contributions also from the Atlantic (high flux density) and Pacific (large area) basins. In the Southern Ocean, GOBMs suggest a sink of 1.1±0.4 GtC yr⁻¹, in line with the fCO₂-1778 products (1.1 [1.0,1.2] GtC yr⁻¹) and atmospheric inversions (1.1±0.2 GtC yr⁻¹). There is similar 1779 agreement in the Pacific Ocean, with GOBMs, fCO2-products, and atmospheric inversions indicating a 1780 1781 sink of 0.6±0.1 GtC yr⁻¹, 0.7 [0.6,0.9] GtC yr⁻¹, and 0.6±0.2 GtC yr⁻¹, respectively. However, in the Atlantic Ocean, GOBMs simulate a sink of 0.5±0.1 GtC yr⁻¹, noticeably lower than both the fCO₂-1782 products (0.8 [0.7,0.9] GtC yr⁻¹) and atmospheric inversions (0.8±0.1 GtC yr⁻¹). It is important to note 1783 the fCO₂-products and atmospheric inversions have a substantial and uncertain river flux adjustment in 1784 the Atlantic Ocean (0.3 GtC yr⁻¹) that also leads to a mean offset between GOBMs and fCO₂-1785 products/inversions in the latitude band of the tropics (Figure 14). The Indian Ocean due its smaller size 1786 and the Arctic Ocean due to its size and sea-ice cover that prevents air-sea gas-exchange are responsible 1787 for smaller but non negligible Socian fluxes (Indian Ocean: (0.3±0.1 GtC yr⁻¹, 0.3 [0.3,0.4] GtC yr⁻¹, 1788 and 0.3±0.1 GtC yr⁻¹ for GOBMs, fCO₂-products, and atmospheric inversions, respectively, and Arctic 1789 Ocean: (0.1±0.03 GtC yr⁻¹, 0.2 [0.1,0.3] GtC yr⁻¹, and 0.1±0.04 GtC yr⁻¹ for GOBMs, fCO₂-products, 1790 1791 and atmospheric inversions, respectively). Note that the Socean numbers presented here deviate from
- 1796 **3.8.3** Fire emissions in 2025

1793

1794

1795

1797 Fire emissions so far in 2025 have been below the average of recent decades, chiefly due to the lowest 1798 emissions on record since 2003 across the tropics. Figure S14 shows global and regional emissions 1799 estimates for the period 1st Jan-30th September in each year 2003-2025. Estimates derive from two 1800 global fire emissions products: the global fire emissions database (GFED, version 4.1s; van der Werf et 1801 al., 2017), and the global fire assimilation system (GFAS, operated by the Copernicus Atmosphere 1802 Service; Kaiser et al., 2012). The two products estimate that global emissions from fires were 1.2-1.4 GtC (the range reflecting the difference between the two fire emission datasets, actual uncertainties are 1803 larger and estimates are likely conservative, see Chen et al. (2023)) during January-September 2025. 1804

numbers reported in RECCAP-2 where the net air-sea CO₂ flux is reported (i.e. without river flux

as major uncertainty, e.g. Sarma et al., 2023, DeVries et al., 2023).

adjustment for fCO2-products and inversions, and with river flux adjustment subtracted from GOBMs

in most chapters, or comparing unadjusted datasets with discussion of uncertain regional riverine fluxes





1805	These estimates are 19-20% below the 2015-2024 average for the same months (1.5-1.7 GtC). Both the
1806	GFED4.1s and GFAS products show the second-lowest January-September fire emissions since 2003
1807	(2022 is the lowest year in both products).
1808	Notably, the year 2025 follows two years with above-average global fire emissions (Figure S14), with
1809	global emissions through September totalling 1.7-2.1 GtC in 2023 and 1.6-2.2 GtC in 2024. These high
1810	emissions totals were caused by high emissions in North America in 2023 principally in Canada; Jones
1811	et al., 2024b), and in both North America and South America in 2024 (principally in Canada and Brazil;
1812	Kelley et al., 2025). For example, in January-September 2024, GFED4.1s suggests that global
1813	emissions totalled 2.2 GtC, the highest total on record for these months and 32% above the average for
1814	the decade prior (2014-2023; GFAS also suggests that emissions were 11% above the average for
1815	January-September).
1816	Despite low global fire emissions so far in 2025, a pattern of extremely high fire emissions from
1817	Canada has now persisted for three consecutive years commencing with the record-breaking year in
1818	2023 (Jones et al., 2024b, Byrne et al., 2024; Kelley et al., 2025). In January-September 2025, fire
1819	emissions from Canada (0.3-0.4 GtC) were slightly greater than in the same months of 2024 (0.2-0.3
1820	GtC yr ⁻¹) and around half as large as those in the same months of 2023 (0.5-0.8 GtC). The emissions
1821	totals for Canada in January-September 2025 were 2.2 times the average of January-September periods
1822	during the prior decade 2015-2024 and 4-6 times greater than the average of those months in 2003-2022
1823	[excluding the record-breaking year in 2023]; Figure S14). According to GFED4.1s, January-
1824	September fire emissions from Canada in just the past three years (1.5 GtC) exceeded the country's
1825	total January-September fire emissions throughout the 20 years prior (1.2 GtC during 2003-2022). The
1826	continued anomaly in Canada propagated to the Northern Hemisphere, where January-September 2025
1827	emissions of 0.4-0.5 GtC were 13-21% above the average of 2015-2024.
1828	Fire emissions anomalies in Africa strongly influence global fire emissions totals because the continent
1829	typically contributed near 50% of global fire emissions during 2015-2024 (average of January-
1830	September periods). For 2025, fire emissions in Africa through September were 0.4-0.6 GtC, 19-25%
1831	below the average of 2015-2024 (0.6-0.8 GtC). Synchronously, emissions through September from
1832	South America were around 0.1 GtC in both GFED4.1s and GFAS systems, less than half of the
1833	average for 2015-2024 (0.2-0.3 GtC), and emissions from Southeast Asia were around 0.05 GtC, also
1834	less than half of the average for 2015-2024 (0.1 GtC in both GFED4.1s and GFAS). Low emissions
1835	from the tropical parts of Africa, South America, and Southeast Asia contribute to low emissions across
1836	the global tropics so far in 2025 (0.7-0.9 GtC), which were only around two-thirds of the average for
1837	2015-2024 (1.1-1.3 GtC) in both GFED4.1s and GFAS.
1838	We caution that the fire emissions fluxes presented here should not be compared directly with other
1839	fluxes of the budget (e.g. S_{LAND} or E_{LUC}) due to incompatibilities between the observable fire emission





1840	fluxes and what is quantified in the S_{LAND} and E_{LUC} components of the budget. The fire emission
1841	estimates from global fire products relate to all fire types that can be observed in Earth Observations
1842	(Giglio et al., 2018; Randerson et al., 2012; Kaiser et al., 2012), including (i) fires occurring as part of
1843	natural disturbance-recovery cycles that would also have occurred in the pre-industrial period (Yue et
1844	al., 2016; Keeley and Pausas, 2019; Zou et al., 2019), (ii) fires occurring above and beyond natural
1845	disturbance-recovery cycle due to changes in climate, CO2 and N fertilisation and to an increased
1846	frequency of extreme drought and heatwave events (Abatzoglou et al., 2019; Jones et al., 2022; Zheng
1847	et al., 2021; Burton et al., 2024), and (iii) fires occurring in relation to land use and land use change,
1848	such as deforestation fires and agricultural fires (van der Werf et al., 2010; Magi et al., 2012). In the
1849	context of the global carbon budget, fire emissions associated with (ii) should be included in the S_{LAND}
1850	component, fire emissions associated with (iii) should already be accounted for in the $E_{\text{\tiny LUC}}$ component,
1851	while fire emissions associated with (i) should not be included in the global carbon budget as part of the
1852	natural carbon cycle. However, it is not currently possible to derive specific estimates for fluxes (i), (ii),
1853	and (iii) using global fire emission products such as GFED or GFAS. In addition, the fire emissions
1854	estimates from global fire emissions products represent a gross flux of carbon to the atmosphere,
1855	whereas the S_{LAND} component of the budget is a net flux that should also include post-fire recovery
1856	fluxes. Even if emissions from fires of type (ii) could be separated from those of type (i), these fluxes
1857	may be partially or wholly offset in subsequent years by post-fire fluxes as vegetation recovers,
1858	sequestering carbon from the atmosphere to the terrestrial biosphere (Yue et al., 2016; Jones et al.,
1859	2024c). Increases in forest fire emissions and severity (emissions per unit area) globally during the past
1860	two decades have highlighted the increasing potential for fire emissions fluxes to outweigh post-fire
1861	recovery fluxes, though long-term monitoring of vegetation recovery is required to quantify the net
1862	effect on terrestrial C storage (Jones et al., 2024c).

3.9 Closing the global carbon cycle

1863

1865

1864 3.9.1 Partitioning of cumulative emissions and sink fluxes

1866	atmosphere (290 \pm 5 GtC; 39%), ocean (200 \pm 40 GtC; 27%), and land (175 \pm 50 GtC; 24%). The
1867	cumulative land sink is lower than the cumulative land-use emissions (250 ±65 GtC), making the
1868	global land a source of 75 ± 80 GtC over the whole 1850-2024 period (Table 8).
1869	The use of nearly independent estimates for the individual terms of the global carbon budget shows a
1870	cumulative budget imbalance of 80 GtC (11% of total emissions) during 1850-2024 (Table 8), which
1871	suggests that emissions could be slightly too high by the same proportion or that the combined land and
1872	ocean sinks are underestimated (by up to 20%). A large part of the B_{IM} occurs over the first half of the
1873	20th century (Figure 3, red dashed line) and could originate from the estimation of significant increase
1874	in E_{FOS} and E_{LUC} between the mid 1920s and the mid 1960s which is unmatched by a similar growth in

Emissions during the period 1850-2024 amounted to 745 ± 65 GtC and were partitioned among the





1875	atmospheric CO ₂ concentration as recorded in ice cores (Figure 3). Also, we now correct the S _{LAND}
1876	estimate for historical reduction in forest cover (see Section 2.6). This reduces the S_{LAND} estimate by
1877	about 40 GtC over the 1850-2024 period, contributing to the increase of the historical budget imbalance
1878	in comparison to GCB2024 (Friedlingstein et al., 2025a).
1879	For the more recent 1959-2024 period where direct atmospheric CO ₂ measurements are available, total
1880	emissions (EFOS + ELUC) amounted to 530 ± 50 GtC, of which 420 ± 20 GtC (79%) were caused by
1881	fossil CO_2 emissions, and 110 ± 45 GtC (21%) by land-use change (Table 8). The total emissions were
1882	partitioned among the atmosphere (230 \pm 5 GtC; 44%), ocean (145 \pm 30 GtC; 27%), and the land (120
1883	\pm 30 GtC; 23%), with a budget imbalance of 35 GtC (7% of total emissions). All components except
1884	land-use change emissions have significantly grown since the 1960s, with important interannual
1885	variability in the growth rate in atmospheric CO ₂ concentration primarily mirrored in the land CO ₂ sink
1886	(Figure 4), and some decadal variability in all terms (Table 7). Differences with previous budget
1887	releases are documented in Figure S15.
1888	The global carbon budget averaged over the last decade (2015-2024) is shown in Figure 2 and Table 7.
1889	For this period, 88% of the total emissions ($E_{FOS} + E_{LUC}$) were from fossil CO_2 emissions (E_{FOS}), and
1890	12% from land-use change (E _{LUC}). The total emissions were partitioned among the atmosphere (50%),
1891	ocean (29%) and land (21%), with a near zero budget imbalance (0.1%, <0.1 GtC yr ⁻¹). We note that,
1892	compared to GCB2024, we largely reduced the B_{IM} over the 2015-2024 period, but at the cost of
1893	increasing the B_{IM} over the 1959-2024 period.
1894	For single years, the budget imbalance can be larger (Figure 4f). For 2024, the combination of our
1895	estimated anthropogenic sources ($11.6 \pm 0.9 \; \text{GtC yr}^{-1}$) and partitioning in atmosphere, land and ocean
1896	$(13.3 \pm 0.9~\text{GtC yr}^{-1})$ leads to a large negative B_{IM} of -1.7 GtC (Table 7), indicating that, despite the
1897	lower than average land sink in 2024, the combined land and ocean sink is still too large to explain the
1898	record-high atmospheric CO ₂ growth rate of 2024.
1899	3.9.2 Trend and variability in the carbon budget imbalance
1900	The carbon budget imbalance (B _{IM} ; Eq. 1, Figure 4f) quantifies the mismatch between the estimated
1901	total emissions and the estimated changes in the atmosphere, land, and ocean reservoirs. The budget
1902	imbalance from 1959 to 2024 is small (35 GtC cumulated over the period, i.e. 0.5 GtC yr ⁻¹ on average)
1903	and shows no significant trend over the 1959-2024 period (Figure 4). The process models (GOBMs and
1904	DGVMs) and fCO ₂ -products have been selected to match observational constraints in the 1990s, but no
1905	further constraints have been applied to their representation of trend and variability. Therefore, the
1906	small mean and trend in the budget imbalance can be seen as evidence of a coherent community
1907	understanding of the emissions and their partitioning on those time scales (Figure 4). However, the





1908 budget imbalance shows substantial variability of the order of ±1 GtC yr⁻¹, particularly over semi-1909 decadal time scales, although most of the variability is within the uncertainty of the estimates. 1910 We cannot attribute the cause of the budget imbalance with our analysis, we only note that the budget 1911 imbalance is unlikely to be explained by errors in the emissions alone because of its large semi-decadal 1912 variability component, a variability that is atypical of emissions, and also because the budget imbalance 1913 has not increased in the past 60 years despite a near tripling in anthropogenic emissions (Figure 4). 1914 Errors in SLAND and SOCEAN are more likely to be the main cause for the budget imbalance, especially on 1915 interannual to semi-decadal timescales. For example, underestimation of the S_{LAND} by DGVMs has 1916 been reported following the eruption of Mount Pinatubo in 1991 possibly due to missing responses to 1917 changes in diffuse radiation (Mercado et al., 2009). Although we account for aerosol effects on solar 1918 radiation quantity and quality (diffuse vs direct), most DGVMs only used the former as input (i.e., total 1919 solar radiation) (Table S1). Thus, the ensemble mean may not capture the full effects of volcanic 1920 eruptions, i.e. associated with high light scattering sulphate aerosols, on the land carbon sink 1921 (O'Sullivan et al., 2021), potentially explaining the large positive B_{IM} in 1991-1992. DGVMs are 1922 suspected to underestimate the land sink reduction in response to El Niño events (see Section 3.7.3), 1923 which could explain the large negative B_{IM} in 1986-1987, 1997-1998 or 2023-2024). Quasi-decadal 1924 variability in the ocean sink has also been reported, with all methods agreeing on smaller than expected 1925 ocean CO2 sink in the 1990s and a larger than expected sink in the 2000s (Figure 10b; Landschützer et 1926 al., 2016, DeVries et al., 2019, Hauck et al., 2020, McKinley et al., 2020, Gruber et al., 2023) and the 1927 climate-driven variability could be substantial but is not well constrained (DeVries et al., 2023, Müller 1928 et al., 2023). Errors in sink estimates could also be partly driven by errors in the climatic forcing data, 1929 particularly precipitation for S_{LAND} and wind for S_{OCEAN}. 1930 Although the budget imbalance is near zero for the most recent decade, it could be due to a 1931 compensation of errors. We cannot exclude an overestimation of CO₂ emissions, particularly from land-1932 use change, given their large uncertainty, as has been suggested elsewhere (Piao et al., 2018), and/or an 1933 underestimate of the land or ocean sinks. A larger estimate of the atmosphere-land CO2 flux (SLAND-1934 ELUC) over the extra-tropics would reconcile bottom-up model results with inversion estimates (Figure 1935 14). Likewise, a larger S_{OCEAN} is also possible given the higher estimates from the fCO₂-products and 1936 the oxygen based estimates (see Table 6 and Figure 10b), the underestimation of interior ocean 1937 anthropogenic carbon accumulation in the GOBMs (Section 3.6.5, Müller et al., 2023), or known biases 1938 of ocean models (e.g., Terhaar et al., 2022; 2024). More integrated use of observations in the global 1939 carbon budget, either on their own or for further constraining model results, should help resolve some 1940 of the budget imbalance.

1942





4 Tracking progress towards mitigation targets

1943 driven by the rapid growth in emissions in China. In the last decade, however, the global growth rate 1944 has slowly declined, reaching a low +0.8% per year over 2015-2024. While this slowdown in global 1945 fossil CO₂ emissions growth is welcome, global fossil CO₂ emissions continue to grow, far from the 1946 rapid emission decreases needed to be consistent with the temperature goals of the Paris Agreement. 1947 Since the 1990s, the average growth rate of fossil CO₂ emissions has continuously declined across the 1948 group of developed countries of the Organisation for Economic Co-operation and Development 1949 (OECD), with emissions peaking in around 2005 and declining at 1.5% yr⁻¹ in the decade 2015-2024, 1950 compared to a decline of 0.9% yr⁻¹ during the 2005-2014 period (Table 9). In the non-OECD countries, 1951 emissions rose 4.6% yr⁻¹ from 2005-2014, but growth has lowered to 2.1% yr⁻¹ from 2015-2024. In the 1952 decade 2015-2024, territorial fossil CO2 emissions decreased significantly (at the 95% confidence level) 1953 in 35 countries whose economies grew significantly (also at the 95% confidence level): Andorra, 1954 Australia, Austria, Belgium, Bulgaria, Czechia, Denmark, Estonia, Finland, France, Germany, Greece, 1955 Hungary, Ireland, Israel, Jordan, Latvia, Luxembourg, Netherlands, New Zealand, Norway, Poland, 1956 Portugal, South Korea, Romania, Serbia, Slovakia, Slovenia, Spain, Sweden, Switzerland, Taiwan, Thailand, United Kingdom, and USA (updated from Le Quéré et al., 2019). Altogether, these 35 1957 1958 countries emitted 2.7 GtC yr⁻¹ (9.7 GtCO₂ yr⁻¹) on average over the last decade, about 27% of world 1959 CO2 fossil emissions. For comparison, over the previous decade (2005-2014), 18 countries showed a 1960 significant decrease in territorial fossil CO2 emissions while significantly growing their economy 1961 (Austria, Belgium, Bulgaria, Czechia, France, Germany, Luxembourg, North Macedonia, Netherlands, New Zealand, Romania, Serbia, Slovakia, Sweden, Switzerland, United Kingdom, USA, Uzbekistan). 1962 1963 These 18 countries emitted an average 2.0 GtC/yr over 2005–2014, or 20% of the global total. 1964 Decomposing emission changes into the components of growth, a Kaya decomposition, helps give an 1965 initial understanding of the drivers of emission changes (Peters et al., 2017b). The reduction in growth in global fossil CO2 emissions in the last decade (2015-2024, 0.8% yr⁻¹) relative to the previous decade 1966 $(2005-2014, 2.2\% \text{ yr}^1)$ is due to slightly weaker economic growth $(3.5\% \text{ yr}^1 \text{ to } 2.4\% \text{ yr}^1)$, increasing 1967 declines in CO₂ emissions per unit energy (0% yr⁻¹ to 0.7% yr⁻¹), and weakening declines in energy per 1968 1969 unit GDP (1.6% yr⁻¹ to 1.3% yr⁻¹) (Figure S17). Fossil CO₂ emission declines in the USA and the EU27 1970 are primarily driven by sustained or increasing declines in energy per GDP and CO2 emissions per unit 1971 energy. China has seen emissions growth decline from 6.7% yr⁻¹ in the 2005-2014 decade to 2.5% yr⁻¹ 1972 from 2015-2024, driven by weaker economic growth (five percentage points), offset by a considerable weakening in the rate of reduction in the energy per GDP (four percentage points), with sustained 1973 1974 improvements in CO₂ emissions per unit energy (Figure S17). India has had strong economic growth 1975 that is not offset by declines in energy per GDP or declines in CO2 emissions per unit energy, driving

The average growth in global fossil CO₂ emissions peaked at nearly +3% per year during the 2000s,





1976 up fossil CO2 emissions. In the rest of the world, economic growth has slowed considerably in the last 1977 decade, and carbon intensity has increased, with declines in energy per GDP unable to counteract these 1978 increases leading to growing emissions. Despite the high deployment of renewables in some countries 1979 (e.g., China, India), fossil energy sources continue to grow to meet growing energy demand (Le Quéré 1980 et al., 2019). In summary, the carbon intensity of energy has consistently decreased over the past 1981 decade globally (-0.7% yr⁻¹), indicating decarbonisation of the global energy system, with declines in 1982 China (-1.4% yr⁻¹), the European Union (-1.5% yr⁻¹), the USA (-1.3% yr⁻¹), but no change in India and 1983 increases (carbonisation) in the Rest of the World. The global decarbonation trends are not sufficient to 1984 offset the growth in global energy demand, with energy demand growing faster than expected due to 1985 weakening declines in energy per GDP in China, US, and globally. 1986 The slower growth of global fossil CO₂ emissions in the last decade is due in part to the emergence of climate policy (Eskander and Fankhauser 2020; Le Quere et al 2019; Hoppe et al., 2023) and 1987 1988 technological change, which is leading to a shift from coal to gas and growth in renewable energies, and 1989 reduced expansion of coal capacity. At the aggregated global level, decarbonisation shows a strong and 1990 growing signal in the last decade, with smaller contributions from lower economic growth and declines 1991 in energy per GDP. Altogether, global fossil CO2 emissions are still growing, far from the reductions 1992 needed to meet the ambitious climate goals of the UNFCCC Paris agreement. 1993 Last, we update the remaining carbon budget (RCB) based on two studies, the IPCC AR6 (Canadell et 1994 al., 2021) and the revision of the IPCC AR6 estimates (Forster et al., 2025, Lamboll et al., 2023). We 1995 update the RCB assessed by the IPCC AR6 (Canadell et al., 2021), accounting for the 2020 to 2025 1996 GCB estimated anthropogenic emissions from fossil combustion (E_{FOS}) and land use change (E_{LUC}). 1997 From January 2026, the IPCC AR6 RCB (50% likelihood) for limiting global warming to 1.5°C, 1.7°C 1998 and 2°C is estimated to amount to 70, 165, and 300 GtC (250, 600, 1100 GtCO₂). The Forster et al. 1999 (2025) study proposed a significantly lower RCB than IPCC AR6, with the largest reduction being due 2000 to an update of the climate emulator (MAGICC) used to estimate the warming contribution of non-CO2 2001 agents, and to the warming (i.e. emissions) that occurred over the 2020-2024 period. We update the 2002 Forster et al., budget accounting for the 2025 GCB estimated anthropogenic emissions. From January 2003 2026, the Forster et al., (2025) RCB (50% likelihood) for limiting global warming to 1.5°C, 1.7°C and 2004 2°C is estimated to amount to 25, 120, and 275 GtC (90, 450, 1010 GtCO₂), significantly smaller than 2005 the updated IPCC AR6 estimate. Both the original IPCC AR6 and Forster et al. (2025) estimates 2006 include the Earth System uncertainty on the climate response to cumulative CO₂ emissions, which is 2007 reflected through the percent likelihood of exceeding the given temperature threshold, an additional 2008 uncertainty of ±220GtCO₂ due to alternative non-CO₂ emission scenarios, and other sources of 2009 uncertainties (see Canadell et al., 2021). The two sets of estimates overlap when considering all 2010 uncertainties.

2041

2042

2043

2044

2045





2012 remaining carbon (50% likelihood) for limiting global warming to 1.5°C, 1.7°C and 2°C of respectively 2013 45, 145, and 290 GtC (170, 525, 1055 GtCO₂) starting from January 2026. We emphasise the large 2014 uncertainties, particularly when close to the global warming limit of 1.5°C. These 1.5°C, 1.7°C and 2°C 2015 remaining carbon budgets correspond respectively to about 4, 12 and 25 years from the beginning of 2016 2026, at the 2025 level of total anthropogenic CO₂ emissions. Reaching net-zero CO₂ emissions by 2017 2050 entails cutting total anthropogenic CO₂ emissions by about 0.5 GtC (1.7 GtCO₂), 4% of 2025 2018 emissions, each year on average, comparable to the decrease in E_{FOS} observed in 2020 during the 2019 COVID-19 pandemic. However, this would lead to cumulative emissions over 2025-2050 of 140 GtC 2020 (520 GtCO₂), well above the remaining carbon budget of 50 GtC to limit global warming to 1.5°C, but 2021 still within the remaining budget of 145 GtC to limit warming to 1.7°C (in phase with the "well below 2022 2°C" ambition of the Paris Agreement). 2023 5 Discussion 2024 Each year when the global carbon budget is published, each flux component is updated for all previous 2025 years to consider corrections that are the result of further scrutiny and verification of the underlying 2026 data in the primary input datasets. Annual estimates may be updated with improvements in data quality 2027 and timeliness (e.g., to eliminate the need for extrapolation of forcing data such as land use). Of all 2028 terms in the global budget, only the fossil CO₂ emissions and the growth rate in atmospheric CO₂ 2029 concentration are based primarily on empirical inputs supporting annual estimates in this carbon 2030 budget. The carbon budget imbalance, yet an imperfect measure, provides a strong indication of the 2031 limitations in observations, in understanding and representing processes in models, and/or in the 2032 integration of the carbon budget components. 2033 The persistent unexplained variability in the carbon budget imbalance limits our ability to verify 2034 reported emissions (Peters et al., 2017a) and suggests we do not yet have a complete understanding of 2035 the underlying carbon cycle dynamics on annual to decadal timescales. Resolving most of this 2036 unexplained variability should be possible through different and complementary approaches. First, as 2037 intended with our annual updates, the imbalance as an error term should be reduced by improvements 2038 of individual components of the global carbon budget that follow from improving the underlying data 2039 and statistics and by improving the models through the resolution of some of the key uncertainties 2040 detailed in Table 10. Second, additional clues to the origin and processes responsible for the variability

Here, we take the average of our update of both IPCC AR6 and Forster et al. (2025) estimates, giving a

in the budget imbalance could be obtained through a closer scrutiny of carbon variability in light of

biogeochemical observations to better understand the land-ocean partitioning of the carbon imbalance

such as the constraint from atmospheric oxygen. Finally, additional information could also be obtained

through better inclusion of process knowledge at the regional level. The limit for reducing the carbon

other Earth system data (e.g., heat balance, water balance), and the use of a wider range of





2046 budget imbalance is yet unclear, but most certainly not yet reached given the possibilities for 2047 improvements that lie ahead. 2048 Estimates of global fossil CO2 emissions from different datasets are in relatively good agreement when 2049 the different system boundaries of these datasets are considered (Andrew, 2020a). While estimates of 2050 E_{FOS} are derived from reported activity data requiring much fewer complex transformations than some 2051 other components of the budget, uncertainties remain, and one reason for the apparently low variation 2052 between datasets is precisely the reliance on the same underlying reported energy data. The budget 2053 excludes some sources of fossil CO2 emissions, which available evidence suggests are relatively small 2054 (<1%) (see Supplement S.8.2). We have added emissions from lime production in China and the US, 2055 but these are still absent in reporting from most other non-Annex I countries, and before 1990 in other 2056 Annex I countries. 2057 Estimates of E_{LUC} suffer from a range of intertwined issues (Obermeier et al., 2025), including the poor 2058 knowledge of historical land-cover and land-use change (particularly before the 1960s when FAO 2059 reporting started), the rudimentary representation of management processes in most models, and the 2060 diversity in methodologies and boundary conditions used across methods (e.g., Arneth et al., 2017; 2061 Pongratz et al., 2014; Bastos et al., 2021). Uncertainties in current and historical carbon stocks in soils 2062 and vegetation also contribute to uncertainty in E_{LUC} estimates. Major efforts are thus necessary to 2063 resolve the different issues concerning E_{LUC} (Obermeier et al., 2025). The large uncertainty and limited 2064 reliability of E_{LUC} estimates are particularly concerning given the growing importance of E_{LUC} for 2065 climate mitigation strategies, and the large issues in the quantification of the cumulative emissions over 2066 the historical period that arise from large uncertainties in E_{LUC}. 2067 By adding the natural land sink in managed forests estimated by DGVMs (part of S_{LAND} in this budget) 2068 to the budget E_{LUC} estimate, we reconcile most of the large gap between our E_{LUC} estimate and the land-2069 use flux estimates from NGHGIs (Figure 8). This reconciliation (translation) can be used as potential 2070 adjustment in the policy context, for instance to help assess the collective countries' progress towards 2071 the goal of the Paris Agreement avoiding double-accounting for the natural sink in managed forests. In 2072 the absence of this translation, collective progress would appear better than it is (Grassi et al., 2021). A 2073 clear understanding of these implications is thus essential for policymakers for developing effective 2074 climate targets (Grassi et al., 2025). The application of this translation is also recommended in the 2075 UNFCCC Synthesis report for the first Global Stocktake (UNFCCC, 2022) whenever a comparison 2076 between LULUCF fluxes reported by countries and the global emission estimates of the IPCC is 2077 conducted. However, this translation should be seen as a short-term and pragmatic fix based on existing 2078 data, rather than a definitive solution to bridge the differences between global models and national 2079 inventories. Platforms for dataset comparisons (e.g., Melo et al., 2025) help strengthening the dialogue 2080 across communities and identify the additional steps needed to understand and reconcile the remaining





2081 differences, some of which are relevant at the country level (Grassi, et al., 2023, Schwingshackl, et al., 2082 2022). 2083 The comparison of GOBMs, fCO2-products, and inversions highlights discrepancies in the temporal 2084 evolution of Socean in the Southern Ocean and northern high-latitudes (Figure 14, Hauck et al., 2023a) 2085 and in the mean Socian in the tropics. A large part of the uncertainty in the mean fluxes stems from the 2086 regional distribution of the river flux adjustment term. The current distribution simulates the largest 2087 share of the outgassing to occur in the tropics (Lacroix et al., 2020). The long-standing sparse data 2088 coverage of fCO2 observations in the Southern compared to the Northern Hemisphere (e.g., Takahashi et al., 2009) continues to exist (Bakker et al., 2016, 2025a, Figure S5) and to lead to substantially higher 2089 2090 uncertainty in the Social estimate for the Southern Hemisphere (Watson et al., 2020, Gloege et al., 2091 2021, Hauck et al., 2023a). This discrepancy, which also hampers model improvement, points to the 2092 need for increased high-quality fCO2 observations especially in the Southern Ocean. At the same time, 2093 model uncertainty is illustrated by the large spread of individual GOBM estimates (indicated by 2094 shading in Figure 14) and highlights the need for model improvement, now also supported by the 2095 IOMB benchmarking. The issue of diverging trends in Social from different methods remains a matter 2096 of concern. Recent and on-going work suggests that the fCO2-products may overestimate the trend 2097 although biases in the fCO2-product ensemble may partly cancel out (Supplement section S3.4). A data-2098 constrained model approach suggests that the GOBMs underestimate the amplitude of decadal 2099 variability, but that the fCO₂-products overestimate the trend (Mayot et al., 2024). The various methods, 2100 now also including ocean interior observation-based estimates, agree within uncertainties on the mean 2101 ocean sink in the last decade, although the independent estimate from atmospheric oxygen 2102 measurements still shows the largest sink estimate for the past decade and has a steeper trend (Table 6). 2103 However, the estimate is consistent within uncertainties with Socean, with the relatively larger ocean 2104 sink in the fCO₂-products and some of the GOBMs. The assessment of the net land-atmosphere 2105 exchange from DGVMs and atmospheric inversions also shows substantial discrepancy, particularly for 2106 the estimate of the net land flux over the northern extra-tropic. This discrepancy highlights the 2107 difficulty to quantify complex processes (CO2 fertilisation, nitrogen deposition and fertilisers, climate 2108 change and variability, land management, etc.) that collectively determine the net land CO2 flux. 2109 Resolving the differences in the Northern Hemisphere land sink will require the consideration and 2110 inclusion of larger volumes of observations. 2111 The adjustments introduced in this budget for SLAND and SOCEAN to account for known biases (RSS for 2112 DGVMs, cold skin/warm layer for fCO2 products, ocean sink underestimation for GOBMs) lead to a 2113 smaller net land sink (S_{LAND}-E_{LUC}) and a larger ocean sink (S_{OCEAN}), more in line with the atmospheric 2114 inversions and independent oxygen based estimates (Table 7), and also consistent with a recent study 2115 based on satellite derived changes in aboveground biomass over the 2000-2019 period (Randerson et 2116 al., 2025).





2117 We provide metrics for the evaluation of the ocean and land models and the atmospheric inversions 2118 (Figure S6-S8 and S13, Table S11). These metrics expand the use of observations in the global carbon 2119 budget, helping 1) to support improvements in the ocean and land carbon models that produce the sink 2120 estimates, and 2) to constrain the representation of key underlying processes in the models and to 2121 allocate the regional partitioning of the CO₂ fluxes. The use of process-based metrics in an objective 2122 evaluation framework (IOMB) targeted to evaluate the simulation of Social in the ocean 2123 biogeochemistry models is an important advance. This is another step in the endeavour to use a broader 2124 range of observations and more stringent model evaluation that we hope will support continued 2125 improvements in the models and in the annual estimates of the global carbon budget. 2126 We assessed before that a sustained decrease of -1% in global emissions could be detected at the 66% 2127 likelihood level after a decade only (Peters et al., 2017a). Similarly, a change in behaviour of the land 2128 and/or ocean carbon sink would take as long to detect, and much longer if it emerges more slowly. To 2129 continue reducing the carbon imbalance on annual to decadal time scales, regionalising the carbon 2130 budget, and integrating multiple variables are powerful ways to shorten the detection limit and ensure 2131 the research community can rapidly identify issues of concern in the evolution of the global carbon 2132 cycle under the current rapid and unprecedented changing environmental conditions. 2133

6 Conclusions

2134 The estimation of global CO₂ emissions and sinks is a major effort by the carbon cycle research 2135 community that requires a careful compilation and synthesis of measurements, statistical estimates, and 2136 model results. The delivery of an annual carbon budget serves two purposes. First, there is a large 2137 demand for up-to-date information on the state of the anthropogenic perturbation of the climate system 2138 and its underpinning causes. A broad stakeholder community relies on the datasets associated with the 2139 annual carbon budget including scientists, policy makers, businesses, journalists, and non-governmental 2140 organisations engaged in adapting to and mitigating human-driven climate change. Second, over the last 2141 decades we have seen unprecedented changes in the human and biophysical environments (e.g., 2142 changes in the growth of fossil fuel emissions, impact of COVID-19 pandemic, Earth's warming, 2143 extreme events, and strength of the carbon sinks), which call for frequent assessments of the state of the 2144 planet, a better quantification of the causes of changes in the contemporary global carbon cycle, and an improved capacity to anticipate its evolution in the future. Building this scientific understanding to meet 2145 2146 the extraordinary climate mitigation challenge requires frequent, robust, transparent, and traceable 2147 datasets and methods that can be scrutinised and replicated. This paper via 'living data' helps to keep 2148 track of new budget updates.





2149	7 Data availability
2150 2151 2152 2153 2154	The data presented here are made available in the belief that their wide dissemination will lead to greater understanding and new scientific insights of how the carbon cycle works, how humans are altering it, and how we can mitigate the resulting human-driven climate change. Full contact details and information on how to cite the data shown here are given at the top of each page in the accompanying database and summarised in Table 2.
2155	The accompanying database includes three Excel files organised in the following spreadsheets:
2156	File Global_Carbon_Budget_2025v1.0.xlsx includes the following:
2157	1. Summary
2158	2. The global carbon budget (1959-2024);
2159	3. The historical global carbon budget (1750-2024);
2160 2161	4. Global CO ₂ emissions from fossil fuels and cement production by fuel type, and the per-capita emissions (1850-2024);
2162	5. CO ₂ emissions from land-use change from the individual bookkeeping models (1959-2024);
2163 2164	6. Ocean CO ₂ sink from the individual global ocean biogeochemistry models and fCO ₂ -products (1959-2024);
2165	7. Terrestrial CO ₂ sink from the individual DGVMs (1959-2024);
2166	8. Cement carbonation CO ₂ sink (1959-2024).
2167	File National_Fossil_Carbon_Emissions_2025v1.0.xlsx includes the following:
2168	1. Summary
2169	2. Territorial country CO ₂ emissions from fossil fuels and cement production (1850-2024);
2170 2171 2172	 Consumption country CO₂ emissions from fossil fuels and cement production and emissions transfer from the international trade of goods and services (1990-2020) using CDIAC/UNFCCC data as reference;
2173	4. Emissions transfers (Consumption minus territorial emissions; 1990-2020);
2174	5. Country definitions.
2175	File National_LandUseChange_Carbon_Emissions_2024v1.0.xlsx includes the following:

1. Summary

2176





2177 2. Territorial country CO₂ emissions from Land Use Change (1850-2024) from three bookkeeping 2178 2179 All three spreadsheets are published by the Integrated Carbon Observation System (ICOS) Carbon 2180 Portal and are available at https://doi.org/10.18160/GCP-2025 (Friedlingstein et al., 2025c). National 2181 emissions data are also available at https://doi.org/10.5281/zenodo.5569234 (Andrew and Peters, 2025), 2182 from the Global Carbon Atlas (http://www.globalcarbonatlas.org/, last access: 23 October 2025) and 2183 from Our World in Data (https://ourworldindata.org/co2-emissions, last access: 23 October 2025). 2184 **Author contributions** 2185 PF, MOS, MWJ, DCEB, RMA, JH, PL, CLQ, HL, ITL, GPP, WP, JP, CSc, and SS designed the study, 2186 conducted the analysis, and wrote the paper with input from JGC and PC. RMA, GPP, JIK and TK 2187 produced the fossil CO2 emissions and their uncertainties and analysed the emissions data. ME and GM 2188 provided fossil fuel emission data. ZL provided the Carbon Monitor fossil emission projection. JP, CSc, 2189 TG and ZQ provided the bookkeeping land-use change emissions with synthesis by JP and CSc. KH 2190 and JDM provided the estimates of non-vegetation CDR fluxes. LB, MAC, ÖG, NG, TI, TJ, LR, JS, 2191 RS, and HTs provided an update of the global ocean biogeochemical models; LD, DJF, MG, LG, YI, 2192 AJ, GMK, CR, JZ, and PC provided an update of the ocean fCO2-data products, with synthesis on both 2193 streams by JH, PL and AR. SRA, LBa, NRB, AB, CFB, MC, MPE, KE, WE, RAF, TGk, CL, NM, 2194 DRM, SN, AO, AMO, DP, GR, IS, AJS, CSw, ST, BT, SJvdV, EVO, and RW provided ocean fCO2 2195 measurements for the year 2024, with synthesis by DCEB and SDJ. KA, PA, THC, JHE, AFo, BG, JG, 2196 AI, AKJ, EK, JK, EM, JM, LM, TN, QS, TLS, HT, APW, WY, XYa, XYu and CK provided an update 2197 of the Dynamic Global Vegetation Models, with synthesis by SS and MOS. RB, FF, HL, VS, DS, and 2198 HiT provided estimates of land and ocean sinks from Earth System Models, as well as a projection of 2199 the atmospheric growth rate for 2025, with synthesis by HL. FC, NC, LF, ARJ, FJ, ITL, JL, LRN, YN, 2200 CR, XT, YK, and ZL provided an updated atmospheric inversion, WP, FC, and ITL developed the 2201 protocol and produced the synthesis and evaluation of the atmospheric inversions. EJM and RFK 2202 provided the atmospheric oxygen estimate of surface net carbon sinks. RMA provided projections of 2203 the 2025 fossil emissions and atmospheric CO2 growth rate. PL provided the predictions of the 2025





2204 ocean sink. IBMB, LPC, KKG, GCH, TMR and GRvdW provided forcing data for land-use change. FT 2205 and GG provided data for the land-use change NGHGI harmonisation. XL provided the atmospheric 2206 CO2 data. SP provided the satellite OCO-2 atmospheric CO2 growth rate. MWJ provided the historical 2207 atmospheric CO₂ concentration and growth rate. IH provided the climate forcing data for the DGVMs. 2208 NP provided the nitrogen fertilizer forcing data for the DGVMs. MOS and NB produced the aerosol 2209 diffuse radiative forcing for the DGVMs. PCM provided the iLAMB evaluation of the DGVMs. NOC 2210 and MGS provided the iOMB evaluation of the GOBMs. PR provided the historical land carbon export 2211 estimate, MWJ provided the emissions prior for use in the inversion systems. XD provided seasonal 2212 emissions data, based on GRACED (Global gridded daily CO₂ emissions dataset), for most recent years 2213 for the emission prior. PF, MO and MWJ coordinated the effort, revised all figures, tables, text and 2214 numbers to ensure the update was clear from the 2024 edition and in line with the 2215 globalcarbonatlas.org. 2216 2217 Competing interests. 2218 At least one of the authors is a member of the editorial board of Earth System Science Data 2219 2220 Acknowledgements 2221 First, we wish to thank Richard 'Skee' Houghton for his tremendous contribution to the Global Carbon 2222 Budget since its inception, pioneering the estimate of land use change emissions with bookkeeping 2223 models. We thank all people and institutions who provided the data used in this global carbon budget 2224 2025 and the Global Carbon Project members for their input throughout the development of this 2225 publication. We thank Christian Ethé, Xavier Perrot, Damian Loher, Fatemeh Chegini, Fabrice Lacroix, 2226 Yangyang Zhao, Paridhi Rustogi, Sarah Berthet, Aurore Voldoire, Laurent Oziel, T. Toyoda, Y. 2227 Kitamura, K. Toyama, H. Nakano, L. S. Urakawa, Philip Townsend, Nathaniel O. Collier, Min Xu, James 2228 D. Shutler, Andrew J. Watson, T. Holding, I.G.C. Ashton, D. K. Woolf, Lonneke Goddijn-Murphy, 2229 Richard Sims, Stefanie Falk, Pengyue Du, Peter Lawrence, Sean Swenson, Daniel Kennedy, Sam Levis, 2230 Erik Kluzek, Lachlan Whyborn, Drew Holzworth, Ian Harman, Naiqing Pan, Shufen Pan for their 2231 involvement in the development, use, and analysis of the models and data products used here. We thank 2232 Kim Currie, Hannelore Theetaert, and Coraline Leseurre who contributed to the provision of surface





2233 ocean CO2 observations for the year 2024 (see Table A5). We also thank Kevin O'Brien and Eugene 2234 Burger of NOAA's Pacific Marine Environmental Laboratory and Alex Kozyr of NOAA's National Centers for Environmental Information, for their contribution to surface ocean CO2 data and metadata 2235 2236 management. We thank the scientists, institutions, and funding agencies responsible for the collection 2237 and quality control of the data in SOCAT as well as the International Ocean Carbon Coordination Project 2238 (IOCCP) and the Surface Ocean Lower Atmosphere Study (SOLAS) program for their support. ITL and 2239 WP thank the CarbonTracker Europe team at Wageningen University, including Remco de Kok, Joram 2240 Hooghiem and Auke van der Woude. The inverse modelling team thanks all data providers of 2241 atmospheric CO2 data provided through multiple ObsPack products. HL thanks Tatiana Ilyina for supporting the coordination of ESMs' contributions to GCBs, and Sebastian Brune and Kristina Frölich 2242 2243 for helping with the MPI-ESM1-2-LR assimilation. Zhangcai Qin thanks Ziwang Fu and Dr. Yakun Zhu 2244 for contributing to LUCE modeling. We thank Ram Alkama and Simone Rossi for helping in filtering SLAND data from DGVMs with managed forest area and Joana Melo for extracting and processing data 2245 from NGHGIs. FT acknowledges support of member countries to the FAO regular budget and 2246 2247 FAOSTAT. The conclusions in this paper are the authors' only and do not represent FAO views and position on the subject matter. This is PMEL contribution 5802. MC thanks Tobias Steinhoff (MACID), 2248 2249 Lukasz Pawlikowski, Ian Murphy and Gordon Furey (P&O Maritime Services), and Aodhan Fitzgerald 2250 (Marine Institute) for their support. TG and the VLIZ team are thankful to the management group and 2251 crew of the research vessels Simon Stevin, Skagerak and Neil Armstrong for all the support and help they 2252 provided. pCO2 measurements on the Marion Dufresne were collected in the frame of the French 2253 COOL/OISO long-term monitoring program with support from the National Institute of Sciences of the 2254 Universe (INSU), the French Polar Institute (IPEV) and the French Oceanographic Fleet (FOF). AMO thanks the captain and crew on the Sea-Cargo Express for their help. DP would like to thank Kevin 2255 2256 Sullivan for processing and quality controlling AOML data and facilitating submission to SOCATv2025. 2257 GR thanks the "Finnmaid science and tech-teams" at IOW and SYKE for their support, and is indebted 2258 to the crew of the ship and the people involved at Finnlines. IS thanks the captain and crew on the G. O. 2259 Sars for their help. BT and EvO thank Australia's Integrated Marine Observing System (IMOS) for 2260 sourcing CO2 data. IMOS is enabled by the National Collaborative Research Infrastructure Strategy 2261 (NCRIS). SJV thanks Andrew Marriner for maintaining the pCO₂ underway system on the RV Tangaroa. 2262 PCM thanks Tristan Quaife, Eddy Robertson, Emily Black and Anthony Walker for support. FC thanks 2263 Adrien Martinez who maintained the atmospheric transport model for the CAMS inversion. We 2264 acknowledge the contributions of Jeongmin Yun, Anthony Bloom, and Kevin Bowman to the CMS-Flux 2265 inversion submission. YN thanks Suman Maity who performed the NISMON-GOSAT inversion. LF 2266 thanks Paul I. Palmer and acknowledges ongoing support from the National Centre for Earth Observation. 2267 Xiangjun Tian thanks Zhe Jin, Yilong Wang, Hongqin Zhang, Min Zhao, Tao Wang, Jinzhi Ding, and 2268 Shilong Piao for their contributions to the GONGGA inversion system. We thank Ning Zeng, Yun Liu, 2269 Eugenia Kalnay, and Gassem Asrar for their contributions to the COLA system. CarbonTracker CT2025





2270 results provided by NOAA GML, Boulder, Colorado, USA from the website at 2271 http://carbontracker.noaa.gov. FJ thanks Weimin Ju for running the BEPS model. LN thanks Shamil Maksyutov, Rajesh Janardanan and Tsuneo Matsunaga for contributing to NTFVAR inverse model study. 2272 2273 YK acknowledges Bo Zheng from Tsinghua University for his contribution to the THU inversion system. 2274 RSA thanks William Merryfield, Woosung Lee, Jason Cole for their help to set up and produce the model 2275 runs. The IPSL contribution was achieved thanks to the valuable contributions of Patricia Cadule, Juliette Mignot and Olivier Torres. GAM acknowledges contributions from Amanda Fay to updating the LDEO-2276 2277 HPD fCO2 product. JRM thanks Gesa Meyer for assistance setting up the DGVM simulations. LMD 2278 thanks Pedro. M. S. Monteiro (SCS-SU) and Sandy Thomalla (SOCCO-CSIR) for their continued support 2279 to make the CSIR-ML6 fCO2-product up-to-date. CFB is grateful to the technicians and crew of the 2280 research vessel Víctor Angelescu for all the support and assistance they provided. This is INIDEP 2281 contribution 2460.

2282

2283

Financial and computing support

2284 This research was supported by the following sources of funding: Instituto Nacional de Investrigación y 2285 Desarrollo Pesquero (INIDEP) (Argentina); Joint Technical Commission of the Maritime Front 2286 (CTMFM, Argentina-Uruguay) (Argentina); Integrated Marine Observing System (IMOS) (Australia); 2287 National Environmental Science Program (NESP) (Australia); Research Foundation Flanders (grant no. 2288 I001821N) (Belgium); ICOS (Integrated Carbon Observing System) Belgium (Belgium); Tula 2289 Foundation (Canada); National Key Research and Development Program of China (grant no. 2290 2023YFF0805400) (China); Horizon Europe (NextGenCarbon: grant no. 101184989) (EC); Horizon 2291 Europe (RESCUE: grant no. 101056939) (EC); Horizon 2020 (ESM2025: grant no. 101003536) (EC); 2292 Horizon Europe (TRICUSO: grant no. 101199028) (EC); Horizon Europe (GreenFeedBack: grant no. 2293 101056921) (EC); H2020 (JERICO-S3: grant no. 871153) (EC); Horizon Europe (GEORGE: grant no. 2294 101094716) (EC); Copernicus Atmosphere Monitoring Service, implemented by ECMWF on behalf of the European Commission (Grant no. CAMS2 55 bis) (EC); MOB TAC project of the European 2295 2296 Copernicus Marine Environment Monitoring Service (EC); Horizon Europe (TipESM: grant no. 2297 101137673) (EC); Horizon Europe (OceanICU: grant no. 101083922) (EC); Climate Space RECCAP-2 2298 (grant no. 4000144908/24/1-LR) (European Space Agency); EO-LINCS (European Space Agency); 2299 Ocean Carbon for Climate (grant no. 3-18399/24/I-NB) (European Space Agency); Satellite-based 2300 observations of Carbon in the Ocean: Pools, Fluxes and Exchanges (grant no. 4000142532/23/I-DT) 2301 (European Space Agency); THRAC3E (grant no. 4000149569/25/I-AG) (European Space Agency); ; 2302 ICOS Germany (Germany); Federal Ministry of Education and Research (BMBF) (STEPSEC: grant no. 2303 01LS2102A) (Germany); Marine Institute (Ireland); Japan Meteorological Agency (Japan); Global 2304 Environmental Research Coordination System, Ministry of the Environment (grant nos. E2152 and





2305 E2252) (Japan); NIES GOSAT Project (Japan); the Environment Research and Technology Development Fund (JPMEERF24S12200) of the Environmental Restoration and Conservation Agency 2306 2307 provided by Ministry of the Environment of Japan (Japan); Environment Research and Technology 2308 Development Fund (grant no. JPMEERF24S12205, Co-PI: P. K. Patra) of the Environmental Restoration 2309 and Conservation Agency of Japan, and the Arctic Challenge for Sustainability phase III project (ArCS-2310 3; grant no. JPMXD1720251001; Co-PI: P. K. Patra) (Japan); Environment Research and Technology 2311 Development Fund (grant no. JPMEERF24S12206) of the Environmental Restoration and Conservation 2312 Agency of Japan (Japan); Ministry of Business, Innovation and Employment (Strategic Science 2313 Investment Fund via the NIWA Ocean-Climate Interaction programme) (New Zealand); Research Council of Norway (ICOS-3, grant no. 350341) (Norway); Research Council of Norway (grant no. 2314 2315 352474) (Norway); Research Council of Norway (grant no. 352204) (Norway); South African 2316 Department of Science, Technology and Innovation (grant no. DSI/CON C3184/2023) (South Africa); 2317 UK Research and Innovation (Horizon Europe GreenFeedBack: grant no. 10040851) (UK); NCAS at the 2318 University of Reading (UK); NERC NE/V011103/1 "Frontiers of instability in marine ecosystems and 2319 carbon export"UK Natural Environment Research Council (NE/V01417X/1) (UK); Department of 2320 Energy, Office of Science, Office of Biological and Environmental Research (USA); NOAA (Global 2321 Ocean Monitoring and Observing Program: Open Funder Registry no. 100018302) (USA); NOAA 2322 (Ocean Acidification Program: Open Funder Registry no. 100018228) (USA); NOAA (Cooperative 2323 Agreement NA20OAR4320472) (USA); NOAA (Cooperative Agreement NA-03-AR4320179) (USA); Alaska Ocean Observing System (USA); NASA Carbon Monitoring System (grant no. 2324 2325 80NSSC25K7221) (USA); NASA Early Career Investigator Program in Earth Science (grant no. 2326 80NSSC24K1632) (USA); NASA Land Cover and Land Use Change Program (Grants: 2327 80NSSC24K0920 and 80NSSC25K7497) (USA); NSF (Cooperative Agreement No. 1852977) (USA); 2328 NASA Orbiting Carbon Observatory Science Team Program (grant no. NNH23ZDA001N-OCOST) 2329 (USA); NASA Carbon Monitoring System (grant no.NNH22ZDA001N-CMS) (USA); Work of J.L. and 2330 S.P. was conducted at the Jet Propulsion Laboratory, California Institute of Technology, under a contract 2331 with the National Aeronautics and Space Administration (80NM0018D0004) (USA); NOAA 2332 (Cooperative Institute for Marine, Earth and Atmospheric Systems, Award No. NA25NMFX432C0003-2333 T1-01) (USA); NSF (OPP-2329254) (USA); ORNL is managed by UT-Battelle, LLC, for the DOE (grant 2334 no. DE-AC05-1008 00OR22725) (USA); Schmidt Sciences (VESRI CALIPSO) (USA); Schmidt 2335 Sciences (OBVI InMOS) (USA); NSF (OPP-1922922) (USA); NOAA grant NA24NESX432C0001 2336 (Cooperative Institute for Satellite Earth System Studies - CISESS) (USA); NOAA cooperative 2337 agreement NA22OAR4320151 (CIRES: Andrew Jacobson and Xin Lan) (USA); Schmidt Sciences 2338 (CLARiTy project, part of the Virtual Institute for the Carbon Cycle) (USA); Schmidt Sciences (COCO2 2339 project, part of the Virtual Institute for the Carbon Cycle) (USA); NSF (LEAP STC Award no 2019625) 2340 (USA); NASA (grant no. 80NSSC22K0150) (USA); NOAA (GOMO, grant no. NA24OARX431G0151-2341 T1-01) (USA).





2342 The US National Science Foundation (grant nos. OPP-1922922, OPP-2329254), a NOAA cooperative 2343 agreement, the Cooperative Institute for Marine, Earth and Atmospheric Systems (CIMEAS, grant nos. NA20OAR4320278-T1-01 and NA25NMFX432C0003-T3-01S022); although NSF grants 1922922 and 2344 2345 2329254 and NOAA grants NA20OAR4320278-T1-01 and NA25NMFX432C0003-T3-01S022 have 2346 been identified for conflict of interest management based on the overall scope of the project and its potential benefit to the Keeling Curve Foundation, the research findings included in this particular 2347 2348 publication may not necessarily relate to the interests of Keeling Curve Foundation. The terms of this 2349 arrangement have been reviewed and approved by the University of California, San Diego in accordance 2350 with its conflict of interest policies. 2351 We also acknowledge support from the following computing facilities: Australian Community Climate 2352 and Earth System Simulator - National Research Infrastructure (ACCESS-NRI) (Australia); National 2353 Computational Infrastructure (NCI) (Australia); High-Performance Computing Center (HPCC) of Nanjing University for doing the inversions on its blade cluster system (China); HPC computing and 2354 2355 storage resources by GENCI at IDRIS and TGCC thanks to the grant 2024-2201 on the supercomputers Jean Zay's V100 and Joliot Curie's SKL and V100 partitions. (France); The ORCHIDEE simulations 2356 2357 were performed using HPC resources from GENCi-TGCC on grant 2024-00006328 (France); IPSL 2358 Climate Modelling Centre (https://mesocentre.ipsl.fr) (France); HPC resources from GENCI - TGCC 2359 (Grant A005-017403) (France); Deutsches Klimarechenzentrum (DKRZ) (Projects: bm0891, bm1124 2360 and bg1446) (Germany); NIES Supercomputer system, GOSAT Supercomputing Facility (GOCF) (Japan); NEC SX-Aurora TSUBASA at NIES (Japan); Fugaku provided by the RIKEN Center for 2361 2362 Computational Science (Project ID: hp250024) (Japan); JAMSTEC's ES4 Super Computer system 2363 (Japan); Sigma2 - the National Infrastructure for High-Performance Computing and Data Storage in 2364 Norway (Norway); NICIS Centre for High-Performance Computing (South Africa); UK CEDA JASMIN 2365 supercomputer (UK); Compute and Data Environment for Science (CADES) at the Oak Ridge National Laboratory (USA); LEAP Pangeo cloud platform (USA); NASA Ames Supercomputers (USA). 2366

2367





2368	References
2369 2370 2371 2372	Andela, N., Morton, D. C., Giglio, L., Chen, Y., van der Werf, G. R., Kasibhatla, P. S., DeFries, R. S., Collatz, G. J., Hantson, S., Kloster, S., Bachelet, D., Forrest, M., Lasslop, G., Li, F., Mangeon, S., Melton, J. R., Yue, C., and Randerson, J. T.: A human-driven decline in global burned area, Science, 356, 1356–1362, https://doi.org/10.1126/science.aal4108, 2017.
2373 2374	Andrew, R. M.: A comparison of estimates of global carbon dioxide emissions from fossil carbon sources, Earth Syst. Sci. Data, 12, 1437–1465, https://doi.org/10.5194/essd-12-1437-2020, 2020a.
2375 2376	Andrew, R. M.: Timely estimates of India's annual and monthly fossil CO2 emissions, Earth Syst. Sci. Data, 12, 2411–2421, https://doi.org/10.5194/essd-12-2411-2020, 2020b.
2377 2378 2379	Andrew, R. M.: Towards near real-time, monthly fossil CO2 emissions estimates for the European Union with current-year projections, Atmospheric Pollution Research, 12, 101229, https://doi.org/10.1016/j.apr.2021.101229, 2021.
2380 2381	$And rew, R.\ M., \&\ Peters, G.\ P.: The\ Global\ Carbon\ Project's\ fossil\ CO2\ emissions\ dataset\ (Version\ 251022)\ [Data\ set].\ Zenodo.\ https://doi.org/10.5281/zenodo.5569234,\ 2025.$
2382 2383 2384 2385 2386	Aragão, L. E. O. C., Anderson, L. O., Fonseca, M. G., Rosan, T. M., Vedovato, L. B., Wagner, F. H., Silva, C. V. J., Silva Junior, C. H. L., Arai, E., Aguiar, A. P., Barlow, J., Berenguer, E., Deeter, M. N., Domingues, L. G., Gatti L., Gloor, M., Malhi, Y., Marengo, J. A., Miller, J. B., Phillips, O. L., and Saatchi, S.: 21st Century drought-related fires counteract the decline of Amazon deforestation carbon emissions, Nat Commun, 9, 536, https://doi.org/10.1038/s41467-017-02771-y, 2018.
2387 2388 2389	Archer, D., Eby, M., Brovkin, V., Ridgwell, A., Cao, L., Mikolajewicz, U., Caldeira, K., Matsumoto, K., Munhoven, G., Montenegro, A., and Tokos, K.: Atmospheric Lifetime of Fossil Fuel Carbon Dioxide, Annu. Rev. Earth Planet. Sci., 37, 117–134, https://doi.org/10.1146/annurev.earth.031208.100206, 2009.
2390 2391 2392 2393	Arneth, A., Sitch, S., Pongratz, J., Stocker, B. D., Ciais, P., Poulter, B., Bayer, A. D., Bondeau, A., Calle, L., Chini L. P., Gasser, T., Fader, M., Friedlingstein, P., Kato, E., Li, W., Lindeskog, M., Nabel, J. E. M. S., Pugh, T. A. M., Robertson, E., Viovy, N., Yue, C., and Zaehle, S.: Historical carbon dioxide emissions caused by land-use changes are possibly larger than assumed, Nature Geosci, 10, 79–84, https://doi.org/10.1038/ngeo2882, 2017.
2394 2395 2396	Asaadi, A., Arora, V. K., Melton, J. R., and Bartlett, P.: An improved parameterization of leaf area index (LAI) seasonality in the Canadian Land Surface Scheme (CLASS) and Canadian Terrestrial Ecosystem Model (CTEM) modelling framework, 15, 6885–6907, https://doi.org/10.5194/bg-15-6885-2018, 2018.
2397 2398 2399	Aumont, O., Orr, J. C., Monfray, P., Ludwig, W., Amiotte-Suchet, P., and Probst, JL.: Riverine-driven interhemispheric transport of carbon, Global Biogeochem. Cycles, 15, 393–405, https://doi.org/10.1029/1999GB001238, 2001.
2400 2401	Aumont, O., Ethé, C., Tagliabue, A., Bopp, L., and Gehlen, M.: PISCES-v2: an ocean biogeochemical model for carbon and ecosystem studies, 8, 2465–2513, https://doi.org/10.5194/gmd-8-2465-2015, 2015.
2402 2403 2404 2405 2406 2407 2408 2409 2410 2411 2412 2413	Babiker, M., G. Berndes, K. Blok, B. Cohen, A. Cowie, O. Geden, V. Ginzburg, A. Leip, P. Smith, M. Sugiyama, F. Yamba, Al Khourdajie, A., Arneth, A., Lima de Azevedo, I. M., Bataille, C., Beerling, D., Bezner Kerr, R., Bradley, J., Buck, H. J., Cabeza, L. F., Calvin, K., Campbell, D., Carnicer Cols, J., Daioglou, V., Harmsen, M., Höglund-Isaksson, L., House, J. I., Keller, D., de Kleijne, K., Kugelberg, S., Makarov, I., Meza, F., Minx, J. C., Morecroft, M., Nabuurs, G. J., Neufeldt, H., Novikova, A., Nugroho, S. B., Oschlies, A., Parmesan, C., Peters, G. P., Poore, J., Portugal-Pereira, J., Postigo, J. C., Pradhan, P., Renforth, P., Rivera-Ferre, M. G., Roe, S., Singh, P. K., Slade, R., Smith, S. M., Tirado von der Pahlen, M. C., and Toribio Ramirez, D.: Cross sectoral perspectives. In: Climate Change 2022: Mitigation of Climate Change (P.R. Shukla, J. Skea, R. Slade, A. Al Khourdajie, R. van Diemen, D. McCollum, M. Pathak, S. Some, P. Vyas, R. Fradera, M. Belkacemi, A. Hasija, G. Lisboa, S. Luz, J. Malley, (eds.)]. Cambridge University Press, Cambridge, UK and New York, NY, USA. doi: 10.1017/9781009157926.014. 2022





- 2414 Baccini, A., Walker, W., Carvalho, L., Farina, M., Sulla-Menashe, D., and Houghton, R. A.: Tropical forests are a
- 2415 net carbon source based on aboveground measurements of gain and loss, Science, 358, 230-234,
- 2416 https://doi.org/10.1126/science.aam5962, 2017.
- 2417 Bakker, D. C. E., Pfeil, B., Landa, C. S., Metzl, N., O'Brien, K. M., Olsen, A., Smith, K., Cosca, C., Harasawa, S.,
- 2418 Jones, S. D., Nakaoka, S., Nojiri, Y., Schuster, U., Steinhoff, T., Sweeney, C., Takahashi, T., Tilbrook, B., Wada,
- 2419 C., Wanninkhof, R., Alin, S. R., Balestrini, C. F., Barbero, L., Bates, N. R., Bianchi, A. A., Bonou, F., Boutin, J.,
- 2420 Bozec, Y., Burger, E. F., Cai, W.-J., Castle, R. D., Chen, L., Chierici, M., Currie, K., Evans, W., Featherstone, C.,
- 2421 2422 Feely, R. A., Fransson, A., Goyet, C., Greenwood, N., Gregor, L., Hankin, S., Hardman-Mountford, N. J., Harlay, J., Hauck, J., Hoppema, M., Humphreys, M. P., Hunt, C. W., Huss, B., Ibánhez, J. S. P., Johannessen, T., Keeling,
- 2423 R., Kitidis, V., Körtzinger, A., Kozyr, A., Krasakopoulou, E., Kuwata, A., Landschützer, P., Lauvset, S. K.,
- 2424 Lefèvre, N., Lo Monaco, C., Manke, A., Mathis, J. T., Merlivat, L., Millero, F. J., Monteiro, P. M. S., Munro, D.
- 2425 R., Murata, A., Newberger, T., Omar, A. M., Ono, T., Paterson, K., Pearce, D., Pierrot, D., Robbins, L. L., Saito,
- 2426 S., Salisbury, J., Schlitzer, R., Schneider, B., Schweitzer, R., Sieger, R., Skjelvan, I., Sullivan, K. F., Sutherland, S. 2427 C., Sutton, A. J., Tadokoro, K., Telszewski, M., Tuma, M., van Heuven, S. M. A. C., Vandemark, D., Ward, B.,
- 2428 Watson, A. J., and Xu, S.: A multi-decade record of high-quality CO2 data in version 3 of the Surface Ocean CO2
- 2429 Atlas (SOCAT), Earth Syst. Sci. Data, 8, 383-413, https://doi.org/10.5194/essd-8-383-2016, 2016.
- 2430 Bakker, D. C. E., Alin, S. R., Aramaki, T., Barbero, L., Bates, N. R., Gkritzalis, T., Jones, S. D., Kozyr, A.,
- 2431 Lauvset, S. K., Macovei, V., Metzl, N., Munro, D. R., Nakaoka, S.-i., O'Brien, K. M., Olsen, A., Pierrot, D.,
- 2432 Steinhoff, T., Sullivan, K. F., Sutton, A. J., Sweeney, C., Wada, C., Wanninkhof, R., Akl, J., Arbilla, L. A., Azetsu-
- 2433 Scott, K., Battisti, R., Beatty, C. M., Becker, M., Benoit-Cattin, A., Berghoff, C. F., Bittig, H. C., Bonin, J. A.,
- 2434 Bott, R., Bozzano, R., Burger, E. F., Brunetti, F., Cantoni, C., Castelli, G., Chambers, D. P., Chierici, M., Corbo,
- A., Cronin, M., Cross, J. N., Currie, K. I., Dentico, C., Emerson, S. R., Enochs, I., Enright, M. P., Enyo, K., 2435 2436 Ericson, Y., Evans, W., Fay, A. R., Feely, R. A., Fragiacomo, E., Fransson, A., Gehrung, M., Giani, M., Glockzin,
- 2437 M., Hamnca, S., Holodkov, N., Hoppema, M., Ibánhez, J. S. P., Kadono, K., Kamb, L., Kralj, M., Kristensin, T. O.,
- 2438 Laudicella, V. A., Lefèvre, N., Leseurre, C., Lo Monaco, C., Maenner Jones, S. M., Maenza, R. A., McAuliffe, A.
- 2439 M., Mdokwana, B. W., Monacci, N. M., Musielewicz, S., Neill, C., Newberger, T., Nojiri, Y., Ohman, M. D.,
- 2440 Ólafsdóttir, S. R., Olivier, L., Omar, A., Osborne, J., Pensieri, S., Petersen, W., Plueddemann, A. J., Rehder, G.,
- 2441 Roden, N. P., Rutgersson, A., Sallée, J.-B., Sanders, R., Sarpe, D., Schirnik, C., Schlitzer, R., Send, U., Skjelvan,
- 2442 I., Sutherland, S., C., T'Jampens, M., Tamsitt, V., Telszewski, M., Theetaert, H., Tilbrook, B., Trull, T., Tsanwani,
- 2443 M., Van de Velde, S., Van Heuven, S. M. A. C., Veccia, M. H., Voynova, Y. G., Weller, R. A., Williams, N. L.:
- 2444 Surface Ocean CO2 Atlas Database Version 2025 (SOCATv2025) (NCEI Accession 0304549), NOAA National
- 2445 Centers for Environmental Information, Dataset, https://doi.org/10.25921/648f-fv35, 2025a.
- 2446 Bakker, D. C. E., Alin, S. R., Aramaki, T., Barbero, L., Bates, N. R., Gkritzalis, T., Jones, S. D., Kozyr, A.,
- 2447 Lauvset, S. K., Macovei, V. A., Metzl, N., Munro, D. R., Nakaoka, S.i., O'Brien, K. M., Olsen, A., Pierrot, D.
- 2448 Steinhoff, T., Sullivan, K. F., Sutton, A. J., Sweeney, C., Wada, C., Wanninkhof, R: SOCAT version 2025: Open
- 2449 ocean CO2 data submissions stabilise, https://socat.info/index.php/posters/, Poster published on 05/06/2025. Last
- 2450 access 23 October 2025, 2025b.
- 2451 Ballantyne, A. P., Alden, C. B., Miller, J. B., Tans, P. P., and White, J. W. C.: Increase in observed net carbon
- 2452 dioxide uptake by land and oceans during the past 50 years, Nature, 488, 70-72,
- 2453 https://doi.org/10.1038/nature11299, 2012.
- 2454 Ballantyne, A. P., Andres, R., Houghton, R., Stocker, B. D., Wanninkhof, R., Anderegg, W., Cooper, L. A.,
- 2455 DeGrandpre, M., Tans, P. P., Miller, J. B., Alden, C., and White, J. W. C.: Audit of the global carbon budget:
- 2456 estimate errors and their impact on uptake uncertainty, Biogeosciences, 12, 2565-2584, https://doi.org/10.5194/bg-
- 2457 12-2565-2015, 2015.
- 2458 Bar-On, Y. M., Li, X., O'Sullivan, M., Wigneron, J-P., Sitch, S., Ciais, P., Frankenberg, C., Fischer, W. W.: Recent
- 2459 gains in global terrestrial carbon stocks are mostly stored in nonliving pools, Science 387, 1291–1295, 2025.
- 2460 Bastos, A., Hartung, K., Nützel, T. B., Nabel, J. E. M. S., Houghton, R. A., and Pongratz, J.: Comparison of
- 2461 uncertainties in land-use change fluxes from bookkeeping model parameterisation, 12, 745-762,
- 2462 https://doi.org/10.5194/esd-12-745-2021, 2021.
- 2463 Battle, M. O., Raynor, R., Kesler, S., and Keeling, R.: Technical Note: The impact of industrial activity on the
- 2464 amount of atmospheric O2, Atmospheric Chem. Phys. Discuss., 1-17, https://doi.org/10.5194/acp-2022-765, 2023.





- 2465 Bellenger, H., Bopp, L., Ethé, C., Ho, D., Duvel, J. P., Flavoni, S., Guez, L., Kataoka, T., Perrot, X., Parc, L., and
- 2466 Watanabe, M.: Sensitivity of the Global Ocean Carbon Sink to the Ocean Skin in a Climate Model, J. Geophys.
- 2467 Res. Oceans, 128, e2022JC019479, https://doi.org/10.1029/2022JC019479, 2023.
- 2468 Bennington, V., Gloege, L., and McKinley, G. A.: Variability in the Global Ocean Carbon Sink From 1959 to 2020
- 2469 by Correcting Models with Observations, Geophys. Res. Lett., 49, e2022GL098632,
- 2470 https://doi.org/10.1029/2022GL098632, 2022.
- 2471 Bernardello, R., Sicardi, V., Lapin, V., Ortega, P., Ruprich-Robert, Y., Tourigny, E. and Ferrer, E.: Ocean
- 2472 biogeochemical reconstructions to estimate historical ocean CO 2 uptake. Earth System Dynamics, 15(5), pp.1255-
- 2473 1275, https://doi.org/10.5194/esd-15-1255-2024, 2024.
- 2474 Berthet, S., Séférian, R., Bricaud, C., Chevallier, M., Voldoire, A., and Ethé, C.: Evaluation of an Online Grid-
- Coarsening Algorithm in a Global Eddy-Admitting Ocean Biogeochemical Model, J. Adv. Model Earth Sy., 11, 2475
- 2476 1759-1783, https://doi.org/10.1029/2019MS001644, 2019.
- 2477 Bethke, I., Wang, Y., Counillon, F., Keenlyside, N., Kimmritz, M., Fransner, F., Samuelsen, A., Langehaug, H.,
- 2478 Svendsen, L., Chiu, P.-G., Passos, L., Bentsen, M., Guo, C., Gupta, A., Tjiputra, J., Kirkevåg, A., Olivié, D.,
- 2479 Seland, Ø., Solsvik Vågane, J., Fan, Y., and Eldevik, T.: NorCPM1 and its contribution to CMIP6 DCPP, Geosci.
- 2480 Model Dev., 14, 7073–7116, https://doi.org/10.5194/gmd-14-7073-2021, 2021.
- 2481 Betts, R. A., Jones, C. D., Knight, J. R., Keeling, R. F., and Kennedy, J. J.: El Niño and a record CO2 rise, Nat.
- 2482 Clim. Change, 6, 806-810, https://doi.org/10.1038/nclimate3063, 2016.
- 2483 Bilbao, R., Wild, S., Ortega, P., Acosta-Navarro, J., Arsouze, T., Bretonnière, P.A., Caron, L.P., Castrillo, M.,
- 2484 Cruz-García, R., Cvijanovic, I. and Doblas-Reyes, F.J.: Assessment of a full-field initialised decadal climate
- 2485 prediction system with the CMIP6 version of EC-Earth. Earth System Dynamics Discussions, 2020, pp.1-30,
- 2486 https://doi.org/10.5194/esd-12-173-2021, 2020.
- 2487 Bloom, A. A. and Williams, M.: Constraining ecosystem carbon dynamics in a data-limited world: integrating
- 2488 ecological "common sense" in a model-data fusion framework, Biogeosciences, 12, 1299-1315,
- 2489 https://doi.org/10.5194/bg-12-1299-2015, 2015.
- 2490 Bloom, A. A., Exbrayat, J.-F., van der Velde, I. R., Feng, L., and Williams, M.: The decadal state of the terrestrial
- 2491 carbon cycle: Global retrievals of terrestrial carbon allocation, pools, and residence times, Proc. Natl. Acad. Sci.,
- 2492 113, 1285–1290, https://doi.org/10.1073/pnas.1515160113, 2016.
- 2493 Boer, G. J., Smith, D. M., Cassou, C., Doblas-Reyes, F., Danabasoglu, G., Kirtman, B., Kushnir, Y., Kimoto, M.,
- 2494 Meehl, G. A., Msadek, R., Mueller, W. A., Taylor, K. E., Zwiers, F., Rixen, M., Ruprich-Robert, Y., and Eade, R.:
- 2495 The Decadal Climate Prediction Project (DCPP) contribution to CMIP6, Geosci. Model Dev., 9, 3751–3777,
- 2496 https://doi.org/10.5194/gmd-9-3751-2016, 2016.
- 2497 Boucher, O., Servonnat, J., Albright, A. L., Aumont, O., Balkanski, Y., Bastrikov, V., Bekki, S., Bonnet, R., Bony,
- 2498 S., Bopp, L., Braconnot, P., Brockmann, P., Cadule, P., Caubel, A., Cheruy, F., Codron, F., Cozic, A., Cugnet, D.,
- 2499 D'Andrea, F., Davini, P., de Lavergne, C., Denvil, S., Deshayes, J., Devilliers, M., Ducharne, A., Dufresne, J.-L.,
- 2500 Dupont, E., Éthé, C., Fairhead, L., Falletti, L., Flavoni, S., Foujols, M.-A., Gardoll, S., Gastineau, G., Ghattas, J.,
- 2501 Grandpeix, J.-Y., Guenet, B., Guez, E., Lionel, Guilyardi, E., Guimberteau, M., Hauglustaine, D., Hourdin, F.,
- 2502 Idelkadi, A., Joussaume, S., Kageyama, M., Khodri, M., Krinner, G., Lebas, N., Levavasseur, G., Lévy, C., Li, L., 2503
- Lott, F., Lurton, T., Luyssaert, S., Madec, G., Madeleine, J.-B., Maignan, F., Marchand, M., Marti, O., Mellul, L., Meurdesoif, Y., Mignot, J., Musat, I., Ottlé, C., Peylin, P., Planton, Y., Polcher, J., Rio, C., Rochetin, N., Rousset, 2504
- 2505 C., Sepulchre, P., Sima, A., Swingedouw, D., Thiéblemont, R., Traore, A. K., Vancoppenolle, M., Vial, J., Vialard,
- 2506 J., Viovy, N., and Vuichard, N.: Presentation and Evaluation of the IPSL-CM6A-LR Climate Model, J. Adv.
- 2507 Model. Earth Syst., 12, e2019MS002010, https://doi.org/10.1029/2019MS002010, 2020.
- 2508 Bourgeois, T., Goris, N., Schwinger, J., and Tjiputra, J. F.: Stratification constrains future heat and carbon uptake
- 2509 in the Southern Ocean between 30°S and 55°S, Nat. Commun., 13, 340, https://doi.org/10.1038/s41467-022-
- 2510 27979-5, 2022.
- 2511 Bourgoin, C., Beuchle, R., Branco, A., Carreiras, J., Ceccherini, G., Oom, D., San-Miguel-Ayanz, J., and Sedano,
- 2512 F.: Extensive fire-driven degradation in 2024 marks worst Amazon forest disturbance in over 2 decades,
- 2513 Biogeosciences, 22, 5247–5256, https://doi.org/10.5194/bg-22-5247-2025, 2025.





- 2514 Bray, E.: 2017 Minerals Yearbook: Aluminum [Advance Release], Tech. rep., U.S. Geological Survey, https://d9-
- 2515 wret.s3-us-west-2.amazonaws.com/assets/palladium/production/atoms/files/myb1-2017-alumi.pdf, 2020
- 2516 Brienen, R. J. W., Caldwell, L., Duchesne, L., Voelker, S., Barichivich, J., Baliva, M., Ceccantini, G., Di Filippo,
- 2517 A., Helama, S., Locosselli, G. M., Lopez, L., Piovesan, G., Schöngart, J., Villalba, R., and Gloor, E.: Forest carbon
- 2518 sink neutralized by pervasive growth-lifespan trade-offs, Nat. Commun., 11, 4241, https://doi.org/10.1038/s41467-
- 2519 020-17966-z, 2020.
- Brienen, R. J. W., Phillips, O. L., Feldpausch, T. R., Gloor, E., Baker, T. R., Lloyd, J., Lopez-Gonzalez, G., 2520
- 2521 Monteagudo-Mendoza, A., Malhi, Y., Lewis, S. L., Vásquez Martinez, R., Alexiades, M., Álvarez Dávila, E.,
- 2522 Alvarez-Loayza, P., Andrade, A., Aragão, L. E. O. C., Araujo-Murakami, A., Arets, E. J. M. M., Arroyo, L.,
- 2523 Aymard C., G. A., Bánki, O. S., Baraloto, C., Barroso, J., Bonal, D., Boot, R. G. A., Camargo, J. L. C., Castilho, C.
- 2524 V., Chama, V., Chao, K. J., Chave, J., Comiskey, J. A., Cornejo Valverde, F., da Costa, L., de Oliveira, E. A., Di
- 2525 Fiore, A., Erwin, T. L., Fauset, S., Forsthofer, M., Galbraith, D. R., Grahame, E. S., Groot, N., Hérault, B.,
- Higuchi, N., Honorio Coronado, E. N., Keeling, H., Killeen, T. J., Laurance, W. F., Laurance, S., Licona, J.,
- 2526 2527 Magnussen, W. E., Marimon, B. S., Marimon-Junior, B. H., Mendoza, C., Neill, D. A., Nogueira, E. M., Núñez, P.,
- 2528 Pallqui Camacho, N. C., Parada, A., Pardo-Molina, G., Peacock, J., Peña-Claros, M., Pickavance, G. C., Pitman, N.
- 2529 C. A., Poorter, L., Prieto, A., Quesada, C. A., Ramírez, F., Ramírez-Angulo, H., Restrepo, Z., Roopsind, A., Rudas,
- A., Salomão, R. P., Schwarz, M., Silva, N., Silva-Espejo, J. E., Silveira, M., Stropp, J., Talbot, J., ter Steege, H., 2530
- 2531 Teran-Aguilar, J., Terborgh, J., Thomas-Caesar, R., Toledo, M., Torello-Raventos, M., Umetsu, R. K., van der
- 2532 Heijden, G. M. F., van der Hout, P., Guimarães Vieira, I. C., Vieira, S. A., Vilanova, E., Vos, V. A., and Zagt, R.
- 2533 J.: Long-term decline of the Amazon carbon sink, 519, 344–348, https://doi.org/10.1038/nature14283, 2015.
- Bronselaer, B., Winton, M., Russell, J., Sabine, C. L., and Khatiwala, S.: Agreement of CMIP5 Simulated and
- 2535 Observed Ocean Anthropogenic CO2 Uptake, Geophys. Res. Lett., 44, 12,298-12,305,
- 2536 https://doi.org/10.1002/2017GL074435, 2017.
- 2537 Bruno, M. and Joos, F.: Terrestrial carbon storage during the past 200 years: A Monte Carlo Analysis of CO 2 data
- 2538 from ice core and atmospheric measurements, Global Biogeochem. Cycles, 11, 111-124,
- 2539 https://doi.org/10.1029/96GB03611, 1997.
- 2540 Burrows, S. M., Maltrud, M., Yang, X., Zhu, Q., Jeffery, N., Shi, X., Ricciuto, D., Wang, S., Bisht, G., Tang, J.,
- 2541 Wolfe, J., Harrop, B. E., Singh, B., Brent, L., Baldwin, S., Zhou, T., Cameron-Smith, P., Keen, N., Collier, N., Xu,
- 2542 M., Hunke, E. C., Elliott, S. M., Turner, A. K., Li, H., Wang, H., Golaz, J.-C., Bond-Lamberty, B., Hoffman, F. M., 2543 Riley, W. J., Thornton, P. E., Calvin, K., and Leung, L. R.: The DOE E3SM v1.1 Biogeochemistry Configuration:
- 2544 Description and Simulated Ecosystem-Climate Responses to Historical Changes in Forcing, J. Adv. Model. Earth
- 2545 Syst., 12, e2019MS001766, https://doi.org/10.1029/2019MS001766, 2020.
- 2546 Bunsen, F., Nissen, C., and Hauck, J.: The Impact of Recent Climate Change on the Global Ocean Carbon Sink.
- 2547 Geophysical Research Letters, 51(4), e2023GL107030, https://doi.org/10.1029/2023GL107030, 2024.
- 2548 Burton, C., Betts, R., Cardoso, M., Feldpausch, T. R., Harper, A., Jones, C. D., Kelley, D. I., Robertson, E., and
- 2549 Wiltshire, A.: Representation of fire, land-use change and vegetation dynamics in the Joint UK Land Environment
- 2550 Simulator vn4.9 (JULES), Geosci. Model Dev., 12, 179–193, https://doi.org/10.5194/gmd-12-179-2019, 2019.
- 2551 Burton, C., Lampe, S., Kelley, D. I., Thiery, W., Hantson, S., Christidis, N., Gudmundsson, L., Forrest, M., Burke,
- 2552 E., Chang, J., Huang, H., Ito, A., Kou-Giesbrecht, S., Lasslop, G., Li, W., Nieradzik, L., Li, F., Chen, Y.,
- Randerson, J., Reyer, C. P. O., and Mengel, M.: Global burned area increasingly explained by climate change, 2553
- 2554 Nature Climate Change, https://doi.org/10.1038/s41558-024-02140-w, 2024.
- 2555 Bushinsky, S. M., Landschützer, P., Rödenbeck, C., Gray, A. R., Baker, D., Mazloff, M. R., Resplandy, L.,
- 2556 Johnson, K. S., and Sarmiento, J. L.: Reassessing Southern Ocean Air-Sea CO 2 Flux Estimates With the Addition
- 2557 of Biogeochemical Float Observations, Global Biogeochem. Cycles, 33, 1370-1388,
- 2558 https://doi.org/10.1029/2019GB006176, 2019.
- 2559 Byrne, B., Liu, J., Bowman, K.W., Pascolini-Campbell, M., Chatterjee, A., Pandey, S., Miyazaki, K., van der Werf,
- 2560 G.R., Wunch, D., Wennberg, P.O., Roehl, C.M., and Sinha, S.: Carbon emissions from the 2023 Canadian
- 2561 wildfires. Nature, 633, 835-839, https://doi.org/10.1038/s41586-024-07878-z, 2024.
- 2562 Canadell, J. G., Le Quere, C., Raupach, M. R., Field, C. B., Buitenhuis, E. T., Ciais, P., Conway, T. J., Gillett, N.
- 2563 P., Houghton, R. A., and Marland, G.: Contributions to accelerating atmospheric CO2 growth from economic





- 2564 activity, carbon intensity, and efficiency of natural sinks, Proceedings of the National Academy of Sciences, 104,
- 2565 18866-18870, https://doi.org/10.1073/pnas.0702737104, 2007.
- 2566 Canadell, J. G., Monteiro, P. M. S., Costa, M. H., Cotrim da Cunha, L., Cox, P. M., Eliseev, A. V., Henson, S.,
- 2567 Ishii, M., Jaccard, S., Koven, C., Lohila, A., Patra, P. K., Piao, S., Rogelj, J., Syampungani, S., Zaehle, S., and
- 2568 Zickfeld, K.: Global Carbon and other Biogeochemical Cycles and Feedbacks. In: Climate Change 2021: The
- 2569 Physical Science Basis. Contribution of Working Group I to the Sixth Assessment Report of the Intergovernmental 2570 Panel on Climate Change [Masson-Delmotte, V., P. Zhai, A. Pirani, S. L. Connors, C. Péan, S. Berger, N. Caud, Y.
- Chen, L. Goldfarb, M. I. Gomis, M. Huang, K. Leitzell, E. Lonnoy, J.B.R. Matthews, T. K. Maycock, T.
- 2571 2572 Waterfield, O. Yelekçi, R. Yu and B. Zhou (eds.)]. Cambridge University Press, Cambridge, United Kingdom and
- 2573 New York, NY, USA, pp. 673-816, https://doi.org/10.1017/9781009157896.007., 2021.
- 2574 Cao, Z., Myers, R. J., Lupton, R. C., Duan, H., Sacchi, R., Zhou, N., Reed Miller, T., Cullen, J. M., Ge, Q., and
- 2575 Liu, G.: The sponge effect and carbon emission mitigation potentials of the global cement cycle, Nat Commun, 11,
- 2576 3777, https://doi.org/10.1038/s41467-020-17583-w, 2020.
- 2577 Carbon Monitor: Year in Review: Global carbon emissions and decarbonization in 2024, available at:
- 2578 https://carbonmonitor.org/, last access: 23 October 2025, 2025.
- 2579 Centro Nacional de Monitoramento e Alertas de Desastres Naturais (CEMADEN): Monitoramento de secas e
- 2580 impactos no Brasil - Agosto 2024, available at: https://www.gov.br/cemaden/pt-
- 2581 br/assuntos/monitoramento/monitoramento-de-seca-para-o-brasil/monitoramento-de-secas-e-impactos-no-brasil-
- 2582 agosto-2024, last access: 23 October 2025.
- 2583 Céspedes, J., Sylvester, J. M., Pérez-Marulanda, L., Paz-Garcia, P., Reymondin, L., Khodadadi, M., Tello, J. J., and
- 2584 Castro-Nunez, A.: Has global deforestation accelerated due to the COVID-19 pandemic?, J. For. Res., 34, 1153-
- 2585 1165, https://doi.org/10.1007/s11676-022-01561-7, 2023.
- 2586 Chandra, N., Patra, P. K., Niwa, Y., Ito, A., Iida, Y., Goto, D., Morimoto, S., Kondo, M., Takigawa, M., Hajima,
- 2587 T., and Watanabe, M.: Estimated regional CO2 flux and uncertainty based on an ensemble of atmospheric CO2
- 2588 inversions, Atmospheric Chem. Phys., 22, 9215–9243, https://doi.org/10.5194/acp-22-9215-2022, 2022.
- 2589 Chatfield, C.: The Holt-Winters Forecasting Procedure, J. Roy. Stat. Soc. C., 27, 264-279,
- 2590 https://doi.org/10.2307/2347162, 1978.
- 2591 Chau, T. T. T., Gehlen, M., and Chevallier, F.: A seamless ensemble-based reconstruction of surface ocean pCO2
- 2592 and air-sea CO2 fluxes over the global coastal and open oceans, Biogeosciences, 19, 1087-1109,
- 2593 https://doi.org/10.5194/bg-19-1087-2022, 2022.
- 2594 Chen, Y., Hall, J., Van Wees, D., Andela, N., Hantson, S., Giglio, L., Van Der Werf, G. R., Morton, D. C., and
- 2595 Randerson, J. T.: Multi-decadal trends and variability in burned area from the fifth version of the Global Fire
- 2596 Emissions Database (GFED5), Earth Syst. Sci. Data, 15, 5227-5259, https://doi.org/10.5194/essd-15-5227-2023,
- 2597
- 2598 Chevallier, F., Fisher, M., Peylin, P., Serrar, S., Bousquet, P., Bréon, F.-M., Chédin, A., and Ciais, P.: Inferring CO
- 2599 2 sources and sinks from satellite observations: Method and application to TOVS data, J. Geophys. Res., 110,
- D24309, https://doi.org/10.1029/2005JD006390, 2005. 2600
- 2601 Chevallier, F., Martinez, A., Lloret, Z., Takache, S., and Cozic, A.: Offline Atmospheric Transport on a Global
- 2602 Mesh of Hexagons, JGR Atmospheres, 130, e2025JD043579, https://doi.org/10.1029/2025JD043579, 2025.
- 2603 Ciais, P., Sabine, C., Bala, G., Bopp, L., Brovkin, V., Canadell, J. G., Chhabra, A., DeFries, R., Galloway, J.,
- 2604 Heimann, M., Jones, C., Le Quéré, C., Myneni, R., Piao, S., Thornton, P., Willem, J., Friedlingstein, P., and
- 2605 Munhoven, G.: Carbon and Other Biogeochemical Cycles, in Climate Change 2013: The Physical Science Basis,
- 2606 Contribution of Working Group I to the Fifth Assessment Report of the Intergovernmental Panel on Climate 2607
- Change, edited by: Intergovernmental Panel on Climate Change, Cambridge University Press, Cambridge, United 2608
- Kingdom and New York, NY, USA, https://doi.org/10.1017/CBO9781107415324.015, 2013.
- 2609 Ciais, P., Tan, J., Wang, X., Roedenbeck, C., Chevallier, F., Piao, S.-L., Moriarty, R., Broquet, G., Le Quéré, C.,
- Canadell, J. G., Peng, S., Poulter, B., Liu, Z., and Tans, P.: Five decades of northern land carbon uptake revealed 2610
- 2611 by the interhemispheric CO2 gradient, Nature, 568, 221-225, https://doi.org/10.1038/s41586-019-1078-6, 2019.





- 2612 Ciais, P., Bastos, A., Chevallier, F., Lauerwald, R., Poulter, B., Canadell, P., Hugelius, G., Jackson, R. B., Jain, A.,
- Jones, M., Kondo, M., Luijkx, I. T., Patra, P. K., Peters, W., Pongratz, J., Petrescu, A. M. R., Piao, S., Qiu, C., Von
- Randow, C., Regnier, P., Saunois, M., Scholes, R., Shvidenko, A., Tian, H., Yang, H., Wang, X., and Zheng, B.:
- 2615 Definitions and methods to estimate regional land carbon fluxes for the second phase of the REgional Carbon
- 2616 Cycle Assessment and Processes Project (RECCAP-2), Geosci. Model Dev., 15, 1289–1316,
- 2617 https://doi.org/10.5194/gmd-15-1289-2022, 2022.
- Ciais, P., Ke, P., Yao, Y., Sitch, S., Li, W., Xu, Y., Du, X., Gui, X., Bastos, A., Zaehle, S., Poulter, B., Colligan, T.,
- van der Woude, A. M., Peters, W., Liu, Z., Jin, Z., Tian, X., Wang, Y., Liu, J., Pandey, S., O'Dell, C., Bian, J.,
- Zhou, C., Miller, J., Lan, X., Goncalves De Souza, J., O'Sullivan, M., Friedlingstein, P., van der Werf, G. R.,
- 2621 Peters, G. P., and Chevallier, F.: Low latency global carbon budget indicates reduced land carbon sink in the year
- 2622 2024, National Science Review, submitted.
- 2623 Collier, N., Hoffman, F. M., Lawrence, D. M., Keppel-Aleks, G., Koven, C. D., Riley, W. J., Mu, M., and
- 2624 Randerson, J. T.: The International Land Model Benchmarking (ILAMB) System: Design, Theory, and
- 2625 Implementation, J. Adv. Model. Earth Syst., 10, 2731–2754, https://doi.org/10.1029/2018MS001354, 2018.
- 2626 Conchedda, G. and Tubiello, F. N.: Drainage of organic soils and GHG emissions: Validation with country data,
- Biosphere Biogeosciences, https://doi.org/10.5194/essd-2020-202, 2020.
- 2628 Cox, P. M., Pearson, D., Booth, B. B., Friedlingstein, P., Huntingford, C., Jones, C. D., and Luke, C. M.:
- 2629 Sensitivity of tropical carbon to climate change constrained by carbon dioxide variability, Nature, 494, 341–344,
- 2630 https://doi.org/10.1038/nature11882, 2013.
- 2631 De Kauwe, M. G., Medlyn, B. E., Zaehle, S., Walker, A. P., Dietze, M. C., Wang, Y.-P., Luo, Y., Jain, A. K., El-
- 2632 Masri, B., Hickler, T., Wårlind, D., Weng, E., Parton, W. J., Thornton, P. E., Wang, S., Prentice, I. C., Asao, S.,
- Smith, B., McCarthy, H. R., Iversen, C. M., Hanson, P. J., Warren, J. M., Oren, R., and Norby, R. J.: Where does
- the carbon go? A model—data intercomparison of vegetation carbon allocation and turnover processes at two
- temperate forest free-air CO2 enrichment sites, New Phytol., 203, 883–899, https://doi.org/10.1111/nph.12847,
- 2636 2014
- 2637 Delire, C., Séférian, R., Decharme, B., Alkama, R., Calvet, J.-C., Carrer, D., Gibelin, A.-L., Joetzjer, E., Morel, X.,
- Rocher, M., and Tzanos, D.: The Global Land Carbon Cycle Simulated With ISBA-CTRIP: Improvements Over
- 2639 the Last Decade, J. Adv. Model. Earth Syst., 12, e2019MS001886, https://doi.org/10.1029/2019MS001886, 2020.
- 2640 Denman, K. L., Brasseur, G., Chidthaisong, A., Ciais, P., Cox, P. M., Dickinson, R. E., Hauglustaine, D., Heinze,
- 2641 C., Holland, E., Jacob, D., Lohmann, U., Ramachandran, S., Leite da Silva Dias, P., Wofsy, S. C., and Zhang, X.:
 2642 Couplings Between Changes in the Climate System and Biogeochemistry, in: Climate Change 2007: The Physical
- 2643 Science Basis. Contribution of Working Group I to the Fourth Assessment Report of the Intergovernmental Panel
- 2644 on Climate Change, edited by: Solomon, S., Qin, D., Manning, M., Marquis, M., Averyt, K., Tignor, M. M. B.,
- 2645 Miller, H. L., and Chen, Z. L., Cambridge University Press, Cambridge, UK and New York, USA, 499–587, ISBN:
- 2646 9780521705967, 2007.
- 2647 Denvil-Sommer, A., Gehlen, M., and Vrac, M.: Observation system simulation experiments in the Atlantic Ocean
- for enhanced surface ocean pCO2 reconstructions, Ocean Sci., 17, 1011–1030, https://doi.org/10.5194/os-17-1011-
- 2649 2021, 2021.
- 2650 DeVries, T., Holzer, M., and Primeau, F.: Recent increase in oceanic carbon uptake driven by weaker upper-ocean
- 2651 overturning, Nature, 542, 215–218, https://doi.org/10.1038/nature21068, 2017.
- 2652 DeVries, T.: The oceanic anthropogenic CO 2 sink: Storage, air-sea fluxes, and transports over the industrial era,
- 2653 Global Biogeochem. Cycles, 28, 631–647, https://doi.org/10.1002/2013GB004739, 2014.
- 2654 DeVries, T., Quéré, C. L., Andrews, O., Berthet, S., Hauck, J., Ilyina, T., Landschützer, P., Lenton, A., Lima, I. D.,
- 2655 Nowicki, M., Schwinger, J., and Séférian, R.: Decadal trends in the ocean carbon sink, PNAS, 116, 11646–11651,
- 2656 https://doi.org/10.1073/pnas.1900371116, 2019.
- 2657 DeVries, T.: Atmospheric CO2 and Sea Surface Temperature Variability Cannot Explain Recent Decadal
- Variability of the Ocean CO2 Sink, Geophysical Research Letters, 49, e2021GL096018,
- 2659 https://doi.org/10.1029/2021GL096018, 2022.





- 2660 DeVries, T., Yamamoto, K., Wanninkhof, R., Gruber, N., Hauck, J., Müller, J. D., Bopp, L., Carroll, D., Carter, B.,
- Chau, T.-T.-T., Doney, S. C., Gehlen, M., Gloege, L., Gregor, L., Henson, S., Kim, J. H., Iida, Y., Ilyina, T.,
- Landschützer, P., Le Quéré, C., Munro, D., Nissen, C., Patara, L., Pérez, F. F., Resplandy, L., Rodgers, K. B.,
- 2663 Schwinger, J., Séférian, R., Sicardi, V., Terhaar, J., Triñanes, J., Tsujino, H., Watson, A., Yasunaka, S., and Zeng,
- 2664 J.: Magnitude, trends, and variability of the global ocean carbon sink from 1985-2018, Glob. Biogeochem. Cycles,
- 2665 n/a, e2023GB007780, https://doi.org/10.1029/2023GB007780, 2023.
- Döscher, R., Acosta, M., Alessandri, A., Anthoni, P., Arneth, A., Arsouze, T., Bergmann, T., Bernadello, R.,
- Bousetta, S., Caron, L.P. and Carver, G.: The EC-earth3 Earth system model for the climate model intercomparison
- project 6. Geoscientific Model Development Discussions, 2021, pp.1-90, https://doi.org/10.5194/gmd-15-2973-
- 2669 2022, 2021.
- 2670 Doney, S. C., Lima, I., Feely, R. A., Glover, D. M., Lindsay, K., Mahowald, N., Moore, J. K., and Wanninkhof, R.:
- Mechanisms governing interannual variability in upper-ocean inorganic carbon system and air-sea CO2 fluxes:
- 2672 Physical climate and atmospheric dust, Deep Sea Research Part II: Topical Studies in Oceanography, 56, 640–655,
- 2673 https://doi.org/10.1016/j.dsr2.2008.12.006, 2009.
- 2674 Dong, Y., Bakker, D. C. E., Bell, T. G., Huang, B., Landschützer, P., Liss, P. S., and Yang, M.: Update on the
- 2675 Temperature Corrections of Global Air-Sea CO2 Flux Estimates, Glob. Biogeochem. Cycles, 36, e2022GB007360,
- 2676 https://doi.org/10.1029/2022GB007360, 2022.
- 2677 Dong, Y., Bakker, D. C. E., Bell, T. G., Yang, M., Landschützer, P., Hauck, J., Rödenbeck, C., Kitidis, V.,
- 2678 Bushinsky, S. M., and Liss, P. S. (2024). Direct observational evidence of strong CO2 uptake in the Southern
- 2679 Ocean. Science Advances, 10(30), eadn5781, https://doi.org/10.1126/sciadv.adn5781, 2024a.
- 2680 Dong, Y., Bakker, D. C. E., and Landschützer, P.: Accuracy of ocean CO2 uptake estimates at a risk by a reduction
- in the data collection. Geophysical Research Letters, 51, e2024GL108502, https://doi.org/10.1029/2024GL108502,
- 2682 2024b.
- 2683 Dorgeist, L., Schwingshackl, C., Bultan, S., and Pongratz, J.: A consistent budgeting of terrestrial carbon fluxes.
- 2684 Nature Communications, 15(1), 7426, https://doi.org/10.1038/s41467-024-51126-x, 2024.
- 2685 Dou, X., Wang, Y., Ciais, P., Chevallier, F., Davis, S. J., Crippa, M., Janssens-Maenhout, G., Guizzardi, D.,
- 2686 Solazzo, E., Yan, F., Huo, D., Zheng, B., Zhu, B., Cui, D., Ke, P., Sun, T., Wang, H., Zhang, Q., Gentine, P., Deng,
- Z., and Liu, Z.: Near-real-time global gridded daily CO2 emissions, The Innovation, 3, 100182,
- 2688 https://doi.org/10.1016/j.xinn.2021.100182, 2022.
- 2689 Eckes-Shephard, A. H., Argles, A. P. K., Brzeziecki, B., Cox, P. M., De Kauwe, M. G., Esquivel-Muelbert, A.,
- Fisher, R. A., Hurtt, G. C., Knauer, J., Koven, C. D., Lehtonen, A., Luyssaert, S., Marqués, L., Ma, L., Marie, G.,
- 2691 Moore, J. R., Needham, J. F., Olin, S., Peltoniemi, M., Piltz, K., Sato, H., Sitch, S., Stocker, B. D., Weng, E.,
- 2692 Zuleta, D., and Pugh, T. A. M. Pugh: Demography, dynamics and data: building confidence for simulating changes
- in the world's forests, New Phytologist, doi: 10.1111/nph.70643, 2025.
- Edson, J. B., Jampana, V., Weller, R. A., Bigorre, S. P., Plueddemann, A. J., Fairall, C. W., Miller, S. D., Mahrt,
- L., Vickers, D., and Hersbach, H.: On the Exchange of Momentum over the Open Ocean, J. Phys. Oceanogr., 43,
- 2696 1589–1610, https://doi.org/10.1175/JPO-D-12-0173.1, 2013.
- 2697 EIA: Short-Term Energy Outlook: October 2025. U.S. Energy Information Administration [Data set]. Available at:
- 2698 http://www.eia.gov/forecasts/steo/outlook.cfm, last access: 23 October 2025, 2023.
- 2699 Ehmen, T. F., Mackay, N. S., and Watson, A.: The Spatiotemporal Distribution of Dissolved Inorganic Carbon in
- 2700 the Global Ocean Interior: Reconstructed through Machine Learning, ESS Open Archive, id.
- 2701 essoar.173687460.04244614/v1, available at: https://doi.org/10.22541/essoar.173687460.04244614/v1, last access:
- 2702 23 Octover 2025, 2025.
- Embury, O., Merchant, C.J., Good, S.A., Rayner, N.A., Høyer, J.L., Atkinson, C., Block, T., Alerskans, E.,
- 2704 Pearson, K.J., Worsfold, M. and McCarroll, N. and Donlon, C.: Satellite-based time-series of sea-surface
- temperature since 1980 for climate applications. Scientific Data, 11(1), 326, https://doi.org/10.1038/s41597-024-
- 2706 03147-w, 2024.
- 2707 Erb, K.-H., Kastner, T., Luyssaert, S., Houghton, R. A., Kuemmerle, T., Olofsson, P., and Haberl, H.: Bias in the
- attribution of forest carbon sinks, Nature Clim Change, 3, 854–856, https://doi.org/10.1038/nclimate2004, 2013.





- Erb, K.-H., Kastner, T., Plutzar, C., Bais, A. L. S., Carvalhais, N., Fetzel, T., Gingrich, S., Haberl, H., Lauk, C.,
- 2710 Niedertscheider, M., Pongratz, J., Thurner, M., and Luyssaert, S.: Unexpectedly large impact of forest management
- 2711 and grazing on global vegetation biomass, Nature, 553, 73-76, https://doi.org/10.1038/nature25138, 2018.
- 2712 Erb, M. and Marland G.: Global, Regional, and National Fossil-Fuel CO2 Emisisons: 1751-2022 CDIAC-FF,
- 2713 Research Institute for Environment, Energy, and Economics, Appalachian State University.
- 2714 https://rieee.appstate.edu/projects-programs/cdiac/, last access: 23 October 2025, 2025.
- 2715 Eskander, S. M. S. U. and Fankhauser, S.: Reduction in greenhouse gas emissions from national climate legislation,
- 2716 Nat. Clim. Chang., 10, 750–756, https://doi.org/10.1038/s41558-020-0831-z, 2020.
- 2717 Etheridge, D. M., Steele, L. P., Langenfelds, R. L., Francey, R. J., Barnola, J.-M., and Morgan, V. I.: Natural and
- 2718 anthropogenic changes in atmospheric CO 2 over the last 1000 years from air in Antarctic ice and firn, J. Geophys.
- 2719 Res., 101, 4115-4128, https://doi.org/10.1029/95JD03410, 1996.
- FAO, Food and Agriculture Organization of the United Nations (FAO): Impact of the Ukraine-Russia conflict on 2720
- 2721 global food security and related matters under the mandate of the Food and Agriculture Organization of the United
- 2722 Nations (FAO), Hundred and Seventieth Session of the Council, https://www.fao.org/3/nj164en/nj164en.pdf, last
- 2723 access: 23 October 2025, 2023.
- 2724 FAO: FAOSTAT Emissions from drained organic soils. Available at http://www.fao.org/faostat/en/#data/GV, last
- 2725 access: 23 October 2025, 2025a.
- 2726 FAO: Forest emissions and removals - Global, regional and country trends 1990-2025.FAOSTAT Analytical
- 2727 Briefs, No. 114. Rome., available at: https://doi.org/10.4060/cd7163en, last access: 23 October 2025, 2025b.
- 2728 FAO: Land statistics 2001-2023 - Global, regional and country trends. FAOSTAT Analytical Briefs, No.107.
- 2729 Rome, available at: https://doi.org/10.4060/cd5765en, last access: 23 October 2025, 2025c.
- 2730 FAO: FAOSTAT Emissions totals database, available at: https://faostat.fao.org/internal/en/#data/GT, FAO, Rome,
- 2731 , last access: 23 October 2025, 2025d.
- 2732 Fay, A. R., Gregor, L., Landschützer, P., McKinley, G. A., Gruber, N., Gehlen, M., Iida, Y., Laruelle, G. G.,
- 2733 Rödenbeck, C., Roobaert, A., and Zeng, J.: SeaFlux: harmonization of air-sea CO2 fluxes from surface pCO2 data
- 2734 products using a standardized approach, Earth System Science Data, 13, 4693-4710, https://doi.org/10.5194/essd-
- 2735 13-4693-2021, 2021.
- 2736 Fay, A. R., McKinley, G. A., Lovenduski, N. S., Eddebbar, Y., Levy, M. N., Long, M. C., Olivarez, H. C., and
- 2737 Rustagi, R. R.: Immediate and Long-Lasting Impacts of the Mt. Pinatubo Eruption on Ocean Oxygen and Carbon
- 2738 Inventories. Global Biogeochemical Cycles, 37(2). https://doi.org/10.1029/2022gb007513, 2023.
- 2739 Fay, A. R., Carroll, D., McKinley, G. A., Menemenlis, D., and Zhang, H.: Scale-Dependent Drivers of Air-Sea
- 2740 CO2 Flux Variability, Geophysical Research Letters, 51, e2024GL111911, https://doi.org/10.1029/2024GL111911,
- 2741 2024.
- 2742 Fay, A. R., Heimdal, T. H., Acquaviva, V., Shaum, A. P., and McKinley, G. A.: Sensitivity of Ocean Carbon Sink
- 2743 Estimates to Rare Observations, Geophysical Research Letters, 52, e2025GL117961,
- 2744 https://doi.org/10.1029/2025GL117961, 2025.
- 2745 Felzer, B. S.: Carbon, nitrogen, and water response to climate and land use changes in Pennsylvania during the
- 2746 20th and 21st centuries, Ecological Modelling, 240, 49-63, https://doi.org/10.1016/j.ecolmodel.2012.05.003, 2012.
- 2747 Felzer, B. S. and Jiang, M.: Effect of Land Use and Land Cover Change in Context of Growth Enhancements in the
- 2748 United States Since 1700: Net Source or Sink?, JGR Biogeosciences, 123, 3439-3457,
- 2749 https://doi.org/10.1029/2017JG004378, 2018.
- Felzer, B. S., Cronin, T. W., Melillo, J. M., Kicklighter, D. W., and Schlosser, C. A.: Importance of carbon-2750
- 2751 2752 nitrogen interactions and ozone on ecosystem hydrology during the 21st century, J. Geophys. Res., 114,
- 2008JG000826, https://doi.org/10.1029/2008JG000826, 2009.
- Felzer, B. S., Cronin, T. W., Melillo, J. M., Kicklighter, D. W., Schlosser, C. A., and Dangal, S. R. S.: Nitrogen
- 2754 effect on carbon-water coupling in forests, grasslands, and shrublands in the arid western United States, J.
- 2755 Geophys. Res., 116, G03023, https://doi.org/10.1029/2010JG001621, 2011.





- Feng, L., Palmer, P. I., Bösch, H., and Dance, S.: Estimating surface CO2 fluxes from space-borne CO2 dry air
- 2757 mole fraction observations using an ensemble Kalman Filter, Atmospheric Chem. Phys., 9, 2619-2633,
- 2758 https://doi.org/10.5194/acp-9-2619-2009, 2009.
- 2759 Feng, L., Palmer, P. I., Parker, R. J., Deutscher, N. M., Feist, D. G., Kivi, R., Morino, I., and Sussmann, R.:
- 2760 Estimates of European uptake of CO2 inferred from GOSAT XCO2 retrievals: sensitivity to measurement bias
- 2761 inside and outside Europe, Atmos. Chem. Phys., 16, 1289-1302, https://doi.org/10.5194/acp-16-1289-2016, 2016.
- Fisher, R. A., Muszala, S., Verteinstein, M., Lawrence, P., Xu, C., McDowell, N. G., Knox, R. G., Koven, C., 2762
- 2763 Holm, J., Rogers, B. M., Spessa, A., Lawrence, D., and Bonan, G.: Taking off the training wheels: the properties of
- 2764 a dynamic vegetation model without climate envelopes, CLM4.5(ED), Geosci. Model Dev., 8, 3593-3619,
- 2765 https://doi.org/10.5194/gmd-8-3593-2015, 2015.
- 2766 Flanagan, D.: 2017 Minerals Yearbook: Copper [Advance Release], Tech. rep., U.S. Geological Survey,
- https://pubs.usgs.gov/myb/vol1/2017/myb1-2017-copper.pdf, 2021. 2767
- 2768 Ford, D. J., Blannin, J., Watts, J., Watson, A. J., Landschützer, P., Jersild, A., and Shutler, J. D.: A Comprehensive
- 2769 Analysis of Air-Sea CO2 Flux Uncertainties Constructed From Surface Ocean Data Products, Global
- 2770 Biogeochemical Cycles, 38, e2024GB008188, https://doi.org/10.1029/2024GB008188, 2024.
- 2771 Ford, D. J., Shutler, J. D., Ashton, I., Sims, R. P., and Holding, T.: Recalculated (depth and temperature consistent)
- 2772 $surface\ ocean\ CO_2\ at las\ (SOCAT)\ version\ 2025\ (v0-1),\ https://doi.org/10.5281/ZENODO.15656803,\ 2025.$
- 2773 Forster, P. M., Smith, C., Walsh, T., Lamb, W. F., Lamboll, R., Cassou, C., Hauser, M., Hausfather, Z., Lee, J.-Y.,
- 2774 Palmer, M. D., Von Schuckmann, K., Slangen, A. B. A., Szopa, S., Trewin, B., Yun, J., Gillett, N. P., Jenkins, S.,
- 2775 Matthews, H. D., Raghavan, K., Ribes, A., Rogelj, J., Rosen, D., Zhang, X., Allen, M., Aleluia Reis, L., Andrew,
- 2776 R. M., Betts, R. A., Borger, A., Broersma, J. A., Burgess, S. N., Cheng, L., Friedlingstein, P., Domingues, C. M.,
- 2777 Gambarini, M., Gasser, T., Gütschow, J., Ishii, M., Kadow, C., Kennedy, J., Killick, R. E., Krummel, P. B., Liné, 2778 A., Monselesan, D. P., Morice, C., Mühle, J., Naik, V., Peters, G. P., Pirani, A., Pongratz, J., Minx, J. C., Rigby,
- 2779 M., Rohde, R., Savita, A., Seneviratne, S. I., Thorne, P., Wells, C., Western, L. M., Van Der Werf, G. R., Wijffels,
- 2780 S. E., Masson-Delmotte, V., and Zhai, P.: Indicators of Global Climate Change 2024: annual update of key
- 2781 indicators of the state of the climate system and human influence, Earth Syst. Sci. Data, 17, 2641-2680,
- 2782 https://doi.org/10.5194/essd-17-2641-2025, 2025.
- 2783 Friedlingstein, P., Houghton, R. A., Marland, G., Hackler, J., Boden, T. A., Conway, T. J., Canadell, J. G.,
- 2784 Raupach, M. R., Ciais, P., and Le Quéré, C.: Update on CO2 emissions, Nature Geosci, 3, 811-812,
- 2785 https://doi.org/10.1038/ngeo1022, 2010.
- 2786 Friedlingstein, P., Andrew, R. M., Rogelj, J., Peters, G. P., Canadell, J. G., Knutti, R., Luderer, G., Raupach, M. R.,
- 2787 Schaeffer, M., van Vuuren, D. P., and Le Quéré, C.: Persistent growth of CO2 emissions and implications for
- 2788 reaching climate targets, Nature Geosci, 7, 709-715, https://doi.org/10.1038/ngeo2248, 2014.
- 2789 Friedlingstein, P., Jones, M. W., O'Sullivan, M., Andrew, R. M., Hauck, J., Peters, G. P., Peters, W., Pongratz, J.,
- 2790 Sitch, S., Le Quéré, C., Bakker, D. C. E., Canadell, J. G., Ciais, P., Jackson, R. B., Anthoni, P., Barbero, L., Bastos,
- 2791 A., Bastrikov, V., Becker, M., Bopp, L., Buitenhuis, E., Chandra, N., Chevallier, F., Chini, L. P., Currie, K. I.,
- 2792 Feely, R. A., Gehlen, M., Gilfillan, D., Gkritzalis, T., Goll, D. S., Gruber, N., Gutekunst, S., Harris, I., Haverd, V.,
- 2793 Houghton, R. A., Hurtt, G., Ilyina, T., Jain, A. K., Joetzjer, E., Kaplan, J. O., Kato, E., Klein Goldewijk, K.,
- 2794 Korsbakken, J. I., Landschützer, P., Lauvset, S. K., Lefèvre, N., Lenton, A., Lienert, S., Lombardozzi, D., Marland,
- 2795 G., McGuire, P. C., Melton, J. R., Metzl, N., Munro, D. R., Nabel, J. E. M. S., Nakaoka, S.-I., Neill, C., Omar, A.
- 2796 M., Ono, T., Peregon, A., Pierrot, D., Poulter, B., Rehder, G., Resplandy, L., Robertson, E., Rödenbeck, C.,
- 2797 Séférian, R., Schwinger, J., Smith, N., Tans, P. P., Tian, H., Tilbrook, B., Tubiello, F. N., van der Werf, G. R.,
- 2798 Wiltshire, A. J., and Zaehle, S.: Global Carbon Budget 2019, Earth Syst. Sci. Data, 11, 1783-1838,
- 2799 https://doi.org/10.5194/essd-11-1783-2019, 2019.
- 2800 Friedlingstein, P., O'Sullivan, M., Jones, M. W., Andrew, R. M., Hauck, J., Olsen, A., Peters, G. P., Peters, W.,
- 2801 Pongratz, J., Sitch, S., Le Quéré, C., Canadell, J. G., Ciais, P., Jackson, R. B., Alin, S., Aragão, L. E. O. C., Arneth,
- 2802 A., Arora, V., Bates, N. R., Becker, M., Benoit-Cattin, A., Bittig, H. C., Bopp, L., Bultan, S., Chandra, N., 2803 Chevallier, F., Chini, L. P., Evans, W., Florentie, L., Forster, P. M., Gasser, T., Gehlen, M., Gilfillan, D.,
- 2804
- Gkritzalis, T., Gregor, L., Gruber, N., Harris, I., Hartung, K., Haverd, V., Houghton, R. A., Ilyina, T., Jain, A. K., Joetzjer, E., Kadono, K., Kato, E., Kitidis, V., Korsbakken, J. I., Landschützer, P., Lefèvre, N., Lenton, A., Lienert, 2805
- 2806 S., Liu, Z., Lombardozzi, D., Marland, G., Metzl, N., Munro, D. R., Nabel, J. E. M. S., Nakaoka, S.-I., Niwa, Y.,
- 2807 O'Brien, K., Ono, T., Palmer, P. I., Pierrot, D., Poulter, B., Resplandy, L., Robertson, E., Rödenbeck, C.,





- 2808 Schwinger, J., Séférian, R., Skjelvan, I., Smith, A. J. P., Sutton, A. J., Tanhua, T., Tans, P. P., Tian, H., Tilbrook,
- 2809 B., van der Werf, G., Vuichard, N., Walker, A. P., Wanninkhof, R., Watson, A. J., Willis, D., Wiltshire, A. J.,
- 2810 Yuan, W., Yue, X., and Zaehle, S.: Global Carbon Budget 2020, Earth Syst. Sci. Data, 12, 3269–3340,
- 2811 https://doi.org/10.5194/essd-12-3269-2020, 2020.
- 2812 Friedlingstein, P., Jones, M. W., O'Sullivan, M., Andrew, R. M., Bakker, D. C. E., Hauck, J., Le Quéré, C., Peters,
- 2813 G. P., Peters, W., Pongratz, J., Sitch, S., Canadell, J. G., Ciais, P., Jackson, R. B., Alin, S. R., Anthoni, P., Bates, N.
- 2814 R., Becker, M., Bellouin, N., Bopp, L., Chau, T. T. T., Chevallier, F., Chini, L. P., Cronin, M., Currie, K. I.,
- 2815 Decharme, B., Djeutchouang, L. M., Dou, X., Evans, W., Feely, R. A., Feng, L., Gasser, T., Gilfillan, D.,
- 2816 Gkritzalis, T., Grassi, G., Gregor, L., Gruber, N., Gürses, Ö., Harris, I., Houghton, R. A., Hurtt, G. C., Iida, Y.,
- 2817 Ilyina, T., Luijkx, I. T., Jain, A., Jones, S. D., Kato, E., Kennedy, D., Klein Goldewijk, K., Knauer, J., Korsbakken, 2818 J. I., Körtzinger, A., Landschützer, P., Lauvset, S. K., Lefèvre, N., Lienert, S., Liu, J., Marland, G., McGuire, P. C.,
- 2819 Melton, J. R., Munro, D. R., Nabel, J. E. M. S., Nakaoka, S.-I., Niwa, Y., Ono, T., Pierrot, D., Poulter, B., Rehder,
- 2820 G., Resplandy, L., Robertson, E., Rödenbeck, C., Rosan, T. M., Schwinger, J., Schwingshackl, C., Séférian, R.,
- 2821 Sutton, A. J., Sweeney, C., Tanhua, T., Tans, P. P., Tian, H., Tilbrook, B., Tubiello, F., van der Werf, G. R.,
- 2822 Vuichard, N., Wada, C., Wanninkhof, R., Watson, A. J., Willis, D., Wiltshire, A. J., Yuan, W., Yue, C., Yue, X.,
- 2823 Zaehle, S., and Zeng, J.: Global Carbon Budget 2021, Earth Syst. Sci. Data, 14, 1917-2005,
- 2824 https://doi.org/10.5194/essd-14-1917-2022, 2022a.
- 2825 Friedlingstein, P., O'Sullivan, M., Jones, M. W., Andrew, R. M., Gregor, L., Hauck, J., Le Quéré, C., Luijkx, I. T.,
- 2826 Olsen, A., Peters, G. P., Peters, W., Pongratz, J., Schwingshackl, C., Sitch, S., Canadell, J. G., Ciais, P., Jackson, R.
- 2827 B., Alin, S. R., Alkama, R., Arneth, A., Arora, V. K., Bates, N. R., Becker, M., Bellouin, N., Bittig, H. C., Bopp,
- 2828 L., Chevallier, F., Chini, L. P., Cronin, M., Evans, W., Falk, S., Feely, R. A., Gasser, T., Gehlen, M., Gkritzalis, T., 2829
- Gloege, L., Grassi, G., Gruber, N., Gürses, Ö., Harris, I., Hefner, M., Houghton, R. A., Hurtt, G. C., Iida, Y., Ilyina,
- 2830 T., Jain, A. K., Jersild, A., Kadono, K., Kato, E., Kennedy, D., Klein Goldewijk, K., Knauer, J., Korsbakken, J. I.,
- 2831 Landschützer, P., Lefèvre, N., Lindsay, K., Liu, J., Liu, Z., Marland, G., Mayot, N., McGrath, M. J., Metzl, N.,
- 2832 Monacci, N. M., Munro, D. R., Nakaoka, S., Niwa, Y., O'Brien, K., Ono, T., Palmer, P. I., Pan, N., Pierrot, D.,
- 2833 Pocock, K., Poulter, B., Resplandy, L., Robertson, E., Rödenbeck, C., Rodriguez, C., Rosan, T. M., Schwinger, J., 2834 Séférian, R., Shutler, J. D., Skjelvan, I., Steinhoff, T., Sun, Q., Sutton, A. J., Sweeney, C., Takao, S., Tanhua, T.,
- 2835
- Tans, P. P., Tian, X., Tian, H., Tilbrook, B., Tsujino, H., Tubiello, F., van der Werf, G. R., Walker, A. P., 2836 Wanninkhof, R., Whitehead, C., Willstrand Wranne, A., Wright, R., Yuan, W., Yue, C., Yue, X., Zaehle, S., Zeng,
- 2837 J., and Zheng, B.: Global Carbon Budget 2022, Earth Syst. Sci. Data, 14, 4811-4900, https://doi.org/10.5194/essd-
- 2838 14-4811-2022, 2022b.
- 2839 Friedlingstein, P., O'Sullivan, M., Jones, M. W., Andrew, R. M., Bakker, D. C. E., Hauck, J., Landschützer, P., Le
- 2840 Quéré, C., Luijkx, I. T., Peters, G. P., Peters, W., Pongratz, J., Schwingshackl, C., Sitch, S., Canadell, J. G., Ciais,
- 2841 P., Jackson, R. B., Alin, S. R., Anthoni, P., Barbero, L., Bates, N. R., Becker, M., Bellouin, N., Decharme, B.,
- 2842 Bopp, L., Brasika, I. B. M., Cadule, P., Chamberlain, M. A., Chandra, N., Chau, T.-T.-T., Chevallier, F., Chini, L. 2843 P., Cronin, M., Dou, X., Enyo, K., Evans, W., Falk, S., Feely, R. A., Feng, L., Ford, D. J., Gasser, T., Ghattas, J.,
- 2844 Gkritzalis, T., Grassi, G., Gregor, L., Gruber, N., Gürses, Ö., Harris, I., Hefner, M., Heinke, J., Houghton, R. A.,
- 2845 Hurtt, G. C., Iida, Y., Ilyina, T., Jacobson, A. R., Jain, A. K., Jarníková, T., Jersild, A., Jiang, F., Jin, Z., Joos, F.,
- 2846 Kato, E., Keeling, R. F., Kennedy, D., Klein Goldewijk, K., Knauer, J., Korsbakken, J. I., Körtzinger, A., Lan, X.,
- 2847 Lefèvre, N., Li, H., Liu, J., Liu, Z., Ma, L., Marland, G., Mayot, N., McGuire, P. C., McKinley, G. A., Meyer, G.,
- 2848 Morgan, E. J., Munro, D. R., Nakaoka, S., Niwa, Y., O'Brien, K. M., Olsen, A., Omar, A. M., Ono, T., Paulsen, M.,
- Pierrot, D., Pocock, K., Poulter, B., Powis, C. M., Rehder, G., Resplandy, L., Robertson, E., Rödenbeck, C., Rosan, 2849
- 2850 T. M., Schwinger, J., Séférian, R., Smallman, T. L., Smith, S. M., Sospedra-Alfonso, R., Sun, Q., Sutton, A. J.,
- 2851 Sweeney, C., Takao, S., Tans, P. P., Tian, H., Tilbrook, B., Tsujino, H., Tubiello, F., van der Werf, G. R., van
- 2852 Ooijen, E., Wanninkhof, R., Watanabe, M., Wimart-Rousseau, C., Yang, D., Yang, X., Yuan, W., Yue, X., Zaehle,
- 2853 S., Zeng, J., and Zheng, B.: Global Carbon Budget 2023, Earth Syst. Sci. Data, 15, 5301–5369,
- 2854 https://doi.org/10.5194/essd-15-5301-2023, 2023.
- 2855 Friedlingstein, P., O'Sullivan, M., Jones, M. W., Andrew, R. M., Hauck, J., Landschützer, P., Le Quéré, C., Li, H.,
- 2856 Luijkx, I. T., Olsen, A., Peters, G. P., Peters, W., Pongratz, J., Schwingshackl, C., Sitch, S., Canadell, J. G., Ciais,
- 2857 P., Jackson, R. B., Alin, S. R., Arneth, A., Arora, V., Bates, N. R., Becker, M., Bellouin, N., Berghoff, C. F., Bittig,
- 2858 H. C., Bopp, L., Cadule, P., Campbell, K., Chamberlain, M. A., Chandra, N., Chevallier, F., Chini, L. P., Colligan,
- 2859 T., Decayeux, J., Djeutchouang, L. M., Dou, X., Duran Rojas, C., Enyo, K., Evans, W., Fay, A. R., Feely, R. A.,
- 2860 Ford, D. J., Foster, A., Gasser, T., Gehlen, M., Gkritzalis, T., Grassi, G., Gregor, L., Gruber, N., Gürses, Ö., Harris,
- 2861 I., Hefner, M., Heinke, J., Hurtt, G. C., Iida, Y., Ilyina, T., Jacobson, A. R., Jain, A. K., Jarníková, T., Jersild, A.,
- 2862 Jiang, F., Jin, Z., Kato, E., Keeling, R. F., Klein Goldewijk, K., Knauer, J., Korsbakken, J. I., Lan, X., Lauvset, S. 2863 K., Lefèvre, N., Liu, Z., Liu, J., Ma, L., Maksyutov, S., Marland, G., Mayot, N., McGuire, P. C., Metzl, N.,
- 2864 Monacci, N. M., Morgan, E. J., Nakaoka, S.-I., Neill, C., Niwa, Y., Nützel, T., Olivier, L., Ono, T., Palmer, P. I., 2865 Pierrot, D., Qin, Z., Resplandy, L., Roobaert, A., Rosan, T. M., Rödenbeck, C., Schwinger, J., Smallman, T. L.,





- 2866 Smith, S. M., Sospedra-Alfonso, R., Steinhoff, T., Sun, Q., Sutton, A. J., Séférian, R., Takao, S., Tatebe, H., Tian,
- 2867 H., Tilbrook, B., Torres, O., Tourigny, E., Tsujino, H., Tubiello, F., van der Werf, G., Wanninkhof, R., Wang, X.,
- Yang, D., Yang, X., Yu, Z., Yuan, W., Yue, X., Zaehle, S., Zeng, N., and Zeng, J.: Global Carbon Budget 2024,
- 2869 Earth Syst. Sci. Data, 17, 965–1039, https://doi.org/10.5194/essd-17-965-2025, 2025a.
- 2870 Friedlingstein, P., Le Quéré, C., O'Sullivan, M., Hauck, J., Landschützer, P., Luijkx, I.T., Li, H., van der Woude,
- 2871 A., Schwingshackl, C., Pongratz, P., Regnier, P., Andrew, R.M., Bakker, D.C.E., Canadell, J.G., Ciais, P., Gasser,
- T., Jones, M.W., Lan, X., Morgan, E., Olsen, A., Peters, G.P., Peters, W., Sitch, S., and Tian, H.: Emerging climate
- impact on carbon sinks in a consolidated carbon budget, Nature, https://doi.org/10.1038/s41586-025-09802-5,
- 2874 2025b.
- Friedlingstein, P., O'Sullivan, M., Jones, M. W., Andrew, R. M., Bakker, D. C. E., Hauck, J., Landschützer, P., Le
- 2876 Quéré, C., Li, H., Luijkx, I. T., Peters, G. P., Peters, W., Pongratz, J., Schwingshackl, C., Sitch, S., Canadell, J. G.,
- 2877 Ciais, P., Aas, K., Alin, S. R., Anthoni, P., Barbero, L., Bates, N. R., Bellouin, N., Benoit-Cattin, A., Berghoff, C.
- 2878 F., Bernardello, R., Bopp, L., Brasika, I. B. M., Chamberlain, M. A., Chandra, N., Chevallier, F., Chini, L. P.,
- 2879 Collier, N. O., Colligan, T. H., Cronin, M., Djeutchouang, L. M., Dou, X., Enright, M. P., Enyo, K., Erb, M.,
- Evans, W., Feely, R. A., Feng, L., Ford, D. J., Foster, A., Fransner, F., Gasser, T., Gehlen, M., Gkritzalis, T.,
- 2881 Goncalves De Souza, J., Grassi, G., Gregor, L., Gruber, N., Guenet, B., Gürses, Ö., Harrington, K., Harris, I.,
- Heinke, J., Hurtt, G. C., Iida, Y., Ilyina, T., Ito, A., Jacobson, A. R., Jain, A. K., Jarníková, T., Jersild, A., Jiang, F.,
- Jones, S. D., Kato, E., Keeling, R. F., Klein Goldewijk, K., Knauer, J., Kong, Y., Korsbakken, J. I., Koven, C.,
- Kunimitsu, T., Lan, X., Liu, J., Liu, Z., Liu, Z., Lo Monaco, C., Ma, L., Marland, G., McGuire, P. C., McKinley,
- 2885 G. A., Melton, J. R., Monacci, N., Monier, E., Morgan, E. J., Munro, D. R., Müller, J. D., Nakaoka, S., Nayagam,
- L. R., Niwa, Y., Nutzel, T., Olsen, A., Omar, A. M., Pan, N., Pandey, S., Pierrot, D., Qin, Z., Regnier, P., Rehder,
- 2887 G., Resplandy, L., Roobaert, A., Rosan, T. M., Rödenbeck, C., Schwinger, J., Skjelvan, I., Smallman, T. L., Spada,
- 2888 V., Sreeush, M. G., Sun, Q., Sutton, A. J., Sweeney, C., Swingedouw, D., Séférian, R., Takao, S., Tatebe, H., Tian,
- 2889 H., Tian, X., Tilbrook, B., Tsujino, H., Tubiello, F., van Ooijen, E., van der Werf, G. R., van de Velde, S. J.,
- 2890 Walker, A. P., Wanninkhof, R., Yang, X., Yuan, W., Yue, X., and Zeng, J..: Supplemental data of the Global
- Carbon Budget 2025, ICOS-ERIC Carbon Portal, https://doi.org/10.18160/GCP-2025, 2025c.
- 2892 Fu, W., Moore, J. K., Primeau, F., Collier, N., Ogunro, O. O., Hoffman, F. M., and Randerson, J. T.: Evaluation of
- 2893 Ocean Biogeochemistry and Carbon Cycling in CMIP Earth System Models With the International Ocean Model
- 2894 Benchmarking (IOMB) Software System, JGR Oceans, 127, e2022JC018965,
- $2895 \qquad https://doi.org/10.1029/2022JC018965, 2022. \\$
- 2896 Ganzenmüller, R., Bultan, S., Winkler, K., Fuchs, R., Zabel, F., and Pongratz, J.: Land-use change emissions based
- on high-resolution activity data substantially lower than previously estimated, Environ. Res. Lett., 17, 064050,
- 2898 https://doi.org/10.1088/1748-9326/ac70d8, 2022.
- 2899 Gasser, T., Crepin, L., Quilcaille, Y., Houghton, R. A., Ciais, P., and Obersteiner, M.: Historical CO2 emissions
- 2900 from land use and land cover change and their uncertainty, Biogeosciences, 17, 4075–4101,
- 2901 https://doi.org/10.5194/bg-17-4075-2020, 2020.
- 2902 Gaubert, B., Stephens, B. B., Basu, S., Chevallier, F., Deng, F., Kort, E. A., Patra, P. K., Peters, W., Rödenbeck,
- 2903 C., Saeki, T., Schimel, D., Van der Laan-Luijkx, I., Wofsy, S., and Yin, Y.: Global atmospheric CO2 inverse
- 2904 models converging on neutral tropical land exchange, but disagreeing on fossil fuel and atmospheric growth rate,
- 2905 Biogeosciences, 16, 117–134, https://doi.org/10.5194/bg-16-117-2019, 2019.
- 2906 Gauthier, C. B., Melton, J. R., Meyer, G., Raj Deepak, S. N., and Sonnentag, O.: Parameter Optimization for
- 2907 Global Soil Carbon Simulations: Not a Simple Problem, J Adv Model Earth Syst, 17, e2024MS004577,
- 2908 https://doi.org/10.1029/2024MS004577, 2025.
- 2909 GCP: The Global Carbon Budget 2007, available at: http://www.
- 2910 globalcarbonproject.org/carbonbudget/archive.htm, last access: 23 October 2025, 2007.
- 2911 Giglio, L., Schroeder, W., and Justice, C. O.: The collection 6 MODIS active fire detection algorithm and fire
- 2912 products, Remote Sensing of Environment, 178, 31–41, https://doi.org/10.1016/j.rse.2016.02.054, 2016.
- 2913 Gitz V, Ciais P. Amplifying effects of land-use change on future atmospheric CO2 levels. Global Biogeochemical
- 2914 Cycles. https://doi.org/10.1029/2002GB001963, 2003.
- 2915 Gloege, L., McKinley, G. A., Landschützer, P., Fay, A. R., Frölicher, T. L., Fyfe, J. C., Ilyina, T., Jones, S.,
- 2916 Lovenduski, N. S., Rodgers, K. B., Schlunegger, S., and Takano, Y.: Quantifying Errors in Observationally Based





- 2917 Estimates of Ocean Carbon Sink Variability, Global Biogeochem. Cy., 35, e2020GB006788,
- 2918 https://doi.org/10.1029/2020GB006788, 2021.
- 2919 Gloege, L., Yan, M., Zheng, T., and McKinley, G. A.: Improved Quantification of Ocean Carbon Uptake by Using
- 2920 Machine Learning to Merge Global Models and pCO2 Data, J. Adv. Model. Earth Syst., 14, e2021MS002620,
- 2921 https://doi.org/10.1029/2021MS002620, 2022.
- 2922 Golar, G., Malik, A., Muis, H., Herman, A., Nurudin, N., and Lukman, L.: The social-economic impact of COVID-
- 2923 19 pandemic: implications for potential forest degradation, Heliyon, 6, e05354,
- 2924 https://doi.org/10.1016/j.heliyon.2020.e05354, 2020.
- 2925 Goris, N., Tjiputra, J. F., Olsen, A., Schwinger, J., Lauvset, S. K., and Jeansson, E.: Constraining Projection-Based
- 2926 Estimates of the Future North Atlantic Carbon Uptake, J. Clim., 31, 3959–3978, https://doi.org/10.1175/JCLI-D-

- 2927 17-0564.1, 2018.
- Grassi, G., House, J., Kurz, W. A., Cescatti, A., Houghton, R. A., Peters, G. P., Sanz, M. J., Viñas, R. A., Alkama, 2929 R., Arneth, A., Bondeau, A., Dentener, F., Fader, M., Federici, S., Friedlingstein, P., Jain, A. K., Kato, E., Koven,
- 2930 C. D., Lee, D., Nabel, J. E. M. S., Nassikas, A. A., Perugini, L., Rossi, S., Šitch, S., Viovy, N., Wiltshire, A., and
- Zaehle, S.: Reconciling global-model estimates and country reporting of anthropogenic forest CO2 sinks, Nature 2931
- 2932 Clim Change, 8, 914–920, https://doi.org/10.1038/s41558-018-0283-x, 2018.
- 2933 Grassi, G., Stehfest, E., Rogelj, J., van Vuuren, D., Cescatti, A., House, J., Nabuurs, G.-J., Rossi, S., Alkama, R.,
- 2934 Viñas, R. A., Calvin, K., Ceccherini, G., Federici, S., Fujimori, S., Gusti, M., Hasegawa, T., Havlik, P.,
- 2935 Humpenöder, F., Korosuo, A., Perugini, L., Tubiello, F. N., and Popp, A.: Critical adjustment of land mitigation
- 2936 pathways for assessing countries' climate progress, Nat. Clim. Chang., 11, 425-434,
- 2937 https://doi.org/10.1038/s41558-021-01033-6, 2021.
- 2938 Grassi, G., Schwingshackl, C., Gasser, T., Houghton, R. A., Sitch, S., Canadell, J. G., Cescatti, A., Ciais, P.,
- 2939 Federici, S., Friedlingstein, P., Kurz, W. A., Sanz Sanchez, M. J., Abad Viñas, R., Alkama, R., Bultan, S.,
- 2940 Ceccherini, G., Falk, S., Kato, E., Kennedy, D., Knauer, J., Korosuo, A., Melo, J., McGrath, M. J., Nabel, J. E. M.
- 2941 S., Poulter, B., Romanovskaya, A. A., Rossi, S., Tian, H., Walker, A. P., Yuan, W., Yue, X., and Pongratz, J.:
- 2942 Harmonising the land-use flux estimates of global models and national inventories for 2000-2020, Earth Syst. Sci.
- 2943 Data, 15, 1093–1114, https://doi.org/10.5194/essd-15-1093-2023, 2023.
- 2944 Grassi, G., Peters, G. P., Canadell, J. G., Cescatti, A., Federici, S., Gidden, M. J., Harris, N., Herold, M., Krug, T.,
- 2945 O'Sullivan, M., Pongratz, J., Sanz, M. J., Schwingshackl, C., and Van Vuuren, D.: Improving land-use emission
- 2946 estimates under the Paris Agreement, Nat Sustain, 8, 579-581, https://doi.org/10.1038/s41893-025-01565-1, 2025.
- 2947 Gregor, L., Lebehot, A. D., Kok, S., and Scheel Monteiro, P. M.: A comparative assessment of the uncertainties of
- 2948 global surface ocean CO2 estimates using a machine-learning ensemble (CSIR-ML6 version 2019a)-have we hit 2949 the wall?. Geoscientific Model Development, 12(12), 5113-5136, https://doi.org/10.5194/gmd-12-5113-2019,
- 2950
- 2951 Gregor, L., Shutler, J., and Gruber, N.: High-resolution variability of the ocean carbon sink. Global
- 2952 Biogeochemical Cycles, 38(8), e2024GB008127, https://doi.org/10.1029/2024GB008127, 2024.
- 2953 Gruber, N., Bakker, D. C. E., DeVries, T., Gregor, L., Hauck, J., Landschützer, P., McKinley, G. A., and Müller, J.
- 2954 D.: Trends and variability in the ocean carbon sink, Nat. Rev. Earth Environ., 4, 119-134,
- 2955 https://doi.org/10.1038/s43017-022-00381-x, 2023.
- 2956 Gruber, N., Clement, D., Carter, B. R., Feely, R. A., van Heuven, S., Hoppema, M., Ishii, M., Key, R. M., Kozyr,
- 2957 A., Lauvset, S. K., Lo Monaco, C., Mathis, J. T., Murata, A., Olsen, A., Perez, F. F., Sabine, C. L., Tanhua, T., and
- 2958 Wanninkhof, R.: The oceanic sink for anthropogenic CO2 from 1994 to 2007, 363, 1193-1199,
- 2959 https://doi.org/10.1126/science.aau5153, 2019.
- 2960 Guan, D., Liu, Z., Geng, Y., Lindner, S., and Hubacek, K.: The gigatonne gap in China's carbon dioxide
- 2961 inventories, Nature Clim Change, 2, 672-675, https://doi.org/10.1038/nclimate1560, 2012.
- 2962 Gulev, S. K., Thorne, P. W., Ahn, J., Dentener, F. J., Domingues, C. M., Gerland, S., Gong, D. S., Kaufman, S.,
- 2963 Nnamchi, H. C., Quaas, J., Rivera, J. A., Sathyendranath, S., Smith, S. L., Trewin, B., von Shuckmann, K., and
- 2964 Vose, R. S.: Changing State of the Climate System. In: Climate Change 2021: The Physical Science Basis.
- 2965 Contribution of Working Group I to the Sixth Assessment Report of the Intergovernmental Panel on Climate





- 2966 Change [Masson-Delmotte, V., Zhai, P., Pirani, A., Connors, S. L., Péan, C., Berger, S., Caud, N., Chen, Y.,
- 2967 Goldfarb, L., Gomis, M. I., Huang, M., Leitzell, K., Lonnoy, E., Matthews, J.B.R., Maycock, T.K., Waterfield, T.,
- 2968 Yelekçi, O., Yu, R. and Zhou, B. (eds.)]. Cambridge University Press, Cambridge, United Kingdom and New
- 2969 York, NY, USA, pp. 287–422, https://doi.org/10.1017/9781009157896.004, 2021.
- 2970 Guo, R., Wang, J., Bing, L., Tong, D., Ciais, P., Davis, S. J., Andrew, R. M., Xi, F., and Liu, Z.: Global CO2
- 2971 uptake by cement from 1930 to 2019, 13, 1791–1805, https://doi.org/10.5194/essd-13-1791-2021, 2021.
- 2972 Gürses, Ö., Oziel, L., Karakuş, O., Sidorenko, D., Völker, C., Ye, Y., Zeising, M., Butzin, M., and Hauck, J.:
- Ocean biogeochemistry in the coupled ocean—sea ice-biogeochemistry model FESOM2.1–REcoM3, Geosci.
- 2974 Model Dev., 16, 4883–4936, https://doi.org/10.5194/gmd-16-4883-2023, 2023.
- 2975 Gütschow, J., Jeffery, M. L., Gieseke, R., Gebel, R., Stevens, D., Krapp, M., and Rocha, M.: The PRIMAP-hist
- 2976 national historical emissions time series, 8, 571–603, https://doi.org/10.5194/essd-8-571-2016, 2016.
- 2977 Gütschow, J., Busch, D. and Pflüger, M.: The PRIMAP-hist national historical emissions time series (1750-2023)
- 2978 v2.6, Zenodo [Data set], https://doi.org/10.5281/zenodo.13752654, 2023.
- 2979 Hall, B. D., Crotwell, A. M., Kitzis, D. R., Mefford, T., Miller, B. R., Schibig, M. F., and Tans, P. P.: Revision of
- the World Meteorological Organization Global Atmosphere Watch (WMO/GAW) CO2 calibration scale, 14,
- 2981 3015–3032, https://doi.org/10.5194/amt-14-3015-2021, 2021.
- 2982 Hansis, E., Davis, S. J., and Pongratz, J.: Relevance of methodological choices for accounting of land use change
- 2983 carbon fluxes, Global Biogeochem. Cycles, 29, 1230–1246, https://doi.org/10.1002/2014GB004997, 2015.
- 2984 Hauck, J., Nissen, C., Landschützer, P., Rödenbeck, C., Bushinsky, S., and Olsen, A.: Sparse observations induce
- 2985 large biases in estimates of the global ocean CO2 sink: an ocean model subsampling experiment, Philos. Trans. R.
- 2986 Soc. Math. Phys. Eng. Sci., 381, 20220063, https://doi.org/10.1098/rsta.2022.0063, 2023a.
- Hauck, J., Gregor, L., Nissen, C., Patara, L., Hague, M., Mongwe, P., Bushinsky, S., Doney, S. C., Gruber, N., Le
- 2988 Quéré, C., Manizza, M., Mazloff, M., Monteiro, P. M. S., and Terhaar, J.: The Southern Ocean Carbon Cycle
- 2989 1985–2018: Mean, Seasonal Cycle, Trends, and Storage. Global Biogeochemical Cycles, 37(11), e2023GB007848,
- 2990 https://doi.org/10.1029/2023GB007848, 2023b.
- 2991 Hauck, J., Zeising, M., Le Quéré, C., Gruber, N., Bakker, D. C. E., Bopp, L., Chau, T. T. T., Gürses, Ö., Ilyina, T.,
- 2992 Landschützer, P., Lenton, A., Resplandy, L., Rödenbeck, C., Schwinger, J., and Séférian, R.: Consistency and
- 2993 Challenges in the Ocean Carbon Sink Estimate for the Global Carbon Budget, Front. Mar. Sci., 7, 571720,
- 2994 https://doi.org/10.3389/fmars.2020.571720, 2020.
- 2995 Haverd, V., Smith, B., Nieradzik, L., Briggs, P. R., Woodgate, W., Trudinger, C. M., Canadell, J. G., and Cuntz,
- 2996 M.: A new version of the CABLE land surface model (Subversion revision r4601) incorporating land use and land
- 2997 cover change, woody vegetation demography, and a novel optimisation-based approach to plant coordination of
- 2998 photosynthesis, Geosci. Model Dev., 11, 2995–3026, https://doi.org/10.5194/gmd-11-2995-2018, 2018.
- Heinke, J., Rolinski, S., and Müller, C.: Modelling the role of livestock grazing in C and N cycling in grasslands
- 3000 with LPJmL5.0-grazing, Geosci. Model Dev., 16, 2455–2475, https://doi.org/10.5194/gmd-16-2455-2023, 2023.
- Hickler, T., Smith, B., Prentice, I. C., Mjöfors, K., Miller, P., Arneth, A., and Sykes, M. T.: CO2 fertilization in
- 3002 temperate FACE experiments not representative of boreal and tropical forests, Glob. Change Biol., 14, 1531–1542,
- 3003 https://doi.org/10.1111/j.1365-2486.2008.01598.x, 2008.
- Hoesly, R. M., Smith, S. J., Feng, L., Klimont, Z., Janssens-Maenhout, G., Pitkanen, T., Seibert, J. J., Vu, L.,
- 3005 Andres, R. J., Bolt, R. M., Bond, T. C., Dawidowski, L., Kholod, N., Kurokawa, J., Li, M., Liu, L., Lu, Z., Moura,
- 3006 M. C. P., O'Rourke, P. R., and Zhang, Q.: Historical (1750–2014) anthropogenic emissions of reactive gases and
- 3007 aerosols from the Community Emissions Data System (CEDS), Geosci. Model Dev., 11, 369–408,
- 3008 https://doi.org/10.5194/gmd-11-369-2018, 2018.
- Hoesly, R., Smith, S. J., Prime, N., Ahsan, H., Suchyta, H., O'Rourke, P., Crippa, M., Klimont, Z., Guizzardi, D.,
- Behrendt, J., Feng, L., Harkins, C., McDonald, B., Mott, A., McDuffie, A., Nicholson, M. and Wang, S.: CEDS
- 3011 v_2024_07_08 Release Emission Data, Zenodo [Data set], https://doi.org/10.5281/zenodo.12803196, 2024.





- 3012 Hong, C., Burney, J. A., Pongratz, J., Nabel, J. E. M. S., Mueller, N. D., Jackson, R. B., and Davis, S. J.: Global
- 3013 and regional drivers of land-use emissions in 1961–2017, Nature, 589, 554–561, https://doi.org/10.1038/s41586-
- 3014 020-03138-y, 2021.
- Holding, T., Ashton, I. G., Shutler, J. D., Land, P. E., Nightingale, P. D., Rees, A. P., Brown, I., Piolle, J.-F., Kock,
- A., Bange, H. W., Woolf, D. K., Goddijn-Murphy, L., Pereira, R., Paul, F., Girard-Ardhuin, F., Chapron, B.,
- 3017 Rehder, G., Ardhuin, F., and Donlon, C. J.: The FluxEngine air-sea gas flux toolbox: simplified interface and
- 3018 extensions for in situ analyses and multiple sparingly soluble gases, Ocean Sci., 15, 1707–1728,
- 3019 https://doi.org/10.5194/os-15-1707-2019, 2019.
- 3020 Hoppe, J., Hinder, B., Rafaty, R., Patt, A., and Grubb, M.: Three Decades of Climate Mitigation Policy: What Has
- 3021 It Delivered?, Annu. Rev. Environ. Resour., 48, 615–650, https://doi.org/10.1146/annurev-environ-112321-
- 3022 103821, 2023.
- 3023 Houghton, R. A. and Castanho, A.: Annual emissions of carbon from land use, land-use change, and forestry from
- 3024 1850 to 2020, Earth Syst. Sci. Data, 15, 2025–2054, https://doi.org/10.5194/essd-15-2025-2023, 2023.
- 3025 Houghton, R. A., House, J. I., Pongratz, J., van der Werf, G. R., DeFries, R. S., Hansen, M. C., Le Quéré, C., and
- 3026 Ramankutty, N.: Carbon emissions from land use and land-cover change, Biogeosciences, 9, 5125-5142,
- 3027 https://doi.org/10.5194/bg-9-5125-2012, 2012.
- 3028 Houghton, R. A. and Nassikas, A. A.: Global and regional fluxes of carbon from land use and land cover change
- 3029 1850-2015: Carbon Emissions From Land Use, Global Biogeochem. Cycles, 31, 456-472,
- 3030 https://doi.org/10.1002/2016GB005546, 2017.
- Huang, B., Thorne, P. W., Banzon, V. F., Boyer, T., Chepurin, G., Lawrimore, J. H., Menne, M. J., Smith, T. M.,
- Vose, R. S., and Zhang, H.-M.: NOAA Extended Reconstructed Sea Surface Temperature (ERSST), Version 5,
- 3033 https://doi.org/10.7289/V5T72FNM, 2017.
- 3034 Hubau, W., Lewis, S.L., Phillips, O.L., Affum-Baffoe, K., Beeckman, H., Cuní-Sanchez, A., Daniels, A.K.,
- 3035 Ewango, C.E.N., Fauset, S., Mukinzi, J.M., Sheil, D., Sonké, B., Sullivan, M.J.P., Sunderland, T.C.H., Taedoumg,
- H., Thomas, S.C., White, L.J.T., Abernethy, K.A., Adu-Bredu, S., Amani, C.A., Baker, T.R., Banin, L.F., Baya, F.,
- 3037 Begne, S.K., Bennett, A.C., Benedet, F., Bitariho, R., Bocko, Y.E., Boeckx, P., Boundja, P., Brienen, R.J.W., 3038 Brncic, T., Chezeaux, E., Chuyong, G.B., Clark, C.J., Collins, M., Comiskey, J.A., Coomes, D.A., Dargie, G.C., de
- Haulleville, T., Kamdem, M.N.D., Doucet, J.-L., Esquivel-Muelbert, A., Feldpausch, T.R., Fofanah, A., Foli, E.G.,
- Gilpin, M., Gloor, E., Gonmadje, C., Gourlet-Fleury, S., Hall, J.S., Hamilton, A.C., Harris, D.J., Hart, T.B.,
- Hockemba, M.B.N., Hladik, A., Ifo, S.A., Jeffery, K.J., Jucker, T., Yakusu, E.K., Kearsley, E., Kenfack, D., Koch,
- 3042 A., Leal, M.E., Levesley, A., Lindsell, J.A., Lisingo, J., Lopez-Gonzalez, G., Lovett, J.C., Makana, J.-R., Malhi, 3043 Y., Marshall, A.R., Martin, J., Martin, E.H., Mbayu, F.M., Medijbe, V.P., Mihindou, V., Mitchard, E.T.A., Moor
- Y., Marshall, A.R., Martin, J., Martin, E.H., Mbayu, F.M., Medjibe, V.P., Mihindou, V., Mitchard, E.T.A., Moore,
 S., Munishi, P.K.T., Bengone, N.N., Ojo, L., Ondo, F.E., Peh, K.S.-H., Pickavance, G.C., Poulsen, A.D., Poulsen,
- J.R., Qie, L., Reitsma, J., Rovero, F., Swaine, M.D., Talbot, J., Taplin, J., Taylor, D.M., Thomas, D.W., Toirambe,
- 3046 B., Mukendi, J.T., Tuagben, D., Umunay, P.M., van der Heijden, G.M.F., Verbeeck, H., Vleminckx, J., Willcock,
- 3047 S., Wöll, H., Woods, J.T., Zemagho, L.: Asynchronous carbon sink saturation in African and Amazonian tropical
- 3048 forests, Nature, 579, 80–87, https://doi.org/10.1038/s41586-020-2035-0, 2020.
- Humphrey, V., Zscheischler, J., Ciais, P., Gudmundsson, L., Sitch, S., and Seneviratne, S. I.: Sensitivity of
- atmospheric CO2 growth rate to observed changes in terrestrial water storage, Nature, 560, 628–631,
- 3051 https://doi.org/10.1038/s41586-018-0424-4, 2018.
- Humphrey, V., Berg, A., Ciais, P., Gentine, P., Jung, M., Reichstein, M., Seneviratne, S. I., and Frankenberg, C.:
- 3053 Soil moisture–atmosphere feedback dominates land carbon uptake variability, Nature, 592, 65–69,
- 3054 https://doi.org/10.1038/s41586-021-03325-5, 2021.
- Huntzinger, D. N., Michalak, A. M., Schwalm, C., Ciais, P., King, A. W., Fang, Y., Schaefer, K., Wei, Y., Cook,
- 3056 R. B., Fisher, J. B., Hayes, D., Huang, M., Ito, A., Jain, A. K., Lei, H., Lu, C., Maignan, F., Mao, J., Parazoo, N.,
- Peng, S., Poulter, B., Ricciuto, D., Shi, X., Tian, H., Wang, W., Zeng, N., and Zhao, F.: Uncertainty in the response
- of terrestrial carbon sink to environmental drivers undermines carbon-climate feedback predictions, Sci Rep, 7,
- 3059 4765, https://doi.org/10.1038/s41598-017-03818-2, 2017.
- 3060 Iida, Y., Takatani, Y., Kojima, A., and Ishii, M.: Global trends of ocean CO2 sink and ocean acidification: an
- 3061 observation-based reconstruction of surface ocean inorganic carbon variables, J Oceanogr, 77, 323–358,
- 3062 https://doi.org/10.1007/s10872-020-00571-5, 2021.





- Ilyina, T., Li, H., Spring, A., Müller, W. A., Bopp, L., Chikamoto, M. O., Danabasoglu, G., Dobrynin, M., Dunne,
- 3064 J., Fransner, F., Friedlingstein, P., Lee, W., Lovenduski, N. S., Merryfield, W. j., Mignot, J., Park, J. y., Séférian,
- 3065 R., Sospedra-Alfonso, R., Watanabe, M., and Yeager, S.: Predictable Variations of the Carbon Sinks and
- 3066 Atmospheric CO2 Growth in a Multi-Model Framework, Geophys. Res. Lett., 48, e2020GL090695,
- 3067 https://doi.org/10.1029/2020GL090695, 2021.
- 3068 IMF: International Monetary Fund: World Economic Outlook, available at: http://www.imf.org, last access: 23
- 3069 October 2025, 2025.
- Instituto Nacional de Pesquisas Espaciais (INPE): Portal TerraBrasilis, available at: 3070
- 3071 http://terrabrasilis.dpi.inpe.br/en/home-page/, last access: 23 October 2025.
- 3072 Ito, A.: Disequilibrium of terrestrial ecosystem CO2 budget caused by disturbance-induced emissions and non-CO2
- 3073 carbon export flows: a global model assessment, Earth Syst. Dynam., 10, 685-709, https://doi.org/10.5194/esd-10-
- 3074 685-2019, 2019.
- 3075 Ito, A. and Inatomi, M.: Use of a process-based model for assessing the methane budgets of global terrestrial
- 3076 ecosystems and evaluation of uncertainty, 9, 759-773, https://doi.org/10.5194/bg-9-759-2012, 2012.
- 3077 Jackson, R. B., Canadell, J. G., Le Quéré, C., Andrew, R. M., Korsbakken, J. I., Peters, G. P., and Nakicenovic, N.:
- 3078 Reaching peak emissions, Nature Clim Change, 6, 7–10, https://doi.org/10.1038/nclimate2892, 2016.
- 3079 Jackson, R. B., Le Quéré, C., Andrew, R. M., Canadell, J. G., Korsbakken, J. I., Liu, Z., Peters, G. P., and Zheng,
- 3080 B.: Global energy growth is outpacing decarbonization, Environ. Res. Lett., 13, 120401,
- 3081 https://doi.org/10.1088/1748-9326/aaf303, 2018.
- 3082 Jackson, R. B., Friedlingstein, P., Andrew, R. M., Canadell, J. G., Le Quéré, C., and Peters, G. P.: Persistent fossil
- 3083 fuel growth threatens the Paris Agreement and planetary health, Environ. Res. Lett., 14, 121001,
- 3084 https://doi.org/10.1088/1748-9326/ab57b3, 2019.
- 3085 Jackson, R. B., Friedlingstein, P., Quéré, C. L., Abernethy, S., Andrew, R. M., Canadell, J. G., Ciais, P., Davis, S.
- 3086 J., Deng, Z., Liu, Z., Korsbakken, J. I., and Peters, G. P.: Global fossil carbon emissions rebound near pre-COVID-
- 3087 19 levels, Environ. Res. Lett., 17, 031001, https://doi.org/10.1088/1748-9326/ac55b6, 2022.
- 3088 Jacobson, A. R., Schuldt, K. N., Tans, P., Andrews, A., Miller, J. B., Oda, T., Basu, S., Mund, J., Weir, B., Ott, L.,
- 3089 Aalto, T., Abshire, J. B., Aikin, K., Aoki, S., Apadula, F., Arnold, S., Baier, B., Bartyzel, J., Beyersdorf, A.,
- 3090 Biermann, T., Biraud, S. C., Boenisch, H., Brailsford, G., Brand, W. A., Chen, G., Chen, H., Chmura, L., Clark, S.,
- 3091 Colomb, A., Commane, R., Conil, S., Couret, C., Cox, A., Cristofanelli, P., Cuevas, E., Curcoll, R., Daube, B.,
- 3092 Davis, K. J., De Wekker, S., Della Coletta, J., Delmotte, M., DiGangi, E., DiGangi, J. P., di Sarra, A. G.,
- 3093 Dlugokencky, E., Elkins, J. W., Emmenegger, L., Fang, S., Fischer, M. L., Forster, G., Frumau, A., Galkowski, M.,
- 3094 Gatti, L. V., Gehrlein, T., Gerbig, C., Gheusi, F., Gloor, E., Gomez-Trueba, V., Goto, D., Griffis, T., Hammer, S.,
- 3095 Hanson, C., Haszpra, L., Hatakka, J., Heimann, M., Heliasz, M., Hensen, A., Hermansen, O., Hintsa, E., Holst, J., 3096
- Ivakhov, V., Jaffe, D. A., Jordan, A., Joubert, W., Karion, A., Kawa, S. R., Kazan, V., Keeling, R. F., Keronen, P., 3097 Kneuer, T., Kolari, P., Komínková, K., Kort, E., Kozlova, E., Krummel, P., Kubistin, D., Labuschagne, C., Lam,
- 3098 D. H. Y., Lan, X., Langenfelds, R. L., Laurent, O., Laurila, T., Lauvaux, T., Lavric, J., Law, B. E., Lee, J., Lee, O.
- 3099 S. M., Lehner, I., Lehtinen, K., Leppert, R., Leskinen, A., Leuenberger, M., Levin, I., Levula, J., Lin, J., Lindauer,
- 3100 M., Loh, Z., Lopez, M., Luijkx, I. T., Lunder, C. R., Machida, T., Mammarella, I., Manca, G., Manning, A.,
- 3101 Manning, A., Marek, M. V., Martin, M. Y., Matsueda, H., McKain, K., Meijer, H., Meinhardt, F., Merchant, L.,
- 3102 Mihalopoulos, N., Miles, N. L., Miller, C. E., Mitchell, L., Mölder, M., Montzka, S., Moore, F., Moossen, H.,
- 3103 Morgan, E., Morgui, J.-A., Morimoto, S., Müller-Williams, J., Munger, J. W., Munro, D., Myhre, C. L., Nakaoka,
- 3104 S.-I., Necki, J., Newman, S., Nichol, S., Niwa, Y., Obersteiner, F., O'Doherty, S., Paplawsky, B., Peischl, J.,
- 3105 Peltola, O., Piacentino, S., Pichon, J.-M., Pickers, P., Piper, S., Pitt, J., Plass-Dülmer, C., Platt, S. M., Prinzivalli, 3106 S., Ramonet, M., Ramos, R., Reyes-Sanchez, E., Richardson, S. J., Riris, H., Rivas, P. P., Ryerson, T., Saito, K.,
- 3107 Sargent, M., Sasakawa, M., Scheeren, B., Schuck, T., Schumacher, M., Seifert, T., Sha, M. K., Shepson, P., Shook,
- 3108 M., Sloop, C. D., Smith, P., Stanley, K., Steinbacher, M., Stephens, B., Sweeney, C., Thoning, K., Timas, H., Torn,
- 3109 M., Tørseth, K., Trisolino, P., Turnbull, J., van den Bulk, P., van Dinther, D., Vermeulen, A., Viner, B., Vitkova, 3110 G., Walker, S., Watson, A., Wofsy, S. C., Worsey, J., Worthy, D., Young, D., Zaehle, S., Zahn, A., and Zimnoch,
- M.: CarbonTracker CT2022, NOAA GML [Data set], https://doi.org/10.25925/Z1GJ-3254, 2023a. 3111
- 3112 Jacobson, A. R., Schuldt, K. N., Tans, P., Andrews, A., Miller, J. B., Oda, T., Basu, S., Mund, J., Weir, B., Ott, L.,
- 3113 Aalto, T., Abshire, J. B., Aikin, K., Aoki, S., Apadula, F., Arnold, S., Baier, B., Bartyzel, J., Beyersdorf, A.,
- 3114 Biermann, T., Biraud, S. C., Boenisch, H., Brailsford, G., Brand, W. A., Chen, G., Chen, H., Chmura, L., Clark, S.,





- 3115 Colomb, A., Commane, R., Conil, S., Couret, C., Cox, A., Cristofanelli, P., Cuevas, E., Curcoll, R., Daube, B.,
- 3116 Davis, K. J., De Wekker, S., Della Coletta, J., Delmotte, M., DiGangi, E., DiGangi, J. P., di Sarra, A. G.,
- Dlugokencky, E., Elkins, J. W., Emmenegger, L., Fang, S., Fischer, M. L., Forster, G., Frumau, A., Galkowski, M.,
- 3118 Gatti, L. V., Gehrlein, T., Gerbig, C., Gheusi, F., Gloor, E., Gomez-Trueba, V., Goto, D., Griffis, T., Hammer, S.,
- 3119 Hanson, C., Haszpra, L., Hatakka, J., Heimann, M., Heliasz, M., Hensen, A., Hermansen, O., Hintsa, E., Holst, J.,
- Ivakhov, V., Jaffe, D. A., Jordan, A., Joubert, W., Karion, A., Kawa, S. R., Kazan, V., Keeling, R. F., Keronen, P.,
 Kneuer, T., Kolari, P., Komínková, K., Kort, E., Kozlova, E., Krummel, P., Kubistin, D., Labuschagne, C., Lam,
- 3122 D. H. Y., Lan, X., Langenfelds, R. L., Laurent, O., Laurila, T., Lauvaux, T., Lavric, J., Law, B. E., Lee, J., Lee, O.
- 3123 S. M., Lehner, I., Lehtinen, K., Leppert, R., Leskinen, A., Leuenberger, M., Levin, I., Levula, J., Lin, J., Lindauer,
- M., Loh, Z., Lopez, M., Luijkx, I. T., Lunder, C. R., Machida, T., Mammarella, I., Manca, G., Manning, A.,
- Manning, A., Marek, M. V., Martin, M. Y., Matsueda, H., McKain, K., Meijer, H., Meinhardt, F., Merchant, L.,
- Mihalopoulos, N., Miles, N. L., Miller, C. E., Mitchell, L., Mölder, M., Montzka, S., Moore, F., Moossen, H.,
- 3127 Morgan, E., Morgui, J.-A., Morimoto, S., Müller-Williams, J., Munger, J. W., Munro, D., Myhre, C. L., Nakaoka,
- 3128 S.-I., Necki, J., Newman, S., Nichol, S., Niwa, Y., Obersteiner, F., O'Doherty, S., Paplawsky, B., Peischl, J.,
- 3129 Peltola, O., Piacentino, S., Pichon, J.-M., Pickers, P., Piper, S., Pitt, J., Plass-Dülmer, C., Platt, S. M., Prinzivalli,
- 3130 S., Ramonet, M., Ramos, R., Reyes-Sanchez, E., Richardson, S. J., Riris, H., Rivas, P. P., Ryerson, T., Saito, K.,
- 3131 Sargent, M., Sasakawa, M., Scheeren, B., Schuck, T., Schumacher, M., Seifert, T., Sha, M. K., Shepson, P., Shook,
- 3132 M., Sloop, C. D., Smith, P., Stanley, K., Steinbacher, M., Stephens, B., Sweeney, C., Thoning, K., Timas, H., Torn,
- M., Stoop, C. D., Smith, P., Stanley, K., Steinoacher, M., Stephens, B., Sweeney, C., Honning, K., Himas, H., Torni M., Tørseth, K., Trisolino, P., Turnbull, J., van den Bulk, P., van Dinther, D., Vermeulen, A., Viner, B., Vitkova,
- 3134 G., Walker, S., Watson, A., Wofsy, S. C., Worsey, J., Worthy, D., Young, D., Zaehle, S., Zahn, A., and Zimnoch,
- 3135 M.: CarbonTracker CT-NRT.v2023-3, NOAA GML [Data set], https://doi.org/10.25925/7TAF-J322, 2023b.
- Jain, A. K., Meiyappan, P., Song, Y., and House, J. I.: CO2 emissions from land-use change affected more by
- 3137 nitrogen cycle, than by the choice of land-cover data, Global Change Biology, 19, 2893–2906,
- 3138 https://doi.org/10.1111/gcb.12207, 2013.
- Jain, P., Barber, Q. E., Taylor, S. W., Whitman, E., Castellanos Acuna, D., Boulanger, Y., Chavardès, R. D., Chen,
- J., Englefield, P., Flannigan, M., Girardin, M. P., Hanes, C. C., Little, J., Morrison, K., Skakun, R. S., Thompson,
- D. K., Wang, X., Parisien, M.-A.: Drivers and Impacts of the Record-Breaking 2023 Wildfire Season in Canada.
- 3142 Nature Communications, 15(1), p.6764, https://doi.org/10.1038/s41467-024-51154-7, 2024.
- 3143 Janssens-Maenhout, G., Crippa, M., Guizzardi, D., Muntean, M., Schaaf, E., Dentener, F., Bergamaschi, P.,
- Pagliari, V., Olivier, J. G. J., Peters, J. A. H. W., van Aardenne, J. A., Monni, S., Doering, U., Petrescu, A. M. R.,
- Solazzo, E., and Oreggioni, G. D.: EDGAR v4.3.2 Global Atlas of the three major greenhouse gas emissions for
- 3146 the period 1970–2012, Earth Syst. Sci. Data, 11, 959–1002, https://doi.org/10.5194/essd-11-959-2019, 2019.
- 3147 Jean-Michel, L., Eric, G., Romain, B.-B., Gilles, G., Angélique, M., Marie, D., Clément, B., Mathieu, H., Olivier,
- 3148 L. G., Charly, R., Tony, C., Charles-Emmanuel, T., Florent, G., Giovanni, R., Mounir, B., Yann, D., and Pierre-
- 3149 Yves, L. T.: The Copernicus Global 1/12° Oceanic and Sea Ice GLORYS12 Reanalysis, Front. Earth Sci., 9, 2021.
- 3150 Jiang, F., Ju, W., He, W., Wu, M., Wang, H., Wang, J., Jia, M., Feng, S., Zhang, L., and Chen, J. M.: A 10-year
- 3151 global monthly averaged terrestrial net ecosystem exchange dataset inferred from the ACOS GOSAT v9 XCO2
- 3152 retrievals (GCAS2021), Earth Syst. Sci. Data, 14, 3013–3037, https://doi.org/10.5194/essd-14-3013-2022, 2022.
- 3153 Jiang, F., Wang, H., Chen, J. M., Ju, W., Tian, X., Feng, S., Li, G., Chen, Z., Zhang, S., Lu, X., Liu, J., Wang, H.,
- Wang, J., He, W., and Wu, M.: Regional CO2 fluxes from 2010 to 2015 inferred from GOSAT XCO2 retrievals
- 3155 using a new version of the Global Carbon Assimilation System, Atmospheric Chem. Phys., 21, 1963–1985,
- 3156 https://doi.org/10.5194/acp-21-1963-2021, 2021.
- Jin, Y., Keeling, R. F., Stephens, B. B., Long, M. C., Patra, P. K., Rödenbeck, C., Morgan, E. J., Kort, E. A., and
- 3158 Sweeney, C.: Improved atmospheric constraints on Southern Ocean CO 2 exchange. Proceedings of the National
- 3159 Academy of Sciences, 121(6), e2309333121, https://doi.org/10.1073/pnas.2309333121, 2024.
- Jin, Z., Wang, T., Zhang, H., Wang, Y., Ding, J., and Tian, X.: Constraint of satellite CO2 retrieval on the global
- carbon cycle from a Chinese atmospheric inversion system, Sci. China Earth Sci., 66, 609–618,
- 3162 https://doi.org/10.1007/s11430-022-1036-7, 2023.
- Joos, F. and Spahni, R.: Rates of change in natural and anthropogenic radiative forcing over the past 20,000 years,
- 3164 Proceedings of the National Academy of Sciences, 105, 1425–1430, https://doi.org/10.1073/pnas.0707386105,
- 3165 2008.





- Jones, C. D., Hickman, J. E., Rumbold, S. T., Walton, J., Lamboll, R. D., Skeie, R. B., Fiedler, S., Forster, P. M.,
- Rogelj, J., Abe, M., Botzet, M., Calvin, K., Cassou, C., Cole, J. N. S., Davini, P., Deushi, M., Dix, M., Fyfe, J. C.,
- 3168 Gillett, N. P., Ilyina, T., Kawamiya, M., Kelley, M., Kharin, S., Koshiro, T., Li, H., Mackallah, C., Müller, W. A.,
- 3169 Nabat, P., van Noije, T., Nolan, P., Ohgaito, R., Olivié, D., Oshima, N., Parodi, J., Reerink, T. J., Ren, L.,
- 3170 Romanou, A., Séférian, R., Tang, Y., Timmreck, C., Tjiputra, J., Tourigny, E., Tsigaridis, K., Wang, H., Wu, M., 3171 Wyser, K., Yang, S., Yang, Y., and Ziehn, T.: The Climate Response to Emissions Reductions Due to COVID-19:
- 3172 Initial Results From CovidMIP, Geophys. Res. Lett., 48, e2020GL091883, https://doi.org/10.1029/2020GL091883,
- 3173 2021a.
- Jones, M. W., Abatzoglou, J. T., Veraverbeke, S., Andela, N., Lasslop, G., Forkel, M., Smith, A. J. P., Burton, C.,
- Betts, R. A., van der Werf, G. R., Sitch, S., Canadell, J. G., Santín, C., Kolden, C., Doerr, S. H., and Le Quéré, C.:
- 3176 Global and Regional Trends and Drivers of Fire Under Climate Change, Rev. Geophys., 60, e2020RG000726,
- 3177 https://doi.org/10.1029/2020RG000726, 2022.
- Jones, M. W., Andrew, R. M., Peters, G. P., Janssens-Maenhout, G., De-Gol, A. J., Ciais, P., Patra, P. K.,
- Chevallier, F., and Le Quéré, C.: Gridded fossil CO2 emissions and related O2 combustion consistent with national
- 3180 inventories 1959–2018, Sci Data, 8, 2, https://doi.org/10.1038/s41597-020-00779-6, 2021b.
- Jones, M. W., Andrew, R. M., Peters, G. P., Janssens-Maenhout, G., De-Gol, A. J., Dou, X., Liu, Z., Pickers, P.,
- 3182 Ciais, P., Patra, P. K., Chevallier, F., and Le Quéré, C.: Gridded fossil CO2 emissions and related O2 combustion
- 3183 consistent with national inventories, Zenodo [Data set], https://doi.org/10.5281/zenodo.17467681, 2025.
- Jones, M. W., Kelley, D. I., Burton, C. A., Di Giuseppe, F., Barbosa, M. L. F., Brambleby, E., Hartley, A. J.,
- Lombardi, A., Mataveli, G., McNorton, J. R., Spuler, F. R., Wessel, J. B., Abatzoglou, J. T., Anderson, L. O.,
- Andela, N., Archibald, S., Armenteras, D., Burke, E., Carmenta, R., Chuvieco, E., Clarke, H., Doerr, S. H.,
- Fernandes, P. M., Giglio, L., Hamilton, D. S., Hantson, S., Harris, S., Jain, P., Kolden, C. A., Kurvits, T., Lampe,
- S., Meier, S., New, S., Parrington, M., Perron, M. M. G., Qu, Y., Ribeiro, N. S., Saharjo, B. H., San-Miguel-Ayanz,
 J., Shuman, J. K., Tanpipat, V., van der Werf, G. R., Veraverbeke, S., and Xanthopoulos, G.: State of Wildfires
- 3190 2023–2024, Earth System Science Data, 16, 3601–3685, https://doi.org/10.5194/essd-16-3601-2024, 2024b.
- Jones, M.W., Veraverbeke, S., Andela, N., Doerr, S.H., Kolden, C., Mataveli, G., Pettinari, M.L., Le Quéré, C.,
- Rosan, T.M., van der Werf, G.R. and van Wees, D.: Global rise in forest fire emissions linked to climate change in
- 3193 the extratropics. Science, 386(6719), p.eadl5889, 2024c.
- Jung, M., Reichstein, M., Schwalm, C. R., Huntingford, C., Sitch, S., Ahlström, A., Arneth, A., Camps-Valls, G.,
- Ciais, P., Friedlingstein, P., Gans, F., Ichii, K., Jain, A. K., Kato, E., Papale, D., Poulter, B., Raduly, B.,
- Rödenbeck, C., Tramontana, G., Viovy, N., Wang, Y.-P., Weber, U., Zaehle, S., and Zeng, N.: Compensatory
- water effects link yearly global land CO2 sink changes to temperature, Nature, 541, 516–520,
- 3198 https://doi.org/10.1038/nature20780, 2017.
- 3199 Kaiser, J. W., Heil, A., Andreae, M. O., Benedetti, A., Chubarova, N., Jones, L., Morcrette, J.-J., Razinger, M.,
- 3200 Schultz, M. G., Suttie, M., and van der Werf, G. R.: Biomass burning emissions estimated with a global fire
- 3201 assimilation system based on observed fire radiative power, Biogeosciences, 9, 527–554,
- 3202 https://doi.org/10.5194/bg-9-527-2012, 2012.
- 3203 Kato, E., Kinoshita, T., Ito, A., Kawamiya, M., and Yamagata, Y.: Evaluation of spatially explicit emission
- 3204 scenario of land-use change and biomass burning using a process-based biogeochemical model, J. Land Use Sci., 8,
- 3205 104–122, https://doi.org/10.1080/1747423X.2011.628705, 2013.
- 3206 Kawasaki, T., Hasumi, H., and Tanaka, Y.: Role of tide-induced vertical mixing in the deep Pacific Ocean
- 3207 circulation, J. Oceanogr., 77, 173–184, https://doi.org/10.1007/s10872-020-00584-0, 2021.
- 3208 Ke, P., Ciais, P., Sitch, S., Li, W., Bastos, A., Liu, Z., Xu, Y., Gui, X., Bian, J., Goll, D. S., Xi, Y., Li, W.,
- O'Sullivan, M., Goncalves de Souza, J., Friedlingstein, P., Chevallier, F.: Low latency carbon budget analysis
- reveals a large decline of the land carbon sink in 2023. National Science Review, p.nwae367,
- 3211 https://doi.org/10.1093/nsr/nwae367, 2024.
- 3212 Keeley, J. E. and Pausas, J. G.: Distinguishing disturbance from perturbations in fire-prone ecosystems, Int. J.
- 3213 Wildland Fire, 28, 282–287, https://doi.org/10.1071/WF18203, 2019.





- Keeling, C. D., Bacastow, R. B., Bainbridge, A. E., Ekdahl, C. A., Guenther, P. R., Waterman, L. S., and Chin, J.
- 3215 F. S.: Atmospheric carbon dioxide variations at Mauna Loa Observatory, Hawaii, Tellus A., 28, 538-551,
- 3216 https://doi.org/10.1111/j.2153-3490.1976.tb00701.x, 1976.
- 3217 Keeling R.F.: Development of an Interferometric Oxygen Analyzer for Precise Measurement of the Atmospheric
- 3218 O2 Mole Fraction, PhD thesis, Harvard University, Cambridge, Massachusetts, available at:
- 3219 https://bluemoon.ucsd.edu/publications/ralph/34 PhDthesis.pdf, last access: 23 October 2025, 1988.
- Keeling, R. F., Manning, A. C., Paplawsky, W. J., and Cox, A. C.: On the long-term stability of reference gases for 3220
- 3221 atmospheric O2/N2 and CO2 measurements, Tellus B Chem. Phys. Meteorol., 59, 3-14,
- 3222 https://doi.org/10.1111/j.1600-0889.2006.00196.x, 2007.
- 3223 Keeling, R. F. and Manning, A. C.: 5.15 - Studies of Recent Changes in Atmospheric O2 Content, in: Treatise on
- 3224 Geochemistry (Second Edition), edited by: Holland, H. D. and Turekian, K. K., Elsevier, Oxford, 385-404,
- 3225 https://doi.org/10.1016/B978-0-08-095975-7.00420-4, 2014.
- 3226 Kelley, D. I., Burton, C., Di Giuseppe, F., Jones, M. W., Barbosa, M. L. F., Brambleby, E., McNorton, J. R., Liu,
- 3227 Z., Bradley, A. S. I., Blackford, K., Burke, E., Ciavarella, A., Di Tomaso, E., Eden, J., Ferreira, I. J. M., Fiedler, L.,
- 3228 Hartley, A. J., Keeping, T. R., Lampe, S., Lombardi, A., Mataveli, G., Qu, Y., Silva, P. S., Spuler, F. R.,
- 3229 Steinmann, C. B., Torres-Vázquez, M. Á., Veiga, R., Van Wees, D., Wessel, J. B., Wright, E., Bilbao, B.,
- Bourbonnais, M., Gao, C., Di Bella, C. M., Dintwe, K., Donovan, V. M., Harris, S., Kukavskaya, E. A., N'Dri, A. 3230
- 3231 B., Santín, C., Selaya, G., Sjöström, J., Abatzoglou, J. T., Andela, N., Carmenta, R., Chuvieco, E., Giglio, L.,
- 3232 Hamilton, D. S., Hantson, S., Meier, S., Parrington, M., Sadegh, M., San-Miguel-Ayanz, J., Sedano, F., Turco, M.,
- 3233 Van Der Werf, G. R., Veraverbeke, S., Anderson, L. O., Clarke, H., Fernandes, P. M., and Kolden, C. A.: State of
- 3234 Wildfires 2024-2025, Earth Syst. Sci. Data, 17, 5377-5488, https://doi.org/10.5194/essd-17-5377-2025, 2025.
- 3235 Keppler, L. and Landschützer, P.: Regional Wind Variability Modulates the Southern Ocean Carbon Sink, Sci Rep,
- 3236 9, 7384, https://doi.org/10.1038/s41598-019-43826-y, 2019.
- 3237 Kharin, V. V., Boer, G. J., Merryfield, W. J., Scinocca, J. F., and Lee, W. -S.: Statistical adjustment of decadal
- 3238 predictions in a changing climate, Geophysical Research Letters, 39, 2012GL052647,
- 3239 https://doi.org/10.1029/2012GL052647, 2012.
- 3240 Khatiwala, S., Primeau, F., and Hall, T.: Reconstruction of the history of anthropogenic CO2 concentrations in the
- 3241 ocean, Nature, 462, 346-349, https://doi.org/10.1038/nature08526, 2009.
- 3242 Khatiwala, S., Tanhua, T., Mikaloff Fletcher, S., Gerber, M., Doney, S. C., Graven, H. D., Gruber, N., McKinley,
- G. A., Murata, A., Ríos, A. F., and Sabine, C. L.: Global ocean storage of anthropogenic carbon, Biogeosciences, 3243
- 3244 10, 2169-2191, https://doi.org/10.5194/bg-10-2169-2013, 2013.
- 3245 Kong, Y., Zheng, B., Zhang, Q., and He, K.: Global and regional carbon budget for 2015-2020 inferred from
- 3246 OCO-2 based on an ensemble Kalman filter coupled with GEOS-Chem, Atmospheric Chem. Phys., 22, 10769-
- 3247 10788, https://doi.org/10.5194/acp-22-10769-2022, 2022.
- 3248 Kou-Giesbrecht, S. and Arora, V. K.: Representing the Dynamic Response of Vegetation to Nitrogen Limitation
- 3249 via Biological Nitrogen Fixation in the CLASSIC Land Model, Global Biogeochemical Cycles, 36,
- 3250 e2022GB007341, https://doi.org/10.1029/2022GB007341, 2022.
- 3251 Korsbakken, J. I., Peters, G. P., and Andrew, R. M.: Uncertainties around reductions in China's coal use and CO2
- 3252 emissions, Nature Clim Change, 6, 687-690, https://doi.org/10.1038/nclimate2963, 2016.
- 3253 Koven, C. D., Knox, R. G., Fisher, R. A., Chambers, J. Q., Christoffersen, B. O., Davies, S. J., Detto, M., Dietze,
- 3254 M. C., Faybishenko, B., Holm, J., Huang, M., Kovenock, M., Kueppers, L. M., Lemieux, G., Massoud, E.,
- 3255 McDowell, N. G., Muller-Landau, H. C., Needham, J. F., Norby, R. J., Powell, T., Rogers, A., Serbin, S. P.,
- 3256 Shuman, J. K., Swann, A. L. S., Varadharajan, C., Walker, A. P., Wright, S. J., and Xu, C.: Benchmarking and 3257
- parameter sensitivity of physiological and vegetation dynamics using the Functionally Assembled Terrestrial
- 3258 Ecosystem Simulator (FATES) at Barro Colorado Island, Panama, Biogeosciences, 17, 3017-3044,
- 3259 https://doi.org/10.5194/bg-17-3017-2020, 2020.
- 3260 Krinner, G., Viovy, N., de Noblet-Ducoudré, N., Ogée, J., Polcher, J., Friedlingstein, P., Ciais, P., Sitch, S., and
- 3261 Prentice, I. C.: A dynamic global vegetation model for studies of the coupled atmosphere-biosphere system:





- 3262 DVGM for coupled climate studies, Global Biogeochem. Cycles, 19, GB1015,
- 3263 https://doi.org/10.1029/2003GB002199, 2005.
- 3264 Lacroix, F., Ilyina, T., and Hartmann, J.: Oceanic CO2 outgassing and biological production hotspots induced by
- 3265 pre-industrial river loads of nutrients and carbon in a global modeling approach, Biogeosciences, 17, 55-88,
- 3266 https://doi.org/10.5194/bg-17-55-2020, 2020.
- 3267 Lacroix, F., Ilyina, T., Mathis, M., Laruelle, G. G., and Regnier, P.: Historical increases in land-derived nutrient
- 3268 inputs may alleviate effects of a changing physical climate on the oceanic carbon cycle, Glob Change Biol, 27,
- 3269 5491–5513, https://doi.org/10.1111/gcb.15822, 2021.
- 3270 Lamboll, R. D., Nicholls, Z. R. J., Smith, C. J., Kikstra, J. S., Byers, E., and Rogelj, J.: Assessing the size and
- 3271 uncertainty of remaining carbon budgets, Nat. Clim. Change, https://doi.org/10.1038/s41558-023-01848-5, 2023.
- 3272 Lamboll, R. D., Jones, C. D., Skeie, R. B., Fiedler, S., Samset, B. H., Gillett, N. P., Rogelj, J., Forster, P. M., 2021:
- 3273 Modifying emissions scenario projections to account for the effects of COVID-19: protocol for CovidMIP, Geosci.
- 3274 Model Dev., 14, 3683–3695, https://doi.org/10.5194/gmd-14-3683-2021, 2021.
- 3275 Lan, X., Tans, P. and Thoning, K.: NOAA Greenhouse Gas Marine Boundary Layer Reference CO2 [Data set].
- 3276 NOAA Global Monitoring Laboratory, https://doi.org/10.15138/DVNP-F961, 2024.
- 3277 Lan, X., Tans, P. and K.W. Thoning: Trends in globally-averaged CO2 determined from NOAA Global Monitoring
- 3278 Laboratory measurements. Version Friday, 05-Sep-2025 12:12:59 MDT, https://doi.org/10.15138/9N0H-ZH07,
- 3279 2025.
- 3280 Lan, X., Tans, P. and Thoning, K. W.: Trends in globally-averaged CO2 determined from NOAA Global
- 3281 Monitoring Laboratory measurements, https://doi.org/10.15138/9N0H-ZH07, 2024b.
- 3282 Landschützer, P., Gruber, N., Haumann, F. A., Rödenbeck, C., Bakker, D. C. E., van Heuven, S., Hoppema, M.,
- 3283 Metzl, N., Sweeney, C., Takahashi, T., Tilbrook, B., and Wanninkhof, R.: The reinvigoration of the Southern
- 3284 Ocean carbon sink, Science, 349, 1221–1224, https://doi.org/10.1126/science.aab2620, 2015.
- 3285 Landschützer, P., Gruber, N., and Bakker, D. C. E.: Decadal variations and trends of the global ocean carbon sink:
- decadal air-sea CO2 flux variability, Global Biogeochem. Cycles, 30, 1396–1417,
- 3287 https://doi.org/10.1002/2015GB005359, 2016.
- 3288 Lapola, D. M., Pinho, P., Barlow, J., Aragão, L. E. O. C., Berenguer, E., Carmenta, R., Liddy, H. M., Seixas, H.,
- 3289 Silva, C. V. J., Silva-Junior, C. H. L., Alencar, A. A. C., Anderson, L. O., Armenteras, D., Brovkin, V., Calders,
- 3290 K., Chambers, J., Chini, L., Costa, M. H., Faria, B. L., Fearnside, P. M., Ferreira, J., Gatti, L., Gutierrez-Velez, V. 3291 H., Han, Z., Hibbard, K., Koven, C., Lawrence, P., Pongratz, J., Portela, B. T. T., Rounsevell, M., Ruane, A. C.,
- H., Han, Z., Hibbard, K., Koven, C., Lawrence, P., Pongratz, J., Portela, B. T. T., Rounsevell, M., Ruane, A. C.,
 Schaldach, R., da Silva, S. S., von Randow, C., Walker, W. S.: The drivers and impacts of Amazon forest
- degradation. Science, 379(6630), p.eabp8622, https://doi.org/10.1126/science.abp8622, 2023.
- Law, R. M., Ziehn, T., Matear, R. J., Lenton, A., Chamberlain, M. A., Stevens, L. E., Wang, Y.-P., Srbinovsky, J.,
- Bi, D., Yan, H., and Vohralik, P. F.: The carbon cycle in the Australian Community Climate and Earth System
- 3296 Simulator (ACCESS-ESM1) Part 1: Model description and pre-industrial simulation, Geosci. Model Dev., 10,
- 3297 2567–2590, https://doi.org/10.5194/gmd-10-2567-2017, 2017.
- 3298 Laughner, J. L., Roche, S., Kiel, M., Toon, G. C., Wunch, D., Baier, B. C., Biraud, S., Chen, H., Kivi, R.,
- 3299 Laemmel, T., McKain, K., Quéhé, P.-Y., Rousogenous, C., Stephens, B. B., Walker, K., and Wennberg, P. O.: A
- new algorithm to generate a priori trace gas profiles for the GGG2020 retrieval algorithm, Atmos. Meas. Tech., 16,
- 3301 1121–1146, https://doi.org/10.5194/amt-16-1121-2023, 2023.
- 3302 Lauvset, S. K., Lange, N., Tanhua, T., Bittig, H. C., Olsen, A., Kozyr, A., Álvarez, M., Azetsu-Scott, K., Brown, P.
- 3303 J., Carter, B. R., Cotrim Da Cunha, L., Hoppema, M., Humphreys, M. P., Ishii, M., Jeansson, E., Murata, A.,
- Müller, J. D., Pérez, F. F., Schirnick, C., Steinfeldt, R., Suzuki, T., Ulfsbo, A., Velo, A., Woosley, R. J., and Key,
- R. M.: The annual update GLODAPv2.2023: the global interior ocean biogeochemical data product, Earth Syst.
- 3306 Sci. Data, 16, 2047–2072, https://doi.org/10.5194/essd-16-2047-2024, 2024.
- Lawrence, D. M., Fisher, R. A., Koven, C. D., Oleson, K. W., Swenson, S. C., Bonan, G., Collier, N., Ghimire, B.,
- van Kampenhout, L., Kennedy, D., Kluzek, E., Lawrence, P. J., Li, F., Li, H., Lombardozzi, D., Riley, W. J.,
- 3309 Sacks, W. J., Shi, M., Vertenstein, M., Wieder, W. R., Xu, C., Ali, A. A., Badger, A. M., Bisht, G., van den





- 3310 Broeke, M., Brunke, M. A., Burns, S. P., Buzan, J., Clark, M., Craig, A., Dahlin, K., Drewniak, B., Fisher, J. B.,
- Flanner, M., Fox, A. M., Gentine, P., Hoffman, F., Keppel-Aleks, G., Knox, R., Kumar, S., Lenaerts, J., Leung, L. 3312 R., Lipscomb, W. H., Lu, Y., Pandey, A., Pelletier, J. D., Perket, J., Randerson, J. T., Ricciuto, D. M., Sanderson,
- R., Lipscomb, W. H., Lu, Y., Pandey, A., Pelletier, J. D., Perket, J., Randerson, J. T., Ricciuto, D. M., Sanderson,
 B. M., Slater, A., Subin, Z. M., Tang, J., Thomas, R. Q., Val Martin, M., and Zeng, X.: The Community Land
- 3314 Model Version 5: Description of New Features, Benchmarking, and Impact of Forcing Uncertainty, J. Adv. Model
- 3315 Earth, Sy., 11, 4245–4287, https://doi.org/10.1029/2018MS001583, 2019.
- 3316 Le Quéré, C., Rödenbeck, C., Buitenhuis, E. T., Conway, T. J., Langenfelds, R., Gomez, A., Labuschagne, C.,
- 3317 Ramonet, M., Nakazawa, T., Metzl, N., Gillett, N., and Heimann, M.: Saturation of the Southern Ocean CO2 Sink
- 3318 Due to Recent Climate Change, Science, 316, 1735–1738, https://doi.org/10.1126/science.1136188, 2007.
- 3319 Le Quéré, C., Raupach, M. R., Canadell, J. G., Marland, G., Bopp, L., Ciais, P., Conway, T. J., Doney, S. C., Feely,
- 3320 R. A., Foster, P., Friedlingstein, P., Gurney, K., Houghton, R. A., House, J. I., Huntingford, C., Levy, P. E., Lomas,
- 3321 M. R., Majkut, J., Metzl, N., Ometto, J. P., Peters, G. P., Prentice, I. C., Randerson, J. T., Running, S. W.,
- Sarmiento, J. L., Schuster, U., Sitch, S., Takahashi, T., Viovy, N., van der Werf, G. R., and Woodward, F. I.:
- Trends in the sources and sinks of carbon dioxide, Nature Geosci, 2, 831–836, https://doi.org/10.1038/ngeo689,
- 3324 2009.
- 3325 Le Quéré, C., Andres, R. J., Boden, T., Conway, T., Houghton, R. A., House, J. I., Marland, G., Peters, G. P., van
- der Werf, G. R., Ahlström, A., Andrew, R. M., Bopp, L., Canadell, J. G., Ciais, P., Doney, S. C., Enright, C.,
- 3327 Friedlingstein, P., Huntingford, C., Jain, A. K., Jourdain, C., Kato, E., Keeling, R. F., Klein Goldewijk, K., Levis,
- 3328 S., Levy, P., Lomas, M., Poulter, B., Raupach, M. R., Schwinger, J., Sitch, S., Stocker, B. D., Viovy, N., Zaehle,
- 3329 S., and Zeng, N.: The global carbon budget 1959–2011, Earth Syst. Sci. Data, 5, 165–185,
- 3330 https://doi.org/10.5194/essd-5-165-2013, 2013.
- 3331 Le Quéré, C., Peters, G. P., Andres, R. J., Andrew, R. M., Boden, T. A., Ciais, P., Friedlingstein, P., Houghton, R.
- A., Marland, G., Moriarty, R., Sitch, S., Tans, P., Arneth, A., Arvanitis, A., Bakker, D. C. E., Bopp, L., Canadell, J.
- 3333 G., Chini, L. P., Doney, S. C., Harper, A., Harris, I., House, J. I., Jain, A. K., Jones, S. D., Kato, E., Keeling, R. F.,
- Klein Goldewijk, K., Körtzinger, A., Koven, C., Lefèvre, N., Maignan, F., Omar, A., Ono, T., Park, G.-H., Pfeil,
- B., Poulter, B., Raupach, M. R., Regnier, P., Rödenbeck, C., Saito, S., Schwinger, J., Segschneider, J., Stocker, B.
- 3336 D., Takahashi, T., Tilbrook, B., van Heuven, S., Viovy, N., Wanninkhof, R., Wiltshire, A., and Zaehle, S.: Global
- 3337 carbon budget 2013, Earth Syst. Sci. Data, 6, 235–263, https://doi.org/10.5194/essd-6-235-2014, 2014.
- 3338 Le Quéré, C., Moriarty, R., Andrew, R. M., Peters, G. P., Ciais, P., Friedlingstein, P., Jones, S. D., Sitch, S., Tans,
- 3339 P., Arneth, A., Boden, T. A., Bopp, L., Bozec, Y., Canadell, J. G., Chini, L. P., Chevallier, F., Cosca, C. E., Harris,
- I., Hoppema, M., Houghton, R. A., House, J. I., Jain, A. K., Johannessen, T., Kato, E., Keeling, R. F., Kitidis, V.,
 Klein Goldewijk, K., Koven, C., Landa, C. S., Landschützer, P., Lenton, A., Lima, I. D., Marland, G., Mathis, J. T.,
- Metzl, N., Nojiri, Y., Olsen, A., Ono, T., Peng, S., Peters, W., Pfeil, B., Poulter, B., Raupach, M. R., Regnier, P.,
- Rödenbeck, C., Saito, S., Salisbury, J. E., Schuster, U., Schwinger, J., Séférian, R., Segschneider, J., Steinhoff, T.,
- 3344 Stocker, B. D., Sutton, A. J., Takahashi, T., Tilbrook, B., van der Werf, G. R., Viovy, N., Wang, Y.-P.,
- Wanninkhof, R., Wiltshire, A., and Zeng, N.: Global carbon budget 2014, Earth Syst. Sci. Data, 7, 47–85,
- 3346 https://doi.org/10.5194/essd-7-47-2015, 2015a.
- 3347 Le Quéré, C., Moriarty, R., Andrew, R. M., Canadell, J. G., Sitch, S., Korsbakken, J. I., Friedlingstein, P., Peters,
- G. P., Andres, R. J., Boden, T. A., Houghton, R. A., House, J. I., Keeling, R. F., Tans, P., Arneth, A., Bakker, D. C.
- E., Barbero, L., Bopp, L., Chang, J., Chevallier, F., Chini, L. P., Ciais, P., Fader, M., Feely, R. A., Gkritzalis, T.,
- Harris, I., Hauck, J., Ilyina, T., Jain, A. K., Kato, E., Kitidis, V., Klein Goldewijk, K., Koven, C., Landschützer, P.,
- Lauvset, S. K., Lefèvre, N., Lenton, A., Lima, I. D., Metzl, N., Millero, F., Munro, D. R., Murata, A., Nabel, J. E.
- M. S., Nakaoka, S., Nojiri, Y., O'Brien, K., Olsen, A., Ono, T., Pérez, F. F., Pfeil, B., Pierrot, D., Poulter, B.,
- Rehder, G., Rödenbeck, C., Saito, S., Schuster, U., Schwinger, J., Séférian, R., Steinhoff, T., Stocker, B. D., Sutton, A. J., Takahashi, T., Tilbrook, B., van der Laan-Luijkx, I. T., van der Werf, G. R., van Heuven, S.,
- 3355 Vandemark, D., Viovy, N., Wiltshire, A., Zaehle, S., and Zeng, N.: Global Carbon Budget 2015, Earth Syst. Sci.
- 3356 Data, 7, 349–396, https://doi.org/10.5194/essd-7-349-2015, 2015b.
- 3357 Le Quéré, C., Andrew, R. M., Canadell, J. G., Sitch, S., Korsbakken, J. I., Peters, G. P., Manning, A. C., Boden, T.
- 3358 A., Tans, P. P., Houghton, R. A., Keeling, R. F., Alin, S., Andrews, O. D., Anthoni, P., Barbero, L., Bopp, L.,
- Chevallier, F., Chini, L. P., Ciais, P., Currie, K., Delire, C., Doney, S. C., Friedlingstein, P., Gkritzalis, T., Harris,
- I., Hauck, J., Haverd, V., Hoppema, M., Klein Goldewijk, K., Jain, A. K., Kato, E., Körtzinger, A., Landschützer,
 P., Lefèvre, N., Lenton, A., Lienert, S., Lombardozzi, D., Melton, J. R., Metzl, N., Millero, F., Monteiro, P. M. S.,
- P., Lefèvre, N., Lenton, A., Lienert, S., Lombardozzi, D., Melton, J. R., Metzl, N., Millero, F., Monteiro, P. M. S.,
 Munro, D. R., Nabel, J. E. M. S., Nakaoka, S., O'Brien, K., Olsen, A., Omar, A. M., Ono, T., Pierrot, D., Poulter,
- 3363 B., Rödenbeck, C., Salisbury, J., Schuster, U., Schwinger, J., Séférian, R., Skjelvan, I., Stocker, B. D., Sutton, A. J.,
- Takahashi, T., Tian, H., Tilbrook, B., van der Laan-Luijkx, I. T., van der Werf, G. R., Viovy, N., Walker, A. P.,





- 3365 Wiltshire, A. J., and Zaehle, S.: Global Carbon Budget 2016, Earth Syst. Sci. Data, 8, 605-649,
- 3366 https://doi.org/10.5194/essd-8-605-2016, 2016.
- 3367 Le Quéré, C., Andrew, R. M., Friedlingstein, P., Sitch, S., Pongratz, J., Manning, A. C., Korsbakken, J. I., Peters,
- 3368 G. P., Canadell, J. G., Jackson, R. B., Boden, T. A., Tans, P. P., Andrews, O. D., Arora, V. K., Bakker, D. C. E.,
- 3369 Barbero, L., Becker, M., Betts, R. A., Bopp, L., Chevallier, F., Chini, L. P., Ciais, P., Cosca, C. E., Cross, J.,
- 3370 Currie, K., Gasser, T., Harris, I., Hauck, J., Haverd, V., Houghton, R. A., Hunt, C. W., Hurtt, G., Ilyina, T., Jain, A.
- 3371 K., Kato, E., Kautz, M., Keeling, R. F., Klein Goldewijk, K., Körtzinger, A., Landschützer, P., Lefèvre, N., Lenton,
- 3372 A., Lienert, S., Lima, I., Lombardozzi, D., Metzl, N., Millero, F., Monteiro, P. M. S., Munro, D. R., Nabel, J. E. M. 3373 S., Nakaoka, S., Nojiri, Y., Padin, X. A., Peregon, A., Pfeil, B., Pierrot, D., Poulter, B., Rehder, G., Reimer, J.,
- 3374 Rödenbeck, C., Schwinger, J., Séférian, R., Skjelvan, I., Stocker, B. D., Tian, H., Tilbrook, B., Tubiello, F. N., van
- 3375 der Laan-Luijkx, I. T., van der Werf, G. R., van Heuven, S., Viovy, N., Vuichard, N., Walker, A. P., Watson, A. J.,
- 3376 Wiltshire, A. J., Zaehle, S., and Zhu, D.: Global Carbon Budget 2017, Earth Syst. Sci. Data, 10, 405-448,
- 3377 https://doi.org/10.5194/essd-10-405-2018, 2018a.
- 3378 Le Quéré, C., Andrew, R. M., Friedlingstein, P., Sitch, S., Hauck, J., Pongratz, J., Pickers, P. A., Korsbakken, J. I.,
- 3379 Peters, G. P., Canadell, J. G., Arneth, A., Arora, V. K., Barbero, L., Bastos, A., Bopp, L., Chevallier, F., Chini, L.
- 3380 P., Ciais, P., Doney, S. C., Gkritzalis, T., Goll, D. S., Harris, I., Haverd, V., Hoffman, F. M., Hoppema, M.,
- 3381 Houghton, R. A., Hurtt, G., Ilyina, T., Jain, A. K., Johannessen, T., Jones, C. D., Kato, E., Keeling, R. F., Klein
- 3382 Goldewijk, K., Landschützer, P., Lefèvre, N., Lienert, S., Liu, Z., Lombardozzi, D., Metzl, N., Munro, D. R.,
- 3383 Nabel, J. E. M. S., Nakaoka, S., Neill, C., Olsen, A., Ono, T., Patra, P., Peregon, A., Peters, W., Peylin, P., Pfeil,
- 3384 B., Pierrot, D., Poulter, B., Rehder, G., Resplandy, L., Robertson, E., Rocher, M., Rödenbeck, C., Schuster, U.,
- Schwinger, J., Séferian, R., Skjelvan, I., Steinhoff, T., Sutton, A., Tans, P. P., Tian, H., Tilbrook, B., Tubiello, F. N., van der Laan-Luijkx, I. T., van der Werf, G. R., Viovy, N., Walker, A. P., Wiltshire, A. J., Wright, R., Zaehle, 3385
- 3386
- 3387 S., and Zheng, B.: Global Carbon Budget 2018, Earth Syst. Sci. Data, 10, 2141–2194, https://doi.org/10.5194/essd-
- 3388 10-2141-2018, 2018b.
- 3389 Le Quéré, C., Korsbakken, J. I., Wilson, C., Tosun, J., Andrew, R., Andres, R. J., Canadell, J. G., Jordan, A.,
- 3390 Peters, G. P., and van Vuuren, D. P.: Drivers of declining CO2 emissions in 18 developed economies, Nat. Clim.
- 3391 Chang., 9, 213-217, https://doi.org/10.1038/s41558-019-0419-7, 2019.
- 3392 Le Quéré, C., Peters, G. P., Friedlingstein, P., Andrew, R. M., Canadell, J. G., Davis, S. J., Jackson, R. B., and
- 3393 Jones, M. W.: Fossil CO2 emissions in the post-COVID-19 era, Nat. Clim. Chang., 11, 197-199,
- 3394 https://doi.org/10.1038/s41558-021-01001-0, 2021.
- 3395 Levitus, S., Antonov, J. I., Boyer, T. P., Baranova, O. K., Garcia, H. E., Locarnini, R. A., Mishonov, A. V.,
- Reagan, J. R., Seidov, D., Yarosh, E. S., and Zweng, M. M.: World ocean heat content and thermosteric sea level 3396
- 3397 change (0-2000 m), 1955-2010, Geophys. Res. Lett., 39, https://doi.org/10.1029/2012GL051106, 2012.
- 3398 Li, H., Ilyina, T., Müller, W. A., and Sienz, F.: Decadal predictions of the North Atlantic CO2 uptake, Nat.
- 3399 Commun., 7, 11076, https://doi.org/10.1038/ncomms11076, 2016.
- Li, H., Ilyina, T., Müller, W. A., and Landschützer, P.: Predicting the variable ocean carbon sink, Sci. Adv., 5, 3400
- 3401 eaav6471, https://doi.org/10.1126/sciadv.aav6471, 2019.
- 3402 Li, H., Ilyina, T., Loughran, T., Spring, A., and Pongratz, J.: Reconstructions and predictions of the global carbon
- 3403 budget with an emission-driven Earth system model, Earth Syst. Dyn., 14, 101-119, https://doi.org/10.5194/esd-
- 3404 14-101-2023, 2023.
- 3405 Li, W., Ciais, P., Peng, S., Yue, C., Wang, Y., Thurner, M., Saatchi, S. S., Arneth, A., Avitabile, V., Carvalhais, N.,
- 3406 Harper, A. B., Kato, E., Koven, C., Liu, Y. Y., Nabel, J. E. M. S., Pan, Y., Pongratz, J., Poulter, B., Pugh, T. A. M.,
- 3407 Santoro, M., Sitch, S., Stocker, B. D., Viovy, N., Wiltshire, A., Yousefpour, R., and Zaehle, S.: Land-use and land-
- 3408 cover change carbon emissions between 1901 and 2012 constrained by biomass observations, Biogeosciences, 14,
- 3409 5053-5067, https://doi.org/10.5194/bg-14-5053-2017, 2017.
- 3410 Liao, E., Resplandy, L., Liu, J., and Bowman, K. W.: Amplification of the Ocean Carbon Sink During El Niños:
- 3411 Role of Poleward Ekman Transport and Influence on Atmospheric CO2, Global Biogeochem. Cy., 34,
- 3412 e2020GB006574, https://doi.org/10.1029/2020GB006574, 2020.
- 3413 Lienert, S. and Joos, F.: A Bayesian ensemble data assimilation to constrain model parameters and land-use carbon
- 3414 emissions, Biogeosciences, 15, 2909–2930, https://doi.org/10.5194/bg-15-2909-2018, 2018.

© Author(s) 2025. CC BY 4.0 License.





- Liu, J., Baskaran, L., Bowman, K., Schimel, D., Bloom, A. A., Parazoo, N. C., Oda, T., Carroll, D., Menemenlis,
- 3416 D., Joiner, J., Commane, R., Daube, B., Gatti, L. V., McKain, K., Miller, J., Stephens, B. B., Sweeney, C., and
- 3417 Wofsy, S.: Carbon Monitoring System Flux Net Biosphere Exchange 2020 (CMS-Flux NBE 2020), 13, 299-330,
- 3418 https://doi.org/10.5194/essd-13-299-2021, 2021.
- 3419 Liu, Z., Guan, D., Wei, W., Davis, S. J., Ciais, P., Bai, J., Peng, S., Zhang, Q., Hubacek, K., Marland, G., Andres,
- 3420 R. J., Crawford-Brown, D., Lin, J., Zhao, H., Hong, C., Boden, T. A., Feng, K., Peters, G. P., Xi, F., Liu, J., Li, Y.,
- 3421 Zhao, Y., Zeng, N., and He, K.: Reduced carbon emission estimates from fossil fuel combustion and cement
- 3422 production in China, Nature, 524, 335-338, https://doi.org/10.1038/nature14677, 2015.
- 3423 Liu, Z., Zeng, N., Liu, Y., Kalnay, E., Asrar, G., Wu, B., Cai, Q., Liu, D., and Han, P.: Improving the joint
- 3424 estimation of CO2 and surface carbon fluxes using a constrained ensemble Kalman filter in COLA (v1.0), Geosci.
- 3425 Model Dev., 15, 5511-5528, https://doi.org/10.5194/gmd-15-5511-2022, 2022.
- 3426 Liu, Z., Ciais, P., Deng, Z., Lei, R., Davis, S. J., Feng, S., Zheng, B., Cui, D., Dou, X., Zhu, B., Guo, R., Ke, P.,
- 3427 Sun, T., Lu, C., He, P., Wang, Y., Yue, X., Wang, Y., Lei, Y., Zhou, H., Cai, Z., Wu, Y., Guo, R., Han, T., Xue, J.,
- 3428 Boucher, O., Boucher, E., Chevallier, F., Tanaka, K., Wei, Y., Zhong, H., Kang, C., Zhang, N., Chen, B., Xi, F.,
- 3429 Liu, M., Bréon, F.-M., Lu, Y., Zhang, Q., Guan, D., Gong, P., Kammen, D. M., He, K., and Schellnhuber, H. J.:
- Near-real-time monitoring of global CO2 emissions reveals the effects of the COVID-19 pandemic, Nat Commun, 3430
- 3431 11, 5172, https://doi.org/10.1038/s41467-020-18922-7, 2020a.
- 3432 Liu, Z., Ciais, P., Deng, Z., Davis, S. J., Zheng, B., Wang, Y., Cui, D., Zhu, B., Dou, X., Ke, P., Sun, T., Guo, R.,
- 3433 Zhong, H., Boucher, O., Bréon, F.-M., Lu, C., Guo, R., Xue, J., Boucher, E., Tanaka, K., and Chevallier, F.:
- 3434 Carbon Monitor, a near-real-time daily dataset of global CO2 emission from fossil fuel and cement production, Sci
- 3435 Data, 7, 392, https://doi.org/10.1038/s41597-020-00708-7, 2020b.
- 3436 Long, M. C., Stephens, B. B., McKain, K., Sweeney, C., Keeling, R. F., Kort, E. A., Morgan, E. J., Bent, J. D.,
- 3437 Chandra, N., Chevallier, F., Commane, R., Daube, B. C., Krummel, P. B., Loh, Z., Luijkx, I. T., Munro, D., Patra,
- 3438 P., Peters, W., Ramonet, M., Rödenbeck, C., Stavert, A., Tans, P., Wofsy, S. C.: Strong Southern Ocean carbon
- 3439 uptake evident in airborne observations. Science, 374(6572), 1275–1280, https://doi.org/10.1126/science.abi4355,
- 3440

3462

- 3441 Lovenduski, N. S., Bonan, G. B., Yeager, S. G., Lindsay, K., and Lombardozzi, D. L.: High predictability of
- 3442 terrestrial carbon fluxes from an initialized decadal prediction system, Environ. Res. Lett., 14, 124074,
- 3443 https://doi.org/10.1088/1748-9326/ab5c55, 2019a.
- 3444 Lovenduski, N. S., Yeager, S. G., Lindsay, K., and Long, M. C.: Predicting near-term variability in ocean carbon
- 3445 uptake, Earth Syst. Dyn., 10, 45-57, https://doi.org/10.5194/esd-10-45-2019, 2019b.
- 3446 Lutz, F., Herzfeld, T., Heinke, J., Rolinski, S., Schaphoff, S., von Bloh, W., Stoorvogel, J. J., and Müller, C.:
- 3447 Simulating the effect of tillage practices with the global ecosystem model LPJmL (version 5.0-tillage), Geosci.
- 3448 Model Dev., 12, 2419-2440, https://doi.org/10.5194/gmd-12-2419-2019, 2019.
- 3449 Ma, L., Hurtt, G., Ott, L., Sahajpal, R., Fisk, J., Lamb, R., Tang, H., Flanagan, S., Chini, L., Chatterjee, A., and
- 3450 Sullivan, J.: Global evaluation of the Ecosystem Demography model (ED v3.0), Geosci. Model Dev., 15, 1971-
- 3451 1994, https://doi.org/10.5194/gmd-15-1971-2022, 2022.
- 3452 Magi, B. I., Rabin, S., Shevliakova, E., and Pacala, S.: Separating agricultural and non-agricultural fire seasonality
- 3453 at regional scales, Biogeosciences, 9, 3003-3012, https://doi.org/10.5194/bg-9-3003-2012, 2012.
- 3454 Maksyutov, S., Oda, T., Saito, M., Janardanan, R., Belikov, D., Kaiser, J. W., Zhuravlev, R., Ganshin, A., Valsala,
- 3455 V. K., Andrews, A., Chmura, L., Dlugokencky, E., Haszpra, L., Langenfelds, R. L., Machida, T., Nakazawa, T.,
- 3456 Ramonet, M., Sweeney, C., and Worthy, D.: Technical note: A high-resolution inverse modelling technique for 3457 estimating surface CO2 fluxes based on the NIES-TM-FLEXPART coupled transport model and its adjoint,
- 3458 Atmos. Chem. Phys., 21, 1245-1266, https://doi.org/10.5194/acp-21-1245-2021, 2021.
- 3459 Masarie, K. A. and Tans, P. P.: Extension and integration of atmospheric carbon dioxide data into a globally
- 3460 consistent measurement record, J. Geophys. Res., 100, 11593, https://doi.org/10.1029/95JD00859, 1995.
- 3461 Mataveli, G., Jones, M.W., Carmenta, R., Sanchez, A., Dutra, D.J., Chaves, M., de Oliveira, G., Anderson, L.O.
- 3463 Change Biology, 30(2), p.e17202, https://doi.org/10.1111/gcb.17202, 2024.

and Aragão, L.E.: Deforestation falls but rise of wildfires continues degrading Brazilian Amazon forests. Global





- 3464 Mather, A. S.: The transition from deforestation to reforestation in Europe, in: Agricultural technologies and
- tropical deforestation (eds. Angelsen, A.; Kaimowitz, D.), CABI in association with centre for international
- 3466 Forestry Research, 35–52, 2001.
- 3467 Mauritsen, T., Bader, J., Becker, T., Behrens, J., Bittner, M., Brokopf, R., Brovkin, V., Claussen, M., Crueger, T.,
- Esch, M., Fast, I., Fiedler, S., Fläschner, D., Gayler, V., Giorgetta, M., Goll, D. S., Haak, H., Hagemann, S.,
- 3469 Hedemann, C., Hohenegger, C., Ilyina, T., Jahns, T., Jimenéz-de-la-Cuesta, D., Jungclaus, J., Kleinen, T., Kloster,
- 3470 S., Kracher, D., Kinne, S., Kleberg, D., Lasslop, G., Kornblueh, L., Marotzke, J., Matei, D., Meraner, K.,
- Mikolajewicz, U., Modali, K., Möbis, B., Müller, W. A., Nabel, J. E. M. S., Nam, C. C. W., Notz, D., Nyawira, S.-
- 3472 S., Paulsen, H., Peters, K., Pincus, R., Pohlmann, H., Pongratz, J., Popp, M., Raddatz, T. J., Rast, S., Redler, R.,
- Reick, C. H., Rohrschneider, T., Schemann, V., Schmidt, H., Schnur, R., Schulzweida, U., Six, K. D., Stein, L.,
- 3474 Stemmler, I., Stevens, B., von Storch, J.-S., Tian, F., Voigt, A., Vrese, P., Wieners, K.-H., Wilkenskjeld, S.,
- 3475 Winkler, A., and Roeckner, E.: Developments in the MPI-M Earth System Model version 1.2 (MPI-ESM1.2) and
- 3476 Its Response to Increasing CO2, J. Adv. Model Earth Sy., 11, 998–1038, https://doi.org/10.1029/2018MS001400,
- 3477 2019.
- 3478 Mayot, N., Buitenhuis, E. T., Wright, R. M., Hauck, J., Bakker, D. C. E., and Le Quéré, C.: Constraining the trend
- 3479 in the ocean CO2 sink during 2000–2022. Nat Commun 15, 8429, https://doi.org/10.1038/s41467-024-52641-7,
- 3480 2024.
- 3481 McGrath, M. J., Luyssaert, S., Meyfroidt, P., Kaplan, J. O., Bürgi, M., Chen, Y., Erb, K., Gimmi, U., McInerney,
- D., Naudts, K., Otto, J., Pasztor, F., Ryder, J., Schelhaas, M.-J., and Valade, A.: Reconstructing European forest
- 3483 management from 1600 to 2010, 12, 4291–4316, https://doi.org/10.5194/bg-12-4291-2015, 2015.
- 3484 McKinley, G. A., Fay, A. R., Eddebbar, Y. A., Gloege, L., and Lovenduski, N. S.: External Forcing Explains
- Recent Decadal Variability of the Ocean Carbon Sink, AGU Advances, 1, e2019AV000149,
- 3486 https://doi.org/10.1029/2019AV000149, 2020.
- 3487 McKinley, G. A., Fay, A. R., Lovenduski, N. S., and Pilcher, D. J.: Natural Variability and Anthropogenic Trends
- in the Ocean Carbon Sink, Annu. Rev. Mar. Sci., 9, 125–150, https://doi.org/10.1146/annurev-marine-010816-
- 3489 060529, 2017.
- 3490 Meiyappan, P., Jain, A. K., and House, J. I.: Increased influence of nitrogen limitation on CO 2 emissions from
- future land use and land use change, Global Biogeochem. Cycles, 29, 1524–1548,
- 3492 https://doi.org/10.1002/2015GB005086, 2015.
- 3493 Melo, J., Rossi, S., Achard, F., Alkama, R., Canadell, J. G., Federici, S., Friedlingstein, P., Gibbs, D., Harris, N.,
- Heinrich, V., O'Sullivan, M., Peters, G., Pongratz, J., Rose, M., Roman-Cuesta, R., Sanz Sanchez, M. J.,
- 3495 Schwingshackl, C., Sitch, S., and Grassi, G.: The LULUCF Data Hub: translating global land use emissions
- estimates into the national GHG inventory framework (Version 3.0, 2025 NGHGI release) (3.0),
- 3497 https://doi.org/10.5281/ZENODO.17140775, 2025.
- 3498 Melton, J. R., Arora, V. K., Wisernig-Cojoc, E., Seiler, C., Fortier, M., Chan, E., and Teckentrup, L.: CLASSIC
- 3499 v1.0: the open-source community successor to the Canadian Land Surface Scheme (CLASS) and the Canadian
- 3500 Terrestrial Ecosystem Model (CTEM) Part 1: Model framework and site-level performance, Geosci. Model Dev.,
- $3501 \qquad 13, 2825-2850, https://doi.org/10.5194/gmd-13-2825-2020, 2020. \\$
- Mercado, L. M., Bellouin, N., Sitch, S., Boucher, O., Huntingford, C., Wild, M., and Cox, P. M.: Impact of
- changes in diffuse radiation on the global land carbon sink, Nature, 458, 1014–1017,
- 3504 https://doi.org/10.1038/nature07949, 2009.
- 3505 Merchant, C. J., Embury, O., Bulgin, C. E., Block, T., Corlett, G. K., Fiedler, E., Good, S. A., Mittaz, J., Rayner,
- N. A., Berry, D., Eastwood, S., Taylor, M., Tsushima, Y., Waterfall, A., Wilson, R., and Donlon, C.: Satellite-
- 3507 based time-series of sea-surface temperature since 1981 for climate applications, Sci. Data, 6, 223,
- 3508 https://doi.org/10.1038/s41597-019-0236-x, 2019.
- 3509 Moorcroft, P. R., Hurtt, G. C., and Pacala, S. W.: A Method for Scaling Vegetation Dynamics: The Ecosystem
- 3510 Demography Model (ed), Ecol. Monogr., 71, 557–586, https://doi.org/10.1890/0012-
- 3511 9615(2001)071[0557:AMFSVD]2.0.CO;2, 2001.





- Müller, J. D., Gruber, N., Carter, B., Feely, R., Ishii, M., Lange, N., Lauvset, S. K., Murata, A., Olsen, A., Pérez, F.
- 3513 F., Sabine, C., Tanhua, T., Wanninkhof, R., and Zhu, D.: Decadal Trends in the Oceanic Storage of Anthropogenic
- 3514 Carbon From 1994 to 2014, AGU Adv., 4, e2023AV000875, https://doi.org/10.1029/2023AV000875, 2023.
- 3515 Müller, J. D., Gruber, N., Schneuwly, A., Bakker, D. C. E., Gehlen, M., Gregor, L., Hauck, J., Landschützer, P.,
- and McKinley, G. A.: Unexpected decline in the ocean carbon sink under record-high sea surface temperatures in
- 3517 2023, Nat. Clim. Chang., 15, 978–985, https://doi.org/10.1038/s41558-025-02380-4, 2025.
- 3518 Müller, J. and Joos, F.: Committed and projected future changes in global peatlands continued transient model
- 3519 simulations since the Last Glacial Maximum, Biogeosciences, 18, 3657–3687, https://doi.org/10.5194/bg-18-3657-
- 3520 2021, 2021.
- 3521 Nayagam, L., Maksyutov, S., Oda, T., Janardanan, R., Trisolino, P., Zeng J., Kaiser, J.W. and Matsunaga, T.: A
- 3522 top-down estimation of subnational CO2 budget using a global high-resolution inverse model with data from
- 3523 regional surface networks, Environ. Res. Lett., 19, 0140312024, https://doi.org/10.1088/1748-9326/ad0f74, 2024.
- 3524 NCEP: National Centers for Environmental Prediction. ONI Index. Cold & Warm Episodes by Season [Data set],
- available at: https://www.cpc.ncep.noaa.gov/products/analysis_monitoring/ensostuff/ONI_v5.php, last access: 23
- 3526 October 2025, 2025.
- Nayagam, L., Maksyutov, S., Janardanan, R., Oda, T., Tiwari, Y. K., Sreenivas, G., Datye, A., Jain, C. D., Ratnam,
- 3528 M. V., Sinha, V., Hakkim, H., Terao, Y., Naja, M., Ahmed, Md. K., Mukai, H., Zeng, J., Kaiser, J. W., Someya,
- 3529 Y., Yoshida, Y., and Matsunaga, T.: Indian Land Carbon Sink Estimated from Surface and GOSAT Observations,
- 3530 Remote Sensing, 17, 450, https://doi.org/10.3390/rs17030450, 2025.
- Nevison, C.D., Mahowald, N.M., Doney, S.C., Lima, I.D. and Cassar, N.:. Impact of variable air-sea O 2 and CO 2
- fluxes on atmospheric potential oxygen (APO) and land-ocean carbon sink partitioning. Biogeosciences, 5(3),
- 3533 pp.875-889, https://doi.org/10.5194/bg-5-875-2008, 2008.
- Niu, G.-Y., Yang, Z.-L., Mitchell, K. E., Chen, F., Ek, M. B., Barlage, M., Kumar, A., Manning, K., Niyogi, D.,
- Rosero, E., Tewari, M., and Xia, Y.: The community Noah land surface model with multiparameterization options
- 3536 (Noah-MP): 1. Model description and evaluation with local-scale measurements, J. Geophys. Res. Atmospheres,
- 3537 116, https://doi.org/10.1029/2010JD015139, 2011.
- Niwa, Y., Ishijima, K., Ito, A., and Iida, Y.: Toward a long-term atmospheric CO2 inversion for elucidating natural
- 3539 carbon fluxes: technical notes of NISMON-CO2 v2021.1, Prog. Earth Planet Sci., 9, 42,
- 3540 https://doi.org/10.1186/s40645-022-00502-6, 2022.
- 3541 Niwa, Y., Fujii, Y., Sawa, Y., Iida, Y., Ito, A., Satoh, M., Imasu, R., Tsuboi, K., Matsueda, H., and Saigusa, N.: A
- 3542 4D-Var inversion system based on the icosahedral grid model (NICAM-TM 4D-Var v1.0) Part 2: Optimization
- scheme and identical twin experiment of atmospheric CO<sub>2</sub> inversion, Geosci. Model Dev.,
- 3544 10, 2201–2219, https://doi.org/10.5194/gmd-10-2201-2017, 2017.
- Niwa, Y., Langenfelds, R., Krummel, P., Loh, Zoe, Worthy, Doug, Hatakka, Juha, Aalto, Tuula, Ramonet, Michel,
- Delmotte, Marc, Schmidt, Martina, Gheusi, Francois, Mihalopoulos, N., Morgui, J.A., Andrews, Arlyn,
- Dlugokencky, Ed, Lee, John, Sweeney, Colm, Thoning, Kirk, Tans, Pieter, De Wekker, Stephan, Fischer, Marc L.,
- 3548 Jaffe, Dan, McKain, Kathryn, Viner, Brian, Miller, John B., Karion, Anna, Miller, Charles, Sloop, Christopher D.,
- 3549 Saito, Kazuyuki, Aoki, Shuji, Morimoto, Shinji, Goto, Daisuke, Steinbacher, Martin, Myhre, Cathrine Lund,
- Hermanssen, Ove, Stephens, Britton, Keeling, Ralph, Afshar, Sara, Paplawsky, Bill, Cox, Adam, Walker, Stephen,
- 3551 Schuldt, Kenneth, Mukai, Hitoshi, Machida, Toshinobu, Sasakawa, Motoki, Nomura, Shohei, Ito, Akihiko, Iida,
- Yosuke, and Jones, Matthew W.: Long-term global CO2 fluxes estimated by NICAM-based Inverse Simulation for
 Monitoring CO2 (NISMON-CO2) (ver.2022.1), National Institute for Environmental Studies Japan [Data set],
- 3554 https://doi.org/10.17595/20201127.001, 2020.
- 3555 Norby, R.J.: Forest productivity response to elevated CO2 in free-air CO2 enrichment experiments: the 23 percent
- solution, revisited, New Phytologist, https://doi.org/10.1111/nph.70162, 2025.
- 3557 Obermeier, W. A., Nabel, J. E. M. S., Loughran, T., Hartung, K., Bastos, A., Havermann, F., Anthoni, P., Arneth,
- A., Goll, D. S., Lienert, S., Lombardozzi, D., Luyssaert, S., McGuire, P. C., Melton, J. R., Poulter, B., Sitch, S.,
- Sullivan, M. O., Tian, H., Walker, A. P., Wiltshire, A. J., Zaehle, S., and Pongratz, J.: Modelled land use and land
- 3560 cover change emissions a spatio-temporal comparison of different approaches, 12, 635–670, https://doi.org/10.5194/esd-12-635-2021, 2021.





- 3562 Obermeier, W. A., Schwingshackl, C., Ganzenmüller, R., Grassi, G., Heinrich, V., Luijkx, I. T., Bastos, A., Ciais,
- 3563 P., Sitch, S., and Pongratz, J.: Differences and uncertainties in land-use CO2 flux estimates, Nat Rev Earth
- 3564 Environ, https://doi.org/10.1038/s43017-025-00730-6, 2025.
- 3565 O'Dell, C. W., Eldering, A., Wennberg, P. O., Crisp, D., Gunson, M. R., Fisher, B., Frankenberg, C., Kiel, M.,
- 3566 Lindqvist, H., Mandrake, L., Merrelli, A., Natraj, V., Nelson, R. R., Osterman, G. B., Payne, V. H., Taylor, T. E.,
- Wunch, D., Drouin, B. J., Oyafuso, F., Chang, A., McDuffie, J., Smyth, M., Baker, D. F., Basu, S., Chevallier, F.,
 Crowell, S. M. R., Feng, L., Palmer, P. I., Dubey, M., García, O. E., Griffith, D. W. T., Hase, F., Iraci, L. T., Kivi,
- 3569 R., Morino, I., Notholt, J., Ohyama, H., Petri, C., Roehl, C. M., Sha, M. K., Strong, K., Sussmann, R., Te, Y.,
- 3570 Uchino, O., and Velazco, V. A.: Improved retrievals of carbon dioxide from Orbiting Carbon Observatory-2 with
- 3571 the version 8 ACOS algorithm, Atmos. Meas. Tech., 11, 6539–6576, https://doi.org/10.5194/amt-11-6539-2018,
- 3572 2018.
- 3573 O'Rourke, P. R., Smith, S. J., Mott, A., Ahsan, H., McDuffie, E. E., Crippa, M., Klimont, Z., McDonald, B., Wang,
- 3574 S., Nicholson, M. B., Feng, L., and Hoesly, R. M.: CEDS v_2021_04_21 Release Emission Data, Zenodo [Data
- 3575 set], https://doi.org/10.5281/zenodo.4741285, 2021.
- 3576 O'Sullivan, M., Zhang, Y., Bellouin, N., Harris, I., Mercado, L. M., Sitch, S., Ciais, P., and Friedlingstein, P.:
- 3577 Aerosol-light interactions reduce the carbon budget imbalance, Environ. Res. Lett., 16, 124072,
- 3578 https://doi.org/10.1088/1748-9326/ac3b77, 2021.
- 3579 O'Sullivan, M., Friedlingstein, P., Sitch, S., Anthoni, P., Arneth, A., Arora, V. K., Bastrikov, V., Delire, C., Goll,
- D. S., Jain, A., Kato, E., Kennedy, D., Knauer, J., Lienert, S., Lombardozzi, D., McGuire, P. C., Melton, J. R.,
- Nabel, J. E. M. S., Pongratz, J., Poulter, B., Séférian, R., Tian, H., Vuichard, N., Walker, A. P., Yuan, W., Yue, X.,
- and Zaehle, S.: Process-oriented analysis of dominant sources of uncertainty in the land carbon sink, Nat.
- 3583 Commun., 13, 4781, https://doi.org/10.1038/s41467-022-32416-8, 2022.
- 3584 O'Sullivan, M., Spracklen, D. V., Batterman, S. A., Arnold, S. R., Gloor, M., and Buermann, W.: Have Synergies
- 3585 Between Nitrogen Deposition and Atmospheric CO2 Driven the Recent Enhancement of the Terrestrial Carbon
- 3586 Sink?, Glob. Biogeochem. Cycles, 33, 163–180, https://doi.org/10.1029/2018GB005922, 2019.
- 3587 O'Sullivan, M., Sitch, S., Friedlingstein, P., Luijkx, I. T., Peters, W., Rosan, T. M., Arneth, A., Arora, V. K.,
- Chandra, N., Chevallier, F., Ciais, P., Falk, S., Feng, L., Gasser, T., Houghton, R. A., Jain, A. K., Kato, E.,
- Kennedy, D., Knauer, J., McGrath, M. J., Niwa, Y., Palmer, P. I., Patra, P. K., Pongratz, J., Poulter, B., Rödenbeck,
- 3590 C., Schwingshackl, C., Sun, Q., Tian, H., Walker, A. P., Yang, D., Yuan, W., Yue, X., and Zaehle, S.: The key role
- of forest disturbance in reconciling estimates of the northern carbon sink. Commun Earth Environ 5, 705,
- 3592 https://doi.org/10.1038/s43247-024-01827-4, 2024.
- 3593 O'Sullivan, M., Friedlingstein, P., Sitch, S., Pongratz, J., Schwingshackl, C., Gasser, T., Ciais, P., Arora, V., Kato,
- E., Knauer, J., Nützel, T., Sun, Q., Yuan. W., and Zaehle, S.: An improved approach to estimate the natural land
- 3595 carbon sink, 27 July 2025, PREPRINT (Version 1) available at Research Square [https://doi.org/10.21203/rs.3.rs-
- 3596 7207206/v1], 2025.
- 3597 Palmer, P. I., Feng, L., Baker, D., Chevallier, F., Bösch, H., and Somkuti, P.: Net carbon emissions from African
- biosphere dominate pan-tropical atmospheric CO2 signal, Nat Commun, 10, 3344, https://doi.org/10.1038/s41467-
- 3599 019-11097-w, 2019.
- Pan, Y., Birdsey, R. A., Fang, J., Houghton, R., Kauppi, P. E., Kurz, W. A., Phillips, O. L., Shvidenko, A., Lewis,
- 3601 S. L., Canadell, J. G., Ciais, P., Jackson, R. B., Pacala, S. W., McGuire, A. D., Piao, S., Rautiainen, A., Sitch, S.,
- and Hayes, D.: A Large and Persistent Carbon Sink in the World's Forests, Science, 333, 988–993,
- 3603 https://doi.org/10.1126/science.1201609, 2011.
- 3604 Pandey, S., Miller, J. B., Basu, S., Liu, J., Weir, B., Byrne, B., Chevallier, F., Bowman, K. W., Liu, Z., Deng, F.,
- 3605 O'Dell, C. W., and Chatterjee, A.: Toward Low-Latency Estimation of Atmospheric CO2 Growth Rates Using
- 3606 Satellite Observations: Evaluating Sampling Errors of Satellite and In Situ Observing Approaches, AGU Advances,
- 3607 5, e2023AV001145, https://doi.org/10.1029/2023AV001145, 2024.
- 3608 Pandey, S., Chevallier, F., Rödenbeck, C., Byrne, B., Chatterjee, A., Liu, J., and Frankenberg, C.: Reduction in
- 3609 Earth's carbon budget imbalance, Nat Commun, 16, 6818, https://doi.org/10.1038/s41467-025-61588-2, 2025.





- 3610 Patra, P. K., Takigawa, M., Watanabe, S., Chandra, N., Ishijima, K., and Yamashita, Y.: Improved Chemical
- 3611 Tracer Simulation by MIROC4.0-based Atmospheric Chemistry-Transport Model (MIROC4-ACTM), SOLA, 14,
- 3612 91–96, https://doi.org/10.2151/sola.2018-016, 2018.
- 3613 Pendrill, F., Persson, U. M., Godar, J., Kastner, T., Moran, D., Schmidt, S., and Wood, R.: Agricultural and
- forestry trade drives large share of tropical deforestation emissions, Global Environmental Change, 56, 1–10,
- 3615 https://doi.org/10.1016/j.gloenvcha.2019.03.002, 2019.
- 3616 Pérez, F. F., Becker, M., Goris, N., Gehlen, M., López-Mozos, M., Tjiputra, J., Olsen, A., Müller, J. D., Huertas, I.
- 3617 E., Chau, T. T., Cainzos, V., Velo, A., Benard, G., Hauck, J., Gruber, N., and Wanninkhof, R.: An Assessment
- 3618 of CO 2 Storage and Sea-Air Fluxes for the Atlantic Ocean and Mediterranean Sea Between 1985 and 2018. Global
- 3619 Biogeochemical Cycles, 38(4), e2023GB007862, https://doi.org/10.1029/2023GB007862, 2024.
- 3620 Peters, G. P., Minx, J. C., Weber, C. L., and Edenhofer, O.: Growth in emission transfers via international trade
- from 1990 to 2008, Proceedings of the National Academy of Sciences, 108, 8903-8908,
- 3622 https://doi.org/10.1073/pnas.1006388108, 2011a.
- 3623 Peters, G. P., Marland, G., Le Quéré, C., Boden, T., Canadell, J. G., and Raupach, M. R.: Rapid growth in CO2
- emissions after the 2008–2009 global financial crisis, Nature Clim Change, 2, 2–4,
- 3625 https://doi.org/10.1038/nclimate1332, 2012a.
- 3626 Peters, G. P., Andrew, R. M., Boden, T., Canadell, J. G., Ciais, P., Le Quéré, C., Marland, G., Raupach, M. R., and
- 3627 Wilson, C.: The challenge to keep global warming below 2 °C, Nature Clim Change, 3, 4–6,
- 3628 https://doi.org/10.1038/nclimate1783, 2013.
- 3629 Peters, G. P., Le Quéré, C., Andrew, R. M., Canadell, J. G., Friedlingstein, P., Ilyina, T., Jackson, R. B., Joos, F.,
- 3630 Korsbakken, J. I., McKinley, G. A., Sitch, S., and Tans, P.: Towards real-time verification of CO2 emissions,
- 3631 Nature Clim Change, 7, 848–850, https://doi.org/10.1038/s41558-017-0013-9, 2017a.
- 3632 Peters, G. P., Andrew, R. M., Canadell, J. G., Fuss, S., Jackson, R. B., Korsbakken, J. I., Le Quéré, C. and
- 3633 Nakicenovic, N.: Key indicators to track current progress and future ambition of the Paris Agreement, 7, 118–122,
- 3634 https://doi.org/10.1038/nclimate3202, 2017b.
- Peters, G. P., Andrew, R. M., Canadell, J. G., Friedlingstein, P., Jackson, R. B., Korsbakken, J. I., Le Quéré, C.,
- and Peregon, A.: Carbon dioxide emissions continue to grow amidst slowly emerging climate policies, Nat. Clim.
- 3637 Chang., 10, 3–6, https://doi.org/10.1038/s41558-019-0659-6, 2020.
- Peters, W., Miller, J. B., Whitaker, J., Denning, A. S., Hirsch, A., Krol, M. C., Zupanski, D., Bruhwiler, L., and
- Tans, P. P.: An ensemble data assimilation system to estimate CO2 surface fluxes from atmospheric trace gas
- 3640 observations, J. Geophys. Res. Atmospheres, 110, https://doi.org/10.1029/2005JD006157, 2005.
- 3641 Petrescu, A. M. R., Peters, G. P., Janssens-Maenhout, G., Ciais, P., Tubiello, F. N., Grassi, G., Nabuurs, G.-J.,
- Leip, A., Carmona-Garcia, G., Winiwarter, W., Höglund-Isaksson, L., Günther, D., Solazzo, E., Kiesow, A.,
- 3643 Bastos, A., Pongratz, J., Nabel, J. E. M. S., Conchedda, G., Pilli, R., Andrew, R. M., Schelhaas, M.-J., and Dolman,
- 3644 A. J.: European anthropogenic AFOLU greenhouse gas emissions: a review and benchmark data, Earth Syst. Sci.
- 3645 Data, 12, 961–1001, https://doi.org/10.5194/essd-12-961-2020, 2020.
- 3646 Pfeil, B., Olsen, A., Bakker, D. C. E., Hankin, S., Koyuk, H., Kozyr, A., Malczyk, J., Manke, A., Metzl, N., Sabine,
- 3647 C. L., Akl, J., Alin, S. R., Bates, N., Bellerby, R. G. J., Borges, A., Boutin, J., Brown, P. J., Cai, W.-J., Chavez, F.
- 3648 P., Chen, A., Cosca, C., Fassbender, A. J., Feely, R. A., González-Dávila, M., Goyet, C., Hales, B., Hardman-
- Mountford, N., Heinze, C., Hood, M., Hoppema, M., Hunt, C. W., Hydes, D., Ishii, M., Johannessen, T., Jones, S.
- D., Key, R. M., Körtzinger, A., Landschützer, P., Lauvset, S. K., Lefèvre, N., Lenton, A., Lourantou, A., Merlivat,
 L., Midorikawa, T., Mintrop, L., Miyazaki, C., Murata, A., Nakadate, A., Nakano, Y., Nakaoka, S., Nojiri, Y.,
- Omar, A. M., Padin, X. A., Park, G.-H., Paterson, K., Perez, F. F., Pierrot, D., Poisson, A., Ríos, A. F., Santana-
- 3653 Casiano, J. M., Salisbury, J., Sarma, V. V. S. S., Schlitzer, R., Schneider, B., Schuster, U., Sieger, R., Skjelvan, I.,
- Steinhoff, T., Suzuki, T., Takahashi, T., Tedesco, K., Telszewski, M., Thomas, H., Tilbrook, B., Tjiputra, J.,
 Vandemark, D., Veness, T., Wanninkhof, R., Watson, A. J., Weiss, R., Wong, C. S., and Yoshikawa-Inoue, H.: A
- uniform, quality controlled Surface Ocean CO2 Atlas (SOCAT), Earth Syst. Sci. Data, 5, 125–143,
- 3657 https://doi.org/10.5194/essd-5-125-2013, 2013.





- Piao, S., Ciais, P., Friedlingstein, P., de Noblet-Ducoudré, N., Cadule, P., Viovy, N., and Wang, T.: Spatiotemporal
- 3659 patterns of terrestrial carbon cycle during the 20th century, Global Biogeochem. Cy., 23, GB4026,
- 3660 https://doi.org/10.1029/2008GB003339, 2009.
- Piao, S., Huang, M., Liu, Z., Wang, X., Ciais, P., Canadell, J. G., Wang, K., Bastos, A., Friedlingstein, P., 3661
- 3662 Houghton, R. A., Le Quéré, C., Liu, Y., Myneni, R. B., Peng, S., Pongratz, J., Sitch, S., Yan, T., Wang, Y., Zhu, Z.,
- 3663 Wu, D., and Wang, T.: Lower land-use emissions responsible for increased net land carbon sink during the slow
- 3664 warming period, Nature Geosci, 11, 739–743, https://doi.org/10.1038/s41561-018-0204-7, 2018.
- Pongratz, J., Reick, C.H., Raddatz, T. and Claussen, M.: Effects of anthropogenic land cover change on the carbon 3665
- 3666 cycle of the last millennium. Global Biogeochemical Cycles, 23(4), doi:10.1029/2009GB003488, 2009.
- 3667 Pongratz, J., Reick, C. H., Houghton, R. A., and House, J. I.: Terminology as a key uncertainty in net land use and
- 3668 land cover change carbon flux estimates, Earth Syst. Dynam., 5, 177-195, https://doi.org/10.5194/esd-5-177-2014,
- 3669
- 3670 Pongratz, J., Smith, S. M., Schwingshackl, C., Dayathilake, L., Gasser, T., Grassi, G. and Pilli, R.: Chapter 7:
- 3671 Current levels of CDR. in The State of Carbon Dioxide Removal 2024 - 2nd Edition,
- 3672 https://doi.org/10.17605/OSF.IOZXSKB, 2024.
- 3673 Poulter, B., Bastos, A., Canadell, J., Ciais, P., Gruber, N., Hauck, J., Jackson, R., Ishii, M., Müller, J., Patra, P., and
- 3674 Tian, H.: Inventorying Earth's Land and Ocean Greenhouse Gases, Eos, 103,
- 3675 https://doi.org/10.1029/2022EO179084, 2022.
- 3676 Poulter, B., Frank, D. C., Hodson, E. L., and Zimmermann, N. E.: Impacts of land cover and climate data selection
- 3677 on understanding terrestrial carbon dynamics and the CO2 airborne fraction, Biogeosciences, 8, 2027-2036,
- 3678 https://doi.org/10.5194/bg-8-2027-2011, 2011.
- 3679 Poulter, B., Freeborn, P. H., Jolly, W. M., and Varner, J. M.: COVID-19 lockdowns drive decline in active fires in
- 3680 southeastern United States, PNAS, 118, e2105666118, https://doi.org/10.1073/pnas.2105666118, 2021.
- 3681 Powis, C. M., Smith, S. M., Minx, J. C., and Gasser, T.: Quantifying global carbon dioxide removal deployment,
- 3682 Environ. Res. Lett., 18, 024022, https://doi.org/10.1088/1748-9326/acb450, 2023.
- 3683 Prentice, I. C., Farquhar, G. D., Fasham, M. J. R., Goulden, M. L., Heimann, M., Jaramillo, V. J., Kheshgi, H. S.,
- 3684 Le Quéré, C., Scholes, R. J., and Wallace, D. W. R.: The Carbon Cycle and Atmospheric Carbon Dioxide, in
- 3685 Climate Change 2001: The Scientific Basis. Contribution of Working Group I to the Third Assessment Report of 3686 the Intergovernmental Panel on Climate Change, edited by: Houghton, J. T., Ding, Y., Griggs, D. J., Noguer, M.,
- 3687 van der Linden, P. J., Dai, X., Maskell, K., and Johnson, C. A., Cambridge University Press, Cambridge, United
- 3688
- Kingdom and New York, NY, USA, 183-237, ISBN: 978-0521014953, 2001.
- 3689 Price, J. T. and Warren, R.: Literature Review of the Potential of "Blue Carbon" Activities to Reduce Emissions,
- 3690 available at: https://avoid-net-uk.cc.ic.ac.uk/wp-content/uploads/delightful-downloads/2016/03/Literature-review-
- 3691 of-the-potential-of-blue-carbon-activities-to-reduce-emissions-AVOID2-WPE2.pdf, last access: 23 October 2025,
- 3692
- 3693 Qin, Y., Xiao, X., Wigneron, J.-P., Ciais, P., Brandt, M., Fan, L., Li, X., Crowell, S., Wu, X., Doughty, R., Zhang,
- 3694 Y., Liu, F., Sitch, S., and Moore, B.: Carbon loss from forest degradation exceeds that from deforestation in the
- 3695 Brazilian Amazon, Nat. Clim. Chang., 11, 442-448, https://doi.org/10.1038/s41558-021-01026-5, 2021.
- Qin, Z., Zhu, Y., Canadell, J.G., Chen, M., Li, T., Mishra, U. and Yuan, W.: Global spatially explicit carbon 3696
- 3697 emissions from land-use change over the past six decades (1961–2020). One Earth, 7(5), pp.835-847,
- 3698 https://doi.org/10.1016/j.oneear.2024.04.002, 2024.
- 3699 Qiu, C., Ciais, P., Zhu, D., Guenet, B., Peng, S., Petrescu, A. M. R., Lauerwald, R., Makowski, D., Gallego-Sala,
- A. V., Charman, D. J., and Brewer, S. C.: Large historical carbon emissions from cultivated northern peatlands, 3700
- 3701 Sci. Adv., 7, eabf1332, https://doi.org/10.1126/sciadv.abf1332, 2021.
- 3702 Randerson, J. T., Chen, Y., van der Werf, G. R., Rogers, B. M., and Morton, D. C.: Global burned area and
- 3703 biomass burning emissions from small fires: BURNED AREA FROM SMALL FIRES, J. Geophys. Res.
- 3704 Biogeosciences, 117, n/a-n/a, https://doi.org/10.1029/2012JG002128, 2012.





- Randerson, J. T., Li, Y., Fu, W., Primeau, F., Kim, J. E., Mu, M., Hoffman, F. M., Trugman, A. T., Yang, L., Wu,
- 3706 C., Wang, J. A., Anderegg, W. R. L., Baccini, A., Friedl, M. A., Saatchi, S. S., Denning, A. S., and Goulden, M. L.:
- The weak land carbon sink hypothesis, Sci. Adv., 11, eadr5489, https://doi.org/10.1126/sciadv.adr5489, 2025.
- 3708 Raupach, M. R., Marland, G., Ciais, P., Le Quere, C., Canadell, J. G., Klepper, G., and Field, C. B.: Global and
- 3709 regional drivers of accelerating CO2 emissions, Proceedings of the National Academy of Sciences, 104, 10288-
- 3710 10293, https://doi.org/10.1073/pnas.0700609104, 2007.
- 3711 Regnier, P., Resplandy, L., Najjar, R. G., and Ciais, P.: The land-to-ocean loops of the global carbon cycle, Nature,
- 3712 603, 401–410, https://doi.org/10.1038/s41586-021-04339-9, 2022.
- Reick, C. H., Gayler, V., Goll, D., Hagemann, S., Heidkamp, M., Nabel, J. E. M. S., Raddatz, T., Roeckner, E.,
- 3714 Schnur, R., 110 and Wilkenskjeld, S.: JSBACH 3 The land component of the MPI Earth System Model:
- 3715 documentation of version 3.2, available at: https://doi.org/10.17617/2.3279802, 2021.
- 3716 Remaud, M., Chevallier, F., Cozic, A., Lin, X., and Bousquet, P.: On the impact of recent developments of the
- 3717 LMDz atmospheric general circulation model on the simulation of CO2 transport, 11, 4489,
- 3718 https://doi.org/10.5194/gmd-11-4489-2018, 2018.
- 3719 Resplandy, L., Keeling, R. F., Rödenbeck, C., Stephens, B. B., Khatiwala, S., Rodgers, K. B., Long, M. C., Bopp,
- 3720 L., and Tans, P. P.: Revision of global carbon fluxes based on a reassessment of oceanic and riverine carbon
- 3721 transport, Nature Geosci, 11, 504–509, https://doi.org/10.1038/s41561-018-0151-3, 2018.
- 3722 Resplandy, L., Keeling, R. F., Eddebbar, Y., Brooks, M., Wang, R., Bopp, L., Long, M. C., Dunne, J. P., Koeve,
- W., and Oschlies, A.: Quantification of ocean heat uptake from changes in atmospheric O2 and CO2 composition,
- 3724 Scientific Reports, 9, 20244, https://doi.org/10.1038/s41598-019-56490-z, 2019.
- Rödenbeck, C., Houweling, S., Gloor, M., and Heimann, M.: CO2 flux history 1982–2001 inferred from
- atmospheric data using a global inversion of atmospheric transport, Atmos Chem Phys, 3, 1919–1964, 2003.
- Rödenbeck, C., Bakker, D. C. E., Metzl, N., Olsen, A., Sabine, C., Cassar, N., Reum, F., Keeling, R. F., and
- Heimann, M.: Interannual sea-air CO2 flux variability from an observation-driven ocean mixed-layer scheme, 11,
- 3729 4599–4613, https://doi.org/10.5194/bg-11-4599-2014, 2014.
- 3730 Rödenbeck, C., Zaehle, S., Keeling, R., and Heimann, M.: History of El Niño impacts on the global carbon cycle
- 3731 1957–2017: a quantification from atmospheric CO2 data, 373, 20170303, https://doi.org/10.1098/rstb.2017.0303,
- 3732 2018
- Rödenbeck, C., DeVries, T., Hauck, J., Le Quéré, C., and Keeling, R. F.: Data-based estimates of interannual sea-
- air CO2 flux variations 1957–2020 and their relation to environmental drivers, Biogeosciences, 19, 2627–2652,
- 3735 https://doi.org/10.5194/bg-19-2627-2022, 2022.
- 3736 Rosan, T. M., Klein Goldewijk, K., Ganzenmüller, R., O'Sullivan, M., Pongratz, J., Mercado, L. M., Aragao, L. E.
- O. C., Heinrich, V., Randow, C. V., Wiltshire, A., Tubiello, F. N., Bastos, A., Friedlingstein, P., and Sitcl, S.: A
- multi-data assessment of land use and land cover emissions from Brazil during 2000–2019, Environ. Res. Lett., 16,
- 3739 074004, https://doi.org/10.1088/1748-9326/ac08c3, 2021.
- Rosan, T. M., Sitch, S., O'Sullivan, M., Basso, L. S., Wilson, C., Silva, C., Gloor, E., Fawcett, D., Heinrich, V.,
- 3741 Souza, J. G. and Bezerra, F.G.S.: Synthesis of the land carbon fluxes of the Amazon region between 2010 and
- 3742 2020. Communications Earth & Environment, 5(1), p.46. https://doi.org/10.1038/s43247-024-01205-0, 2024.
- 3743 Sakamoto, K., H. Nakano, S. Urakawa, T. Toyoda, Y. Kawakami, H. Tsujino, G. Yamanaka, 2023: Reference
- manual for the Meteorological Research Institute Community Ocean Model version 5 (MRI.COMv5), Technical
- Reports of the Meteorological Research Institute, No.87, https://doi.org/10.11483/mritechrepo.87.
- 3746 Sarma, V. V. S. S., Sridevi, B., Metzl, N., Patra, P. K., Lachkar, Z., Chakraborty, K., Goyet, C., Levy, M., Mehari,
- M., and Chandra, N.: Air-Sea Fluxes of CO2 in the Indian Ocean Between 1985 and 2018: A Synthesis Based on
- 3748 Observation-Based Surface CO2, Hindcast and Atmospheric Inversion Models, Glob. Biogeochem. Cycles, 37,
- 3749 e2023GB007694, https://doi.org/10.1029/2023GB007694, 2023.
- 3750 Schaphoff, S., von Bloh, W., Rammig, A., Thonicke, K., Biemans, H., Forkel, M., Gerten, D., Heinke, J.,
- Jägermeyr, J., Knauer, J., Langerwisch, F., Lucht, W., Müller, C., Rolinski, S., and Waha, K.: LPJmL4 a dynamic





- global vegetation model with managed land Part 1: Model description, Geosci. Model Dev., 11, 1343-1375,
- https://doi.org/10.5194/gmd-11-1343-2018, 2018.
- 3754 Schimel, D., Alves, D., Enting, I. G., Heimann, M., Joos, F., Raynaud, D., Wigley, T., Prater, M., Derwent, R.,
- 3755 Ehhalt, D., Fraser, P., Sanhueza, E., Zhou, X., Jonas, P., Charlson, R., Rodhe, H., Sadasivan, S., Shine, K. P.,
- 3756 Fouquart, Y., Ramaswamy, V., Solomon, S., Srinivasan, J., Albritton, D., Derwent, R., Isaksen, I., Lal, M., and
- 3757 Wuebbles, D.: Radiative Forcing of Climate Change, in: Climate Change 1995: The Science of Climate Change,
- 3758 Contribution of Working Group I to the Second Assessment Report of the Intergovernmental Panel on Climate
- 3759 Change [Houghton, J. T., Meira Rilho, L. G., Callander, B. A., Harris, N., Kattenberg, A., and Maskell, K. (eds.)],
- 3760 Cambridge University Press, Cambridge, United Kingdom and New York, NY, USA, ISBN: 978-0521559621,
- 3761
- 3762 Schimel, D., Stephens, B. B., and Fisher, J. B.: Effect of increasing CO 2 on the terrestrial carbon cycle, Proc Natl
- Acad Sci USA, 112, 436-441, https://doi.org/10.1073/pnas.1407302112, 2015. 3763
- 3764 Schuh, A. E., Jacobson, A. R., Basu, S., Weir, B., Baker, D., Bowman, K., Chevallier, F., Crowell, S., Davis, K. J.,
- 3765 Deng, F., Denning, S., Feng, L., Jones, D., Liu, J., and Palmer, P. I.: Quantifying the Impact of Atmospheric
- 3766 Transport Uncertainty on CO 2 Surface Flux Estimates, Global Biogeochem. Cycles, 33, 484-500,
- 3767 https://doi.org/10.1029/2018GB006086, 2019.
- 3768 Schuldt, K. N., Mund, J., Aalto, T., Abshire, J. B., Aikin, K., Allen, G., Andrade, M., Andrews, A., Apadula, F.,
- 3769 Arnold, S., Baier, B., Bakwin, P., Bartyzel, J., Bentz, G., Bergamaschi, P., Beyersdorf, A., Biermann, T., Biraud, S.
- 3770 C., Blanc, P.-E., Boenisch, H., Bowling, D., Brailsford, G., Brand, W. A., Brunner, D., Bui, T. P., Burban, B., 3771
- Bäni, L., Calzolari, F., Chang, C. S., Chen, H., Chen, G., Chmura, L., Clark, S., Climadat, S., Colomb, A., 3772
- Commane, R., Condori, L., Conen, F., Conil, S., Couret, C., Cristofanelli, P., Cuevas, E., Curcoll, R., Daube, B., 3773
- Davis, K. J., De Mazière, M., De Wekker, S., Dean-Day, J. M., Della Coletta, J., Delmotte, M., Di Iorio, T.,
- 3774 DiGangi, E., DiGangi, J. P., Dickerson, R., Elsasser, M., Emmenegger, L., Fang, S., Forster, G., France, J., 3775 Frumau, A., Fuente-Lastra, M., Galkowski, M., Gatti, L. V., Gehrlein, T., Gerbig, C., Gheusi, F., Gloor, E., Goto,
- 3776 D., Griffis, T., Hammer, S., Hanisco, T. F., Hanson, C., Haszpra, L., Hatakka, J., Heimann, M., Heliasz, M., Heltai,
- 3777 D., Henne, S., Hensen, A., Hermans, C., Hermansen, O., Hintsa, E., Hoheisel, A., Holst, J., Iraci, L. T., Ivakhov,
- 3778 V., Jaffe, D. A., Jordan, A., Joubert, W., Kang, H.-Y., Karion, A., Kawa, S. R., Kazan, V., Keeling, R. F., Keronen,
- 3779 P., Kim, J., Klausen, J., Kneuer, T., Ko, M.-Y., Kolari, P., Kominkova, K., Kort, E., Kozlova, E., Krummel, P. B., 3780 Kubistin, D., Kulawik, S. S., Kumps, N., Labuschagne, C., Lam, D. H., Lan, X., Langenfelds, R. L., Lanza, A.,
- 3781 Laurent, O., Laurila, T., Lauvaux, T., Lavric, J., Law, B. E., Lee, C.-H., Lee, J., Lehner, I., Lehtinen, K., Leppert,
- R., Leskinen, A., Leuenberger, M., Leung, W. H., Levin, I., Levula, J., Lin, J., Lindauer, M., Lindroth, A., Loh, Z. 3782 M., Lopez, M., Lunder, C. R., Löfvenius, M. O., Machida, T., Mammarella, I., Manca, G., Manning, A., Manning, 3783
- 3784 A., Marek, M. V., Marklund, P., Marrero, J. E., Martin, M. Y., Martin, D., Martins, G. A., Matsueda, H., McKain,
- 3785 K., Meijer, H., Meinhardt, F., Merchant, L., Metzger, J.-M., Mihalopoulos, N., Miles, N. L., Miller, C. E., Miller, J.
- 3786 B., Mitchell, L., Monteiro, V., Montzka, S., Moossen, H., Moreno, C., Morgan, E., Morgui, J.-A., Morimoto, S., 3787 Munger, J. W., Munro, D., Mutuku, M., Myhre, C. L., Mölder, M., Müller-Williams, J., Nakaoka, S.-I., Necki, J.,
- 3788 Newman, S., Nichol, S., Nisbet, E., Niwa, Y., Njiru, D. M., Noe, S. M., Nojiri, Y., O'Doherty, S., Obersteiner, F.,
- 3789
- Paplawsky, B., Parworth, C. L., Peischl, J., Peltola, O., Peters, W., Philippon, C., Piacentino, S., Pichon, J. M., 3790 Pickers, P., Piper, S., Pitt, J., Plass-Dülmer, C., Platt, S. M., Prinzivalli, S., Ramonet, M., Ramos, R., Ren, X.,
- 3791 Reyes-Sanchez, E., Richardson, S. J., Rigouleau, L.-J., Riris, H., Rivas, P. P., Rothe, M., Roulet, Y.-A., Ryerson,
- 3792 T., Ryoo, J.-M., Sargent, M., Sasakawa, M., Schaefer, H., Scheeren, B., Schmidt, M., Schuck, T., Schumacher, M.,
- 3793 Seibel, J., Seifert, T., Sha, M. K., Shepson, P., Shin, D., Shook, M., Sloop, C. D., Smale, D., Smith, P. D., Spain,
- 3794 G., St. Clair, J. M., Steger, D., Steinbacher, M., Stephens, B., Sweeney, C., Sørensen, L. L., Taipale, R., Takatsuji,
- 3795 S., Tans, P., Thoning, K., Timas, H., Torn, M., Trisolino, P., Turnbull, J., Vermeulen, A., Viner, B., Vitkova, G.,
- 3796 Walker, S., Watson, A., Weiss, R., Weyrauch, D., Wofsy, S. C., Worsey, J., Worthy, D., Xueref-Remy, I., Yates,
- 3797 E. L., Young, D., Yver-Kwok, C., Zaehle, S., Zahn, A., Zellweger, C., Zimnoch, M., de Souza, R. A., di Sarra, A.
- 3798 G., van Dinther, D., van den Bulk, P.: Multi-laboratory compilation of atmospheric carbon dioxide data for the
- 3799 $period\ 1957-2023; obspack_co2_1_GLOBALVIEWplus_v10.1_2024-11-13, https://doi.org/10.25925/20241101, https://doi.org/10$
- 3800
- 3801 Schuldt, K. N., Jacobson, A. R., Aalto, T., Aaltonen, H., Andrews, A., Apadula, F., Arnold, S., Bakwin, P.,
- 3802 Bartyzel, J., Bergamaschi, P., Biermann, T., Biraud, S. C., Blanc, P.-E., Brunner, D., Bäni, L., Calzolari, F., Chen,
- 3803 H., Chmura, L., Colomb, A., Condori, L., Conen, F., Conil, S., Couret, C., Cristofanelli, P., Cuevas, E., De
- 3804 Mazière, M., De Wekker, S., Della Coletta, J., Delmotte, M., Di Iorio, T., Elsasser, M., Emmenegger, L., Forster,
- 3805 G., Frumau, A., Fuente-Lastra, M., Galkowski, M., Gheusi, F., Hammer, S., Haszpra, L., Hatakka, J., Heliasz, M., 3806 Heltai, D., Henne, S., Hensen, A., Hermans, C., Hermansen, O., Hoheisel, A., Holst, J., Jaffe, D. A., Karion, A.,
- 3807 Kazan, V., Keronen, P., Kneuer, T., Kolari, P., Kominkova, K., Krummel, P. B., Kubistin, D., Kumps, N., Lan, X.,
- 3808 Langenfelds, R. L., Lanza, A., Laurent, O., Lee, J., Lehner, I., Lehtinen, K., Leskinen, A., Leuenberger, M., Levin,





- 3809 I., Levula, J., Lindauer, M., Lindroth, A., Loh, Z. M., Lopez, M., Lunder, C. R., Löfvenius, M. O., Mammarella, I.,
- Manca, G., Manning, A., Manning, A., Marek, M. V., Marklund, P., McKain, K., Meijer, H., Meinhardt, F.,
- 3811 Metzger, J.-M., Miller, J. B., Miller, C. E., Myhre, C. L., Mölder, M., Müller-Williams, J., Necki, J., Noe, S. M.,
- 3812 O'Doherty, S., Peltola, O., Philippon, C., Piacentino, S., Pichon, J. M., Pickers, P., Pitt, J., Plass-Dülmer, C., Platt,
- 3813 S. M., Ramonet, M., Ramos, R., Reyes-Sanchez, E., Rigouleau, L.-J., Rivas, P. P., Roulet, Y.-A., Scheeren, B.,
- 3814 Schmidt, M., Schumacher, M., Sha, M. K., Sloop, C. D., Smith, P. D., Steger, D., Steinbacher, M., Sweeney, C.,
- 3815 Sørensen, L. L., Taipale, R., Tans, P., Thoning, K., Trisolino, P., Vermeulen, A., Viner, B., Vitkova, G., Weyrauch,
- D., Worthy, D., Xueref-Remy, I., Young, D., Yver-Kwok, C., Zimnoch, M., di Sarra, A. G., van den Bulk, P.:
- 3817 Multi-laboratory compilation of atmospheric carbon dioxide data for the year 2024;
- 3818 obspack co2 1 NRT v10.1 2025-02-07, https://doi.org/10.25925/20250101, 2025.
- 3819 Schwinger, J., Goris, N., Tjiputra, J. F., Kriest, I., Bentsen, M., Bethke, I., Ilicak, M., Assmann, K. M., and Heinze,
- 3820 C.: Evaluation of NorESM-OC (versions 1 and 1.2), the ocean carbon-cycle stand-alone configuration of the
- Norwegian Earth System Model (NorESM1), Geosci. Model Dev., 9, 2589–2622, https://doi.org/10.5194/gmd-9-
- 3822 2589-2016, 2016.
- 3823 Schwingshackl, C., Obermeier, W. A., Bultan, S., Grassi, G., Canadell, J. G., Friedlingstein, P., Gasser, T.,
- Houghton, R. A., Kurz, W. A., Sitch, S., and Pongratz, J.: Differences in land-based mitigation estimates
- reconciled by separating natural and land-use CO2 fluxes at the country level, One Earth, 5, 1367–1376,
- 3826 https://doi.org/10.1016/j.oneear.2022.11.009, 2022.
- 3827 Séférian, R., Nabat, P., Michou, M., Saint-Martin, D., Voldoire, A., Colin, J., Decharme, B., Delire, C., Berthet, S.,
- 3828 Chevallier, M., Sénési, S., Franchisteguy, L., Vial, J., Mallet, M., Joetzjer, E., Geoffroy, O., Guérémy, J.-F., Moine,
- 3829 M.-P., Msadek, R., Ribes, A., Rocher, M., Roehrig, R., Salas-y-Mélia, D., Sanchez, E., Terray, L., Valcke, S.,
- Waldman, R., Aumont, O., Bopp, L., Deshayes, J., Éthé, C., and Madec, G.: Evaluation of CNRM Earth System
- 3831 Model, CNRM-ESM2-1: Role of Earth System Processes in Present-Day and Future Climate, Journal of Advances
- 3832 in Modeling Earth Systems, 11, 4182–4227, https://doi.org/10.1029/2019MS001791, 2019.
- 3833 Seiler, C., Melton, J. R., Arora, V. K., Sitch, S., Friedlingstein, P., Anthoni, P., Goll, D., Jain, A. K., Joetzjer, E.,
- Lienert, S., Lombardozzi, D., Luyssaert, S., Nabel, J. E. M. S., Tian, H., Vuichard, N., Walker, A. P., Yuan, W.,
- 3835 and Zaehle, S.: Are Terrestrial Biosphere Models Fit for Simulating the Global Land Carbon Sink?, J. Adv. Model.
- 3836 Earth Syst., 14, e2021MS002946, https://doi.org/10.1029/2021MS002946, 2022.
- 3837 Sellar, A. A., Jones, C. G., Mulcahy, J. P., Tang, Y., Yool, A., Wiltshire, A., O'Connor, F. M., Stringer, M., Hill,
- 3838 R., Palmieri, J., Woodward, S., Mora, L., Kuhlbrodt, T., Rumbold, S. T., Kelley, D. I., Ellis, R., Johnson, C. E., 3839 Walton, J., Abraham, N. L., Andrews, M. B., Andrews, T., Archibald, A. T., Berthou, S., Burke, E., Blockley, E.,
- Walton, J., Abraham, N. L., Andrews, M. B., Andrews, T., Archibald, A. T., Berthou, S., Burke, E., Blockley, E.
 Carslaw, K., Dalvi, M., Edwards, J., Folberth, G. A., Gedney, N., Griffiths, P. T., Harper, A. B., Hendry, M. A.,
- Hewitt, A. J., Johnson, B., Jones, A., Jones, C. D., Keeble, J., Liddicoat, S., Morgenstern, O., Parker, R. J., Predoi,
- 3842 V., Robertson, E., Siahaan, A., Smith, R. S., Swaminathan, R., Woodhouse, M. T., Zeng, G., and Zerroukat, M.:
- 3843 UKESM1: Description and Evaluation of the U.K. Earth System Model, J. Adv. Model. Earth Syst., 11, 4513–
- 3844 4558, https://doi.org/10.1029/2019MS001739, 2019.
- 3845 Shu, S., Jain, A. K., Koven, C. D., and Mishra, U.: Estimation of Permafrost SOC Stock and Turnover Time Using
- 3846 a Land Surface Model With Vertical Heterogeneity of Permafrost Soils, Global Biogeochem. Cy., 34,
- 3847 e2020GB006585, https://doi.org/10.1029/2020GB006585, 2020.
- 3848 Shutler, J. D., Land, P. E., Piolle, J.-F., Woolf, D. K., Goddijn-Murphy, L., Paul, F., Girard-Ardhuin, F., Chapron,
- B., and Donlon, C. J.: FluxEngine: A Flexible Processing System for Calculating Atmosphere–Ocean Carbon
- 3850 Dioxide Gas Fluxes and Climatologies, J. Atmospheric Ocean. Technol., 33, 741–756,
- 3851 https://doi.org/10.1175/JTECH-D-14-00204.1, 2016.
- 3852 Silva Junior, C.H., Anderson, L.O., Silva, A.L., Almeida, C.T., Dalagnol, R., Pletsch, M.A., Penha, T.V., Paloschi,
- R.A. and Aragão, L.E.: Fire responses to the 2010 and 2015/2016 Amazonian droughts. Frontiers in Earth Science,
- 3854 7, p.97, https://doi.org/10.3389/feart.2019.00097, 2019.
- 3855 Sitch, S., V. Brovkin, W. von Bloh, D. Van Vuuren, B. Eickhout, and Ganopolski, A.: Impacts of future land cover
- on atmospheric CO2 and climate. Global Biogeochemical Cycles, 19, GB2013. doi:10.1029/2004GB002311, 2005.
- 3857 Sitch, S., Huntingford, C., Gedney, N., Levy, P. E., Lomas, M., Piao, S. L., Betts, R., Ciais, P., Cox, P.,
- Friedlingstein, P., Jones, C. D., Prentice, I. C., and Woodward, F. I.: Evaluation of the terrestrial carbon cycle,
- 3859 future plant geography and climate-carbon cycle feedbacks using five Dynamic Global Vegetation Models





- 3860 (DGVMs): Uncertainty In Land Carbon Cycle Feedbacks, Glob. Change Biol., 14, 2015–2039,
- 3861 https://doi.org/10.1111/j.1365-2486.2008.01626.x, 2008.
- 3862 Sitch, S., O'Sullivan, M., Robertson, E., Friedlingstein, P., Albergel, C., Anthoni, P., Arneth, A., Arora, V. K.,
- Bastos, A., Bastrikov, V., Bellouin, N., Canadell, J. G., Chini, L., Ciais, P., Falk, S., Harris, I., Hurtt, G., Ito, A.,
- Jain, A. K., Jones, M. W., Joos, F., Kato, E., Kennedy, D., Klein Goldewijk, K., Kluzek, E., Knauer, J., Lawrence,
- P. J., Lombardozzi, D., Melton, J. R., Nabel, J. E. M. S., Pan, N., Peylin, P., Pongratz, J., Poulter, B., Rosan, T. M.,
 Sun, Q., Tian, H., Walker, A. P., Weber, U., Yuan, W., Yue, X., Zaehle, S.: Trends and Drivers of Terrestrial
- 3867 Sources and Sinks of Carbon Dioxide: An Overview of the TRENDY Project, Global Biogeochemical Cycles,
- 3868 38(7), e2024GB008102, https://doi.org/10.1029/2024GB008102, 2024.
- 3869 Smallman, T. L., Milodowski, D. T., Neto, E. S., Koren, G., Ometto, J., and Williams, M.: Parameter uncertainty
- dominates C-cycle forecast errors over most of Brazil for the 21st century, Earth Syst. Dyn., 12, 1191–1237,
- 3871 https://doi.org/10.5194/esd-12-1191-2021, 2021.
- 3872 Smith, B., Wårlind, D., Arneth, A., Hickler, T., Leadley, P., Siltberg, J., and Zaehle, S.: Implications of
- 3873 incorporating N cycling and N limitations on primary production in an individual-based dynamic vegetation model,
- 3874 Biogeosciences, 11, 2027–2054, https://doi.org/10.5194/bg-11-2027-2014, 2014.
- 3875 Smith, S. M., Geden, O., Gidden, M. J., Lamb, W. F., Nemet, G. F., Minx, J. C., Buck, H., Burke, J., Cox, E.,
- Edwards, M. R., Fuss, S., Johnstone, I., Müller-Hansen, F., Pongratz, J., Probst, B. S., Roe, S., Schenuit, F.,
- 3877 Schulte, I., and Vaughan, N. E. The State of Carbon Dioxide Removal 2024 2nd Edition,
- 3878 http://dx.doi.org/10.17605/OSF.IO/F85QJ, 2024.
- 3879 Sospedra-Alfonso, R., Merryfield, W. J., Boer, G. J., Kharin, V. V., Lee, W.-S., Seiler, C., and Christian, J. R.:
- Decadal climate predictions with the Canadian Earth System Model version 5 (CanESM5), Geosci. Model Dev.,
- 3881 14, 6863–6891, https://doi.org/10.5194/gmd-14-6863-2021, 2021.
- 3882 Steele, L. P., Dlugokencky, E. J., Lang, P. M., Tans, P. P., Martin, R. C., and Masarie, K. A.: Slowing down of the
- 3883 global accumulation of atmospheric methane during the 1980s, Nature 358, 313–316,
- 3884 https://doi.org/10.1038/358313a0, 1992.
- Stephens, B. B., Gurney, K. R., Tans, P. P., Sweeney, C., Peters, W., Bruhwiler, L., Ciais, P., Ramonet, M.,
- Bousquet, P., Nakazawa, T., Aoki, S., Machida, T., Inoue, G., Vinnichenko, N., Lloyd, J., Jordan, A., Heimann,
- 3887 M., Shibistova, O., Langenfelds, R. L., Steele, L. P., Francey, R. J., and Denning, A. S.: Weak Northern and Strong
- 3888 Tropical Land Carbon Uptake from Vertical Profiles of Atmospheric CO2, Science, 316, 1732–1735,
- 3889 https://doi.org/10.1126/science.1137004, 2007.
- 3890 Stephens, B. B., Keeling, R. F., Heimann, M., Six, K. D., Murnane, R., and Caldeira, K.: Testing global ocean
- 3891 carbon cycle models using measurements of atmospheric O2 and CO2 concentration, Glob. Biogeochem. Cycles,
- 3892 12, 213–230, https://doi.org/10.1029/97GB03500, 1998.
- 3893 Stock, C. A., Dunne, J. P., Luo, J. Y., Ross, A. C., Van Oostende, N., Zadeh, N., Cordero, T. J., Liu, X., and Teng,
- 3894 Y.: Photoacclimation and Photoadaptation Sensitivity in a Global Ocean Ecosystem Model, J Adv Model Earth
- 3895 Syst, 17, e2024MS004701, https://doi.org/10.1029/2024MS004701, 2025.
- 3896 Stocker, T., Qin, D., and Platner, G.-K.: Climate Change 2013: The Physical Science Basis. Contribution of
- Working Group I to the Fifth Assessment Report of the Intergovernmental Panel on Climate Change
- 3898 [Intergovernmental Panel on Climate Change (eds.)], Cambridge University Press, Cambridge, ISBN:
- 3899 9789291691388, 2013.\
- 3900 Swart, N. C., Cole, J. N. S., Kharin, V. V., Lazare, M., Scinocca, J. F., Gillett, N. P., Anstey, J., Arora, V.,
- 3901 Christian, J. R., Hanna, S., Jiao, Y., Lee, W. G., Majaess, F., Saenko, O. A., Seiler, C., Seinen, C., Shao, A.,
- 3902 Sigmond, M., Solheim, L., von Salzen, K., Yang, D., and Winter, B.: The Canadian Earth System Model version 5
- 3903 (CanESM5.0.3), Geosci. Model Dev., 12, 4823–4873, https://doi.org/10.5194/gmd-12-4823-2019, 2019.
- 3904 SX Coal: Monthly coal consumption estimates, http://www.sxcoal.com/, last access: 23 October 2025, 2022.
- Takahashi, T., Sutherland, S. C., Wanninkhof, R., Sweeney, C., Feely, R. A., Chipman, D. W., Hales, B.,
 Friederich, G., Chavez, F., Sabine, C., Watson, A., Bakker, D. C. E., Schuster, U., Metzl, N., Yoshikawa-Inoue, H.,
- 3907 Ishii, M., Midorikawa, T., Nojiri, Y., Körtzinger, A., Steinhoff, T., Hoppema, M., Olafsson, J., Arnarson, T. S.,
- 3908 Tilbrook, B., Johannessen, T., Olsen, A., Bellerby, R., Wong, C. S., Delille, B., Bates, N. R., and de Baar, H. J. W.:





- 3909 Climatological mean and decadal change in surface ocean pCO2, and net sea-air CO2 flux over the global oceans,
- 3910 Deep Sea Research Part II: Topical Studies in Oceanography, 56, 554-577,
- 3911 $https://doi.org/10.1016/j.dsr2.\hat{2}008.12.009,\,2009.$
- 3912 Terhaar, J., Frölicher, T. L., and Joos, F.: Southern Ocean anthropogenic carbon sink constrained by sea surface
- 3913 salinity, Sci. Adv., 7, eabd5964, https://doi.org/10.1126/sciadv.abd5964, 2021.
- 3914 Terhaar, J., Frölicher, T. L., and Joos, F.: Observation-constrained estimates of the global ocean carbon sink from
- 3915 Earth system models, Biogeosciences, 19, 4431–4457, https://doi.org/10.5194/bg-19-4431-2022, 2022.
- 3916 Terhaar, J., Goris, N., Müller, J. D., DeVries, T., Gruber, N., Hauck, J., Perez, F. F., and Séférian, R.: Assessment
- 3917 of Global Ocean Biogeochemistry Models for Ocean Carbon Sink Estimates in RECCAP2 and Recommendations
- 3918 for Future Studies. Journal of Advances in Modeling Earth Systems, 16(3), e2023MS003840,
- 3919 https://doi.org/10.1029/2023MS003840, 2024.
- 3920 Tian, H., Xu, X., Lu, C., Liu, M., Ren, W., Chen, G., Melillo, J., and Liu, J.: Net exchanges of CO2, CH4, and
- 3921 N2O between China's terrestrial ecosystems and the atmosphere and their contributions to global climate warming,
- 3922 J. Geophys. Res. Biogeosciences, 116, G02011, https://doi.org/10.1029/2010JG001393, 2011.
- 3923 Tian, H., Chen, G., Lu, C., Xu, X., Hayes, D. J., Ren, W., Pan, S., Huntzinger, D. N., and Wofsy, S. C.: North
- 3924 American terrestrial CO2 uptake largely offset by CH4 and N2O emissions: toward a full accounting of the
- 3925 greenhouse gas budget, Climatic Change, 129, 413–426, https://doi.org/10.1007/s10584-014-1072-9, 2015.
- 3926 Tjiputra, J. F., Schwinger, J., Bentsen, M., Morée, A. L., Gao, S., Bethke, I., Heinze, C., Goris, N., Gupta, A., He,
- 3927 Y.-C., Olivié, D., Seland, Ø., and Schulz, M.: Ocean biogeochemistry in the Norwegian Earth System Model
- 3928 version 2 (NorESM2), Geosci. Model Dev., 13, 2393-2431, https://doi.org/10.5194/gmd-13-2393-2020, 2020.
- 3929 Tsujino, H., Nakano, H., Sakamoto, K., Urakawa, L.S., Toyama, K., Kosugi, N., Kitamura, Y., Ishii, M.,
- 3930 Nishikawa, S., Nishikawa, H., Sugiyama, T., and Ishikawa, Y.: Impact of increased horizontal resolution of an
- 3931 ocean model on carbon circulation in the North Pacific Ocean. Journal of Advances in Modeling Earth Systems,
- 3932 16, e2023MS003720, https://doi.org/10.1029/2023MS003720, 2024.
- Tubiello, F. N., Conchedda, G., Wanner, N., Federici, S., Rossi, S., and Grassi, G.: Carbon emissions and removals 3933
- 3934 from forests: new estimates, 1990-2020, Earth Syst. Sci. Data, 13, 1681-1691, https://doi.org/10.5194/essd-13-
- 3935 1681-2021, 2021.
- 3936 Tubiello, F., Pekkarinen, A., Branthomme, A., Piccoli, M., Obli-Laryea, G., Ramadan, N., and Conchedda, G.:
- 3937 New FAOSTAT forest emissions and removals estimates: 1990-2025, Earth Syst. Sci. Data Discussions,
- 3938 https://doi.org/10.5194/essd-2025-635, 2025.
- 3939 Tuck, C.: 2022 Mineral Commodity Summary: Iron Ore, Tech. rep., U.S. Geological Survey,
- 3940 https://pubs.usgs.gov/periodicals/mcs2022/mcs2022-iron-ore.pdf, 2022.
- 3941 UNFCCC: Synthesis report for the technical assessment component of the first global stocktake, available at:
- 3942 https://unfccc.int/documents/461466, last access: 23 October 2025, 2022.
- 3943 Vale, M. M., Berenguer, E., Argollo de Menezes, M., Viveiros de Castro, E. B., Pugliese de Siqueira, L., and
- 3944 Portela, R. de C. Q.: The COVID-19 pandemic as an opportunity to weaken environmental protection in Brazil,
- 3945 Biological Conservation, 255, 108994, https://doi.org/10.1016/j.biocon.2021.108994, 2021.
- 3946 van der Laan-Luijkx, I. T., van der Velde, I. R., van der Veen, E., Tsuruta, A., Stanislawska, K., Babenhauserheide,
- A., Zhang, H. F., Liu, Y., He, W., Chen, H., Masarie, K. A., Krol, M. C., and Peters, W.: The CarbonTracker Data 3947
- 3948 Assimilation Shell (CTDAS) v1.0: implementation and global carbon balance 2001-2015, Geosci. Model Dev., 10,
- 3949 2785-2800, https://doi.org/10.5194/gmd-10-2785-2017, 2017.
- 3950
- van der Velde, I. R., van der Werf, G. R., Houweling, S., Maasakkers, J. D., Borsdorff, T., Landgraf, J., Tol, P., van Kempen, T. A., van Hees, R., Hoogeveen, R., Veefkind, J. P., and Aben, I.: Vast CO2 release from Australian 3951
- 3952 fires in 2019-2020 constrained by satellite, Nature, 597, 366-369, https://doi.org/10.1038/s41586-021-03712-y,
- 3953
- 3954 van der Werf, G. R., Randerson, J. T., Giglio, L., Collatz, G. J., Mu, M., Kasibhatla, P. S., Morton, D. C., DeFries,
- 3955 R. S., Jin, Y., and van Leeuwen, T. T.: Global fire emissions and the contribution of deforestation, savanna, forest,





- 3956 agricultural, and peat fires (1997–2009), Atmospheric Chem. Phys., 10, 11707–11735, https://doi.org/10.5194/acp-
- 3957 10-11707-2010, 2010.
- 3958 van der Werf, G. R., Randerson, J. T., Giglio, L., van Leeuwen, T. T., Chen, Y., Rogers, B. M., Mu, M., van Marle,
- 3959 M. J. E., Morton, D. C., Collatz, G. J., Yokelson, R. J., and Kasibhatla, P. S.: Global fire emissions estimates
- 3960 during 1997–2016, Earth Syst. Sci. Data, 9, 697–720, https://doi.org/10.5194/essd-9-697-2017, 2017.
- 3961 van Wees, D., van der Werf, G. R., Randerson, J. T., Andela, N., Chen, Y., and Morton, D. C.: The role of fire in
- 3962 global forest loss dynamics, Glob. Change Biol., 27, 2377–2391, https://doi.org/10.1111/gcb.15591, 2021.
- von Bloh, W., Schaphoff, S., Müller, C., Rolinski, S., Waha, K., and Zaehle, S.: Implementing the nitrogen cycle into the dynamic global vegetation, hydrology, and crop growth model LPJmL (version 5.0), Geosci. Model Dev.,
- 3965 11, 2789–2812, https://doi.org/10.5194/gmd-11-2789-2018, 2018.
- 3966 Vaittinada Ayar, P., Bopp, L., Christian, J. R., Ilyina, T., Krasting, J. P., Séférian, R., Tsujino, H., Watanabe, M.,
- 3967 Yool, A., and Tjiputra, J.: Contrasting projections of the ENSO-driven CO2 flux variability in the equatorial
- 3968 Pacific under high-warming scenario, Earth Syst. Dynam., 13, 1097–1118, https://doi.org/10.5194/esd-13-1097-
- 3969 2022, 2022.
- 3970 Vuichard, N., Messina, P., Luyssaert, S., Guenet, B., Zaehle, S., Ghattas, J., Bastrikov, V., and Peylin, P.:
- 3971 Accounting for carbon and nitrogen interactions in the global terrestrial ecosystem model ORCHIDEE (trunk
- version, rev 4999): multi-scale evaluation of gross primary production, Geosci. Model Dev., 12, 4751–4779,
- 3973 https://doi.org/10.5194/gmd-12-4751-2019, 2019.
- Walker, A. P., Quaife, T., Bodegom, P. M., De Kauwe, M. G., Keenan, T. F., Joiner, J., Lomas, M. R., MacBean,
- N., Xu, C., Yang, X., and Woodward, F. I.: The impact of alternative trait-scaling hypotheses for the maximum
- 3976 photosynthetic carboxylation rate (V cmax) on global gross primary production, New Phytol., 215, 1370–1386,
- 3977 https://doi.org/10.1111/nph.14623, 2017.
- 3978 Walker, A. P., De Kauwe, M. G., Bastos, A., Belmecheri, S., Georgiou, K., Keeling, R. F., McMahon, S. M.,
- 3979 Medlyn, B. E., Moore, D. J. P., Norby, R. J., Zaehle, S., Anderson-Teixeira, K. J., Battipaglia, G., Brienen, R. J.
- W., Cabugao, K. G., Cailleret, M., Campbell, E., Canadell, J. G., Ciais, P., Craig, M. E., Ellsworth, D. S., Farquhar,
 G. D., Fatichi, S., Fisher, J. B., Frank, D. C., Graven, H., Gu, L., Haverd, V., Heilman, K., Heimann, M., Hungate,
- 3982 B. A., Iversen, C. M., Joos, F., Jiang, M., Keenan, T. F., Knauer, J., Körner, C., Leshyk, V. O., Leuzinger, S., Liu,
- 3983 Y., MacBean, N., Malhi, Y., McVicar, T. R., Penuelas, J., Pongratz, J., Powell, A. S., Riutta, T., Sabot, M. E. B.,
- 3984 Schleucher, J., Sitch, S., Smith, W. K., Sulman, B., Taylor, B., Terrer, C., Torn, M. S., Treseder, K. K., Trugman,
- A. T., Trumbore, S. E., van Mantgem, P. J., Voelker, S. L., Whelan, M. E., and Zuidema, P. A.: Integrating the
- evidence for a terrestrial carbon sink caused by increasing atmospheric CO2, New Phytol., 229, 2413–2445,
- 3987 https://doi.org/10.1111/nph.16866, 2021.
- 3988 Watanabe, M., Tatebe, H., Koyama, H., Hajima, T., Watanabe, M., and Kawamiya, M.: Importance of El Niño
- 3989 reproducibility for reconstructing historical CO2 flux variations in the equatorial Pacific, Ocean Sci., 16, 1431–
- 3990 1442, https://doi.org/10.5194/os-16-1431-2020, 2020.
- Watson, A. J., Schuster, U., Shutler, J. D., Holding, T., Ashton, I. G. C., Landschützer, P., Woolf, D. K., and
- 3992 Goddijn-Murphy, L.: Revised estimates of ocean-atmosphere CO2 flux are consistent with ocean carbon inventory,
- 3993 Nat Commun, 11, 4422, https://doi.org/10.1038/s41467-020-18203-3, 2020.
- 3994 Watson, R. T., Rohde, H., Oeschger, H., and Siegenthaler, U.: Greenhouse Gases and Aerosols, in: Climate
- 3995 Change: The IPCC Scientific Assessment. Intergovernmental Panel on Climate Change (IPCC), edited by:
- Houghton, J. T., Jenkins, G. J., and Ephraums, J. J., Cambridge University Press, Cambridge, ISBN: 978-
- 3997 0521403603, 1990.
- 3998 Wenzel, S., Cox, P. M., Eyring, V., and Friedlingstein, P.: Projected land photosynthesis constrained by changes in
- 3999 the seasonal cycle of atmospheric CO2, Nature, 538, 499–501, https://doi.org/10.1038/nature19772, 2016.
- 4000 Wilkenskjeld, S., Kloster, S., Pongratz, J., Raddatz, T., and Reick, C. H.: Comparing the influence of net and gross
- 4001 anthropogenic land-use and land-cover changes on the carbon cycle in the MPI-ESM, Biogeosciences, 11, 4817–
- 4002 4828, https://doi.org/10.5194/bg-11-4817-2014, 2014.





- 4003 Wiltshire, A. J., Burke, E. J., Chadburn, S. E., Jones, C. D., Cox, P. M., Davies-Barnard, T., Friedlingstein, P.,
- 4004 Harper, A. B., Liddicoat, S., Sitch, S., and Zaehle, S.: JULES-CN: a coupled terrestrial carbon-nitrogen scheme
- 4005 (JULES vn5.1), 14, 2161–2186, https://doi.org/10.5194/gmd-14-2161-2021, 2021.
- 4006 Winkler, K., Yang, H., Ganzenmüller, R., Fuchs, R., Ceccherini, G., Duveiller, G., Grassi, G., Pongratz, J., Bastos,
- 4007 A., Shvidenko, A., Araza, A., Herold, M., Wigneron, J.-P., and Ciais, P.: Changes in land use and management led
- 4008 to a decline in Eastern Europe's terrestrial carbon sink, Commun. Earth Environ., 4, 1–14,
- 4009 https://doi.org/10.1038/s43247-023-00893-4, 2023.
- 4010 Woodward, F. I. and Lomas, M. R.: Vegetation dynamics - simulating responses to climatic change, Biol. Rev., 79,
- 4011 643-670, https://doi.org/10.1017/S1464793103006419, 2004.
- 4012 Wright, R. M., Le Quéré, C., Buitenhuis, E., Pitois, S., and Gibbons, M. J.: Role of jellyfish in the plankton
- 4013 ecosystem revealed using a global ocean biogeochemical model, 18, 1291-1320, https://doi.org/10.5194/bg-18-
- 4014 1291-2021, 2021.
- 4015 Wunch, D., Wennberg, P. O., Osterman, G., Fisher, B., Naylor, B., Roehl, C. M., O'Dell, C., Mandrake, L., Viatte,
- 4016 C., Kiel, M., Griffith, D. W. T., Deutscher, N. M., Velazco, V. A., Notholt, J., Warneke, T., Petri, C., De Maziere,
- 4017 M., Sha, M. K., Sussmann, R., Rettinger, M., Pollard, D., Robinson, J., Morino, I., Uchino, O., Hase, F.,
- 4018 Blumenstock, T., Feist, D. G., Arnold, S. G., Strong, K., Mendonca, J., Kivi, R., Heikkinen, P., Iraci, L., Podolske,
- 4019 J., Hillyard, P. W., Kawakami, S., Dubey, M. K., Parker, H. A., Sepulveda, E., García, O. E., Te, Y., Jeseck, P.,
- 4020 Gunson, M. R., Crisp, D., and Eldering, A.: Comparisons of the Orbiting Carbon Observatory-2 (OCO-2) X CO2
- 4021 measurements with TCCON, Atmos. Meas. Tech., 10, 2209-2238, https://doi.org/10.5194/amt-10-2209-2017,
- 4022 2017.
- 4023 Wunder, S., Kaimowitz, D., Jensen, S., and Feder, S.: Coronavirus, macroeconomy, and forests: What likely
- 4024 impacts?, For. Policy Econ., 131, 102536, https://doi.org/10.1016/j.forpol.2021.102536, 2021.
- Xi, F., Davis, S. J., Ciais, P., Crawford-Brown, D., Guan, D., Pade, C., Shi, T., Syddall, M., Lv, J., Ji, L., Bing, L., Wang, J., Wei, W., Yang, K.-H., Lagerblad, B., Galan, I., Andrade, C., Zhang, Y., and Liu, Z.: Substantial global 4025
- 4026
- 4027 carbon uptake by cement carbonation, Nature Geosci, 9, 880-883, https://doi.org/10.1038/ngeo2840, 2016.
- 4028 Xia, J., Chen, Y., Liang, S., Liu, D., and Yuan, W.: Global simulations of carbon allocation coefficients for
- 4029 deciduous vegetation types, Tellus B, 67, 28016, https://doi.org/10.3402/tellusb.v67.28016, 2015.
- 4030 Xia, X., Ren, P., Wang, X., Liu, D., Chen, X., Dan, L., He, B., He, H., Ju, W., Liang, M., Lu, X., Peng, J., Qin, Z.,
- 4031 Xia, J., Zheng, B., Wei, J., Yue, X., Yu, G., Piao, S., and Yuan, W.: The carbon budget of China: 1980-2021,
- 4032 Science Bulletin, 69, 114-124, https://doi.org/10.1016/j.scib.2023.11.016, 2024.
- 4033 Yang, D., Liu, Y., Feng, L., Wang, J., Yao, L., Cai, Z., Zhu, S., Lu, N., and Lyu, D.: The First Global Carbon
- 4034 Dioxide Flux Map Derived from TanSat Measurements, Adv. Atmospheric Sci., 38, 1433-1443,
- 4035 https://doi.org/10.1007/s00376-021-1179-7, 2021.
- 4036 Yang, X., Thornton, P., Ricciuto, D., Wang, Y., and Hoffman, F.: Global evaluation of terrestrial biogeochemistry
- in the Energy Exascale Earth System Model (E3SM) and the role of the phosphorus cycle in the historical 4037
- 4038 terrestrial carbon balance, Biogeosciences, 20, 2813-2836, https://doi.org/10.5194/bg-20-2813-2023, 2023.
- 4039 Yao, Y., Joetzjer, E., Ciais, P., Viovy, N., Cresto Aleina, F., Chave, J., Sack, L., Bartlett, M., Meir, P., Fisher, R.,
- 4040 and Luyssaert, S.: Forest fluxes and mortality response to drought: model description (ORCHIDEE-CAN-NHA
- 4041 r7236) and evaluation at the Caxiuana drought experiment, Geosci. Model Dev., 15, 7809-7833,
- 4042 https://doi.org/10.5194/gmd-15-7809-2022, 2022.
- 4043 Yao, Y., Ciais, P., Viovy, N., Joetzjer, E. and Chave, J.: How drought events during the last century have impacted
- 4044 biomass carbon in Amazonian rainforests. Global Change Biology, 29(3), pp.747-762,
- 4045 https://doi.org/10.1111/gcb.16504, 2023.
- 4046 You, Y., Tian, H., Pan, S., Shi, H., Bian, Z., Gurgel, A., Huang, Y., Kicklighter, D., Liang, X.-Z., Lu, C., Melillo,
- 4047 J., Miao, R., Pan, N., Reilly, J., Ren, W., Xu, R., Yang, J., Yu, Q., and Zhang, J.: Incorporating dynamic crop
- 4048 growth processes and management practices into a terrestrial biosphere model for simulating crop production in the
- 4049 United States: Toward a unified modeling framework, Agricultural and Forest Meteorology, 325, 109144,
- 4050 https://doi.org/10.1016/j.agrformet.2022.109144, 2022.





- 4051 Yu, Z., Ciais, P., Piao, S., Houghton, R. A., Lu, C., Tian, H., Agathokleous, E., Kattel, G. R., Sitch, S., Goll, D.,
- 4052 Yue, X., Walker, A., Friedlingstein, P., Jain, A. K., Liu, S., and Zhou, G.: Forest expansion dominates China's land
- 4053 carbon sink since 1980, Nat. Commun., 13, 5374, https://doi.org/10.1038/s41467-022-32961-2, 2022.
- 4054 Yue, X. and Unger, N.: The Yale Interactive terrestrial Biosphere model version 1.0: description, evaluation and
- implementation into NASA GISS ModelE2, Geosci. Model Dev., 8, 2399–2417, https://doi.org/10.5194/gmd-8-
- 4056 2399-2015, 2015.
- Yue, X., Zhou, H., Tian, C., Ma, Y., Hu, Y., Gong, C., Zheng, H., and Liao, H.: Development and evaluation of the
- interactive Model for Air Pollution and Land Ecosystems (iMAPLE) version 1.0, Geosci. Model Dev., 17, 4621–
- 4059 4642, https://doi.org/10.5194/gmd-17-4621-2024, 2024.
- 4060 Yuan, W., Liu, D., Dong, W., Liu, S., Zhou, G., Yu, G., Zhao, T., Feng, J., Ma, Z., Chen, J., Chen, Y., Chen, S.,
- 4061 Han, S., Huang, J., Li, L., Liu, H., Liu, S., Ma, M., Wang, Y., Xia, J., Xu, W., Zhang, Q., Zhao, X., and Zhao, L.:
- 4062 Multiyear precipitation reduction strongly decreases carbon uptake over northern China, J. Geophys. Res.-Biogeo.,
- 4063 119, 881–896, https://doi.org/10.1002/2014JG002608, 2014.
- 4064 Yue, C., Ciais, P., Zhu, D., Wang, T., Peng, S. S., and Piao, S. L.: How have past fire disturbances contributed to
- the current carbon balance of boreal ecosystems?, Biogeosciences, 13, 675–690, https://doi.org/10.5194/bg-13-675-
- 4066 2016, 2016.
- 4067 Zaehle, S. and Friend, A. D.: Carbon and nitrogen cycle dynamics in the O-CN land surface model: 1. Model
- 4068 description, site-scale evaluation, and sensitivity to parameter estimates: Site-scale evaluation of a C-N model,
- 4069 Global Biogeochem. Cycles, 24, GB1005, https://doi.org/10.1029/2009GB003521, 2010.
- 4070 Zaehle, S., Ciais, P., Friend, A. D., and Prieur, V.: Carbon benefits of anthropogenic reactive nitrogen offset by
- nitrous oxide emissions, Nature Geosci, 4, 601–605, https://doi.org/10.1038/ngeo1207, 2011.
- 4072 Zaehle, S., Medlyn, B. E., De Kauwe, M. G., Walker, A. P., Dietze, M. C., Hickler, T., Luo, Y., Wang, Y.-P., El-
- 4073 Masri, B., Thornton, P., Jain, A., Wang, S., Warlind, D., Weng, E., Parton, W., Iversen, C. M., Gallet-Budynek, A.,
- 4074 McCarthy, H., Finzi, A., Hanson, P. J., Prentice, I. C., Oren, R., and Norby, R. J.: Evaluation of 11 terrestrial
- 4075 carbon-nitrogen cycle models against observations from two temperate Free-Air CO2 Enrichment studies, New
- 4076 Phytol., 202, 803–822, https://doi.org/10.1111/nph.12697, 2014.
- 4077 Zeng, J., Iida, Y., Matsunaga, T., and Shirai, T.: Surface ocean CO2 concentration and air-sea flux estimate by
- 4078 machine learning with modelled variable trends, Front. Mar. Sci., 9, https://doi.org/10.3389/fmars.2022.989233,
- 4079 2022
- 4080 Zheng, B., Ciais, P., Chevallier, F., Chuvieco, E., Chen, Y., and Yang, H.: Increasing forest fire emissions despite
- 4081 the decline in global burned area, Sci. Adv., 7, eabh2646, https://doi.org/10.1126/sciadv.abh2646, 2021.
- 4082 Zhu, Y., Xia, X., Canadell, J. G., Piao, S., Lu, X., Mishra, U., Wang, X., Yuan, W., and Qin, Z.: China's carbon
- 4083 sinks from land-use change underestimated, Nat. Clim. Chang., 15, 428–435, https://doi.org/10.1038/s41558-025-
- 4084 02296-z, 2025.
- 4085 Zou, Y., Wang, Y., Ke, Z., Tian, H., Yang, J., and Liu, Y.: Development of a REgion-Specific Ecosystem
- 4086 Feedback Fire (RESFire) Model in the Community Earth System Model, J. Adv. Model. Earth Syst., 11, 417–445,
- 4087 https://doi.org/10.1029/2018MS001368, 2019.
- 4088 Zscheischler, J., Mahecha, M. D., Avitabile, V., Calle, L., Carvalhais, N., Ciais, P., Gans, F., Gruber, N.,
- 4089 Hartmann, J., Herold, M., Ichii, K., Jung, M., Landschützer, P., Laruelle, G. G., Lauerwald, R., Papale, D., Peylin,
- 4090 P., Poulter, B., Ray, D., Regnier, P., Rödenbeck, C., Roman-Cuesta, R. M., Schwalm, C., Tramontana, G.,
- Tyukavina, A., Valentini, R., van der Werf, G., West, T. O., Wolf, J. E., and Reichstein, M.: Reviews and
- 4092 syntheses: An empirical spatiotemporal description of the global surface-atmosphere carbon fluxes: opportunities
- 4093 and data limitations, Biogeosciences, 14, 3685-3703, https://doi.org/10.5194/bg-14-3685-2017, 2017.





4094 Tables

4095

4096 **Table 1.** Factors used to convert carbon in various units (by convention, Unit $1 = \text{Unit } 2 \times \text{conversion}$).

Unit 1	Unit 2	Conversion	Source
GtC (gigatonnes of carbon)	ppm (parts per million) (a)	2.124 (b)	Ballantyne et al. (2012)
GtC (gigatonnes of carbon)	PgC (petagrams of carbon)	1	SI unit conversion
GtCO2 (gigatonnes of carbon dioxide)	GtC (gigatonnes of carbon)	3.664	44.01/12.011 in mass equivalent

(a) Measurements of atmospheric CO₂ concentration have units of dry-air mole fraction. 'ppm' is an abbreviation for micromole/mol, dry air.

⁽b) The use of a factor of 2.124 assumes that all the atmosphere is well mixed within one year. In reality, only the troposphere is well mixed and the growth rate of CO_2 concentration in the less well-mixed stratosphere is not measured by sites from the NOAA network. Using a factor of 2.124 makes the approximation that the growth rate of CO_2 concentration in the stratosphere equals that of the troposphere on a yearly basis.





4098 Table 2. How to cite the individual components of the global carbon budget presented here.

Component	Primary reference		
Global fossil CO ₂ emissions (EFOS), total and by fuel type	Andrew and Peters (2025)		
National territorial fossil CO ₂ emissions (EFOS)	Erb and Marland (2025), UNFCCC (2022)		
National consumption-based fossil CO ₂ emissions (EFOS) by country (consumption)	Peters et al. (2011a) updated as described in this paper		
Net land-use change flux (ELUC)	This paper (see Table 4 for individual model references).		
Growth rate in atmospheric CO ₂ concentration (GATM)	Lan et al. (2025a)		
Ocean and land CO ₂ sinks (SOCEAN and SLAND)	This paper (see Table 4 for individual model and data products references).		





4100 Table 3. Main methodological changes in the global carbon budget this year (GCB2025). Empty cells mean
 4101 there were no methodological changes introduced that year. Table S9 lists methodological changes from the first
 4102 global carbon budget publication up to 2024.

Fossil fuel emissions		LUC emissions	Reservoirs			Other changes
Global	Country (territorial)		Atmosphere	Ocean	Land	
a ₁	rojection vailable for apan for the rst time	Bookkeeping estimates derived from models that estimate ELUC based on transient carbon densities responding to environmental changes (BLUE, OSCAR, LUCE).	Include an assessment of satellite- derived growth rates	Adjustments applied for known underestimati on of GOBMs and cool surface skin effect in fCO2-products. Suspension of 19 ocean data sets from SOCAT.	Include the RSS adjustment.	

https://doi.org/10.5194/essd-2025-659 Preprint. Discussion started: 13 November 2025

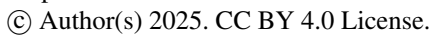






Table 4. References for the process models, bookkeeping models, ocean data products, and atmospheric inversions. All models and products are updated with new data to the end of year 2024.

Model/data name	Reference	Change from Global Carbon Budget 2024 (Friedlingstein et al., 2025a)							
Bookkeeping models for land-use change emissions									
BLUE	Hansis et al. (2015)	Transient C densities used to estimate ELUC							
OSCAR	Gasser et al. (2020)	No change							
LUCE	Qin et al. (2024)	Transient C densities used to estimate ELUC							
Dynamic global	vegetation models								
CABLE-POP	Haverd et al. (2018)	corrected N deposition input data, minor parameter changes							
CLASSIC	Melton et al. (2020), Gauthier et al. (2025), Kou-Giesbrecht and Arora (2022)								
CLM6.0	Lawrence et al. (2019)	New dust scheme, new BGC fire method, updates to MEGAN for BVOCs, parameter updates, new surface datasets, new N fixation method							
CLM-FATES	Fisher et al. (2015), Koven et al. (2020)	New model							
DLEM	Tian et al. (2015), You et al. (2022)	No change							
EDv3	Moorcroft et al. (2001), Ma et al. (2022)	Updated meteorology inputs (i.e. hourly air temperature)							
ELM	Yang et al.(2023), Burrows et al.(2020)	No change							
ELM-FATES	Fisher et al. (2015), Koven et al. (2020), Needham et al. (2025)	New model							
GDSTEM	Felzer et al. (2009), Felzer et al. (2011), Felzer (2012), Felzer and Jiang (2018)	New model							
IBIS	Xia et al., (2024)	No change							
iMAPLE	Yue et al. (2024)	No change.							





ISAM	Jain et al. (2013), Meiyappan et al.	Vertically resolved soil biogeochemistry (carbon and nitrogen)			
	(2015), Shu et al. (2020)	module, following Shu et al. (2020)			
JSBACH	Mauritsen et al. (2019), Reick et al. (2021)	No change			
JULES-ES	Wiltshire et al. (2021), Sellar et al. (2019), Burton et al. (2019)	Minor updates to wildfire parameters			
LPJ-GUESS	Smith et al. (2014)	Wood harvest without the LUH2 secondary mature, young, and non- forest harvest fraction info			
LPJmL	Schaphoff et al. (2018), von Bloh et al. (2018), Lutz et al., (2019), Heinke et al. (2023)	Switch from version 5.7.5 to 5.10.0 incorporating updates to soil temperature scheme, revised N demand and N uptake processes, revised tree phenology, as well as bugfixes and code improvements			
LPJ-EOSIM	Poulter et al. (2011) (d)	Incorporation of new respiration temperature responses and leaf respiration acclimation, updated the soil temperature and water scheme to have 8 layers			
LPX-Bern	Lienert and Joos (2018)	No change			
ORCHIDEEv3	Krinner et al. (2005), Zaehle and Friend (2010), Vuichard et al. (2019)	No change			
SDGVM	Woodward and Lomas (2004), Walker et al. (2017)	Reverted to version used in Friedlingstein et al. (2022), but retaining the recent bug fix to monthly heterotrophic respiration output			
VISIT	Ito and Inatomi (2012), Kato et al. (2013)	No change			
VISIT-UT	Ito (2019)	New model			
Intermediate c	complexity land carbon cycle model				
CARDAMOM	Bloom et al. (2016), Smallman et al. (2021)	Analysis resolution increased from 1 x1 to 0.5x0.5 degree. Estimates of fAPAR from MODIS collection 6.1. New prior constraint on the leaf carbon per unit area parameter (LCA). MODIS burned area forcing was replaced by GFEDv5 burned area estimate			
Global ocean b	niogeochemistry models				
NEMO- PlankTOM12	Wright et all (2021)	No change			
NEMO4.2- PISCES (IPSL)	Aumont et al. (2015)	No change to the model version, but switch to ERA5 forcing - A,B,C,D simulations have been re-run starting from GCB2024 simulation restart fields from 1940 onwards			
MICOM- HAMOCC (NorESM1- OCv1.2)	Schwinger et al. (2016)	No change, model has been re-run to provide monthly CFC/SF ₆ outputs			
MPIOM-	Lacroix et al. (2021)	No change			



НАМОСС6		
NEMO3.6- PISCESv2-gas (CNRM)	Berthet et al. (2019), Séférian et al. (2019)	Updated simulations using 1750 preindustrial conditions instead of 1850. No change in model configuration, except nudging of surface ocean fields applied to minimize the change of atm forcing. The methodology used is based on Sanchez-Gomez et al. (2024)
FESOM2.1-		Switched to ERA5 forcing - A,B,C,D simulations have been re-run
REcoM3	Gürses et al. (2023)	starting from GCB2024 simulation restart fields
MOM6- COBALTv3 (Princeton)	Stock et al., (2025)	New model configuration MOM6-COBALTv3 with ~1° horizontal resolution (360x210). 1) updated ocean biogeochemical module COBALTv3 with an additional fixed nitrogen removal process - anaerobic ammonium oxidation (anammox); 2) updated air-sea gas exchange scheme - wind-wave-bubble formulation; 3) updated riverine carbon and nutrient inputs following R2OMIP protocol (Lacroix et al., 2024, https://zenodo.org/records/13799103); 4) updated river water discharge files.
CESM-ETHZ	Doney et al. (2009)	Compared to the 2024 submission, we changed the forcing to ERA5. To this end, a new spinup was performed, extending over 500 years.
MRI-ESM2-4	Tsujino et al. (2024), Sakamoto et al. (2023)	Iron circulation is modified according to Moore and Braucher (2008) and iron limitation on primary production is adjusted according to this change. Updated atmospheric CO2 for simulations A and C. The JRA-3Q reanalysis (Kosaka et al. 2024) is used to physically force the model. The model is spun up for 1925 years with xCO2=278ppm.
	· · · ·	
ACCESS (CSIRO)	Law et al. (2017)	No change in model since GCB2024, but switched to ERA5 forcing and extended spinup.
fCO2-products	,	
VLIZ-SOMFFN	Landschützer et al. (2016)	Time period extended to 2024
Jena-MLS	Rödenbeck et al. (2014) updated to Rödenbeck et al (2022)	Time period extended to 2024
CMEMS-LSCE-		
FFNNv2	Chau et al. (2022)	Time period extended to 2024
UExP-FNN-U	Watson et al. (2020) and Ford et al. (2024)	Updated to recalculated SOCATv2025 dataset (Ford et al. 2025). Updated salinity dataset to use a tiered approach (described in Gregor et al. 2024) including ESA CCI-SSS (v5.51) and CMEMS GLORYS12V1. Updated time period to 1980 to 2024
NIES-ML3	Zeng et al. (2022)	Time period extended to 2024.
JMA-MLR	lida et al. (2021)	Time period extended to 2024. Updated to recalculated SOCATv2025 dataset (Ford et al. 2025)
OceanSODA- ETHZv2	Gregor et al. (2024)	Time period extended to 2024





LDEO-HPD	Gloege et al. (2022) and Bennington et al. (2022)	Time period extended to 2024					
CSIR-ML6	Gregor et al. (2019)	Time period extended to 2024					
Atmospheric in	versions						
Jena CarboScope	Rödenbeck et al. (2018) & Stephens et al. (2007).	Slight change in station set. Numerical flux resolution 2x2. TM3 run on spatial resolution 6x4 (multiple of 2x2)					
CarbonTracker Europe (CTE)	van der Laan-Luijkx et al. (2017)	Update of prior fluxes and assimilated observations.					
NISMON-CO2	Niwa et al. (2022), Niwa et al. (2017).	Update of prior fluxes, specifically changed GFED to GBEI. Update of the meteorological input to JRA-3Q. Including more CO2 observations.					
CT-NOAA	Jacobson et al. (2025), Byrne et al. (2023), Krol et al. (2005), Peiro et al. (2022)	New air-sea gas exchange and new terrestrial NBE (Jacobson et al., 2025). Unlike previous submissions, CT2025 uses only one set of priors.					
CMS-Flux	Liu et al. (2021)	Update of prior fluxes and assimilated observations.					
CAMS-Satellite	Chevallier et al. (2005) and Chevallier et al. (2025)	Update of the prior fluxes and assimilated observations.					
GONGGA	Jin et al. (2024)	Update of the prior fluxes and assimilated observations.					
COLA	Liu et al. (2022)	Update of the prior fluxes and assimilated observations.					
GCASv2	Jiang et al. (2021) & Emmons et al. (2010)	Update of the prior fluxes and assimilated observations.					
UoE	Feng et al. (2016) & Palmer et al. (2019)	Update of the prior fluxes and assimilated observations.					
MIROC-ACTM	Chandra et al. (2022) & Patra et al. (2018)	Update of assimilated observations and prior fluxes, specifically changed to MiCASA and GFED. Update of the meteorological input to JRA-3Q.					
NTFVAR	Nayagam et al. (2025) & Maksyutov et al. (2021)	Update of prior fluxes and assimilated observations.					
ТНИ	Kong et al. (2022)	New this year, after missing out 1 year. Compared to the previous submission: update of prior fluxes and assimilated observations.					
NISMON- CO2_GOSAT	Niwa et al. (2022), Niwa et al. (2017).	New this year.					
Earth System M	lodels						
CanESM5	Swart et al. (2019), Sospedra-Alfonso et al. (2021)	No change					
EC-Earth3-CC	Döscher et al. (2021), Bilbao et al. (2021), Bernardello et al. (2024)	No change					
IPSL-CM6A- CO2-LR	Boucher et al. (2020)	No change					
MIROC-ES2L	Watanabe et al. (2020)	No change					

https://doi.org/10.5194/essd-2025-659 Preprint. Discussion started: 13 November 2025 © Author(s) 2025. CC BY 4.0 License.





MPI-ESM1-2-LR	Mauritsen et al. (2019), Li et al. (2023)	No change
NorCPM-CC	Tjiputra et al. (2020), Bethke et al. (2021)	New this year.





4108 Table 5. Comparison of results from the bookkeeping method and budget residuals with results from the 4109 DGVMs, as well as additional estimates from atmospheric oxygen, atmospheric inversions and Earth System 4110 Models (ESMs) for different periods, the last decade, and the last year available. All values are in GtC yr¹. The best estimate for GCB2025 (\dot{E}_{LUC}) is calculated with the bookkeeping models (1a) and used in the budget Table 4111 4112 7, see Section 2 and Figure 7 for description of the bookkeeping component fluxes. The best estimate for 4113 GCB2025 (SLAND) is calculated with the DGVMs including the RSS correction (2b), and used in the budget 4114 Table 7. The DGVM uncertainties represent $\pm 1\sigma$ of the decadal or annual (for 2024) estimates from the 4115 individual DGVMs. For the inverse systems the mean and range of available results is given when the number of systems is less than 10, otherwise the $\pm 1\sigma$ is provided. All values are rounded to the nearest 0.1 GtC and 4116 4117 therefore columns do not necessarily add to zero.

4118	Mean	(GtC yr-1))
------	------	------------	---

		1960s	1970s	1980s	1990s	2000s	2010s	2015- 2024	2024
	Bookkeeping (BK) Net flux (1a)	1.9±0 .7	1.7±0 .7	1.7±0 .7	1.7±0 .7	1.7±0 .7	1.6±0 .7	1.4±0 .7	1.3±0 .7
	BK - deforestation (total)	1.8 [1.6,2 .1]	1.8 [1.6,2 .1]	1.7 [1.5,1 .9]	1.9 [1.6,2 .1]	2 [1.7,2 .2]	2 [1.6,2 .4]	1.9 [1.5,2 .3]	1.9 [1.4,2 .4]
	BK - forest regrowth (total)	-0.9 [-1,- 0.7]	-0.9 [-1,- 0.8]	-0.9 [-1,- 0.8]	-1 [- 1.1,- 0.8]	-1.1 [- 1.2,- 0.9]	-1.3 [- 1.4,- 1]	-1.3 [- 1.5,- 1]	-1.3 [- 1.6,- 1]
Land-use change emissions (E _{LUC})	BK - other transitions	0.3 [0.3,0 .3]	0.2 [0.2,0 .3]	0.2 [0.1,0 .3]	0.1 [0.1,0 .2]	0.1 [0,0.1]	0.2 [0.1,0 .2]	0.1 [0.1,0 .1]	0.1 [0.1,0 .1]
	BK - peat drainage & peat fires	0.2 [0.1,0 .2]	0.2 [0.1,0 .2]	0.2 [0.2,0 .2]	0.3 [0.2,0 .3]	0.2 [0.2,0 .3]	0.3 [0.3,0 .3]	0.2 [0.2,0 .3]	0.2 [0.2,0 .2]
	BK - wood harvest & forest management	0.4 [0.1,0 .6]	0.4 [0.1,0 .6]	0.5 [0.1,0 .7]	0.5 [0.1,0 .7]	0.5 [0.1,0 .7]	0.4 [0.1,0 .7]	0.4 [0.1,0 .7]	0.4 [0.1,0 .7]
	DGVMs-net flux (1b)	1.3±0 .5	1.2±0 .5	1.2±0 .5	1.2±0 .5	1.2±0 .6	1.1±0 .6	1±0.6	0.9±0 .5
Terrestrial sink (S _{LAND})	Residual sink from global budget (E _{FOS} +E _{LUC} (1a)-G _{ATM} - S _{OCEAN}) (2a)	1.9±0 .8	2±0.8	1.7±0 .9	2.6±0 .9	2.9±0 .9	3±0.9	2.4±0 .9	0.3±1
(CEAND)	DGVMs (2b)	0.9±0 .3	1.6±0 .5	1.4±0 .6	2±0.5	2.2±0 .6	2.5±0 .7	2.4±0 .8	1.9±0 .9
Net land fluxes (S _{LAND} -E _{LUC})	GCB2025 Budget (2b- 1a)	- 0.9±0 .8	- 0.1±0 .9	- 0.3±0 .9	0.2±0 .9	0.5±0 .9	0.9±1	1±1	0.7±1 .1
	Atmospheric O ₂				1.3±0 .6	0.9±0 .7	1±0.8	0.7±0 .8	-

https://doi.org/10.5194/essd-2025-659 Preprint. Discussion started: 13 November 2025

© Author(s) 2025. CC BY 4.0 License.





	1960s	1970s	1980s	1990s	2000s	2010s	2015- 2024	2024
DGVMs-net (2b-1b)	- 0.3±0 .4	0.4±0 .6	0.2±0 .5	0.8±0 .4	1±0.4	1.4±0 .6	1.4±0 .7	1.1±0 .8
Inversions*	- [-,-]	- [-,-]	- [-,-]	0.7 [0.6,0 .8] (2)	1.4 [1.3,1 .6] (3)	1.5 [1.3,2 .3] (8)	1.3±0 .3 (14)	0.2±0 .7 (14)
ESMs	0 [- 0.7,0. 5]	1.5 [1.2,2]	1.1 [0.5,1 .4]	1.8 [1.2,2 .4]	1.8 [0.4,2 .7]	2 [0.7,3]	2.3 [- 0.1,3. 6]	0.8 [- 2.9- 3.3]

^{*}Estimates are adjusted for the pre-industrial influence of river fluxes, for the cement carbonation sink, and adjusted to common EFOS (Sect. 2.7). The ranges given include varying numbers (in parentheses) of inversions in each decade (Table A4)

⁴¹¹⁹

⁴¹²⁰





4121 Table 6: Comparison of results for the un-adjusted ocean sinks from the fCO₂-products, from global ocean 4122 biogeochemistry models (GOBMs), the best estimate for GCB2025 (adjusted SOCEAN) calculated from fCO2products and GOBMs) and used in the budget Table 7, as well as additional estimates from ocean interior 4123 4124 observation-based changes in the dissolved inorganic carbon (DIC) inventory, atmospheric oxygen, atmospheric 4125 inversions and Earth System Models (ESMs) for different periods, the last decade, and the last year available. All values are in GtC yr⁻¹. Uncertainties represent $\pm 1\sigma$ of the estimates from the GOBMs and inversions (n>10) 4126 and range of ensemble members is given for ensembles with n<10 (fCO₂-products, inversions, ocean interior, 4127 4128 ESMs). The uncertainty of the GCB2025 budget estimate is based on expert judgement (Section 2 and 4129 Supplement S1 to S4) and for oxygen it is the standard deviation of a Monte Carlo ensemble (Section 2.8). Note 4130 that adjustments were applied to the fCO₂-products and two of the ocean interior estimates to match the definition of Socean (see section 2.5.1 and S3.6). 4131

4132 **Mean (GtC yr-1)**

Product	1960s	1970s	1980s	1990s	2000s	2010s	2015- 2024	2024
GCB20 25 Budget	1.3±0. 4		2.1±0. 4	4	4	3.1±0. 4	4	4
fCO ₂ - product s				2.3 [2,3]	2.5 [2.4,2. 9]	3.1 [2.9,3. 5]	3.3 [2.9,3. 9]	3.5 [2.8,4. 2]
GOBMs	1.1±0. 2	1.3±0. 3	1.8±0. 3	2.0±0. 3	2.2±0. 3	2.6±0. 3	2.7±0. 3	2.9±0. 3
Atmosp heric O ₂				2.0±0. 4	2.8±0. 4	3.4±0. 5	3.5±0. 5	-
Inversi ons	- [-,-]	- [-,-]	- [-,-]	[2.2,2.	2.3 [2.2,2. 4] (3)	[2.1,3.	3±0.3 (14)	
Ocean interior	1.1 [-,-	1.3 [-,-]	1.8 [-,-]		2.2 [1.7,2. 5]	3.3 [2.7,4]		-
ESMs	0.7 [0.1,1. 1]	1 [0.4,1. 4]	1.5 [0.7,2]	1.7 [1.1,2. 1]	1.9 [1.5,2. 2]	2.4 [2,2.7]	2.5 [2.2,2. 8]	2.6 [2.2- 3.1]

4133

4134





Table 7: Decadal mean in the five components of the anthropogenic CO_2 budget for different periods, and last year available. All values are in GtC yr⁻¹, and uncertainties are reported as $\pm 1\sigma$. Fossil CO_2 emissions include cement carbonation. The table also shows the budget imbalance (B_{IM}), which provides a measure of the discrepancies among the nearly independent estimates. A positive imbalance means the emissions are overestimated and/or the sinks are too small. All values are rounded to the nearest 0.1 GtC and therefore columns do not necessarily add to zero.

Mean (GtC vr-1)

	mean (Git yr¹)									
		1960s	1970s	1980s	1990s	2000s	2010s	2015- 2024	2024	2025 (Proje ction)
	Fossil CO2 emissi ons (E _{FOS})*	3±0.2	4.7±0 .2	5.4±0 .3	6.4±0 .3	7.8±0 .4	9.5±0 .5	9.8±0 .5	10.3± 0.5	10.4± 0.5
Total emissi ons (E _{FOS} + E _{LUC})	Land- use chang e emissi ons (E _{LUC})	1.9±0 .7	1.7±0 .7	1.7±0 .7	1.7±0 .7	1.7±0 .7	1.6±0 .7	1.4±0 .7	1.3±0 .7	1.1±0 .7
	Total emissi ons	4.9±0 .7	6.4±0 .7	7.1±0 .8	8.1±0 .8	9.5±0 .8	11.1± 0.8	11.2± 0.9	11.6± 0.9	11.5± 0.9
	Growt h rate in atmos CO2 (G _{ATM})	1.7±0 .07	2.8±0 .07	3.4±0 .02	3.1±0 .02	4±0.0 2	5.1±0 .02	5.6±0 .02	7.9±0 .2	4.9±0 .2
Partiti oning	Ocean sink (S _{OCEA} N)	1.3±0 .4	1.6±0 .4	2.1±0 .4	2.3±0 .4	2.6±0 .4	3.1±0 .4	3.2±0 .4	3.4±0 .4	3.2±0 .4
	Terres trial sink (S _{LAND}	0.9±0 .3	1.6±0 .5	1.4±0 .6	2±0.5	2.2±0 .6	2.5±0 .7	2.4±0 .8	1.9±0 .9	3.4±1
Budge t Imbal ance	BIM= E _{FOS} + E _{LUC} - (G _{ATM} +S _{OCEA}	0.9	0.5	0.3	0.7	0.7	0.4	0	-1.7	

https://doi.org/10.5194/essd-2025-659 Preprint. Discussion started: 13 November 2025

© Author(s) 2025. CC BY 4.0 License.





	1960s	1970s	1980s	1990s	2000s	2010s	2015- 2024	2024	2025 (Proje ction)
n+S _{LAN} D)									

^{*}Fossil emissions excluding the cement carbonation sink amount to 3 ± 0.2 GtC yr $^{-1}$, 4.7 ± 0.2 GtC yr $^{-1}$, 5.5 ± 0.3 GtC yr $^{-1}$, 6.4 ± 0.3 GtC yr $^{-1}$, 7.9 ± 0.4 GtC yr $^{-1}$, and 9.7 ± 0.5 GtC yr $^{-1}$ for the decades 1960s to 2010s respectively and to 10 ± 0.5 GtC yr $^{-1}$ for 2024, and 10.5 ± 0.5 GtC yr $^{-1}$ for 2025.





Table 8. Cumulative CO₂ for different time periods in gigatonnes of carbon (GtC). Fossil CO₂ emissions include cement carbonation. The budget imbalance (B_{IM}) provides a measure of the discrepancies among the nearly independent estimates. All values are rounded to the nearest 5 GtC and therefore columns do not necessarily add to zero. Uncertainties are reported as follows: E_{FOS} is 5% of cumulative emissions; E_{LUC} prior to 1959 is 1σ spread from the DGVMs, E_{LUC} post-1959 is 0.7*number of years (where 0.7 GtC yr⁻¹ is the uncertainty on the annual E_{LUC} flux estimate); G_{ATM} uncertainty is held constant at 5 GtC for all time periods; S_{OCEAN} uncertainty is 20% of the cumulative sink (20% relates to the annual uncertainty of 0.4 GtC yr⁻¹, which is ~20% of the current ocean sink); and S_{LAND} is the 1σ spread from the DGVMs estimates.

Mean (GtC yr¹)

		1750-2024	1850-2014	1850-2024	1960-2024	1850-2025
	Fossil CO2 emissions (E _{FOS})	500±25	400±20	495±25	415±20	510±25
Emissions	Land-use change emissions (E _{LUC})	280±65	235±55	250±60	110±45	250±60
	Total emissions	780±70	635±60	745±65	525±50	755±65
	Growth rate in atmos CO2 (G _{ATM})	310±5	235±5	290±5	230±5	295±5
Partitioning	Ocean sink (S _{OCEAN})	210±40	170±35	200±40	145±30	205±40
	Terrestrial sink (S _{LAND})	190±50	150±40	175±50	120±30	175±50
Budget imbalance	BIM=E _{FOS} + E _{LUC} - (G _{ATM} +S _{OCE} _{AN} +S _{LAND})	65	80	80	35	80

 $\begin{array}{c} 4163 \\ 4164 \end{array}$

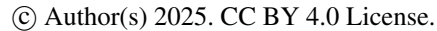






Table 9. Average annual growth rate in fossil CO₂ emissions over the most recent decade (2015-2024) and the previous decade (2005-2014). The data for the World include the cement carbonation sink. IAS are emissions from international aviation and shipping. The rest of the world is defined as World minus China, USA, India, EU27, and IAS.

	World	China	USA	India	EU27	OECD	Non- OEC D	IAS	Rest of the World
2005-	2.1%	6.7%	-1.4%	6.4%-	2.2%	-1.0%	4.6%	1.9%	1.8%
2014									
2015-	0.8%	2.5%	-1.2%	3.6%	-2.5%	-1.5%	2.1%	-1.4%	0.6%
2024									





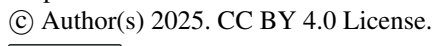
Table 10. Major known sources of uncertainties in each component of the Global Carbon Budget, defined as input data or processes that have a demonstrated effect of at least ±0.3 GtC yr⁻¹.

Source of uncertainty Time scale (years)		Location	Evidence		
Fossil CO2 emission	ns (EFOS; Section 2.	1)			
energy statistics	annual to decadal	global, but mainly China & major developing countries	(Korsbakken et al., 2016, Guan et al., 2012)		
carbon content of coal	annual to decadal	global, but mainly China & major developing countries	(Liu et al., 2015)		
system boundary	annual to decadal	all countries	(Andrew, 2020a)		
Net land-use chang	ge flux (ELUC; sectio	n 2.2)			
land-cover and land-use change statistics	continuous	global; in particular tropics	(Houghton et al., 2012, Gasser et al., 2020, Ganzenmüller et al., 2022, Yu et al. 2022)		
sub-grid-scale transitions annual to dec		global	(Wilkenskjeld et al., 2014, Bastos et al., 2021)		
vegetation annual to deca		global; in particular tropics	(Houghton et al., 2012, Bastos et al., 2021)		
forest degradation (fire, selective logging)	annual to decadal	tropics; Amazon	(Aragão et al., 2018, Qin et al., 2021, Lapola et al., 2023)		
wood and crop harvest	annual to decadal	global; SE Asia	(Arneth et al., 2017, Erb et al., 2018)		
peat burning	multi-decadal trend	global	(van der Werf et al., 2010, 2017)		
Atmospheric grow	th rate (GATM; sect	ion 2.4) no demonst	trated uncertainties larger than ±0.3 GtC yr-1 . The		
uncertainties in an	nual GATM have be	en estimated as ±0.	2 GtC yr-1, although the conversion of the growth		
rate into a global a	nnual flux assuming	instantaneous mixi	ing throughout the atmosphere introduces		
additional errors (s	see Section 2.4.2).				
Ocean sink (SOCEA	N; section 2.5)				
sparsity in surface fCO2 observations	mean, decadal variability and trend	global, in particular southern	(Gloege et al., 2021, Denvil-Sommer et al., 2021, Hauck et al., 2023a; Dong et al., 2024b)		

hemisphere

 ${\sf trend}$

https://doi.org/10.5194/essd-2025-659 Preprint. Discussion started: 13 November 2025







riverine carbon outgassing and its anthropogenic perturbation	annual to decadal	global, in particular partitioning between Tropics and South	(Aumont et al., 2001, Lacroix et al., 2020, Crisp et al., 2022)		
Models underestimate interior ocean anthropogenic carbon storage	annual to decadal	global	(Friedlingstein et al., 2022a, this study, DeVries et al., 2023, Müller et al., 2023)		
near-surface temperature and salinity gradients	mean on all time- scales	global	(Watson et al., 2020, Dong et al., 2022, Bellenger et al., 2023, Dong et al., 2024a)		
Land sink (SLAND;	section 2.6)				
strength of CO2 fertilisation	multi-decadal trend	global	(Wenzel et al., 2016; Walker et al., 2021)		
response to variability in temperature and rainfall	annual to decadal	global; in particular tropics	(Cox et al., 2013; Jung et al., 2017; Humphrey et al., 2018; 2021)		
nutrient limitation and supply	annual to multi- decadal	global	(Zaehle et al., 2014)		
carbon allocation and tissue turnover rates	annual to decadal	global	(De Kauwe et al., 2014; O'Sullivan et al., 2022)		
tree mortality	annual	global in particular tropics	(Hubau et al., 2021; Brienen et al., 2020)		
response to annual		global	(Mercado et al., 2009; O'Sullivan et al., 2021)		





4197 Figures

Atmospheric CO₂ Concentration

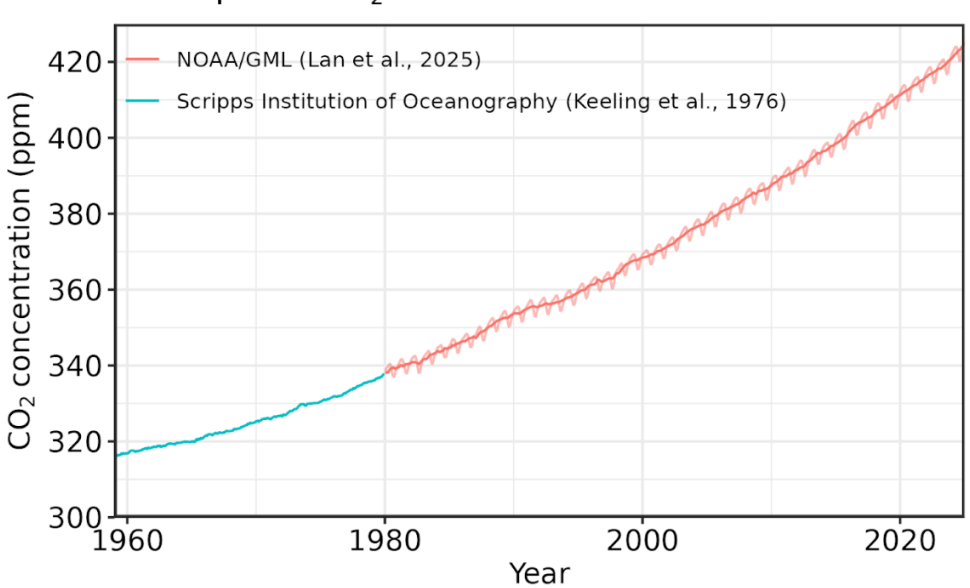


Figure 1. Surface average atmospheric CO₂ concentration (ppm). Since 1980, monthly data are from NOAA/GML (Lan et al., 2025a) and are based on an average of direct atmospheric CO₂ measurements from multiple stations in the marine boundary layer (Masarie and Tans, 1995). The 1958-1979 monthly data are from the Scripps Institution of Oceanography, based on an average of direct atmospheric CO₂ measurements from the Mauna Loa and South Pole stations (Keeling et al., 1976). To account for the difference of mean CO₂ and seasonality between the NOAA/GML and the Scripps station networks used here, the Scripps surface average (from two stations) was de-seasonalised and adjusted to match the NOAA/GML surface average (from multiple stations) by adding the mean difference of 0.667 ppm, calculated here from overlapping data during 1980-2012.





The global carbon cycle

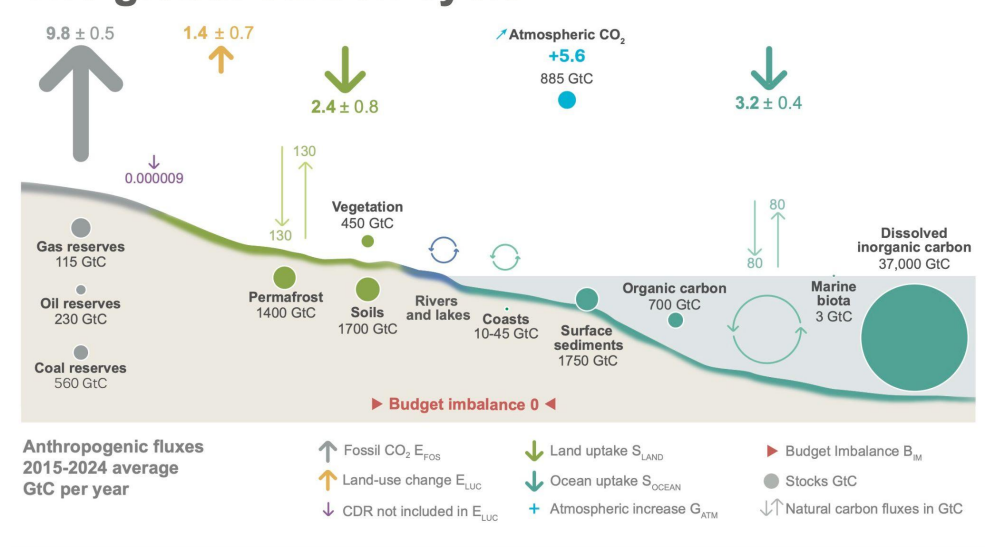
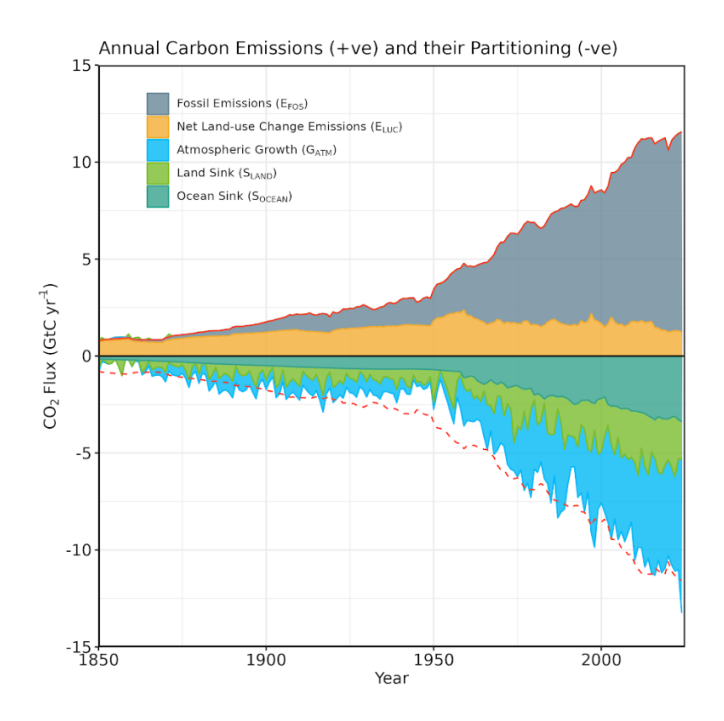


Figure 2. Schematic representation of the overall perturbation of the global carbon cycle caused by anthropogenic activities, averaged globally for the decade 2015-2024. See legends for the corresponding arrows. Fluxes estimates and their 1 standard deviation uncertainty are as reported in Table 7. The CDR estimate is for the year 2024. The uncertainty in the atmospheric CO₂ growth rate is very small (±0.02 GtC yr⁻¹) and is neglected for the figure. The anthropogenic perturbation occurs on top of an active carbon cycle, with fluxes and stocks represented in the background and taken from Canadell et al. (2021) for all numbers, except for the carbon stocks in coasts which is from a literature review of coastal marine sediments (Price and Warren, 2016). Fluxes

are in GtC yr⁻¹ and reservoirs in GtC. This figure was produced by Nigel Hawtin.







4222

4223

4224

4225

4226

4227

4228

4229

4230 4231

4232 4233

4234

4235

4236 4237

Figure 3. Combined components of the global carbon budget as a function of time, for fossil CO₂ emissions (E_{FOS}, including a small sink from cement carbonation; grey) and emissions from land-use change (E_{LUC}; brown), as well as their partitioning among the atmosphere (GATM; cyan), ocean (SOCEAN; blue), and land (SLAND; green). The figure shows annual estimates of each flux (in GtC yr⁻¹) since the year 1850. The partitioning is based on nearly independent estimates from observations (for GATM) and from process model ensembles constrained by data (for S_{OCEAN} and S_{LAND}) and does not exactly add up to the sum of the emissions, resulting in a budget imbalance (B_{IM}) which is represented by the difference between the bottom red line (mirroring total emissions) and the sum of carbon fluxes in the ocean, land, and atmosphere reservoirs. The E_{FOS} estimate is based on a mosaic of different datasets and has an uncertainty of $\pm 5\%$ ($\pm 1\sigma$). The E_{LUC} estimate is from three bookkeeping models (Table 4) with uncertainty of ±0.7 GtC yr⁻¹. The G_{ATM} estimates prior to 1959 are from Joos and Spahni (2008) with uncertainties equivalent to about ±0.1-0.15 GtC yr⁻¹ and from Lan et al. (2025a) since 1959 with uncertainties of about +-0.07 GtC yr⁻¹ during 1959-1979 and ±0.02 GtC yr⁻¹ since 1980. The Socean estimate prior to 1959 is the average from Khatiwala et al. (2013) and DeVries (2014) with uncertainty of about $\pm 30\%$. After 1959, it is the average of an ensemble of models (GOBMs) and an ensemble of fCO_2 products (with adjustments, Table 4) with uncertainties of about ± 0.4 GtC yr⁻¹. The S_{LAND} estimate is the average of an ensemble of models (DGVMs) (Table 4) with uncertainties of about ± 1 GtC yr¹. See the text for more details of each component and their uncertainties.

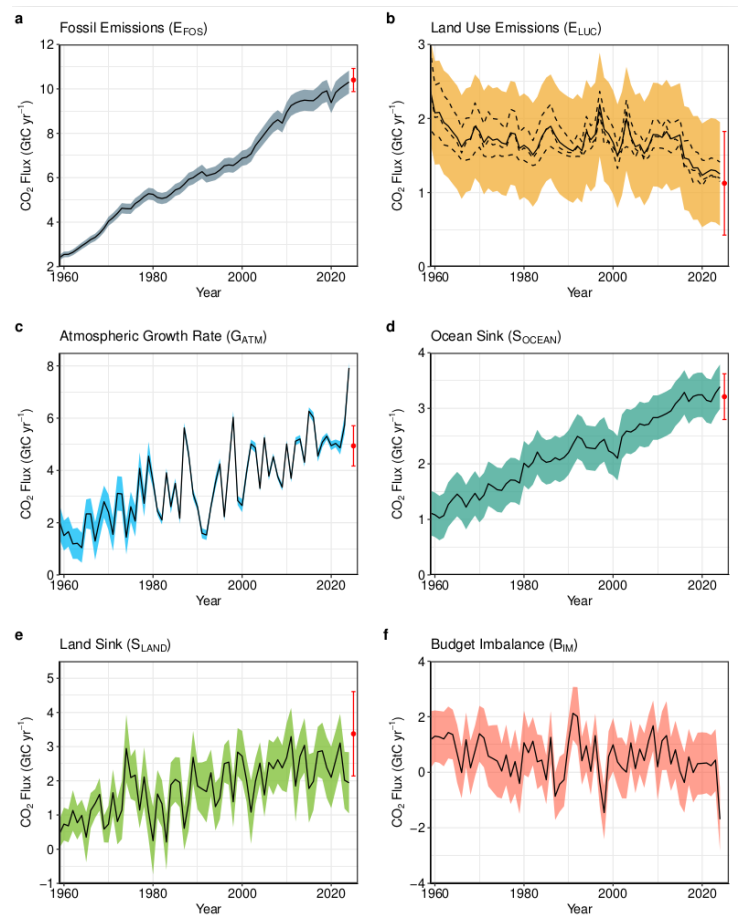


Figure 4. Components of the global carbon budget and their uncertainties as a function of time, presented individually for (a) fossil CO₂, including cement carbonation emissions (E_{FOS}), (b) emissions from land-use change (E_{LUC}), (c) growth rate in atmospheric CO₂ concentration (G_{ATM}), (d) the ocean CO₂ sink (S_{CEAN}), (e) the land CO₂ sink (S_{LAND}), (f) the budget imbalance (B_{IM}) that is not accounted for by the other terms. Individual estimates from the three bookkeeping models are shown as dashed lines for E_{LUC} in panel (b). Positive values of S_{LAND} and S_{OCEAN} represent a flux from the atmosphere to land or the ocean. All data are in GtC yr⁻¹ with the uncertainty bounds representing ± 1 standard deviation in shaded colour. Data sources are as in Figure 3. The red dots indicate our projections for the year 2025 and the red error bars the uncertainty in the 2025 projections (see methods).



42524253

4254

4255

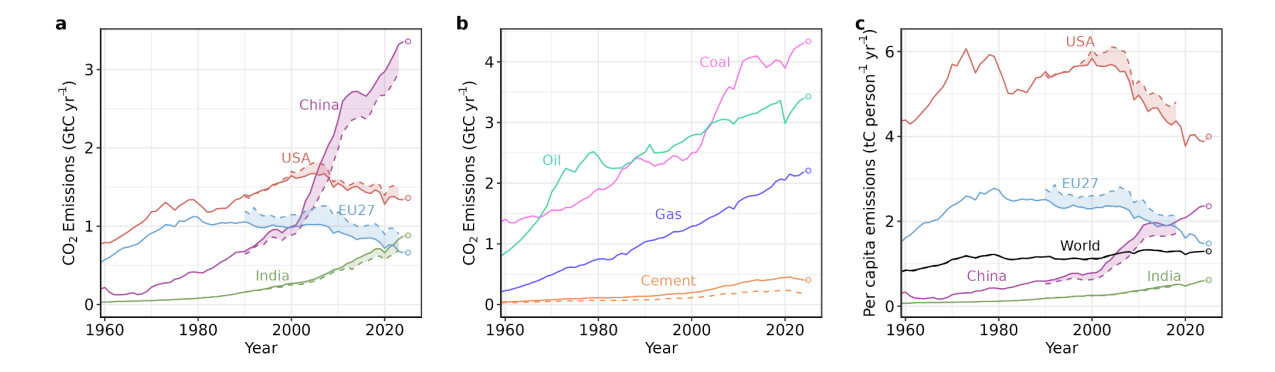


Figure 5. Fossil CO₂ emissions for (a) territorial (solid lines) and consumption (dashed lines) emissions for the top three country emitters (USA, China, India) and for the European Union (EU27), (b) global emissions by fuel type, including coal, oil, gas, and cement, and cement minus cement carbonation (dashed), and (c) per-capita emissions the world and for the large emitters as in panel (a). Territorial emissions are from Andrew & Peters (2025), while consumption-based emissions are updated from Peters et al. (2011a). See Section 2.1 and Supplement S.1 for details of the calculations and data sources.



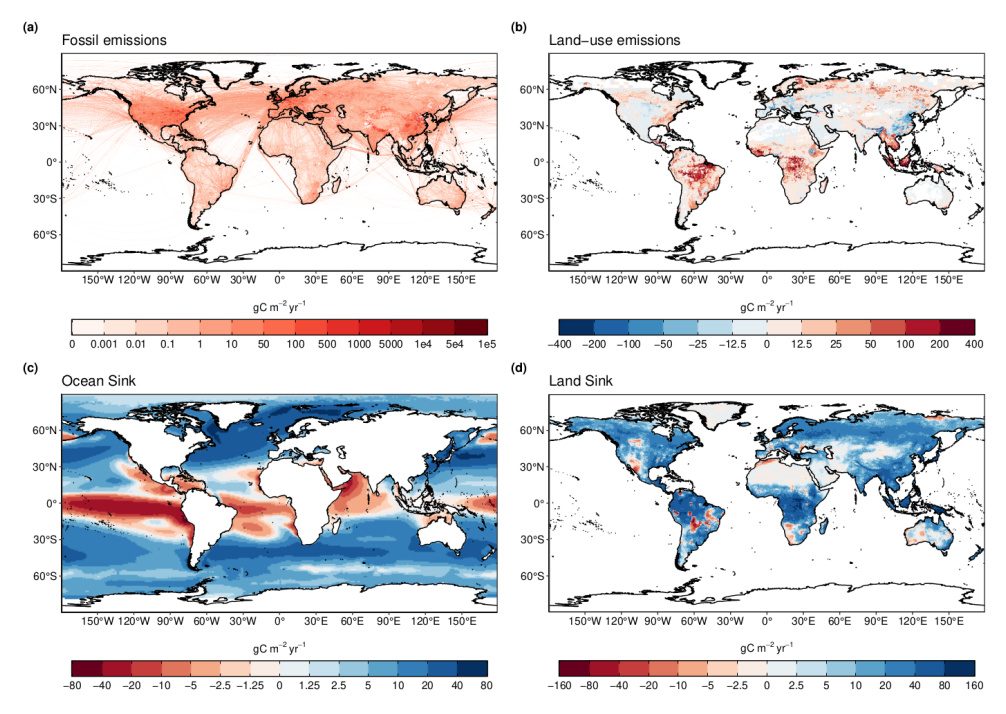


Figure 6. The 2015-2024 decadal mean components of the global carbon budget, presented for (a) fossil CO₂ emissions (E_{FOS}), (b) land-use change emissions (E_{LUC}), (c) the ocean CO₂ sink (S_{OCEAN}), and (d) the land CO₂ sink (S_{LAND}). Positive values for E_{FOS} and E_{LUC} represent a flux to the atmosphere, whereas positive values of S_{OCEAN} and S_{LAND} represent a flux from the atmosphere to the ocean or the land (carbon sink). In all panels, red colours represent a source (flux from the land/ocean to the atmosphere), blue colours represent a sink (flux from the atmosphere into the land/ocean). All units are in gC m⁻² yr⁻¹. Note the different scales in each panel. E_{FOS} data shown is from GCP-GridFEDv2025.0 and does not include cement carbonation. The E_{LUC} map shows the average E_{LUC} from the three bookkeeping models plus emissions from peat drainage and peat fires. BLUE and LUCE provide spatially explicit estimates at 0.25° resolution. Gridded E_{LUC} estimates for OSCAR are derived by spatially distributing their national data based on the spatial patterns of BLUE gross fluxes in each country (see Schwingshackl et al., 2022, for more details about the methodology). S_{OCEAN} data shown is the average of un-adjusted GOBMs and fCO₂-products means, using GOBMs simulation A, no adjustment for bias and drift applied to the gridded fields (see Section 2.5). S_{LAND} data shown is the average of the DGVMs for simulation S2 with the RSS adjustment included (see Section 2.6).

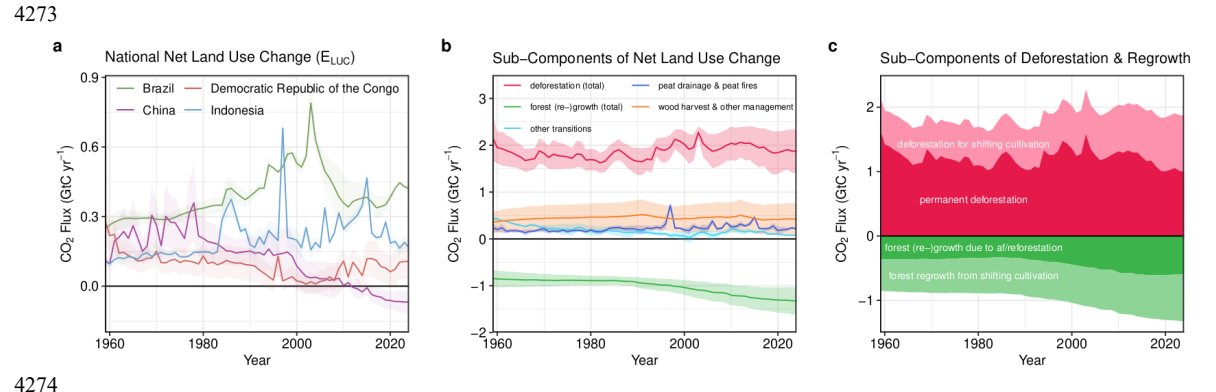


Figure 7. Net CO₂ exchanges between the atmosphere and the terrestrial biosphere related to land use change. (a) Net CO₂ emissions from land-use change from the four countries with largest cumulative emissions since 1959. Values shown are the average of the three bookkeeping models, with shaded regions as ±1σ uncertainty. (b) Sub-components of E_{LUC}: (i) emissions from deforestation (including permanent deforestation and deforestation in shifting cultivation cycles), (ii) emissions from peat drainage & peat fires, (iii) removals from forest (re-)growth (including forest (re-)growth due to afforestation and reforestation and forest regrowth in shifting cultivation cycles), (iv) fluxes from wood harvest and other forest management (comprising slash and product decay following wood harvest, regrowth after wood harvest, and fire suppression), and (v) emissions and removals related to other land-use transitions. The sum of the five components is E_{LUC} shown in Figure 4b. (c) Sub-components of 'deforestation (total)' and of 'forest (re-)growth (total)': (i) deforestation in shifting cultivation cycles, (ii) permanent deforestation, (iii) forest (re-)growth due to afforestation and/or reforestation, and (iv) forest regrowth in shifting cultivation cycles.





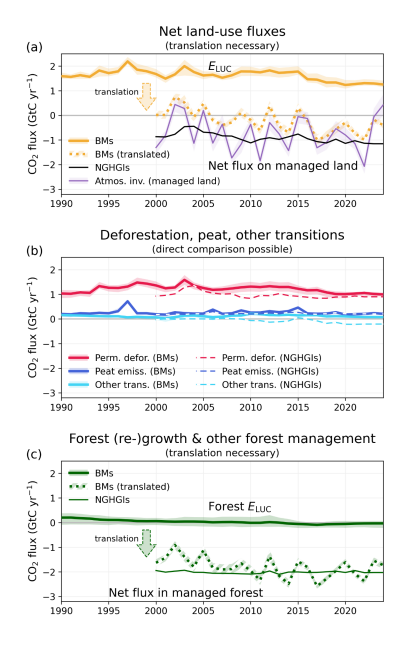


Figure 8. Comparison of land-use flux estimates from bookkeeping models (BMs; following the GCB definition of E_{LUC}), national GHG inventories (NGHGIs; following IPCC guidelines and thus including all carbon fluxes on managed land), and atmospheric inversion systems (considering fluxes on managed land only). To compare BM results with NGHGIs, a translation is necessary for some subcomponents. (a) Net land-use fluxes, for which a translation of BMs is necessary, (b) subcomponents permanent deforestation, peat drainage & peat fires, and other transitions, which can be directly compared and (c) subcomponent forest (re-)growth & other forest management, for which a translation is necessary. The lines represent the mean of 3 BMs and 14 atmospheric inversion estimates, respectively; Shaded areas denote the full range across BM estimates and the standard deviation for atmospheric inversions, respectively. The subcomponent forest (re-)growth & other forest management includes removals from forest (re-)growth (permanent), emissions and removals from wood harvest & other forest management, and emissions and removals in shifting cultivation cycles. The translation of BM estimates to NGHGI estimates in (a) and (c) is done by adding the natural land sink in managed forests to the BM estimates (see also Table S10). The GCB definition of E_{LUC} and the NGHGI definition of land-use fluxes are equally valid, each in its own context. For illustrative purposes we only show the translation of BM estimates to the NGHGI definition. NGHGI data are from the LULUCF data hub V3.1 (Melo et al. 2025).





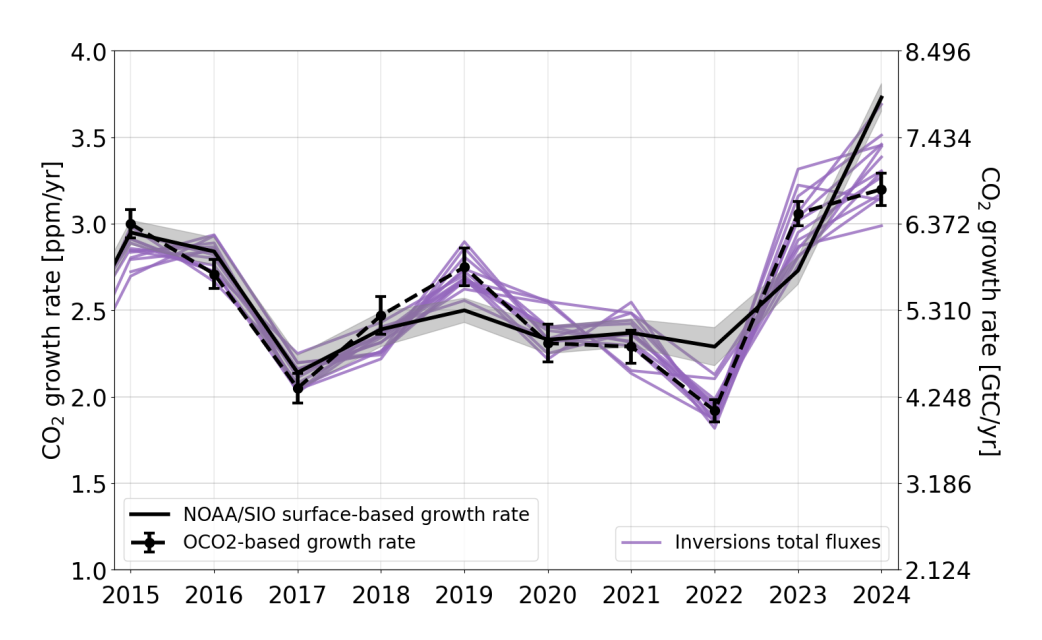


Figure 9: Annual atmospheric CO₂ growth rates based on observations from the surface network (by NOAA (National Oceanic and Atmospheric Administration) and SIO (Scripps Institution of Oceanography), as well as using the Growth Rate from Satellite Observations (GRESO) approach using OCO-2 based XCO₂ observations in ppm yr⁻¹ with uncertainties. To obtain G_{ATM}, the surface observation-based growth rate in units of ppm yr⁻¹ is converted to units of GtC yr⁻¹ by multiplying by a conversion factor (CF) of 2.124 GtC per ppm, assuming instantaneous mixing of CO₂ throughout the atmosphere. The purple lines are the atmospheric growth rates (in GtC yr⁻¹) calculated as the sum of the fluxes derived by the atmospheric inversions. Note that the right hand axis shows the growth rate in GtC yr⁻¹, with intervals of the conversion factor.





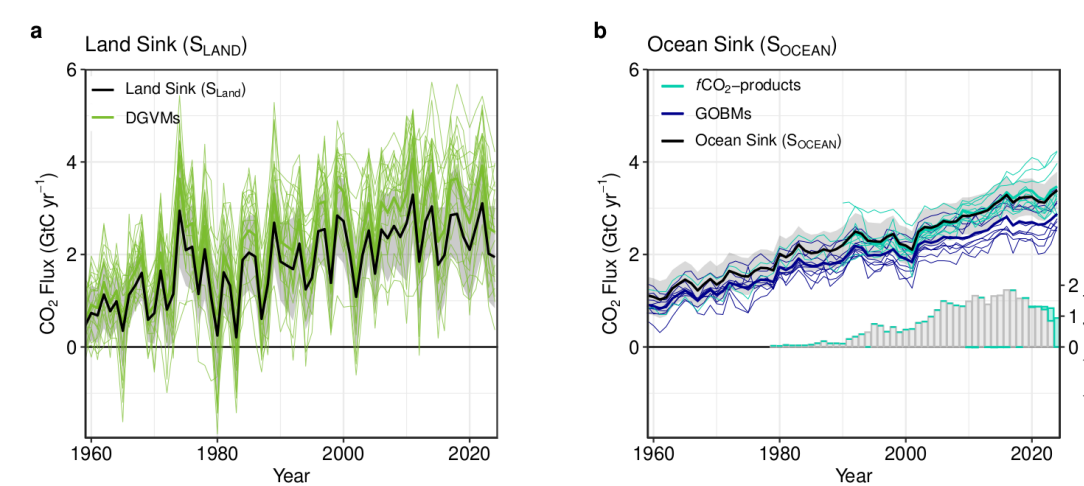


Figure 10. (a) The land CO₂ sink (S_{LAND}) estimated by individual DGVMs (thin green lines). The DGVM multimodel mean is shown as the thick green line. The S_{LAND} budget estimate (black with ±1σ uncertainty), is the DGVM multi-model mean adjusted for the RSS bias (i.e. reduced by 19%). (b) Comparison of the anthropogenic atmosphere-ocean CO₂ flux showing the budget values of S_{OCEAN} (black; with the uncertainty in grey shading), individual ocean models (royal blue), and the ocean fCO₂-products (cyan). Adjustments were applied to S_{OCEAN} (black) for the known underestimation in GOBMs and the warm layer/cool skin effect for fCO₂-products. Individual model lines as well as GOBM and fCO₂-product ensemble means (thick cyan and royal blue lines) do not include these adjustments, with the exception of 2 fCO₂-products (UExP-FNN-U and JMA-MLR) that include temperature corrections as part of their air-sea CO₂ flux calculation (see section 2.5). Two fCO₂-products (Jena-MLS, LDEO-HPD) extend back to 1959. All fCO₂-products were adjusted for the preindustrial ocean source of CO₂ from river input to the ocean, by subtracting a source of 0.65 GtC yr⁻¹ to make them comparable to S_{OCEAN} (see Section 2.5). The bar-plot in the lower right illustrates the number of monthly gridded values in the SOCAT v2025 dataset (Bakker et al., 2025a). Grey bars indicate the number of grid cells in SOCAT v2024, and coloured bars indicate the newly added grid cells in v2025.

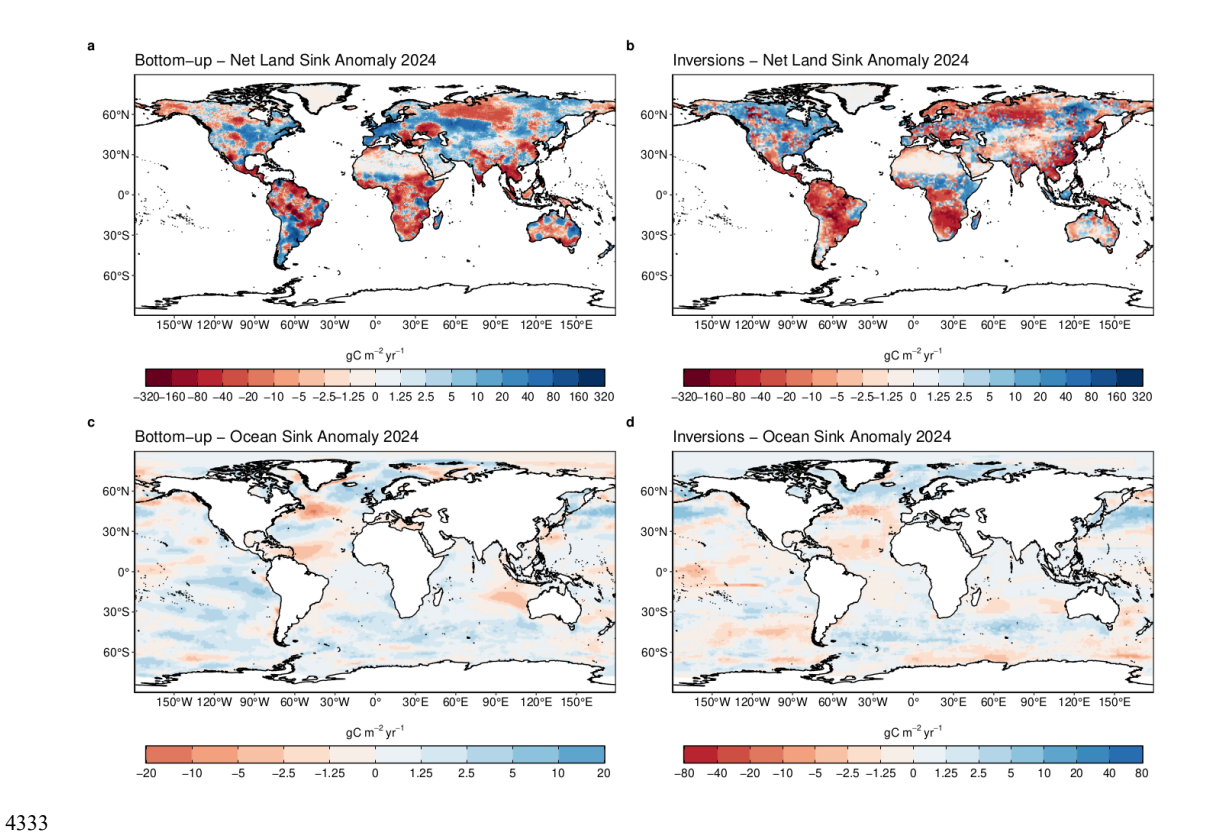


Figure 11. Anomalies in land and ocean sinks for 2024. Maps show the 2024 fluxes relative to the 2015-2024 decadal mean. Units are gC m⁻² yr⁻¹. (a) The bottom-up anomaly in the net land flux combines both the anomaly in S_{LAND} from DGVMs and in E_{LUC} from bookkeeping models, although the E_{LUC} contribution to the anomaly is minimal. Panel (b) shows the mean anomaly in the net land flux across 14 inversions. Panel (c) shows the mean anomaly from GOBMs and fCO_2 product ensemble means. The mean anomaly for GOBMs and fCO_2 products is first calculated, and then the mean of the two products is shown. Panel (d) shows the mean anomaly in ocean

4334

4335

4336

4337

43384339

4340

4341

fluxes across 14 inversions.





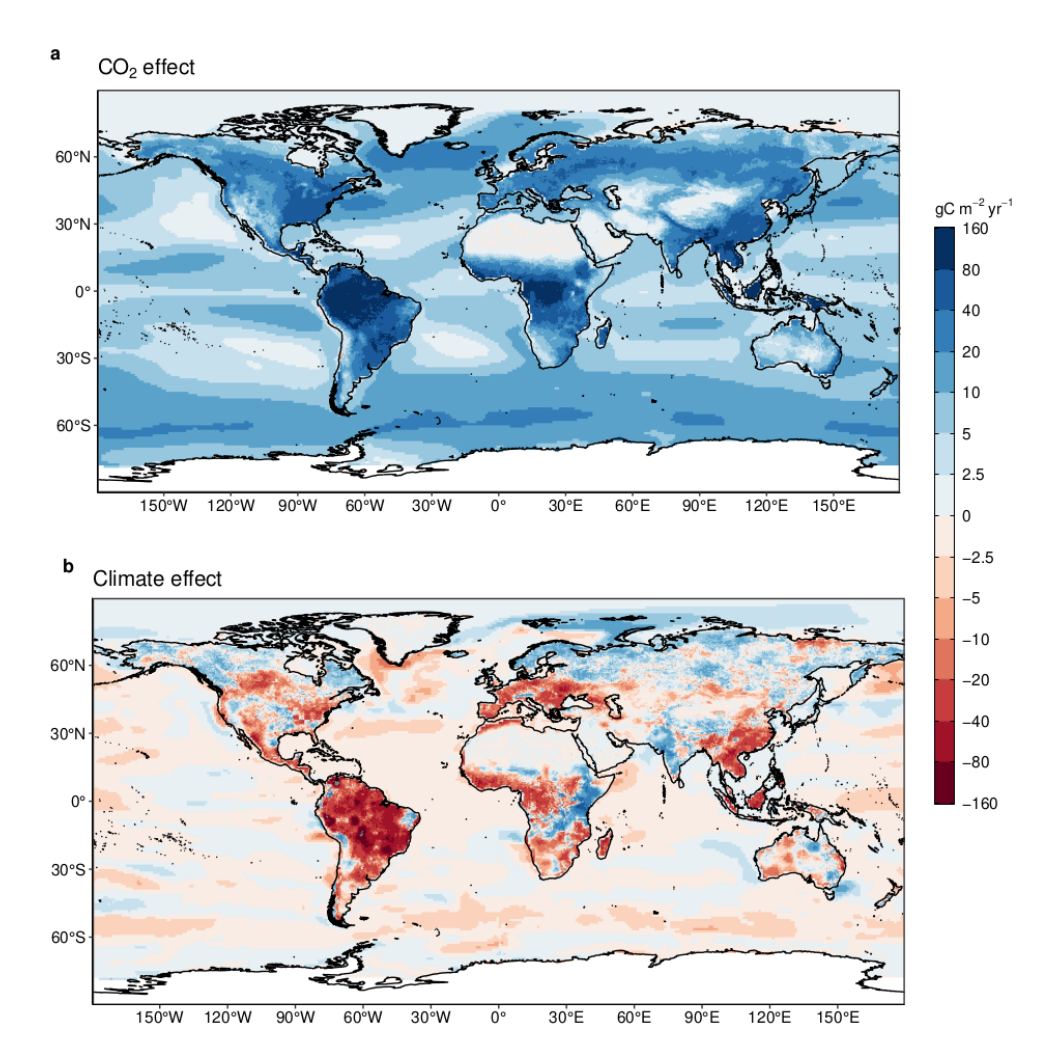


Figure 12. Attribution of the atmosphere-ocean (S_{OCEAN}) and atmosphere-land (S_{LAND}) CO₂ fluxes to (a) increasing atmospheric CO₂ concentrations and (b) changes in climate, averaged over the previous decade 2015-2024. All data shown is from the processed-based GOBMs and DGVMs. Note that the sum of ocean CO₂ and climate effects shown here will not equal the ocean sink shown in Figure 6, which includes the *f*CO₂-products. No adjustments were applied to the DGVMs or GOBMs. See Supplement S.3.2 and S.4.1 for attribution methodology. Units are in gC m⁻² yr⁻¹ (note the non-linear colour scale). Positive values (blue) are CO₂ sinks, negative values (red) are CO₂ sources.

estimates.

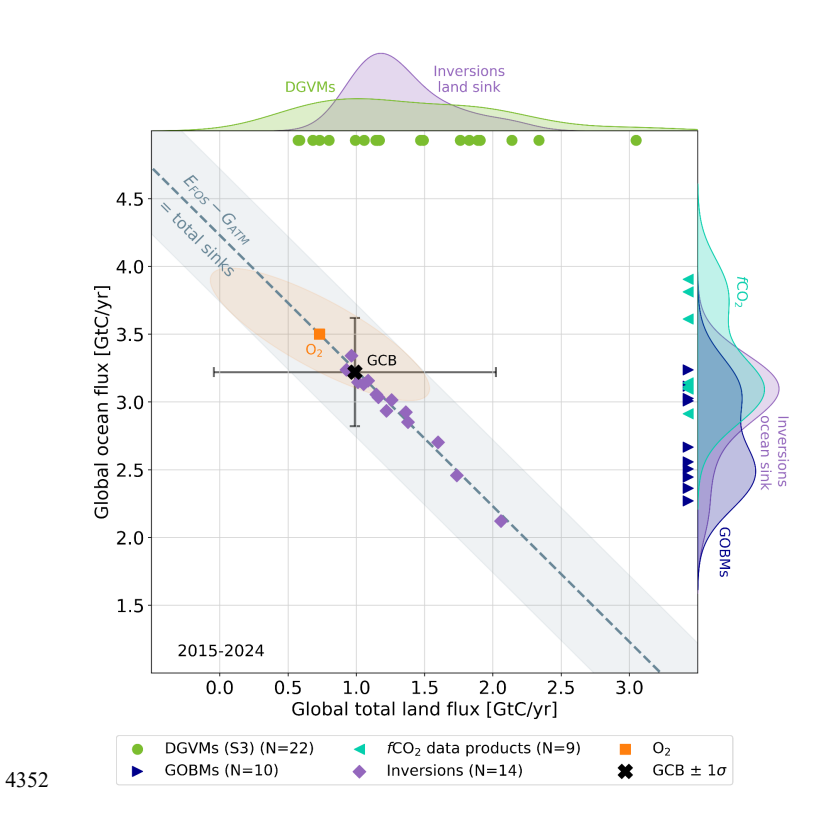


Figure 13. The 2015-2024 decadal mean global net atmosphere-ocean and net atmosphere-land fluxes derived from the ocean models and fCO₂ products (y-axis, right and left pointing blue triangles respectively), and from the DGVMs (x-axis, green symbols), and the same fluxes estimated from the atmospheric inversions (purple symbols). The shaded distributions show the densities of the ensembles of individual estimates. The black central cross ('GCB') is the mean (±1σ) of Socean and (Sland – Eluc) as assessed in this budget. The grey diagonal line represents the constraint on the global land + ocean net flux, i.e. global fossil fuel emissions minus the atmospheric growth rate from this budget (E_{FOS} – G_{ATM}). The orange square represents the same global net atmosphere-ocean and atmosphere-land fluxes as estimated from the atmospheric O₂ constraint (the ellipse drawn around the central atmospheric O₂ estimate is a contour representing the 1σ uncertainty of the land and ocean fluxes as a joint probability distribution). Positive values are CO₂ sinks. Note that the inverse estimates have been scaled for a minor difference between E_{FOS} and GridFEDv2O25.1 (Jones et al., 2025). The 'GCB' central mean estimate includes the S_{LAND} and S_{OCEAN} global adjustments. The inversions and fCO₂ products include the river adjustment (see Section 2). No further adjustments were applied to the individual bottom-up

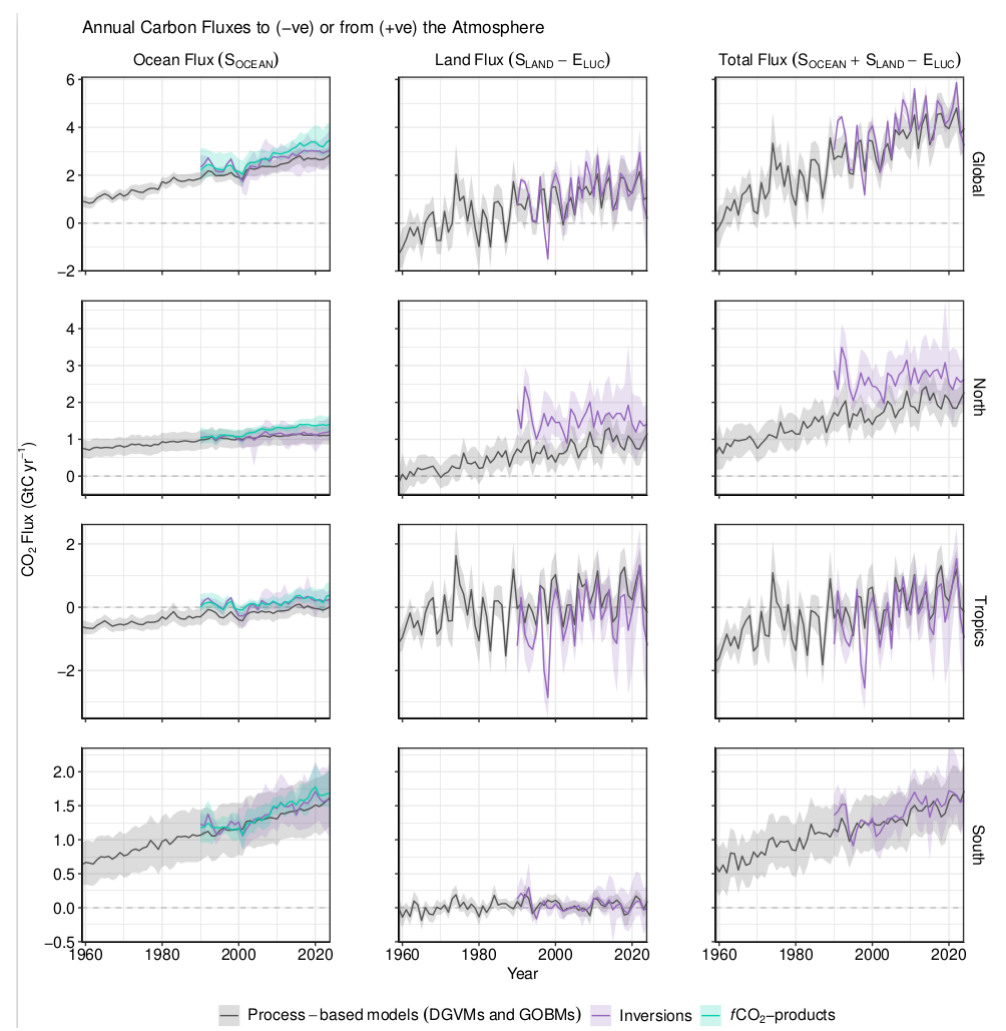


Figure 14. CO_2 fluxes between the atmosphere and the Earth's surface separated between land and oceans, globally and in three latitude bands. The ocean flux is S_{OCEAN} and the land flux is the net atmosphere-land fluxes from the DGVMs. The latitude bands are (top row) global, (2^{nd} row) north (>30°N), (3^{rd} row) tropics ($30^{\circ}S_{30^{\circ}N}$), and (bottom row) south (<30°S), and over ocean (left column), land (middle column), and total (right column). Estimates are shown for: process-based models (DGVMs for land, GOBMs for oceans); inversion systems (land and ocean); and fCO_2 -products (ocean only). Positive values are CO_2 sinks. Mean estimates from the combination of the process models for the land and oceans are shown (black line) with ± 1 σ of the model ensemble (grey shading). For the total uncertainty in the process-based estimate of the total sink, uncertainties are summed in quadrature. Mean estimates from the atmospheric inversions are shown (purple lines) with their full spread (purple shading). Mean estimates from the fCO_2 -products are shown for the ocean domain (light blue

https://doi.org/10.5194/essd-2025-659 Preprint. Discussion started: 13 November 2025 © Author(s) 2025. CC BY 4.0 License.

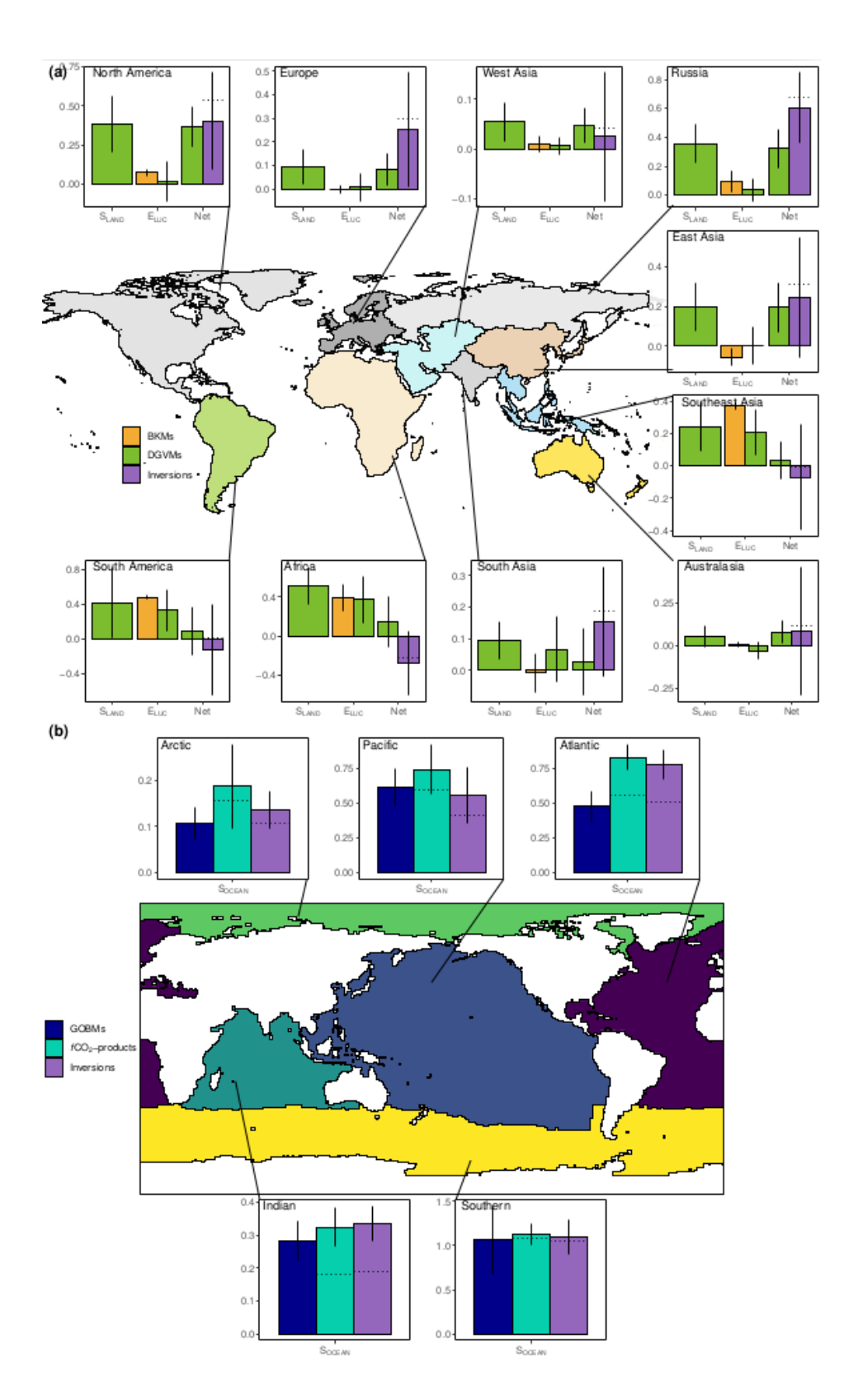




4378	lines) with full model spread (light blue shading). The global S_{OCEAN} (upper left) and the sum of S_{OCEAN} in all
4379	three regions represents the anthropogenic atmosphere-to-ocean flux based on the assumption that the pre-
4380	industrial ocean sink was 0 GtC yr^1 when riverine fluxes are not considered. This assumption does not hold at
4381	the regional level, where pre-industrial fluxes can be significantly different from zero. Hence, the regional
4382	panels for Socean represent a combination of natural and anthropogenic fluxes.
4383	
4384	







https://doi.org/10.5194/essd-2025-659 Preprint. Discussion started: 13 November 2025 © Author(s) 2025. CC BY 4.0 License.





Figure 15. Decadal mean (a) land and (b) ocean fluxes for RECCAP-2 regions over 2015-
2024. For land fluxes, S_{LAND} is estimated by the DGVMs (green bars), with the error bar as
$\pm 1\sigma$ spread among models. A positive S_{LAND} is a net transfer of carbon from the atmosphere to
the land. $E_{\text{\tiny LUC}}$ fluxes are shown for both DGVMs (green) and bookkeeping models (orange),
again with the uncertainty calculated as the $\pm 1\sigma$ spread. Note, a positive E_{LUC} flux indicates a
loss of carbon from the land. For the DGVMs, S_{LAND} and E_{LUC} are adjusted for RSS bias. The
net land flux is shown for both DGVMs (green) and atmospheric inversions (purple),
including the full model spread for inversions. The ocean sink ($S_{\mbox{\scriptsize OCEAN}})$ is estimated by
GOBMs (royal blue), fCO2-products (cyan), and atmospheric inversions (purple). No
adjustments were applied to GOBMs and fCO2-products at regional scale. Uncertainty is
estimated as the $\pm 1\sigma$ spread for GOBMs, and the full model spread for the other two datasets.
The dotted lines show the fCO ₂ -products and inversion results without river flux adjustment.
Positive values are CO ₂ sinks.